DISSERTATION

submitted to the

Combined Faculties of Natural Sciences and Mathematics

Ruperto-Carola University Heidelberg, Germany

for the degree

Doctor of Natural Sciences (PhD)

presented by

Manuel Rhiel, M.Sc.

born in Marburg (Wehrda)

Date of oral examination: 28.02.2018

Vesicular Proteomics:

Isoforms of the COPI and COPII coats

-

Implications in Protein Sorting and Disease

1st Referee: Prof. Dr. Felix T. Wieland

2nd Referee: Prof. Dr. Thomas Söllner

Table of contents

Abstract

As for many proteins, subunits of the COPI and COPII vesicular coats have diverged during evolution. To date, multiple isoforms of almost all proteins involved in the formation of these vesicles can be found in higher organisms. While work of others and our own lab has established an important role of the four Sec24 isoforms in the process of cargo/machinery recruitment into COPII vesicles, it remains largely elusive what purpose the isoforms of the coatomer subunits γ- and ζ-COP as well as of the small GTPase Arf (Arf1-6) serve in COPI formation. To investigate a putative role of these proteins in the recruitment of specific proteins into COPI vesicles, and deepen our current understanding of the roles of COPII coat isoforms, we established a method to purify *in vitro* reconstituted vesicles from SILAC-labeled cells in order to assess and compare their protein content. By doing so we were able to narrow down a concise set of proteins that represents the proteome of these two classes of early secretory pathway vesicular carriers. In contrast to the COPII system, we found that neither isoforms of γ- or ζ-COP, nor any of the four vesicle-generating isoforms of Arf seem to have any influence on the content composition of COPI vesicles. However, while the isoforms of coatomer seem to be capable of recruiting cargo proteins with virtually identical efficacy, Arf1 could be distinguished as the most potent COPI-forming GTPase isoform.

We further investigated disease-related mutations identified in one particular Sec24 isoform, Sec24D. These mutations were recently shown to be the sole cause for the development of a syndromic form of *osteogenesis imperfecta*, which is better known as brittle bone disease. We could show that one single point mutation within Sec24D, the conversion of serine in position 1015 to phenylalanine, completely abrogates the ability of this protein to bind to the ER-Golgi Q_a-SNARE protein Syntaxin5 in direct interaction studies. As a consequence, COPII vesicles formed by this Sec24D variant were largely depleted in not only Syntaxin5 but also its partner ER-Golgi SNAREs GS27 and Bet1.

Moreover we studied fibroblast cells derived from a patient that carries the Sec24D^{S1015F} mutation in one allele and a point mutation that causes a premature stop-codon within the second allele of the gene. In such cells, the level of all four ER-Golgi SNAREs and also some intra-Golgi SNARE proteins was markedly reduced. However, the distribution of Syntaxin5 under steady state conditions reflected that of control cells.

Zusammenfassung

Im Verlauf der Evolution kam es zur Diversifikation vieler Proteine, darunter auch Untereinheiten der COPI und COPII Vesikelhüllen-Proteine. Inzwischen ist klar, dass von fast allen Proteinen, welche bei der Entstehung von COPI oder COPII Vesikeln in höheren Organismen eine Rolle spielen, mehrere Isoformen existieren. Während eine entscheidende Rolle der vier Isoformen von Sec24 beim Prozess der Maschinerie-/Frachtaufnahme in COPII Vesikel durch die Arbeiten Anderer und unseres Labors etabliert wurde, bleibt die Frage nach der Funktion der Isoformen der Coatomer Untereinheiten γ- und ζ-COP beziehungsweise der kleinen GTPase Arf (Arf1-6) bei der COPI Biogenese bisher unbeantwortet. Um eine mögliche Rolle dieser Proteine im Zusammenhang mit spezifischer Protein in COPI Vesikel zu untersuchen und unser bestehendes Verständnis dieser Rolle für COPII Vesikelhüllen-Proteine zu vertiefen, haben wir eine neue Methode zur Aufreinigung von *in vitro* rekonstituierten Vesikeln aus SILAC-markierten Zellen etabliert um deren Inhalt untersuchen und vergleichen zu können. Hierdurch war es uns möglich eine präzise Aufstellung jener Proteine vorzunehmen, die in Vesikeln des frühen sekretorischen Wegs zu finden sind. Wir konnten feststellen, dass Isoformen von γ- oder ζ-COP, beziehungsweise der vier Vesikel-formenden Isoformen von Arf keinen wesentlichen Einfluss auf den Protein-Inhalt von COPI Vesikeln haben, anders als im COPII System. Wir konnten jedoch beobachten, dass Arf1 die potenteste Isoform aller COPI-formenden GTPasen ist, während die Fähigkeit zur Frachtaufnahmen bei den Coatomer Isoformen sehr ähnlich zu sein scheint.

Desweiteren haben wir krankheitsausprägende Mutationen in einer bestimmten Sec24 Isoform - Sec24D - untersucht. Diese kürzlich identifizierten Mutationen führen als einzige Ursache zur Ausprägung einer syndromischen Form von *osteogenesis imperfecta*, besser bekannt als Glasknochenkrankheit. Mithilfe direkter Interaktionsstudien konnten wir zeigen, dass eine einzige Punktmutation in Sec24D, Konversion von Serin in Position 1015 zu Phenylalanin, die Fähigkeit des Proteins an das ER-Golgi Q_a-SNARE Protein Syntaxin5 zu binden, vollständig in blockiert. Als Konsequenz daraus, enthalten COPII Vesikel, die mit dieser Sec24D Variante hergestellt werden sowohl kaum Syntaxin5 als auch nur geringe Mengen der übrigen ER-Golgi SNAREs GS27 und Bet1.

Wir untersuchten zudem Fibroblasten eines Patienten, der zum einen die bereits erwähnte $Sec24D^{S1015F}$ Mutation trägt und dessen zweites Sec24D Allel zudem eine Mutation enthält die in einem verfrühten Stop-Codon resultiert. Die Menge aller vier ER-Golgi und einiger intra-Golgi SNARE Proteine war in diesen Zellen erheblich reduziert. Demgegenüber konnten wir keine abweichende intrazelluläre Verteilung von Syntaxin5 im Vergleich zu Kontrollzellen beobachten.

1 Introduction

1.1 Organelles of the Secretory Pathway and their Discovery

The secretory pathway is an elaborate logistic center that is found in all eukaryotes. The major part of a cells' membrane material forms this system. It can be roughly divided into three major functional units: The endoplasmic reticulum, the Golgi apparatus, and the endosomal system including the plasma membrane. In the following I briefly discuss the discovery of these organelles and try to point out their main functions.

1.1.1 The Endoplasmic Reticulum

In an early electron microscopic study from 1945, Keith Porter and his colleagues discovered structures which they described as "lace-like reticulum" (Porter et al., 1945). The term reticulum became widely accepted and was further specified by the prefix endoplasmic which simply underlines its location within the cytoplasm of a cell (Porter and Kallman, 1952). Over the cause of the following years it became clear that the endoplasmic reticulum (ER) is the largest of organelles which together make up the endomembrane system of a eukaryotic cell. George Palade noticed in the mid 1960s that the ER can be basically divided into two major functional units already based on its appearance under the electron microscope. He observed that some areas of the ER membrane appear to be smooth (smooth ER; sER), other regions seemingly were surrounded by a rough (rough ER; rER), dense outer surface (Palade, 1955, 1956; Palade and Siekevitz, 1956).

Shortly thereafter, first indications pointed towards a role of the rER in protein secretion. It became clear that the dense surface of the rER was formed by "ribosomes", a term coined by Richard B. Roberts that supposedly serve the synthesis of proteins destined to enter the pathway of secretion (Siekevitz and Palade, 1960). In the following decade more and more evidence was gathered in electron microscopic studies and radioactive labeling experiments that supported this idea (Blobel and Sabatini, 1970; Redman and Sabatini, 1966; Sabatini and Blobel, 1970; Sabatini et al., 1966). Together these findings then ultimately led to the proposal of the signal hypothesis by Günther Blobel and David Sabatini in 1971 which predicts the presence of specific targeting signals for protein entry into the secretory pathway. Only four years later, Blobel together with Bernhard Dobberstein

was able to prove the signal hypothesis experimentally in two classic publications (Blobel and Dobberstein, 1975a, b).

It is common knowledge nowadays that the rough ER is the birthplace of secreted proteins. Most of them carry a so-called signal sequence/peptide, a short stretch of amino acids at the N-terminus of the protein (Blobel and Dobberstein, 1975b). This sequence is recognized like a barcode once it emerges from the exit tunnel of the translating ribosome by targeting factors, amongst other proteins (Krieg et al., 1986; Kurzchalia et al., 1986). The most prominent and first discovered ER-targeting factor was the signal recognition particle (SRP) (Walter and Blobel, 1980). When engaged with a ribosome, the SRP-ribosome complex is targeted to the ER membrane (Walter and Blobel, 1981a, b). The nascent chain subsequently elongates while being transcribed through a pore that is formed by the so-called Sec61 translocon in order to reach the lumen or the ER (Crowley et al., 1994; Crowley et al., 1993; Görlich et al., 1992).

In contrast to the rough ER which on EM images often appears as ribosome-studded flat cisternae, the smooth ER is more dilated and vesicular in structure. The difference in shape is linked to its function. The sER is not specified in producing transmembrane and secreted protein, but plays a pivotal role in lipid biosynthesis, synthesis of steroids, detoxification and the regulation of calcium homeostasis (reviewed in Baumann and Walz, 2001; Fagone and Jackowski, 2009; Schwarz and Blower, 2016; Shibata et al., 2006). Moreover, the smooth ER is often viewed as part of a larger fraction of the ER, called the transitional ER (tER) (Palade, 1975). The term transition in this context does not point out the transition from ribosome-associated to ribosome-free regions but rather at its function: It is the region of the ER from where vesicular transport/transition is initiated. The tER is located close to the cis-side of the Golgi (Schweizer et al., 1988). Because of its appearance it is also called vesicular tubular clusters (VTCs) (Bannykh et al., 1996), a name that can be used synonymous with tER. More commonly used nowadays is the term ER-Golgi intermediate compartment (ERGIC) (Klumperman et al., 1998; Schweizer et al., 1990) which points out the chimeric character of this sub-compartment. The export of proteins from the ER is discussed in detail in the following.

1.1.2 The Golgi Apparatus

In contrast to the ER, the Golgi apparatus was discovered long before the invention of electron microscopy. At the end of the 19th century, Italian physician and histologist Camillo Golgi invented a silver-staining method for his studies of neuronal cells. Eventually he recognized reappearing intracellular structures that now carry his name (Golgi, 1989a, b; translations of the original articles

from 1898). Reportedly, the existence of the Golgi apparatus was hotly debated because it could not be observed in living cells but was only visible with the silver-staining technique introduced by Golgi. It took until the advent of electron microscopy when the existence of a membranous organelle that occupied the same regions stained by the Golgi-staining could be ultimately confirmed (Dalton and Felix, 1954; Sjostrand and Hanzon, 1954). Dalton and Felix described the morphology of the Golgi complex as it is generally found in higher organisms. They observed vacuole-like structures, flat profiles, lamellae, and vesicles (Dalton and Felix, 1954, 1956).

Scientist started to understand the function of this organelle during the 1960s. Again, Palade, this time together with co-workers Lucien Caro and James Jamieson, found first evidence for a role of the Golgi apparatus in protein secretion by using a combined approach of autoradiography, electron microscopy, and cellular fractionation (Caro and Palade, 1964; Jamieson and Palade, 1967; Palade, 1975). Simultaneously, employing similar methods, the lab of Charles Lebond could show that the Golgi apparatus is incorporating labeled sugar molecules (Neutra and Leblond, 1966; Whur et al., 1969). This work was further substantiated by parallel studies from other labs which could show that the activity of glycosyltransferases is greatly increased in Golgi-enriched membrane fractions, pointing towards a role of the Golgi in glycosylation (Fleischer et al., 1969; Morre et al., 1969). After having found two major tasks of the Golgi it became clear that the Golgi complex cannot be viewed as one compartment where each region carries out the same functions (Novikoff et al., 1971). Instead, distinct regions of the Golgi are fulfilling very specific tasks (Kornfeld and Kornfeld, 1985).

Nowadays, the cisternae of a Golgi stack are generally divided into a cis-, medial-, and trans-Golgi entity. Each sub-compartment contains a specific set of enzymes that successively drive the maturation of glycosylation that begins in the ER (reviewed in Dunphy and Rothman, 1985; Kornfeld and Kornfeld, 1985). Moreover, looser network-like structures were found both at the cis- and the trans-side of the Golgi. The ERGIC, mentioned in the previous section, is also known as cis-Golgi network (CGN). Here, secretory COPII vesicles from the ER arrive and also retrograde COPI vesicles do form (Appenzeller-Herzog and Hauri, 2006). Furthermore, it has also been shown to play a pivotal in sorting of lysosomal proteins, the initial tagging of which takes place as early as at the CGN-level (Coutinho et al., 2012; Schweizer et al., 1991).

The trans-Golgi network (TGN) on the opposite side of the complex is a very specialized sorting hub. There is no other sub-compartment of the secretory pathway from where more different trafficking routs are taken (Griffiths and Simons, 1986; Gu et al., 2001). The TGN is furthermore the stage at which vesicular transport is no longer driven by the COPI/COPII system. Here other classes of vesicles, of which many are associated with the scaffold clathrin, take over vesicular transport (Robinson, 2004).

1.1.3 Late Secretory Organelles: The Endosomal System

For some secreted proteins, the last packing into a carrier occurs at the TGN from where they are then directly transported towards the plasma membrane (PM). In yeast this is facilitated by packing of such proteins into carriers that are formed by the exomer complex (Wang et al., 2006). In mammals, the same trafficking route seems to exist, although it remains unclear how exactly these carriers form (Bard and Malhotra, 2006; Klemm et al., 2009; Wakana et al., 2012). The TGN-PM trafficking is in general poorly understood when compared to for example the back-and-forth exchange of material between the ER and the Golgi. One possible reason for this might be the presence of another elaborate section of the secretory pathway acting after the Golgi: The endosomal system. Its discovery is preceded by the discovery of the lysosomes by de Duve and his co-workers (Appelmans et al., 1955; De Duve and Wattiaux, 1966; Essner and Novikoff, 1961). First evidence for the existence of a compartment he called “phagosome” came from Werner Straus (Straus, 1964). He observed that internalized horseradish peroxidase was first in a membranous compartment separate from the lysosome with which it would eventually merge over time. Twenty years later, Ira Mellman and co-workers separated those organelles which they named “endosomes” from denser lysosomes (Galloway et al., 1983).

After first discovering the organelle it became rapidly clear that - similar to Golgi complex - the endosome cannot be viewed as a uniform compartment. Endocytic vesicles fuse in order to form an early endosome which are also referred to as sorting endosomes (Gruenberg et al., 1989). Here, molecules to be ultimately degraded via the lysosomal pathway are separated from e.g. receptors which are recycled for another round of recognition and internalization (Maxfield and McGraw, 2004; Mayor et al., 1993). Moreover, trafficking between early endosomes and the TGN has been observed (Bonifacino and Rojas, 2006). The early endosomes will at some point mature to become a late endosome, a process that is regulated in part by Rab GTPases (Huotari and Helenius, 2011). Late endosomes then fuse with one another and with lysosomes in order to form a terminal organelle for the degradation of proteins (Luzio et al., 2010; Luzio et al., 2007).

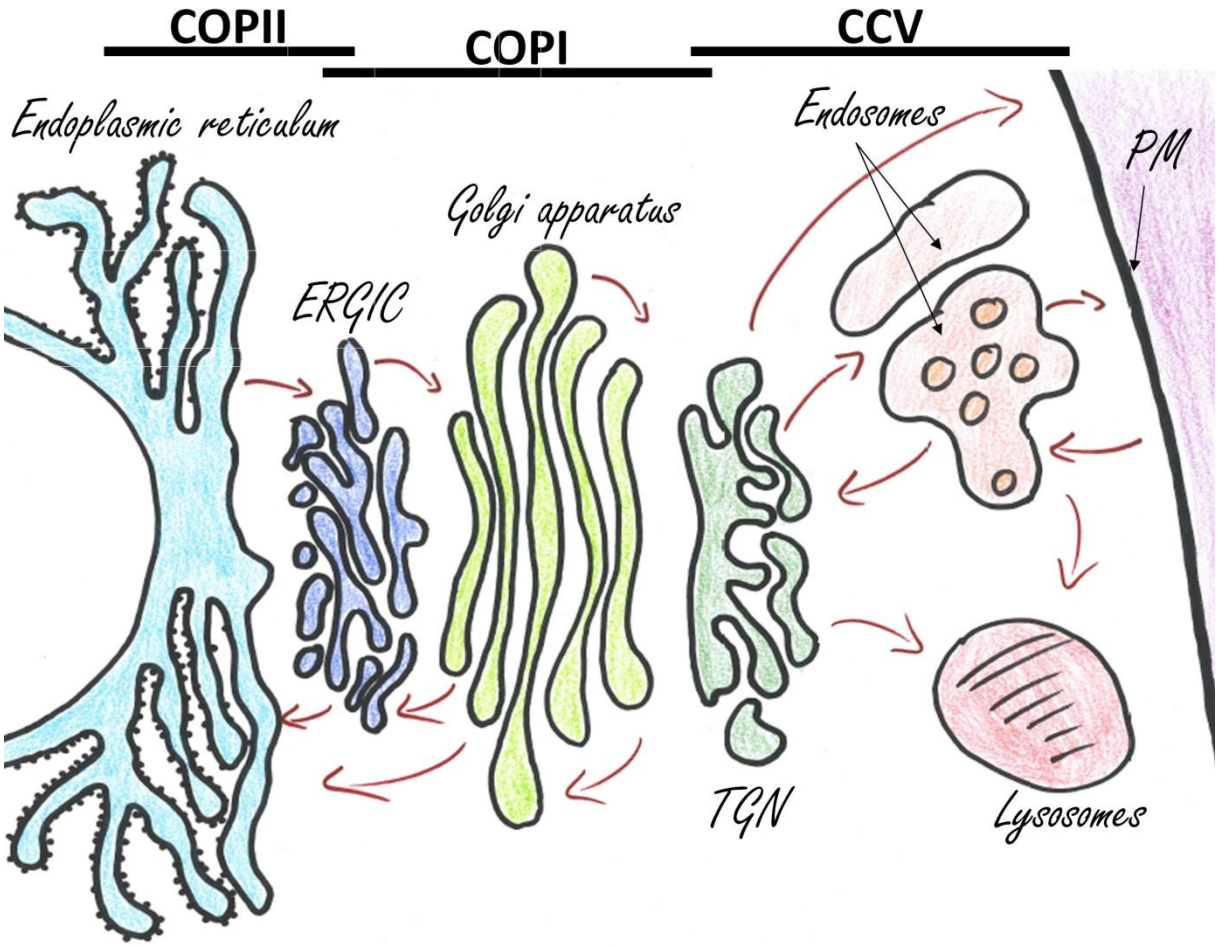

Figure 1.1 Organelles of the Secretory Pathway

Drawn are the organelles of the secretory pathway. Red arrows mark the transport of material. The classes of vesicular coat, which acts at the respective organelles, are indicated above the drawing. For additional information refer to (Bonifacino and Glick, 2004; Robinson, 2004)

1.2 COPII Vesicles: ER to Golgi Transport

The endoplasmic reticulum as the largest of secretory organelles harbors its own vesicular transport system. The current knowledge about the general mechanism of COPII vesicle biogenesis, non-essential accessory protein which support this process, as well as cargo-uptake, is discussed in the following.

1.2.1 COPII Vesicles: Biogenesis

The endoplasmic reticulum (ER) is the first organelle which proteins have to access in order to enter the secretory pathway. From here proteins are transported within an organelle-specific type of vesicles to the Golgi apparatus. The proteins that form the coat of the so-called COPII vesicles were first identified in genetic screen carried out in the lab of Randy Schekman (Novick et al., 1981; Novick et al., 1980). COPII vesicles bud at specialized domains of the ER termed ER-exit sites (ERES) (Orci et al., 1991; Rossanese et al., 1999). These are stable, long-lived structures which can be formed *de novo* (Bevis et al., 2002; Stephens, 2003).

COPII vesicle formation at these sites starts by the activation of secretion-associated Ras-related GTPase 1 (Sar1). This is facilitated by its membrane-bound guanidine nucleotide exchange factor (GEF) Sec12, which exchanges GDP for GTP rendering the protein from a soluble to a membrane associated-state (Barlowe et al., 1993; Barlowe and Schekman, 1995; d'Enfert et al., 1991; Nakano et al., 1988). The activation of Sar1 in mammals seems to occur mainly at ERES as both, Sec12 and Sar1, are enriched in this region of the ER (Kuge et al., 1994; Weissman et al., 2001).

Once bound to GTP, the conformation of Sar1 changes dramatically. It exposes an amphipathic α-helix located at its N-terminus which unlike that of other small GTPases involved in trafficking is not post-translationally modified by a myristoyl group or prenyl moiety (Bi et al., 2002; Huang et al., 2001). The helix is not only pivotal for the membrane binding ability but is furthermore key to the membrane surface activity of Sar1 (Bielli et al., 2005). Membrane-anchored Sar1 binds to single dimers of Sec23/Sec24 with the interaction surface being formed be Sar1 and Sec23 (Bi et al., 2002). The trimeric complex is further believed to interact with acidic lipids of the ER-membrane via a conserved positively charged surface in order to achieve a more stable association (Bi et al., 2002; Matsuoka et al., 1998).

Between the two subunits of the inner coat complex, Sec23/Sec24, there is a strict division of labor. While Sec23 functions as the build-in GTPase activating proteins (GAP) for Sar1 (Yoshihisa et al., 1993), Sec24 is binding to short cytoplasmic tails of membrane proteins, a process that is important for the formation of so-called “pre-budding complexes” (Aridor et al., 1998; Kuehn et al., 1998; Kuehn et al., 1996). These pre-budding complexes alone are not capable of deforming the ER membrane into a bud or vesicle (Lee et al., 2005). This is only achieved by the addition of a second, outer layer of coat which is composed of heterotetramers containing two subunits of each, Sec13 and Sec31. The fact that Sec13/31 functions as the scaffold for COPII formation can already be deduced from its feature of forming empty cages by itself (Stagg et al., 2006). *In vivo*, the outer coat

is recruited via an interaction of the Sec31 subunit with an interface that is formed by Sec23 and Sar1 (Bi et al., 2007). This interaction does not only lead to the formation of a COPII bud but also triggers GTP hydrolysis in Sar1 (Antonny et al., 2001). Another factor that seems to play an important role in modulating Sar1 activity and organization of ERES is Sec16 (Sprangers and Rabouille, 2015).

Scission of the vesicles relies on the ability of Sar1 so deform membranes into tubules or even small vesicles at very high concentrations (Hariri et al., 2014; Lee et al., 2005). While the scission of COPII vesicles is not dependent on the ability of Sar1 to hydrolyze GTP (Adolf et al., 2013; Barlowe et al., 1994) uncoating cannot happen when GTP hydrolysis is blocked (Aridor et al., 1995; Barlowe et al., 1994; Oka and Nakano, 1994). In addition to the core machinery of COPII vesicle biogenesis, several other factors are crucial to ensure an optimal efficacy in cargo of formation, cargo packing and targeting *in vivo* which are thoroughly discussed elsewhere (Venditti et al., 2014; Zanetti et al., 2011).

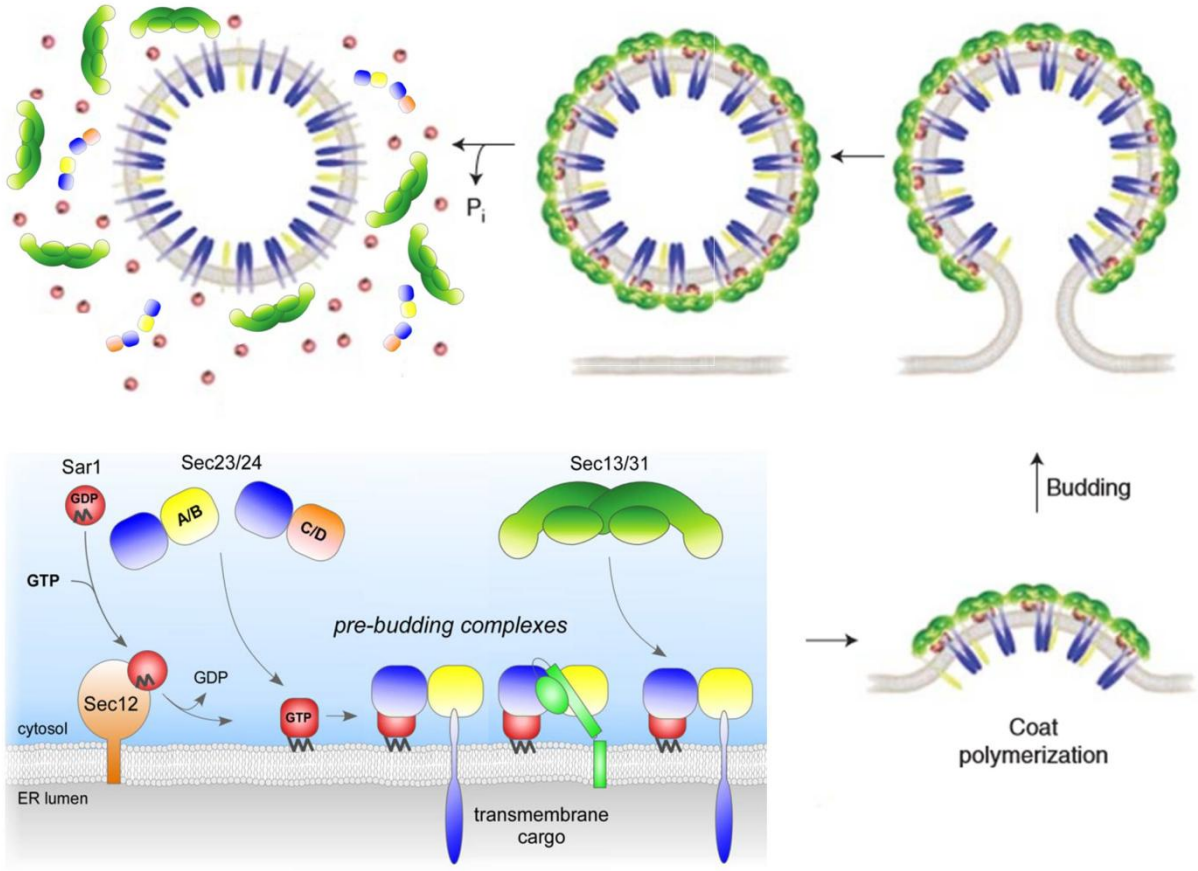

Figure 1.2 COPII Vesicle Biogenesis

At the ER membrane, Sar1 is brought into an active, membrane-bound state by nucleotide exchange to GTP facilitated by Sec12. It in turn recruits the inner COPII coat, various heterodimeric Sec23/Sec24 complexes which together with transmembrane proteins form a pre-budding complex. The outer scaffolds, heterotetrameric Sec13/Sec31 complexes, join the pre-budding complex and polymerize to form a bud that will eventually undergo scission. Hydrolysis of GTP bound to Sar1 is stimulated by its built-in GAP, Sec23, will release the coat and allow fusion of the vesicle with its target membrane. For details and literature please refer to the main text. Images were taken and modified from Adolf et al. (2016) and Popoff et al. (2011a).

1.2.2 COPII vesicles: Cargo sorting

After the finding that COPII vesicles are responsible for the ER-exit of secreted proteins, it was discovered that certain components of the COPII coat modulate the content of these carriers (Aridor et al., 1998; Kuehn et al., 1998; Kuehn et al., 1996). This led to the discovery of the first COPII sorting motif present in the C-terminal cytoplasmic tail of the vesicular stomatitis virus glycoprotein (VSV-G) (Nishimura and Balch, 1997) which is required to concentrate the protein at sites of COPII formation (Nishimura et al., 1999). The VSV-G sorting motif – DxE - is extremely short and its main feature is two acidic residues. Motifs following the same consensus (i.e. DxD/ExE/ExD) have been identified subsequently in non-viral endogenous protein Sys1p/Gap1p in yeast (Malkus et al., 2002; Votsmeier and Gallwitz, 2001) and Kir1.1/Kir2.1 in mammals (Ma et al., 2001). Later it was shown that the regions flanking diacidic motifs are important for their proper function (Ma et al., 2001; Sevier et al., 2000).

Using pulldown assays, reconstitutions and crystallography, the labs of Jonathan Goldberg and Randy Schekman were able to identify the binding site for these sequences present in the COPII components Sec24p in yeast (Miller et al., 2003; Mossessova et al., 2003). They found that not only the classical DxE of Sys1p but also an LxxLE and an LxxME motif present in Bet1p and Sed5p were bound by Sec24p at this interface, which was further referred to as “B-site” (Mossessova et al., 2003). In the same study, a second Sec24p binding site - the “A-site” – was identified. Via this site, Sec24p interacts with the SNARE Sed5p, through a peptide sequence YNNSNPF present in Sed5p that becomes exposed when the ER-Golgi SNARE complex assembles (Mossessova et al., 2003).

Most recently, it was proposed that another type of binding motif (ΦC motifs) which is characterized by bulky, hydrophobic residues at the very C-terminus of transmembrane proteins also binds to the B-site (Ma et al., 2017). Amongst the proteins that carry such a signal are ERGIC53 (Kappeler et al., 1997), the yeast homologues Emp46p and Emp47p (Sato and Nakano, 2002), as well as Erv41p/Erv46p (Otte and Barlowe, 2002), and members of the yeast p24 family (Dominguez et al., 1998). Similar to observations made for p24 in the COPI system, the oligomeric state of proteins carrying COPII sorting signals, can influence their efficient uptake (Springer et al., 2014).

A third distinct binding site, the “C-site”, binds to a conformational epitope formed by the SNARE Sec22b when it is in the so-called closed conformation (Mancias and Goldberg, 2007). The binding motif can only be recognized by two of the four mammalian Sec24 isoforms (Sec24A/B) (Mancias and Goldberg, 2007). This observation is in line with the fact that not all Sec24 proteins have the same potential to bind and recruit cargo proteins in budding yeast several years earlier. The ER-Golgi

SNARE proteins Bet1p, Bos1p, and Sec22p are recruited into COPII vesicles by Sec24p and bind to the coat subunit directly while no such interactions could be observed for its homologue Lst1p (Miller et al., 2002). After the initial findings that the subclasses of Sec24 in yeast and mammals can influence the content of COPII vesicles, more and more isoform specific clients were identified. They are discussed in the following section.

1.2.3 COPII vesicles: Coat Protein Isoforms

As mentioned in the previous section, several isoforms of Sec24 with distinct functions exist in simple eukaryotes such as yeast. This repertoire of isoforms increases vastly when moving to higher organisms. In mammals, various isoforms of four of the five cytosolic proteins essential for COPII vesicle biogenesis have been identified. Sec24, the main cargo sorting subunit has four isoforms (Sec24A-D), Sar1, Sec13, and Sec31 have two isoforms (A/B), each. The Sec24 isoforms, which can be divided into the two subclasses Sec24A/B and Sec24C/D, came to the center of attention roughly ten years ago, when Mancias and Goldberg investigated the binding of ER-Golgi SNARE proteins so the COPII coat. They concluded that the two SNAREs Syntaxin5 (Sed5p in yeast) and GS27 (Bos1p in yeast) bind exclusively to Sec24C/D via an IxM peptide motif (Mancias and Goldberg, 2008). Sec22b and Bet1, the further SNAREs of the complex, were identified as interactors of Sec24A/B via the aforementioned conformational epitope in Sec22b and an YxxCE motif present in Bet1, respectively (Mancias and Goldberg, 2007, 2008). Most recently our lab could show that Bet1 does not bind to Sec24A but to Sec24C/D (Adolf et al., 2016). Moreover, we did not observe any direct binding of either Bet1 or GS27 to Sec24C which together with other experimental data led us to the conclusion that their recruitment into COPII vesicles is facilitated through binding to Syntaxin5 (Adolf et al., 2016).

Isoforms specific cargo sorting by Sec24 has even since become a major interest in the COPII field. Several proteins which are destined to reach the plasma membrane were identified as specific interactors of Sec24A (e.g. PCSK9, γ-Secretase), Sec24B (Vangl2), Sec24C (SERT1, AE1, Claudin-1), or Sec24D (GAT1, NET1, DAT) (Chen et al., 2013; Farhan et al., 2007; Kim et al., 2007; Merte et al., 2010; Otsu et al., 2013; Sucic et al., 2011; Yin et al., 2017). This led to the identification of novel, isoform specific targeting motifs such as the ΦxΦxΦ motif (Φ=bulky, hydrophobic amino acid) or a very short R[I/L] motif (Otsu et al., 2013; Sucic et al., 2013). As briefly pointed out before, not all proteins, e.g. the ER-Golgi SNAREs discriminate between individual isoforms. Most proteins rely on one of the two Sec24 classes in order to be correctly transported. For example, ER export of members of the p24

family and CD59 was shown to rely on Sec24C/D (Bonnon et al., 2010). The observation that p24 proteins are transported by Sec24C/D was recently challenged by a crystallographic study from the Goldberg lab in which they found the cytoplasmic tail of p24 bound to the B-site in Sec24A (Ma et al., 2017). Unpublished data from out lab does not support this finding as we could consistently observe elevated levels of p24 packing in *in vitro* reconstitution experiments only for Sec24C/D.

Since Sec24 is the designated cargo-binding subunit of the COPII coat, much effort concentrated on investigating the role of its isoforms. However, as pointed out at the beginning of this section, also other COPII subunits exist as two distinct isoforms. Until today, however, little is known about their function. Mutations in the genes encoding either Sec23A or Sec23B have been linked to the development of different syndromes. While mutations in Sec23A lead to Cranio-lenticulo-sutural dysplasia (CLSD), Sec23B deficiency could be liked to Congenital Dyserythropoietic Anemia Type II (Bianchi et al., 2009; Boyadjiev et al., 2006). Despite the fact that the development of either syndrome is probably mainly due to the varying expression levels of the two Sec23 isoforms in different tissues, their discovery pointed at possibly diverging roles of the Sar1 isoforms (Fromme et al., 2008; Fromme et al., 2007). Sec23A with an F to L conversion in position 382 which caused CLSD was potent in packing ERGIC53 into COPII vesicles together with Sar1A. However, packing of the same cargo was completely abrogated in combination with Sar1B (Fromme et al., 2007). Although this observation could well be an artifact, the secretion of other large cargo molecules has been linked specifically to Sar1B (Fryer et al., 2014; Jones et al., 2003). In summary, isoforms of Sec23 and Sar1 are poorly understood and virtually no distinct functions have been assigned to the isoforms of Sec31.

1.3 COPI: Transport System of the Golgi Apparatus

Scientists in the Rothman lab in collaboration with Lelio Orci identified a new type of vesicles budding from the Golgi apparatus during the eighties of the last century (Malhotra et al., 1989). The new carriers were named COat Protein complex I (COPI) vesicles. It has early been shown that these carriers play a pivotal role in retrieving escaped ER-residents (Cosson and Letourneur, 1994; Letourneur et al., 1994). A role of COPI vesicles in intra-Golgi transport has ever since their discovery been heavy debated (reviewed by Glick and Luini, 2011; Glick and Nakano, 2009).

In the following section I briefly review the work that has been done to elucidate the fundamental mechanisms that underlie the formation of these carriers.

1.3.1 COPI Vesicles: Biogenesis

It is a common motif of vesicles biogenesis that it starts with the activation of a small GTPase. In case of COPI these GTPases belong to the ADP-ribosylation factor (Arf) family. Nucleotide exchange in Arf can be performed by multiple GEFs (reviewed in Casanova, 2007; Gillingham and Munro, 2007). Associated with COPI trafficking is the Golgi-associated brefeldin A-resistant GEF 1 (GBF1) (Claude et al., 1999; Kawamoto et al., 2002; Zhao et al., 2002).

Despite the fact that several Arf family members have the ability to form COPI vesicles (Liang and Kornfeld, 1997; Popoff et al., 2011b; Volpicelli-Daley et al., 2005), Arf1 was the first COPI-forming GTPase to be identified and is believed to be the most involved Arf isoform (Serafini et al., 1991). Recruitment of Arf1 to the Golgi membrane is supported by transmembrane proteins of the early secretory pathway. The first protein implicated in this context was p23, which was shown to interact directly with Arf1 (Gommel et al., 2001; Majoul et al., 2001). *In vitro* binding experiments showed that this interaction is dependent on the oligomeric state of p23, and the nucleotide-state of Arf1. In order to be recruited, Arf1 needs to be in a GDP-bound state and p23 has to form oligomers (Gommel et al., 2001). The second protein implicated in Arf1 recruitment by means of binding and co-localization experiments was the ER-Golgi SNARE protein GS27 (Honda et al., 2005).

Once recruited to the Golgi membrane and after GBF1 has stimulated nucleotide exchange, Arf1 undergoes a significant structural rearrangement. The N-terminal amphipathic α-helix modified with a myristoyl group at its very end becomes exposed and concomitantly inserts into the lipid bilayer (Antonny et al., 1997; Franco et al., 1995, 1996). Thus anchored Arf1 recruits the outer COPI coat coatomer *en bloc* (Donaldson et al., 1992; Hara-Kuge et al., 1994). Coatomer (CM) is a 550 kDa heptameric complex that consists of the seven subunits α-, β'-, β-, γ-, δ-, ε-, and ζ-COP (Waters et al., 1991). Four of the seven subunits have been implicated in binding directly to Arf: β-, γ-, δ-, β'-COP (Sun et al., 2007; Zhao et al., 1997; Zhao et al., 1999). Structural studies of the COPI coat assembled on the membrane could confirm the direct interaction of three of these subunits, while the interaction of Arf1 with β'-COP was not directly observed (Dodonova et al., 2017; Dodonova et al., 2015).

While Arf1 and coatomer constituted the minimal cytosolic machinery to form COPI vesicles (Bremser et al., 1999; Sohn et al., 1996; Spang et al., 1998), cytoplasmic tails exposed by transmembrane proteins of the Golgi have been identified as having a distinguished role in this process (discussed in more detail below). Especially proteins of the p24/TMED family, p23 and p24, which as dimers bind to the γ-COP subunit, were shown to affect the overall structure of the complex

(Langer et al., 2008; Reinhard et al., 1999). These rearrangements that can be observed in solution are believed to be the equivalent of coat polymerization on a membrane.

Like for COPII vesicles, scission of COPI vesicles can occur even when GTP hydrolysis in Arf1 is blocked (Adolf et al., 2013; Malhotra et al., 1989). Concerning the driver of COPI vesicle scission there are different views. The brefeldin A ADP-ribosylated substrate (BARS) protein and the lipid phosphatic acid (PA) have been implicated in COPI vesicle fission (Yang et al., 2008; Yang et al., 2005). However, as both, BARS and PA were not determined as critical components in a minimal system (Bremser et al., 1999; Spang et al., 1998); their action is most likely restricted to a supportive role. Noteworthy, GTP-loaded Arf1, like Sar1-GTP, displays a strong membrane surface activity and can form tubules from synthetic liposomes by itself (Beck et al., 2008; Krauss et al., 2008). Together with the observation that a dimerization-deficient mutant of Arf1 fails to produce free vesicles, a pivotal role of the small GTPase in vesicle scission has been forwarded (Beck et al., 2011b).

Uncoating of COPI vesicles depends on the hydrolysis of GTP in Arf that is stimulated by members of the ArfGAP family (Reinhard et al., 2003; Tanigawa et al., 1993). Unpublished data from our lab suggests that ArfGAPs in addition to promoting GTP hydrolysis furthermore drive the disassembly of the COPI coat (Ganeva et al., unpublished data).

An extensive review on COPI biogenesis can be found elsewhere (Popoff et al., 2011a).

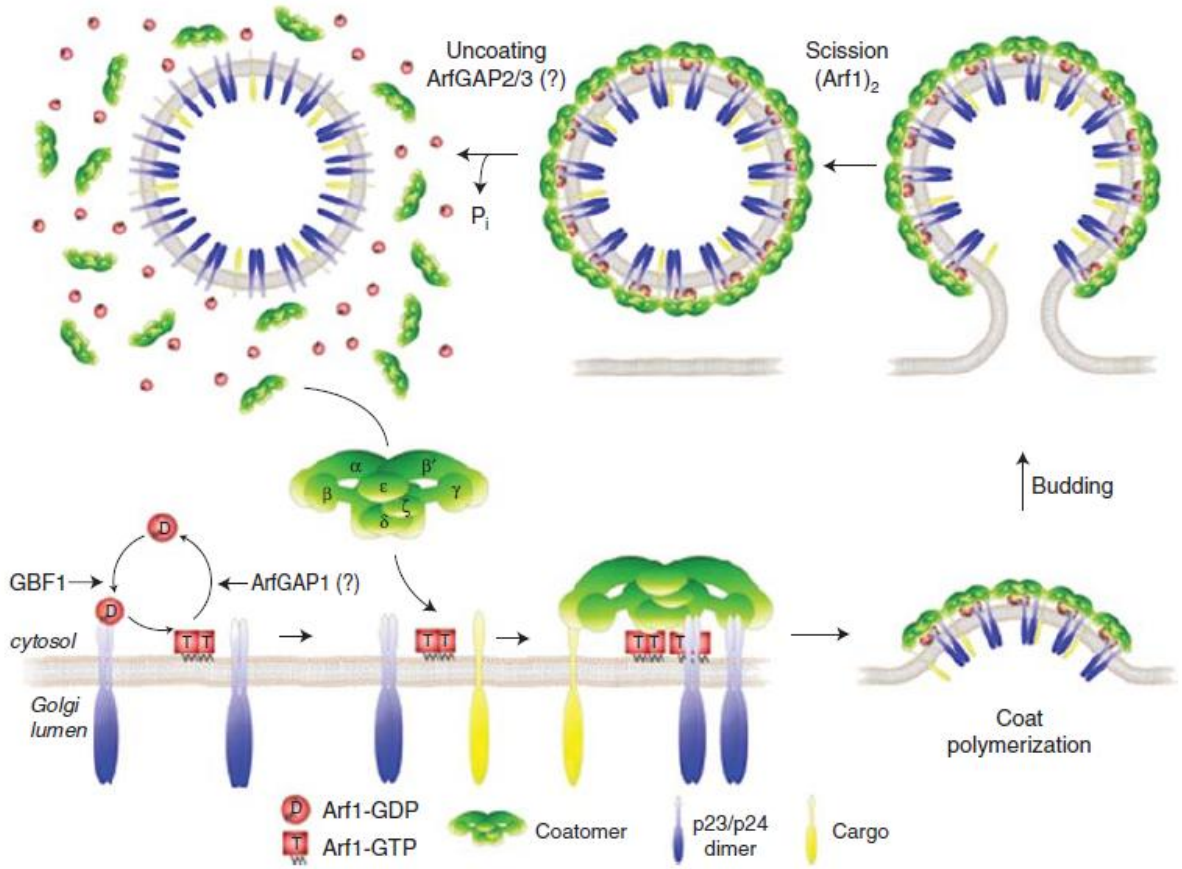

Figure 1.3 COPI Vesicles Biogenesis

Arf1 is recruited to the Golgi membrane through interaction with p23/p24 and activated by its GEF GBF1. ArfGAP1 potentially stimulates GTP hydrolysis at this stage to concentrate cargo. Coatomer is recruited by Arf1-GTP and binds to cytoplasmic tails of various transmembrane proteins. As the local concentration of coat protein rises, they will start to polymerize and form a bud. Vesicle scission is promoted by the small GTPase Arf in its dimeric form. Uncoating of COPI vesicles requires the hydrolysis of GTP stimulated by ArfGAPs. The model was taken from Popoff et al. (2011a). For more detailed information on COPI biogenesis and the accompanying literature please refer to the main text.

1.3.2 COPI Vesicles: Cargo Sorting

In order to make vesicle formation a productive process, it is not only required to correctly assemble the coat but to furthermore concentrate the right proteins at the site of vesicle budding. In the COPI system, selection of the right cargo molecules is driven by direct interactions of five of the seven subunits with short peptide motifs. The initially identified COPI binding motifs are characterized by the presence of two lysine residues at the very C-terminus of the short cytoplasmic tails of transmembrane proteins (Nilsson et al., 1989; Pääbo et al., 1987). These lysine residues can be either directly following one another (KKxx motif) or be separated by one amino acid (KxKxx motif) (Cosson and Letourneur, 1994; Jackson et al., 1990; Schröder-Köhne et al., 1998). Dilysine motifs are recognized be the two large coatomer subunits α-COP and β`-subunit. Both subunits show a

preference for either the KKxx motif (α-COP) or the KxKxx motif (β`-COP) (Eugster et al., 2004; Schröder-Köhne et al., 1998; Schröder et al., 1995) which they recognized with a high specificity via their most N-terminal WD-repeat domains (Jackson et al., 2012). The two best characterized proteins with dilysine motifs are Wbp1 in yeast and ERGIC53 in mammals (Gaynor et al., 1994; Schindler et al., 1993).

Another retrieval motif is characterized by the presence of basic arginine residues (Schutze et al., 1994). The positioning of the residues within the protein is not as strict as for the lysine-based motifs (Michelsen et al., 2005). In contrast to KK-based motifs, binding of arginine-based motifs is mediated by the coatomer subuits β-COP and δ-COP via a binding site that is believed to be homologues to the region in AP complexes that recognize YxxΦ motifs (Michelsen et al., 2007). Functionally, RR motifs serve the same purpose as lysine-based motifs, namely the retrieval of proteins back to the ER. This however often serves the greater purpose to allow for the correct assembly of multimeric complexes at the level of the ER before they are ultimately exported as one functional unit (Brock et al., 2005; O'Kelly et al., 2002; Zerangue et al., 1999).

As mentioned in the beginning, five subunits of coatomer are directly involved in binding to transmembrane proteins. The fifth, so far not mentioned subunit is γ-COP. It has been shown to bind to members of the p24 family (Fiedler et al., 1996; Sohn et al., 1996). The motifs found in these proteins are bipartite. They contain in addition to a basic signature, two pivotal phenylalanine residues (Harter and Wieland, 1998). Moreover, the FFxxBBx_n motif (B=basic amino acid; n≥2) binds to γ-COP only after dimerization hinting at a possible mechanism for the circulation of p24 proteins in the early secretory pathway (Béthune et al., 2006; Harter and Wieland, 1998).

Although heavily studied, the roles that p24 proteins fulfill in the context of COPI trafficking is still not fully understood. While a crucial role during the formation of the vesicles itself has been established earlier (Bremser et al., 1999; Sohn et al., 1996), more recent studies suggest that some p24 proteins are actively involved in the retrieval of (HDEL)/KDEL-bearing ER-residents (Pastor-Cantizano et al., 2017a; Pastor-Cantizano et al., 2017b).

In order to be retrieved to the ER via COPI, luminal proteins need to be concentrated at sites of vesicle formation despite the inability to directly interact with the COPI coat. Thus, they need to be recognized by receptors which can couple them to the coat proteins. The KDEL-receptor was the first such retrieval factor to be identified in the COPI trafficking system (Munro and Pelham, 1987). It posses seven transmembrane domains connected by short loops and its C-terminal tail is facing towards the cytosol. The recognition of the receptor by coatomer happens via a short peptide stretch in the cytosolic tail which contains in addition to two lysine residues a serine that can be

phosphorylated by PKA (Cabrera et al., 2003). This phosphorylation has been shown to be critical for an interaction with coatomer and ArfGAP1 (Cabrera et al., 2003). Where exactly the KDEL-receptor binds to the COPI coat has not been shown, yet. A recent publication suggested a role for δ-COP in KDEL-receptor sorting (Arakel et al., 2016). Via the luminal portion, the receptor binds to more than 50 proteins which bear a KDEL signal at their very C-Terminus which is recognized by the receptor in the early Golgi cisternae (Lewis and Pelham, 1992; Lewis et al., 1990; Majoul et al., 1998). The retrieval of KDEL-tagged proteins, despite happening indirectly, seems to be even more efficient than the retrieval of KKxx-bearing transmembrane proteins (Stornaiuolo et al., 2003). Release of the cargo from its receptors is likely mediated by the pH-difference between the ER and the Golgi (Wilson et al., 1993) as the Golgi complex has a slightly more acidic pH (~6.4) when compared to the ER (~7.2) (Wu et al., 2000).

Other receptors with a different mode of client recognition are for example RER1 or Vps74/GOLPH3. RER1 is important for retrieval of the Sar1-GEF Sec12 (Boehm et al., 1994; Nishikawa and Nakano, 1993) which it binds via its transmembrane domain and in doing so couples it to the COPI coat via a cytosolic motif (Sato et al., 2001). Vps74/GOLPH3 is a more recently discovered adaptor for glycosyltransferases that need to be properly retained in the Golgi. Unlike KDEL-receptor or RER1, recognition of its clients happens via the cytosolic portion of the protein (Eckert et al., 2014; Schmitz et al., 2008; Tu et al., 2008). Furthermore, the soluble proteins of the ArfGAP family, especially ArfGAP1, have been implicated in cargo sorting (Liu et al., 2005; Rein et al., 2002; Shiba and Randazzo, 2014; Spang et al., 2010). The most recently identified COPI sorting motif is characterized by the C-terminal sequence KxD/E. It was found in members of the nonaspanin protein family and serves the retention of these Golgi-residents (Woo et al., 2015).

It is of note that none of the proteins that has been identified to bear a COPI sorting signal is transported to a destination other than the ER or the Golgi. This implies that uptake of secreted cargo is rather passive as has been proposed earlier (Karrenbauer et al., 1990; Wieland et al., 1987).

1.3.3 COPI vesicles: Coat Protein Isoforms

Coatomer consists of seven subunits (Stenbeck et al., 1993; Waters et al., 1991). Out of these seven subunits, γ-COP and ζ-COP two were found in genetic screen to exist as different isoforms which were termed $\gamma_{1/2}$- and $\zeta_{1/2}$-COP (Blagitko et al., 1999; Futatsumori et al., 2000). They were furthermore shown to localize to the Golgi when expressed as tagged versions (Futatsumori et al., 2000). Our lab shortly after studied the endogenous proteins (Wegmann et al., 2004). It was revealed

that in various mouse tissues, the expression levels of γ-COP and ζ-COP isoforms was very similar. No sample showed a marked expression of either isoform (Wegmann et al., 2004). Furthermore, Wegmann et al. probed the composition of coatomer complexes and found that >95 % of endogenous CM has either of the three combinations $\gamma_1\zeta_1$, $\gamma_2\zeta_1$, and $\gamma_1\zeta_2$. Coatomer containing $\gamma_2\zeta_2$ was not found in significant amounts. Subsequently, a $\gamma_1\zeta_1$:$\gamma_2\zeta_1$:$\gamma_1\zeta_2$ ratio of 2:1:2 was proposed (Wegmann et al., 2004). This ratio was roughly confirmed by a follow-up study which came up with a ratio of approximately 2.5:1:1.5 (Moelleken et al., 2007). Latter study was the first to point towards a putative functional difference between the isoforms of coatomer since a very clear divergence of intracellular distribution could be observed. While CM containing γ_1-COP (any therefore also ζ_2-COP) was predominantly located at the cis-Golgi (>70%), γ_2-COP was found mainly associated with the trans-Golgi (>60%). I*n vitro* reconstitution experiments later showed, that all coatomer isoforms, even $\gamma_2\zeta_2$, are capable of forming COPI vesicles with similar efficacy (Sahlmuller et al., 2011). Until today only one further study by Hamlin et al. provides functional data regarding the isoforms of CM. In this study it was shown that the inactive cytosolic kinase Scyl1 interacts specifically with γ_2-COP and furthermore with class II Arfs (Hamlin et al., 2014).

The second family of cytosolic proteins important for COPI vesicle biogenesis are members of the Arf family. Six different isoforms of Arf have been identified in mammals, and simply termed Arf1-6 (Bobak et al., 1989; Kahn et al., 1991; Lee et al., 1992; Price et al., 1988; Tsuchiya et al., 1991). All Arf isoforms except for Arf2 can be found in humans. Based on their sequence identity they can be grouped into three classes. Arf1, Arf2, and Arf3 constitute class I and are ~96% identical. Arf4 and Arf5 form class II (Kahn et al., 2006). They are ~90% identical to one another and show still a high similarity to class I Arfs (~80% identity). The only Arf in class III is Arf6. It shows still a decent amino acid sequence similarity to all other Arfs (~64-70% identity) (Kahn et al., 2006).

The fact that Arf6 forms a separate class is in line with its unique intracellular localization (Cavenagh et al., 1996; D'Souza-Schorey and Stahl, 1995). The lab of Richard Kahn demonstrated that Arf6 is tightly associated with the plasma membrane and that this association is not controlled by its nucleotide state. In contrast they could observe that all other human Arfs are cytosolic and become bound to the endomembrane system only upon activation with GTPγS (Cavenagh et al., 1996). Its unique localization is likely the reason why Arf6 is, besides Arf1, the most studied Arf family member. It has been implicated amongst other things in events of endocytosis, endosomal sorting, actin remodeling, and cholesterol homeostasis (D'Souza-Schorey and Chavrier, 2006; Donaldson, 2003; Schweitzer et al., 2011). The second, intensely-studied Arf isoform, Arf1, has been identified as the main partner of coatomer for the formation of COPI vesicles (Serafini et al., 1991). It is furthermore involved in the biogenesis of clathrin-coated vesicles (see section 1.4.1). However, also Arf1 has been

shown to function beyond membrane trafficking. Early studies have identified Arf1 (and other Arf family members) as a regulator of lipid metabolism by activating e.g. phospholipase D or stimulating PIP_2 biosynthesis (Brown et al., 1993; Cockcroft et al., 1994; Godi et al., 1999). Arf3, Arf4, and Arf5 have been subject of much less investigation. A knockdown study by the Kahn lab showed that each Arf isoform is dispensable. Only when knocked down pairwise were they able to observe effects on protein trafficking and localization as well as organelle integrity (Volpicelli-Daley et al., 2005). The partial redundancy is in line with the fact that Arf3-5, like Arf1, support COPI vesicle biogenesis *in vitro* (Popoff et al., 2011b). Overall our knowledge, especially concerning the functions of class II Arfs is very scarce. Only recently, experimental evidence is gathered which points at distinct molecular roles of these Arfs. Arf4, for example, has been shown to play a specific role in trafficking of Rhodopsin C at late stages of the secretory pathway (Deretic et al., 2005). Additionally, recent studies showed that Arf4/5 in the early secretory pathway behave differently from Arf1. Both Arfs stayed associated with the ERGIC even in their GDP state (Chun et al., 2008; Duijsings et al., 2009). Overall, the mounting biochemical and cell biological data suggests that the Arf family of proteins is not nearly understood. Very comprehensive reviews covering the topic can be found elsewhere (Casanova, 2007; D'Souza-Schorey and Chavrier, 2006; Kahn et al., 2005).

1.4 Clathrin-coated Vesicles (CCVs): Post-Golgi traffic

The first class of vesicles identified were clathrin-coated vesicles (CCVs), during the advent of EM (Kanaseki and Kadota, 1969; Roth and Porter, 1964). Over the course of the last forty years it became clear that CCVs are by far the most diverse group of vesicles, which share common principles and the outer scaffold clathrin. A great review on the topic can be found elsewhere (Robinson, 2015), here I try to briefly outline the important aspects of CCV trafficking including other post-Golgi vesicle types which do not necessarily use clathrin as a scaffold.

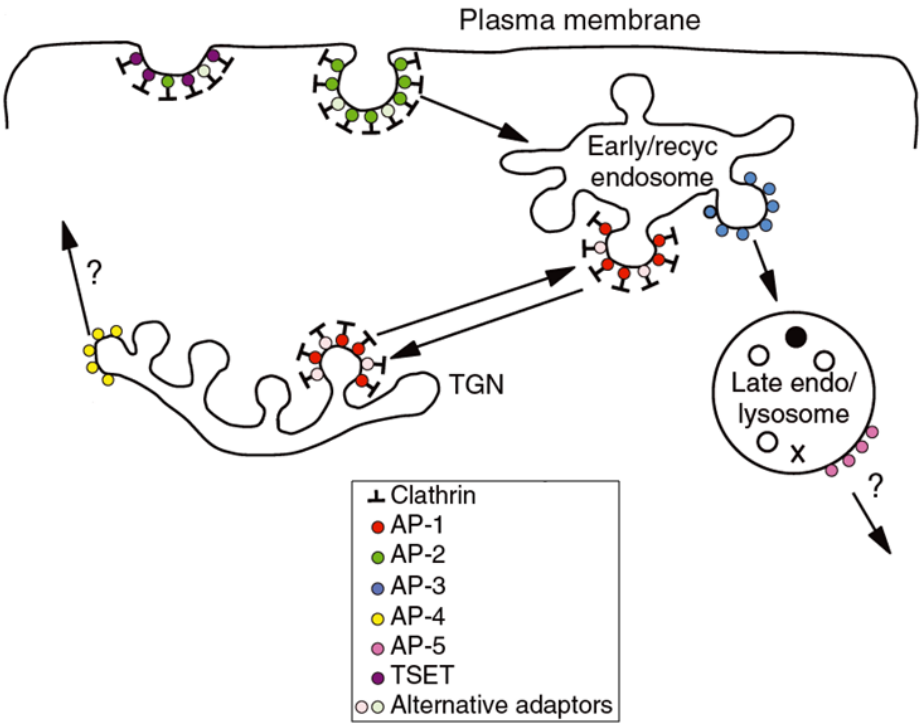

Figure 1.4 Post-Golgi Vesicular Transport

Vesicular transport between post-Golgi stack compartments is largely facilitated by CCVs in concert with adaptor protein complexes AP-1 (TGN-endosomes), AP-2 (endocytosis), and possibly AP-3 (endosomes-lysosomes). AP-4 and AP-5 are clathrin-independent adaptors acting at the TGN and late endosomes/lysosomes, respectively. The AP complexes often work in concert with alternative adaptors such as γ-adaptin ear-containing Arf-binding proteins (GGAs) and epsins at various sites. The most recently discovered endocytic adaptor complex TSET is not found in animals (Hirst et al., 2014). The image was taken from Robinson (2015) and modified.

1.4.1 CCVs: Biogenesis

Shortly after CCVs had been acknowledged as recurring structures in cells of higher organisms, Barbara Pearse purified the key protein for their formation by accident and called it “clathrin” (Pearse, 1976). At the same time, Goldstein and Brown working on uptake of LDL showed that in this process, (clathrin)-coated pits (CCPs) play a fundamental role (Anderson et al., 1977). With this the first functional data for CCVs was being provided.

Insight into the molecular structure of CCVs came from studies which showed that clathrin is not a single protein but a complex composed of three light and three heavy chains (Ungewickell and Branton, 1981) and that the formation of clathrin cages is assisted by “assembly peptides (APs)” (Keen et al., 1979; Zaremba and Keen, 1983). Nowadays, AP is usually translated as adaptor protein (complex), for they not only assemble clathrin but also bind cargo and machinery. AP-1 and AP-2 were the first APs discovered almost simultaneously. They serve trafficking in the TGN/endosomal

system (AP-1) and endocytosis at the plasma membrane (AP-2) (Pearse and Robinson, 1984; Unanue et al., 1981). APs are tetrameric complexes that consist of two large subunits, a medium sized and a small subunit (Owen et al., 2004). Until to date, three additional tetrameric adaptor protein complexes were identified and termed AP-3, AP-4, and AP-5 (Dell'Angelica et al., 1999a; Dell'Angelica et al., 1997; Hirst et al., 2011). In addition there are many other proteins which function as adaptors for clathrin and cargo but are not part of the AP family. Monomeric adaptors belonging into this group are for example AP180/CALM (Morris et al., 1993; Murphy et al., 1991), γ-adaptin ear-containing Arf-binding proteins 1-3 (GGA1-3) (Boman et al., 2000; Dell'Angelica et al., 2000; Puertollano et al., 2001b) and epsin1-3 (Chen et al., 1998; Drake et al., 2000).

The fact that AP-3/4/5 were identified relatively long after the initial discovery of AP-1 and AP-2 can be partially explained by the circumstance that they act completely or partially clathrin-independent. Adaptor protein complex 3 despite having a discrete binding site to clathrin (Dell'Angelica et al., 1997) shows only partial co-localization with the scaffold (Kural et al., 2012; Peden et al., 2004). AP-4 and AP-5 function as adaptors independent of clathrin (Dell'Angelica et al., 1999a; Hirst et al., 2011; Hirst et al., 1999) and seem to use other layers of outer scaffold like SPG11 and SPG15 in case of AP-5 (Hirst et al., 2013).

Membrane recruitment of most of the APs (AP-1/3/4) and all GGAs have in common that it is triggered by a small GTPase of the Arf family (Boehm et al., 2001; Boman et al., 2000; Ooi et al., 1998; Puertollano et al., 2001b; Stamnes and Rothman, 1993; Traub et al., 1993). Alternatively, binding to the lipid Phosphatidylinositol-4,5-bisphosphate (PIP_2), like in the case of AP-2, can substitute for priming of the vesicle formation site by a small GTPase (Gaidarov et al., 1996; Ohno et al., 1995). Noteworthy, Arf6 has been shown to play an indirect role in AP-2 recruitment by binding to the PIP_2-producing kinase (Krauss et al., 2003).

Recruitment to the respective membrane by either Arf or PIP_2 leads to a structural change within AP-1/2 which is referred to as transition from the “locked” to the “unlocked/open” conformation. The open conformation reveals binding sites for both clathrin and cargo (Collins et al., 2002; Heldwein et al., 2004; Jackson et al., 2010; Ren et al., 2013). Clathrin then is recruited from the cytosol and forms a lattice on its adaptors. A recent study suggests that clathrin – at least on the plasma membrane – first builds a flat lattice which then, possibly with the aid of other factors, forms into a CCP (Avinoam et al., 2015).

Similar to their recruitment, also the scission of endocytic CCVs seems to be distinct from that of other late secretory vesicles. A pivotal role in this process is played by the large GTPase dynamin which is the key factor for scission (reviewed by Ferguson and De Camilli, 2012). The exact

mechanism of vesicle scission for all other CCVs is not clear, however, dynamin seems not to be involved (Kural et al., 2012). Possibly, the small GTPase of the Arf family which functions in adaptor recruitment plays a similar role in scission as has been forwarded in the COPI system.

The final step of vesicle biogenesis, shedding of the coat, is a chaperone-assisted process in the CCV system. The clathrin lattice is actively disassembled by an Hsp70/Hsp40 pair, Hsc70 and auxilin (Ungewickell et al., 1995). Uncoating of the inner layer involves again ArfGAPs in case of the Arf-dependent adaptors (reviewed in Randazzo and Hirsch, 2004) and likely other factors in the case of AP-2 CCVs (Semerdjieva et al., 2008)

1.4.2 CCVs: Cargo Sorting

Sorting of proteins by adaptors in the late secretory pathway is mainly driven by two types of signals. The first motif is characterized by the presence of tyrosine. A mutation that led to conversion of the C-terminal tyrosine in the low density lipoprotein receptor (LDLr) was spotted as the cause of familial hypercholesterolemia (Davis et al., 1986). In the same study it was observed that the LDLr was no longer concentrated at sites of CCV formation at the plasma membrane when the NPxY motif was changed to NPxC. The same motif was subsequently identified in ten additional proteins (Chen et al., 1990). It was shown that this particular trafficking signal is used only to mediate internalization at the plasma membrane, while more common, related YxxΦ motifs (Φ=bulky, hydrophobic amino acid) are used in virtually all steps of the late secretory pathway (Aguilar et al., 2001; Ohno et al., 1998). The YxxΦ motif was first identified as the signal for internalization of the mannose-6-phosphate/insulin-like growth factor 2 receptor (Canfield et al., 1991; Jadot et al., 1992). The role of the YxxΦ motif in mediating protein trafficking between other organelles of the post-Golgi compartments was established shortly thereafter (Hunziker et al., 1991; Matter and Mellman, 1994). The promiscuity of this signal is reflected by the fact that it is bound by multiple AP complexes via their µ-subunit (Aguilar et al., 2001; Boll et al., 2002; Ohno et al., 1998). This binding occurs via a site that is distinct from the binding site used by NPxY-bearing receptors in order to get internalized (Ohno et al., 1998).

Besides the NPxY/YxxΦ motifs, a third common targeting signal that contains critical (iso-)leucine residues has been identified first in CD3-γ chain (Letourneur and Klausner, 1992). Because the (usually two) leucines, which are important for the function of the signal are positioned close to glutamate or aspartate residues the motif is often called “acidic dileucine motifs”. The DKQTLL sequence found in CD3-γ chain was the first of the D/ExxxL/[LI] family. This signature drives transportation of a large number of proteins between virtually all organelles of the late secretory

pathway (Bonifacino and Traub, 2003; Chen et al., 1997; Johnson and Kornfeld, 1992). It interacts simultaneously with two subunits of various AP-complexes. One of the two subunits is always the σ-subunit; the second subunit is one of the two large subunits of the respective AP-complexes (Chaudhuri et al., 2007; Doray et al., 2007; Mattera et al., 2011).

The second sub-family of acidic dileucine motifs follows the consensus DxxLL. They are recognized by GGAs via their VHS domain and hence only involved in trafficking between the TGN and endosomes (Misra et al., 2002; Nielsen et al., 2001; Puertollano et al., 2001a; Shiba et al., 2002). Interestingly, while all the sorting motifs so far described in the COPI/COPII system are located within the cytoplasmic regions of transmembrane proteins, acidic dileucine motifs were also identified in soluble proteins e.g. HIV-Nef which down regulates CD4 (Greenberg et al., 1998). Furthermore, the attachment of the soluble ubiquitin to a transmembrane protein can function as a transport signal (reviewed in Piper and Luzio, 2007).

Despite the fact that the number of proteins carrying one of the classical post-Golgi sorting motifs is very large when compared to the COPI/COPII system (Bonifacino and Traub, 2003), they still do not account for all the trafficking events. A very impressive study in this concern was carried out by the Robinson lab in which they screen for endocytic motifs and found that their hits would usually not follow any consensus sequence (Kozik et al., 2010). This points out at a possibly much larger number of signals which have thus far not been assigned.

1.4.3 CCVs: Coat Protein Isoforms

Since the number of coat proteins that do function in post-Golgi transport is greater than the number of coat subunits found in the COPI or COPII system it is not surprising that CCV coat proteins account for the largest number of isoforms in vesicular transport. Apart from the isoforms of Arf, which were already discussed in paragraph 1.3.3, several subunits of the AP complexes have different isoforms. While the four proteins which form the latest discovered clathrin-independent heptameric AP-4 and AP-5 complexes have no isoforms, AP-2 possess one subunit with two isoforms: AP-2$\alpha_{1/2}$. The AP-1 complex has two subunits, AP-1$\mu_{1/2}$/σ_{1-3}, which exist as isoforms, AP-3 even harbors three isotypic subunits, AP-3$\mu_{1/2}$/$\sigma_{1/2}$/$\beta_{1/2}$. Hence, in the AP system alone 6 proteins exist that have different isoforms. The number of isotypic proteins expands, however vastly, when other adaptors are taken into account e.g. Epsin1-3, GGA1-3 (Dell'Angelica et al., 2000).

Evidence for a specific function of some isoforms came from the observation that in cells lacking the polarized cell specific AP-1μ_2 subunit, baso-lateral sorting was disturbed. It could be re-established once the protein was restored (Folsch et al., 1999; Ohno et al., 1999). The AP1-μ_2-containing AP complex was further called AP-1B because it became clear that its function in polarized cells is very distinct from the AP-1A complex containing isoform 1 of AP1-μ (Folsch et al., 2003; Guo et al., 2013). For example does AP-1B but not AP1-A interact with Arf6 (Shteyn et al., 2011).

At around the same time, different isoforms of the AP-3 complex were discovered (Dell'Angelica et al., 1997; Pevsner et al., 1994; Simpson et al., 1996). Like for AP-1, there is one variant which is cell type specific, and one that is ubiquitously expressed. The AP-3B (with AP-3μ_2/β_2) is exclusively expressed in neurons, AP-3A (with AP-3μ_1/β_1) in all tissues (Hirst and Robinson, 1998; Le Borgne and Hoflack, 1998; Robinson and Bonifacino, 2001). The neuronal specific variant has been implicated in the formation of synaptic vesicles from endosomes (Blumstein et al., 2001; Faundez et al., 1998) while AP-3A seems to be involved in transport from the TGN/endosomes to lysosomes (Nakatsu and Ohno, 2003).

Evidence is emerging which indicates that like in the COPII system, isoforms of the various coat subunits participate in specific sorting events. For example AP-1σ_1 is thought to be involved in the trafficking of sortilin (Baltes et al., 2014) and GGA1 in transport of adiponectin (Xie et al., 2006). In general it can be said that these sorting events appear to be more cell-type specific in contrast to isoform-specific packing performed by Sec24 proteins which applies to ubiquitously expressed SNARE proteins (Adolf et al., 2016; Mancias and Goldberg, 2008). More concise information about this topic can be found elsewhere (Bonifacino and Traub, 2003; Nakatsu and Ohno, 2003; Paczkowski et al., 2015; Robinson, 2015).

1.5 Mass Spectrometry (MS)

Mass spectrometry is a powerful tool in chemistry, pharmacology, as well as biochemistry of proteins and lipids. In analogy to the term “genomics” which describes the study of whole genomes, the term proteomics was coined for investigations that aim at the understanding of proteins at a global scale. In the following, basic principles and techniques used in modern proteomics are outlined. For further, more intensive review on this topic, the following articles are well suited (Aebersold and Mann, 2016; Bantscheff et al., 2012; Glish and Vachet, 2003).

1.5.1 Basic principles of MS and Proteomics

Modern mass spectrometry allows for the simultaneous analysis of highly complex biological samples containing thousands of proteins. This discipline, called proteomics, was made possible by two important advancements. The first critical progress was the invention of ionization methods applicable to large, instable analytes such as proteins. Those were electrospray ionization (ESI) developed by John Fenn and, simultaneously, matrix-assisted laser desorption/ionization (MALDI) introduced by Koichi Tanaka (Fenn et al., 1989; Karas and Hillenkamp, 1988). Until then, the analysis of substances by mass spectrometry was limited to small, heat-resistant molecules due to the high energy used for ionization (e.g. electron ionization, EI). The second major breakthrough for proteomics was the progress made in the field of DNA sequencing. Approximately two decades ago, it became possible to sequence whole genomes (Goffeau et al., 1996). This was prerequisite for modern proteomics as it was now possible to develop databases containing all potentially expressed proteins with which mass spectra could be compared (Mann and Wilm, 1994; Perkins et al., 1999).

In a typical modern MS experiment, proteins are separated according to their molecular mass by one- or two-dimensional SDS-PAGE with the second dimension being a focusing of proteins corresponding to their isoelectric point (Laemmli, 1970; O'Farrell, 1975). The gel can then be stained with Coomassie or silver to visualize the proteins. Bands or spots of interest are excised, in-gel digested with a sequence-specific protease, typically trypsin, and subjected to liquid chromatography (LC) (Shevchenko et al., 2006; Shevchenko et al., 1996; Wilm et al., 1996). Following LC, the peptides enter the mass spectrometer where a first MS scan is performed. Subsequently, (potentially pre-selected) precursor ions are fragmented by collision and subjected to a second round of MS scanning (tandem MS). The resulting product ions are detected and their spectra interpreted. In this regard, interpretation means they are usually compared to *in silico* generated databases containing the possible peptide fragments of all proteins which can occur during such an experiment. In doing so it is possible to determine the protein composition of a sample with high accuracy (the experimental setup is explained in more detail in Han et al., 2008 and Karpievitch et al., 2010).

One of the major challenges of protein MS has been to directly compare two or more biological samples with one another. To overcome this problem, mainly two strategies have emerged: protein/peptide labeling of samples and metabolic labeling of studied organisms. The first protein labeling reagents introduced were so-called isotope-coded affinity tags (ICATs) (Gygi et al., 1999). Here, cysteine residues are labeled with an affinity tag (e.g. biotin) which is coupled to the cysteine-reactive group via an isotope-labeled linker. The initially used deuterium for labeling was replaced by C^{13}- and N^{15}-based labels due to the observation that deuterium can cause differences in retention

time during LC (Yi et al., 2005; Zhang et al., 2001). The most popular sample labeling procedure nowadays is isobaric labeling, notably tandem mass tags (TMTs) and isobaric tags for absolute and relative quantification (iTRAQs) (Ross et al., 2004; Thompson et al., 2003; Wiese et al., 2007). These tags, of which a large variety exits, are coupled to the proteins/peptides like ICATs. When intact, they all have identical masses. Only upon fragmentation during tandem MS, reporter ions are produced which allow for the comparison of their precursor and ultimately the biological samples. Since the number of such tags it high, a large number of samples can be analyzed in parallel.

The labeling strategies outlined above are challenged by an intensive modification of the samples prior to MS analysis. These experiments require a high level of accuracy and efficacy during the labeling procedure in order to be quantitative. The second type of labeling methods, metabolic labeling, overcome this potential bias very elegantly by introducing the labels directly into the proteins and allowing them to be incorporated by the studied biological model. The most prominent method, stable isotope labeling by amino acids in cell culture (SILAC), was described 15 years ago (Ong et al., 2002). Although crude labeling methods such as cultivation with heavy nitrogen (N^{15}) is still in use (reviewed by Gouw et al., 2010), most labeling procedures use amino acids with heavy atoms, most frequently lysine and arginine (Ong and Mann, 2007). SILAC experiments are as the name implies usually done with cultured cells but also whole organisms have been isotope-labeled (Gouw et al., 2010). In contrast to post-sample preparation labels such as TMTs, there is a quite limited number SILAC labels available, restricting the number of samples that can be analyzed in parallel. Furthermore, the method is restricted to experiments where a sufficient labeling of proteins can be achieved by the studied organism/cell. However, if these requirements are met, SILAC is the most direct way to compare protein samples by simply calculating the ratio/enrichment of labeled versus non-labeled peptides from their MS intensities.

Noteworthy, there are ways to quantify proteins without introducing a label (Wong and Cagney, 2010). Such methods, but also all labeling methods, do not provide absolute quantification of samples but rather access the relative abundance of proteins in comparison to another sample. Hence absolute quantification is still one of the major challenges for MS in the upcoming years.

1.5.2 Proteomics as a Tool to Study Organelles and Vesicles

Modern mass spectrometry has advanced to a stage that allows the analysis of whole proteomes of classical model organisms such as yeast (de Godoy et al., 2008) or even the proteomes of more complex samples e.g. total human cell lines (Beck et al., 2011a; Nagaraj et al., 2011). Hence the

analysis of a cellular substructure is easily achievable which opens the possibility to study in detail which proteins belong to a certain organelle and how the protein composition of it changes in response to a certain treatment (Gannon et al., 2011; Yates et al., 2005) .

Isolation of the cellular entity of interest can be achieved in different ways. The most simple way is differential centrifugation including density gradient centrifugation that has been used to isolate and study the proteomes of lysosomes (Bagshaw et al., 2005), mitochondria (Sickmann et al., 2003), or multiple organelles in one study (Dunkley et al., 2004; Foster et al., 2006; Gilchrist et al., 2006; Itzhak et al., 2016). Such isolation strategies have been extended by means of affinity purification. Zhang et al. for example labeled cells with biotin and subsequently performed streptavidin affinity purification in order to obtain a fraction highly enriched in plasma membrane (Zhang et al., 2003). Similarly, the Hauri lab has used an antibody against the KDEL receptor in order to isolate the ER-Golgi intermediate compartment from BFA-treated cells (Breuza et al., 2004). In all studies mentioned above, new proteins could be assigned to the respective organelles. But not only have organelles been subjected to MS analysis after enrichment, also vesicles which facilitate the transport between many of these compartments have been studied. To study them, two principal strategies were applied: Isolation of endogenous vesicles and *in vitro* reconstitution.

The first strategy, isolation of endogenous vesicles, was applied to synaptic vesicles and CCVs (Borner et al., 2006; Takamori et al., 2006). In latter experiments, a CCV-enriched fraction was quantitatively compared to a mock fraction from cells where the heavy chain of the pivotal scaffold clathrin was knocked down (Borner et al., 2006). This clever setup has been improved by adaption of fast protein rerouting to mitochondria (“knocksideways”) (Robinson et al., 2010). It was used to mislocalize certain clathrin adaptor proteins. Subsequently, a CCV fraction from these knocksideways cells was prepared and compared to a non-treated control. Whatever proteins are no longer found in the CCV fraction from knocksideways cells are potential interactors of the depleted adaptor (Hirst et al., 2012).

The second approach, *in vitro* reconstitution, has been used to study COPI and COPII vesicles. COPI vesicles were reconstituted from a Golgi-enriched membrane fraction using cytosol and nucleotides (Gilchrist et al., 2006). The more recently published proteomic study of COPII vesicles was performed with yeast microsomes and purified COPII coat components (Margulis et al., 2016). In both cases, quantification was done without any labeling of the samples prior or after vesicle preparation.

In general, proteomic investigation of organelles and vesicles has helped to understand the protein content of these structures and also the flow of material between different cellular compartments. With evolving bioinformatics tools, it is possible to do cellular proteomics using very crude

differential centrifugation as has been demonstrated by the Borner lab (Itzhak et al., 2016). All these developments will round out the intracellular protein landscape. A very comprehensive review on proteomic studies of organelles was written by Yates et al. (2005), the most recent advancement for rapid profiling of cellular organelles can be found in the publication of Itzhak et al. (2016).

1.6 Emerging Role of Coat Proteins in Disease

The first medical afflictions which partially result from protein miss-trafficking were beginning to be understood on a cell biological level during the sixties of the last century (Hashimoto et al., 1965; Hers, 1963). These so-called lysosomal storage disorders (LSDs) represent a broad group of diseases with more than 40 different known syndromes (Vellodi, 2005). One of these syndromes results for example from mutations that cause inactivity of the phosphotransferase that primes lysosomal enzymes for correct targeting by the mannose-6-phosphate (Kornfeld, 1986; Reitman and Kornfeld, 1981; Reitman et al., 1981; Varki et al., 1981). Shorty after this finding, the famous single point mutation that affects the transportation of the LDLr was identified (Davis et al., 1986). Trafficking of the LDL receptor was studied in the first place because its perturbation causes familial hypercholesterolemia (Davis et al., 1986).

The advent of deep sequencing at the turn of the millennium has made it easier to identify such mutations even for rare diseases with only very few patients. Amongst the first mutations identified in this fashion, were a deletion and a non-conservative amino acid conversion affecting the AP-3β_1 subunit of adaptor protein complex 3 (Dell'Angelica et al., 1999b). Those mutations lead to development of the Hermansky-Pudlak syndrome which is characterized by defective lysosomal targeting of proteins ultimately causing albinism and bleeding disorders (Dell'Angelica et al., 1999b; Gahl and Huizing, 1993; Huizing et al., 2002). Ever since then, several mutations in subunits of various AP complex subunits have been implicated in the development of disease. Mutations in AP-1σ_2 were linked to X-linked mental retardation (Cacciagli et al., 2014; Tarpey et al., 2006). Similarly, mutations in the second isoform, AP-1σ_1 cause the severe MEDNIK (mental retardation, enteropathy, deafness, peripheral neuropathy, ichthyosis, and keratodermia) syndrome (Montpetit et al., 2008). Moreover, the two AP complexes AP-4 and AP-5 are tightly linked to hereditary spastic paraplegia (HSP/SPG), a syndrome marked by spasticity of the lower limbs and sometimes mental retardation (reviewed in Fink, 2013, 2014). This connection is so intimate that some of the AP complex subunits were first identified as factors of SPG-development before becoming designated coat components, i.e. SPG11/SPG15 (Hirst et al., 2013; Slabicki et al., 2010).

In recent years, it became clear that not only coat proteins of the late secretory pathway play a role in development of disease, also proteins of the COPI and COPII systems are associated with medical conditions. For example mutations in the small GTPase Sar1B were shown to cause lipid absorption disorders (Jones et al., 2003). Furthermore, mutations within the inner coat subunits Sec23A were associated with Cranio-lenticulo-sutural dysplasia (CLSD) (Boyadjiev et al., 2006; Fromme et al., 2007). The other Sec23 isoform, Sec23B, was shown to play a role in Dyserythropoietic Anemia Type II (Bianchi et al., 2009) and the Cowden syndrome which is characterized by a high risk of epithelial cancer (Yehia et al., 2015). Most recently, mutations within the isoform Sec24D were identified as the cause of syndromic form of *osteogenesis imperfecta* (OI) (Garbes et al., 2015). In the COPI system, mutations of the α-COP subunit could be linked to hereditary autoimmune-mediated lung disease and arthritis (Watkin et al., 2015), while mutations of δ-COP correlated with a craniofacial disorder (Izumi et al., 2016).

Taken together the number of proteins which serve vesicular transport and play a role in the development of various diseases is strongly increasing especially in most recent years.

1.7 Objective

As pointed out in the previous sections, coat proteins and their isoforms can have a major influence on cargo-uptake, and on the directionality of vesicular transport (see 1.2-1.4). These findings are underlined by the fact that mutations within different isoforms of the same coat component can result in completely different medical afflictions (see 1.6). While for many subunits of the COPII and the CCV system data, which assigns them to a certain function, exists, such data is virtually absent for isoforms in the COPI system. Likewise, while the molecular mechanism which leads to the occurrence of a certain syndrome is understood for many of the mutations highlighted in section 1.6, such an explanation is missing for the most recently discovered mutations in Sec24D leading to syndromic *osteogenesis imperfecta* (Garbes et al., 2015). Therefore, in this thesis I worked on the following questions:

- Do isoforms of γ- and ζ-COP influence the steady-state proteome of COPI vesicles?
- Do isoforms of the small GTPase Arf influence the protein content of COPI vesicles?
- What are the shared/diverging proteins in COPI vesicles with different origin?
- What is the molecular mechanism that leads to a syndromic form of *osteogenesis imperfecta* in patients with Sec24D mutations?

2 Results

2.1 Establishing a Workflow for COPI Proteomics

As pointed out in section 1.7, one of the major goals of this study was to investigate the protein content of COPI vesicles prepared with different isoforms of coat proteins. Hence we decided to take advantage of an *in vitro* COPI reconstitution system in which recombinant coat proteins are used to produce vesicles from semi-intact cells (SIC) (Adolf et al., 2013), schematically drawn in figure 2.1. Briefly, the plasma membrane of cells is permeabilized with digitonin and the cytosol removed through washing with a physiological assay buffer. Recombinant coatomer, Arf, and nucleotides are added to the semi-intact cells following an incubation step to allow vesicle formation. Vesicles can be separated from the vast amount of SIC via medium-speed centrifugation (MSP) (Fig. 2.1; Material and Methods).

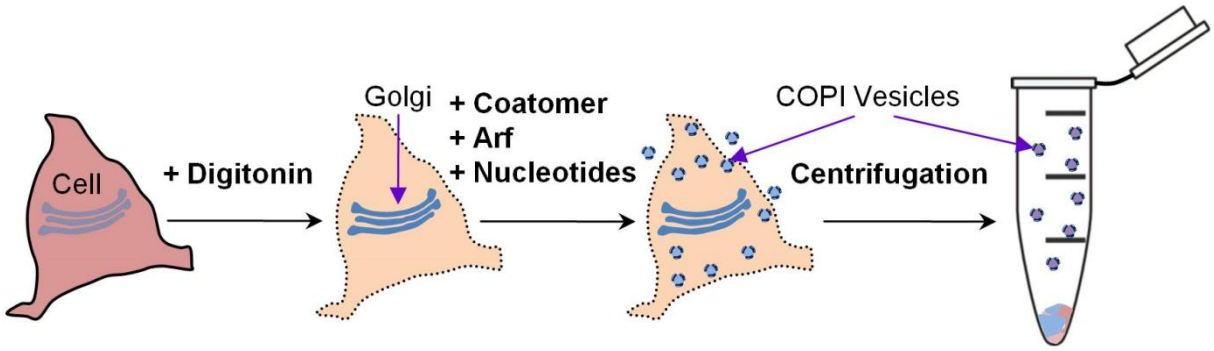

Figure 2.1 COPI Reconstitution from Semi-intact Cells

Cells are permeabilized with digitonin, washed with buffer, and incubated with COPI coat proteins and nucleotides for 30 minutes. Donor membranes can be subsequently separated from the vesicles via medium-speed centrifugation at 14.000 ×g for 10 minutes. For experimental details see Material and Methods.

The vesicle-containing supernatant recovered after MSP contains, besides COPI vesicles, the huge excess of recombinant coat protein used for reconstitution. When performing Western blot analyses it is usually sufficient to subject the supernatant to high-speed centrifugation (HSP) at 100.000 ×g in order to harvest the vesicles (Fig. 2.2). As can be clearly seen, vesicle marker proteins ERGIC53, ERGIC1, and p24 are enriched in the harvested fraction, when all COPI components and nucleotides were present compared to a control reaction without coatomer. In contrast, the non-vesicle marker GM130 is not particularly enriched in the COPI vesicle fraction (Fig 2.2).

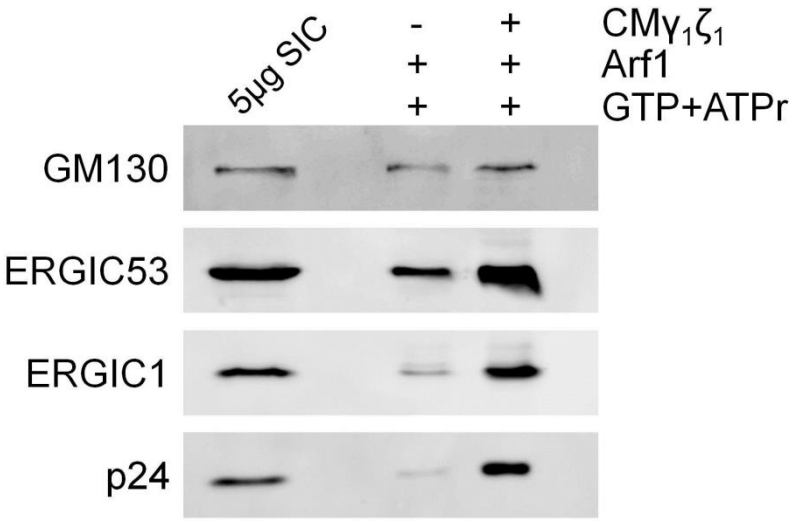

Figure 2.2 Western Blot Analysis of Harvested COPI Vesicles

Representative Western blot analysis of COPI vesicles reconstituted from SIC HeLa using recombinant CM, Arf1, GTP, and ATP regenerating system (ATPr) with 5 µg of SIC loaded as input. Vesicles were isolated via differential centrifugation (MSP and HSP). Indicated on the left are the antibodies used for detection.

Despite the fact that HSPs from vesicle reconstitutions can be analyzed via Western blot, a mass spectrometric analysis of such a sample is not possible. When we tried to directly assess the protein content of such samples, very low quality data was obtained. We attributed this shortcoming to excess coat, which is harvested alongside the vesicles. The majority of peptides, coming from these coat proteins, seemed to hamper the detection of proteins from the vesicle membrane and inside. Thus we decided to purify the reconstituted vesicles by means of density gradient floatation. For this we used the density matrix iodixanol, which had been previously used to purify COPII vesicles (M.Sc. thesis Manuel Rhiel, Adolf et al., unpublished data). Vesicle samples obtained from medium-speed centrifugation were adjusted to a concentration of 40 % iodixanol. The samples were overlaid with a big 30 % and small 20 % layer and the whole gradient centrifuged over night at 250.000 ×g (for details see Material and Methods). Following ultracentrifugation, the gradient, which is schematically depicted in figure 2.3A, was fractionated into ten fractions from top (1) to bottom (10). Each fraction was diluted in assay buffer and subjected to high-speed centrifugation at 100.000 ×g for 2 h in order to harvest vesicles and to some extend free protein. Subsequently, the fractions were analyzed by Western blot and probed for the COPI vesicle marker proteins ERGIC53 and p24 as well as the COPI coat component γ-COP. When either coatomer or nucleotide had been omitted during the budding reaction, faint signals for ERGIC53 and p24 could be detected predominantly in fraction 2, but also fraction 3 (Fig. 2.3B two upper panels). The signal intensities for both proteins increased strongly, when GTP was added to the reaction. Also here, the strongest signals were detected in fraction 2 (Fig. 2.3B second lowest panel). Using a non-hydrolysable GTP analog, GMP-PNP, instead of GTP also

resulted in the detection of strong signals for both COPI marker proteins. However, especially the detection for p24 did not longer give the strongest signal in fraction 2 but rather in fraction 3. Moreover, unlike under all conditions mentioned before, using GMP-PNP lead to the detection of γ-COP in fraction 3 of the gradient (Fig. 2.3B lower panel). Coat detection and the shift of marker proteins from fraction 2 to fraction 3 as observed for the GMP-PNP sample is in line with a higher buoyant density of coated vesicles, compared to uncoated vesicles. It is worth noting that most of the endogenous coatomer was removed from the SIC during the washing step. Hence, the recombinant protein complex, here detected via γ-COP, is in vast excess of the remaining fraction of endogenous proteins (Fig. 2.3B inputs).

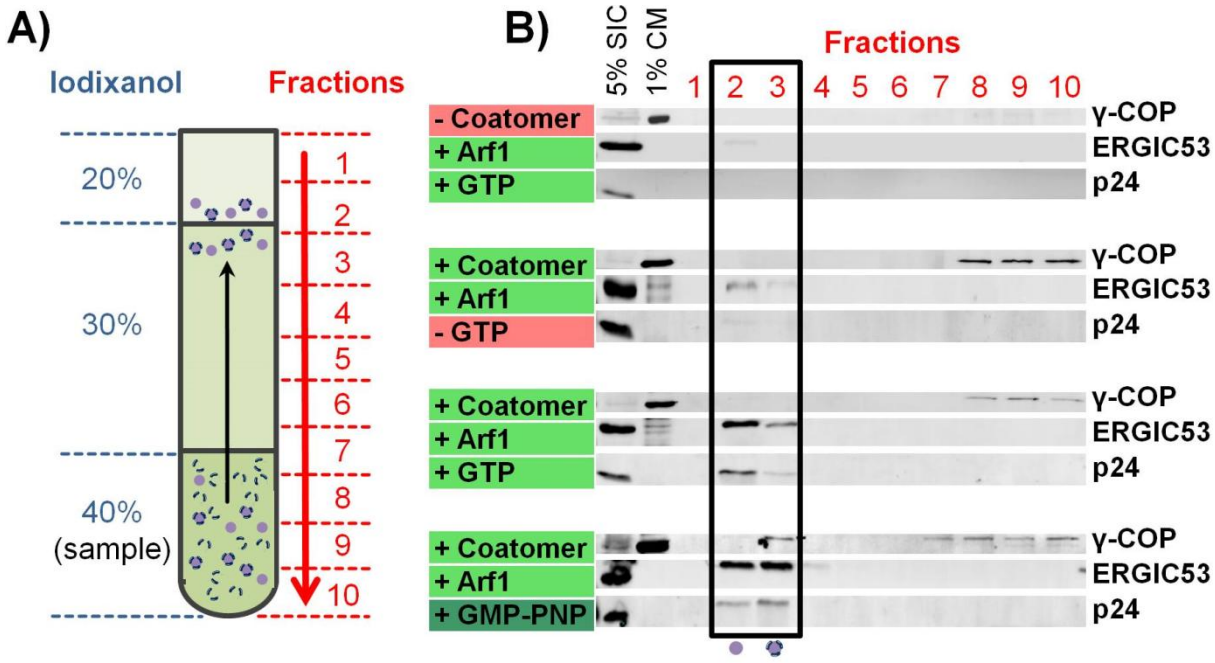

Figure 2.3 COPI Vesicle Purification via Floatation in an Iodixanol Density Gradient

(A) Scheme of the density gradient used for COPI floatation. Samples were adjusted to 40 % and overlaid with 30 % and 20 % density matrix. The black arrow indicated the movement of the vesicles; the red arrow indicates the fractionation procedure from top to bottom. (B) Western blot analysis of the fractions indicated above the blots. Components added/omitted during reconstitutions are depicted on the left. As inputs, 5 % of the SIC and 1% of CM used for the reconstitutions were loaded. Membranes were probed for the presence of the protein indicated on the right. Black box highlights the fractions that contain COPI marker proteins (2 and 3).

In order to further verify that fractions 2 and 3 contain COPI vesicles, they were investigated by electron microscopy. A combined fraction 2/3 was harvested from gradients loaded with reconstitutions performed with GTP, GMP-PNP, or without coatomer and subjected to resin-embedding. From control samples (without CM), no pellet could be obtained. This is not unexpected as the Western blot analysis of this sample displayed only weak signals for COPI marker proteins (Fig. 2.3B second highest panel). For GTP and GMP-PNP reconstitutions, resin-embedded samples could be prepared. Inspection of ultrathin sections from these samples revealed

predominantly vesicle-like structures (Fig. 2.4). The vesicles were not perfectly homogenous in size, ranging from 60-100 nm. Moreover, while the vesicles recovered from the GTP sample appeared almost exclusively uncoated, an electron-dense coat could be observed on many of the vesicle profiles isolated from gradient loaded with the GMP-PNP reconstitution (compare Fig. 2.4 A and B).

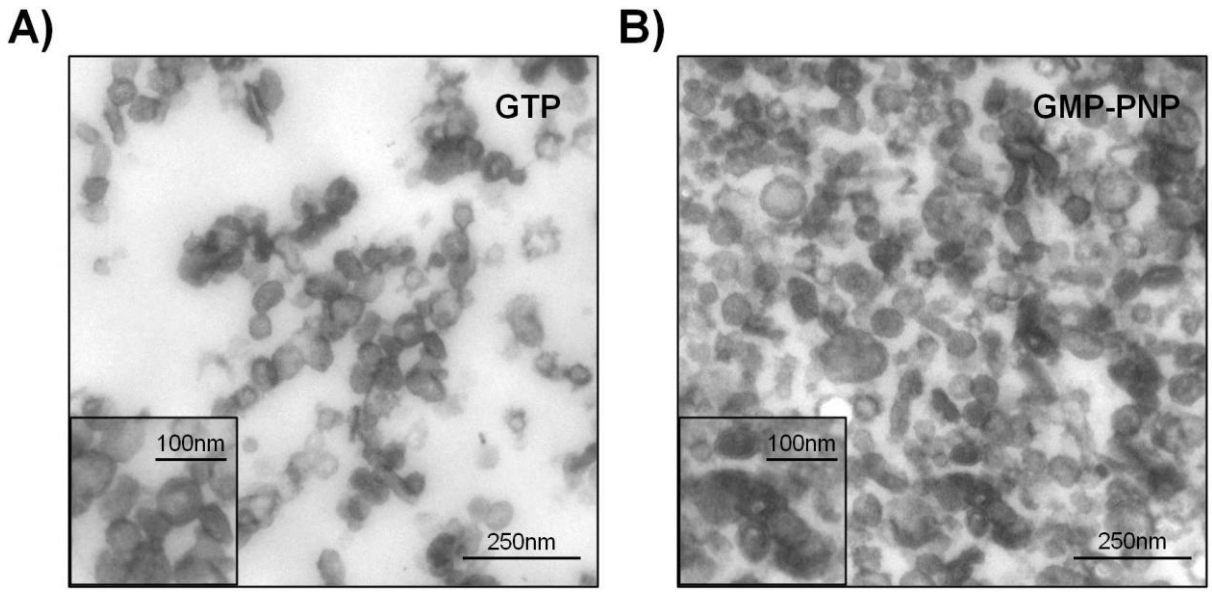

Figure 2.4 Resin-embedding EM of Purified COPI Vesicles

Representative EM images of embedded samples recovered from a combined fraction 2/3 after iodixanol density gradient purification. Reconstitutions were performed either with GTP (A) or non-hydrolysable analog GMP-PNP (B). Scale bars with their respective length are depicted in the main images and insets.

With an assay and purification procedure at hand to obtain a clean fraction of COPI vesicles we needed to choose a method for proteomics. Since semi-intact cells were used as source of Golgi membranes, we decided to use isotope labeling (SILAC) which would allow us to perform quantitative mass spectrometry. The workflow that was employed in order to investigate the protein content of COPI vesicles is outlined in figure 2.5:

i) Cells were in parallel cultivated in heavy medium, containing isotope-labeled arginine and lysine, and light medium with unlabelled amino acids. ii) Once an incorporation of the heavy amino acids >95 % was achieved, cells were expanded and used as donor material for COPI reconstitution. In parallel to the budding reaction, a mock reaction without CM was performed, which contains background levels of COPI marker proteins (Fig. 2.3B), and furthermore all contaminants that are co-purified with the reconstituted vesicles. iii) Samples from the budding reaction and the mock reaction were mixed and processed for LC-MS. iv) The samples from both reactions were analyzed in the same MS run. By comparing the intensities of heavy and light peptides (SILAC ratio) it is possible to quantify the enrichment of proteins in either one of the two samples (Fig. 2.5).

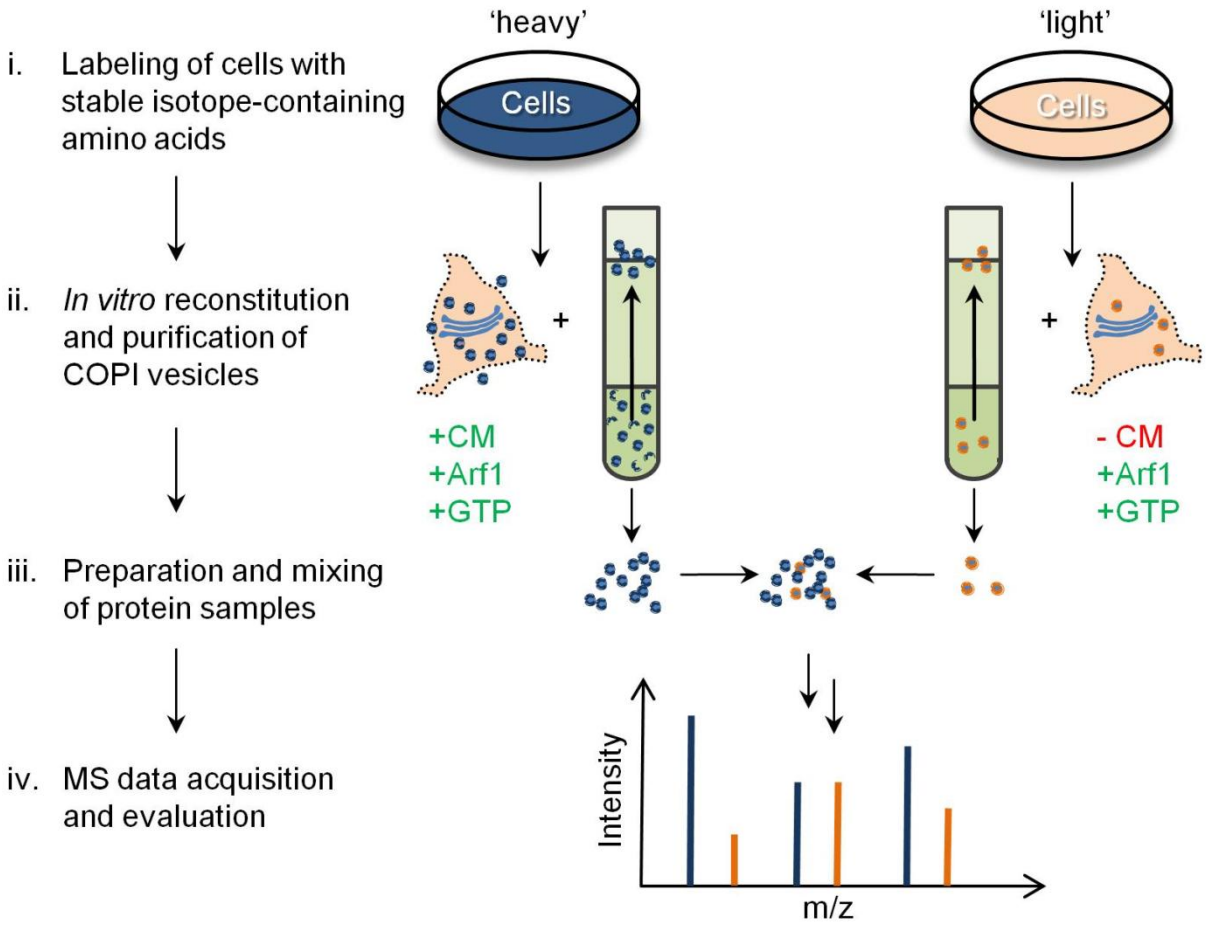

Figure 2.5 Workflow of a SILAC-based COPI Proteomic Experiment

i) Cells were labeled with heavy amino acids. ii) Heavy and light cells were used as membrane source for budding and mock reactions (without CM). The reconstituted (mock) vesicles were purified through density gradient floatation. iii) Vesicle and mock samples were mixed and processed for LC-MS. iv) Samples were analyzed in the same MS run. Labels allow the assignment of each peptide to one of the two samples. From their intensities, quantitative SILAC ratios can be calculated.

2.2 The HeLa Cell COPI Vesicle Core Proteome

In the workflow shown in figure 2.5, the COPI reconstitution was performed from heavy cells, while the mock reaction was carried out with unlabeled cells. In order to make sure that the labeling procedure had no influence on the later sample, the same experiment was performed with switched isotope labels – vesicles light, mock heavy. This general intrinsic control was kept for further SILAC experiments as they were usually performed as label switch replicates.

The SILAC ratios obtained from two independent experiments are displayed in the scatter plot in figure 2.6. Here, each protein detected in both runs is displayed as a dot with its coordinates being its respective SILAC ratios. Obvious contaminants identified by high light/heavy and low heavy/light ratios e.g. keratin species or coat proteins were excluded from the plot. Noteworthy, in the final

experiments, presented here, only coatomer was omitted in the mock reactions. Initially also Arf1 was omitted with the results that subunits of the adaptor protein complex 1 (AP-1) were enriched almost fourfold in the vesicle fraction. Through the addition of Arf1, no AP complex subunit displays SILAC ratios >1.6. From the plot in figure 2.6 it can be clearly seen that the majority of proteins have SILAC ratios of close to one meaning they are neither enriched in the COPI sample nor the mock control. Proteins which are enriched in the COPI vesicle sample spread out towards the upper right corner of the plot, aligning to a virtual diagonal. Values from both independent runs display a high degree of correlation, with an R^2 value of 0.7. This value rises to 0.83 when a single protein with heavily diverging SILAC ratios, Zinc finger protein-like 1 (ZFPL1), which displays SILAC ratios of 29.5 and 4.3, is excluded from the analysis (Fig. 2.6). The cis-Golgi protein ZPFL1, as well as other proteins and protein families that display particularly high SILAC ratios are highlighted in the plot. In particular, 6 members of the p24/TMED family, the two calcium binding proteins nucleobindin 1 and 2 (NUCB1/2), the zinc transporters SLC30A6/7, as well as the ER-Golgi cycling protein ERGIC3, display robust enrichment in the COPI vesicle sample (Fig. 2.6).

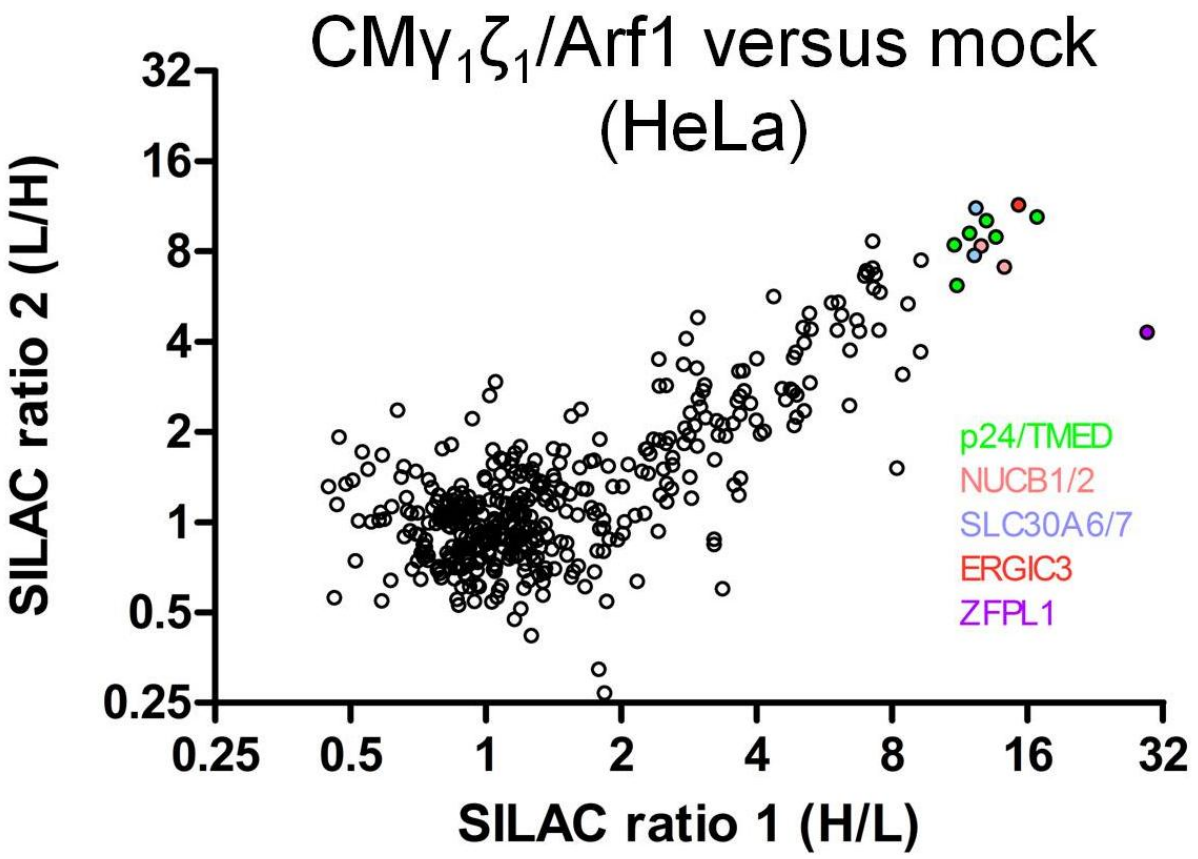

Figure 2.6 The HeLa Cell COPI Proteome

Scatter plot of SILAC ratios obtained from two independent experiments performed according to figure 2.5 with switched labels. $CM\gamma_1\zeta_1$ and Arf1 were used. Contaminants were removed from the datasets. Some proteins and protein families are highlighted in color. R^2 value of the complete dataset is 0.7; it rises to 0.83 when ZFPL1 is neglected.

In total three COPI vesicles versus mock experiments were performed with HeLa cells. 102 proteins were identified in at least 2 experiments, displaying mean SILAC ratios of >2. An additional 20 proteins were identified with SILAC ratios >2 in only one experiment with the SILAC label being carried by the COPI vesicle fraction. Hence, taken together 122 proteins are high fidelity COPI core proteome candidates. A complete list of these proteins is displayed in table 1.

Protein.names	Gene.names	ratio 1 (H/L)	ratio 2 (L/H)	ratio 3 (H/L)	Mean SILAC ratio	SEM
Zinc finger protein-like 1	ZFPL1	29,51	4,30	13,37	15,73	7,37
Transmembrane emp24 domain-containing protein 7	TMED7;TMED7-TICAM2	16,79	10,41	11,29	12,83	2,00
Solute carrier family 35 member E1	SLC35E1	13,62		10,88	12,25	1,37
Endoplasmic reticulum-Golgi intermediate compartment protein 3	ERGIC3	15,26	11,43	9,31	12,00	1,74
Zinc transporter 5	SLC30A5	10,65		12,74	11,69	1,04
Transmembrane emp24 domain-containing protein 10	TMED10	12,96	10,12	9,31	10,80	1,11
Transmembrane emp24 domain-containing protein 4	TMED4	13,61	8,95	9,64	10,73	1,45
Zinc transporter 7	SLC30A7	12,28	11,15	8,67	10,70	1,07
Nucleobindin-1	NUCB1	12,59	8,35	10,50	10,48	1,23
Transmembrane emp24 domain-containing protein 2	RNP24;TMED2	11,88	9,17	9,89	10,31	0,81
Zinc transporter 6	SLC30A6	12,17	7,77		9,97	2,20
Transmembrane emp24 domain-containing protein 9	TMED9	10,99	8,43	9,64	9,68	0,74
Nucleobindin-2;Nesfatin-1	HEL-S-109;NUCB2;Nucb2	14,18	7,08	7,69	9,65	2,27
Transmembrane emp24 domain-containing protein 1	TMED1	11,13	6,16	8,48	8,59	1,44
Endoplasmic reticulum-Golgi intermediate compartment protein 2	ERGIC2	7,24	8,64	8,16	8,01	0,41
VIP36-like protein	LMAN2L	7,24	7,05	8,10	7,46	0,32
Protein RER1	RER1	9,28	7,47	5,56	7,44	1,07
Protein cornichon homolog 4	CNIH4	7,34	6,72		7,03	0,31
Surfeit locus protein 4	SURF4	7,01	6,90	5,96	6,62	0,33
Protein ERGIC-53	LMAN1	6,96	6,63	6,23	6,61	0,21
Protein YIPF;Protein YIPF5	YIPF5	7,07	6,80	5,90	6,59	0,36
Galactosylgalactosylxylosylprotein 3-beta-glucuronosyltransferase 3	B3GAT3	9,24	3,71		6,47	2,77
Vesicular integral-membrane protein VIP36	LMAN2	7,52	5,84	5,63	6,33	0,60
Golgi SNAP receptor complex member 2	GOSR2	8,31		4,30	6,31	2,01
Transmembrane 9 superfamily member 3	TM9SF3;SMBP	8,67	5,36	4,60	6,21	1,25
Rab-like protein 3	RABL3	6,05			6,05	
Beta-1,3-galactosyltransferase 6	B3GALT6	5,88			5,88	
Immediate early response 3-interacting protein 1	IER3IP1	7,28	6,04	4,25	5,85	0,88
Protein YIPF4	YIPF4	8,45	3,10		5,78	2,67
Vesicle transport protein GOT1B	GOLT1B	5,87	5,38	5,72	5,66	0,14
Endoplasmic reticulum mannosyl-oligosaccharide 1,2-alpha-mannosidase;alpha-1,2-Mannosidase	MAN1B1	7,47	4,36	4,60	5,48	1,00
Protein YIF1A	YIF1A	6,08	5,41	4,88	5,46	0,35
Vesicle-trafficking protein SEC22b	SEC22B	6,76	4,34	5,06	5,39	0,72
Endoplasmic reticulum resident protein 44	ERP44	6,17	4,91	4,44	5,17	0,52
Protein kish-A	TMEM167A	5,35		4,93	5,14	0,21

Protein.names	Gene.names	ratio 1 (H/L)	ratio 2 (L/H)	ratio 3 (H/L)	Mean SILAC ratio	SEM
Golgi reassembly-stacking protein 2	GORASP2	4,99			*4,99*	
Protein YIF1B	YIF1B	5,24	4,98	4,37	4,86	0,26
Alpha-(1,6)-fucosyltransferase	FUT8	8,19	1,51		4,85	3,34
ER lumen protein-retaining receptor 1;ER lumen protein-retaining receptor	KDELR1	5,53		4,00	4,76	0,76
Endoplasmic reticulum-Golgi intermediate compartment protein 1	ERGIC1	6,45	3,74	4,01	4,73	0,86
Syntaxin-5	STX5;STX5A	4,88	3,68	5,61	4,72	0,56
Ras-related protein Rab-18	RAB18	5,06	4,45	4,29	4,60	0,24
Clusterin;Clusterin beta chain;Clusterin alpha chain;Clusterin	CLU	4,36	5,66	3,68	4,57	0,58
Protein CASP;Homeobox protein cut-like 1	CUX1;Nbla10317;CUX1-RETc;CUX1-RETa	6,43	2,45		4,44	1,99
Protein YIPF3;Protein YIPF3, 36 kDa form III;Protein YIPF	YIPF3	5,28	4,40	3,29	4,32	0,58
Mannosyl-oligosaccharide 1,2-alpha-mannosidase IB	MAN1A2	6,04	4,37	2,23	4,21	1,10
Polypeptide N-acetylgalactosaminyltransferase 1	GALNT1	5,10	3,96	3,55	4,21	0,46
Protein canopy homolog 2	CNPY2	4,15			4,15	
Lipoprotein lipase	LPL	5,25	2,91		4,08	1,17
Cell growth regulator with EF hand domain protein 1	CGREF1	4,81	2,73		3,77	1,04
Protein disulfide-isomerase	P4HB	4,00	3,51		3,76	0,25
Palmitoyltransferase ZDHHC13;Palmitoyltransferase	ZDHHC13	5,10	2,36		3,73	1,37
Polypeptide N-acetylgalactosaminyltransferase 3;Polypeptide N-acetylgalactosaminyltransferase	GALNT3	4,75	2,78	3,63	3,72	0,57
Peptidyl-prolyl cis-trans isomerase;Peptidyl-prolyl cis-trans isomerase B	HEL-S-39;PPIB	4,84	3,54	2,59	3,65	0,65
Emerin	EMD	2,96	4,82	3,03	3,60	0,61
Reticulocalbin-1	HEL-S-84;RCN1	4,63	2,56		3,60	1,03
Transmembrane protein 115	TMEM115	4,90	2,24		3,57	1,33
Transmembrane emp24 domain-containing protein 5	TMED5	2,79	4,09	3,72	3,53	0,39
Alpha-1,6-mannosyl-glycoprotein 2-beta-N-acetylglucosaminyltransferase	MGAT2	4,55	2,79	3,05	3,46	0,55
Alpha-mannosidase 2;Alpha-mannosidase	MAN2A1	4,91	2,65	2,65	3,41	0,75
ER lumen protein-retaining receptor;ER lumen protein-retaining receptor 2	KDELR2			3,39	*3,39*	
Rho-related BTB domain-containing protein 3	RHOBTB3	3,32			*3,32*	
Glycosyltransferase 8 domain-containing protein 2	GLT8D2	3,26			*3,26*	
Sec1 family domain-containing protein 1	SCFD1	3,75	2,74		3,25	0,50
ADP-ribosylation factor 4	ARF4	3,18			*3,18*	
BET1 homolog	BET1;DKFZp781C0425	3,67	2,63		3,15	0,52
Alpha-2-macroglobulin receptor-associated protein	LRPAP1	3,14			*3,14*	
UbiA prenyltransferase domain-containing protein 1	UBIAD1	4,85	2,10	2,45	3,13	0,86
Vesicle-trafficking protein SEC22a	SEC22A	3,13			*3,13*	

Protein.names	Gene.names	ratio 1 (H/L)	ratio 2 (L/H)	ratio 3 (H/L)	Mean SILAC ratio	SEM
Serpin H1	SERPINH1	3,73	3,20	2,34	3,09	0,41
Galectin-3-binding protein	LGALS3BP	4,15	2,01		3,08	1,07
Thioredoxin domain-containing protein 5	hCG_1811539;TXNDC5;STRF8;DKFZp666I134	2,75	3,36		3,05	0,30
Ras-related protein Rab-2A	RAB2;RAB2A	3,65	3,18	2,27	3,03	0,40
cDNA FLJ76981, highly similar to Homo sapiens golgi autoantigen, golgin subfamily a, 5 (GOLGA5), mRNA	GOLGA5	3,06	2,87		2,97	0,09
Transmembrane emp24 domain-containing protein 3	TMED3	2,42	3,49		2,96	0,54
Calumenin	CALU	3,67	2,29	2,73	2,89	0,41
Probable glutathione peroxidase 8	GPX8	3,04	2,75	2,80	2,86	0,09
Calreticulin	HEL-S-99n;CALR	2,97	2,58		2,77	0,19
Polypeptide N-acetylgalactosaminyltransferase 10;Polypeptide N-acetylgalactosaminyltransferase	GALNT10	3,41	1,94	2,88	2,74	0,43
Alpha-1,3-mannosyl-glycoprotein 2-beta-N-acetylglucosaminyltransferase	MGAT1	3,99	2,19	1,95	2,71	0,64
Insulin-like growth factor-binding protein 7	IGFBP7	2,99	2,42		2,71	0,29
Adipocyte plasma membrane-associated protein	APMAP	2,51	2,86		2,69	0,17
Ras-related protein Rab-6B	RAB6A;RAB6B	3,62	2,53	1,88	2,68	0,51
Exostosin-like 2;Processed exostosin-like 2	EXTL2	2,67			*2,67*	
Protein disulfide-isomerase A6	PDIA6	3,08	2,23		2,66	0,42
Neutral alpha-glucosidase AB	HEL-S-164nA;GANAB	2,43	2,85		2,64	0,21
Transmembrane 9 superfamily member 1	TM9SF1	3,87	2,49	1,52	2,63	0,68
Nucleoporin NDC1	NDC1	2,60			*2,60*	
78 kDa glucose-regulated protein	HEL-S-89n;HSPA5	2,94	3,26	1,48	2,56	0,55
Protein O-linked-mannose beta-1,2-N-acetylglucosaminyltransferase 1	POMGNT1	3,68	1,40		2,54	1,14
Sulfhydryl oxidase 2	QSOX2	3,26	2,18	2,12	2,52	0,37
Alpha-1,3-mannosyl-glycoprotein 4-beta-N-acetylglucosaminyltransferase B	MGAT4B	2,91	2,10		2,50	0,40
Golgi SNAP receptor complex member 1	GOSR1	3,28	1,95	2,28	2,50	0,40
Carbohydrate sulfotransferase 14	CHST14	3,54	2,14	1,82	2,50	0,53
Chondroitin sulfate synthase 2	CHPF	2,45			*2,45*	
SPARC-related modular calcium-binding protein 1	SMOC1	3,56	1,33		2,45	1,12
Beta-1,4-glucuronyltransferase 1	B3GNT6;B4GAT1	3,65	1,23		2,44	1,21
NADH-cytochrome b5 reductase	CYB5R3	2,78	2,06		2,42	0,36
Transmembrane protein 43	TMEM43;FLJ00144			2,39	*2,39*	
Golgin subfamily B member 1	GOLGB1	3,36	2,12	1,67	2,38	0,51
Protein FAM3A	FAM3A	2,32			*2,32*	
Protein CASC4	CASC4	3,22	1,62	2,13	2,32	0,47
Calcium-transporting ATPase;Calcium-transporting ATPase type 2C member 1	ATP2C1	2,76	1,83	2,34	2,31	0,27

Protein.names	Gene.names	ratio 1 (H/L)	ratio 2 (L/H)	ratio 3 (H/L)	Mean SILAC ratio	SEM
Ras-related protein Rab-1B;Putative Ras-related protein Rab-1C	RAB1B;RAB1C	2,84	2,31	1,76	2,31	0,31
45 kDa calcium-binding protein	SDF4	2,83	1,96	2,09	2,29	0,27
DnaJ homolog subfamily B member 11	DNAJB11	2,27			*2,27*	
Very-long-chain enoyl-CoA reductase	TECR	2,26			*2,26*	
Protein SYS1 homolog	SYS1	2,25			*2,25*	
Catechol O-methyltransferase	COMT	2,19			*2,19*	
Transmembrane protein 33	SHINC3;TMEM33	2,52	1,83	2,17	2,17	0,20
Prenylated Rab acceptor protein 1	RABAC1	2,95	1,79	1,67	2,14	0,41
Golgi integral membrane protein 4	GOLIM4	2,36	1,89	2,10	2,12	0,14
Ras-related protein Rab-1A	RAB1A	2,55	1,90	1,84	2,10	0,23
Solute carrier family 35 member E2B;Solute carrier family 35 member E2	hCG_2036609;SLC35E2B;SLC35E2	3,22	0,88		2,05	1,17
GDP-fucose transporter 1	SLC35C1	2,86	1,20		2,03	0,83
Myosin-10	MYH10	3,22	0,84		2,03	1,19
Transmembrane 9 superfamily member 4	TM9SF4	2,84	1,41	1,83	2,03	0,42
Dermatan-sulfate epimerase	DSE	2,28	1,76		2,02	0,26
Glycoprotein endo-alpha-1,2-mannosidase-like protein	MANEAL	4,07	1,97		2,01	1,05
Transforming growth factor-beta-induced protein ig-h3	TGFBI	2,01			*2,01*	
40S ribosomal protein S2	RPS2;OK/KNS-cl.6;rps2	2,27	1,75		2,01	0,26
Cleft lip and palate transmembrane protein 1-like protein	CLPTM1L	1,63	2,38		2,00	0,38

Table 1: Candidate Proteins for the HeLa Cell COPI Core Proteome

List of candidates for the COPI core proteome from HeLa cells as determined by three independent experiments performed according to Fig. 2.5. CM$\gamma_1\zeta_1$, Arf1, and GTP were used for reconstitutions. Given are gene and protein names of the identified proteins, the SILAC ratios (H/L or L/H) from each experiment, the mean SILAC ratio, and standard error of the mean (SEM). Displayed are protein with mean SILAC ratios of >2 or with a SILAC ratio >2 in one of the two experiments in which the vesicle sample was labeled with heavy isotopes (written in italic in the Mean SILAC ratio column).

Apart from the aforementioned proteins highlighted in figure 2.6, other ER-Golgi cycling proteins (e.g. ERGIC53/LMAN1, RER1, KDEL receptor), trafficking and fusion machinery such as SNAREs (e.g. Sec22b, Stx5, and GOSR1) and Rab proteins (e.g. Rab2A, Rab6A, and Rab18) alongside a large number of Golgi-localized enzymes (e.g. MAN1A2, ZDHHC13, GALNT1) were identified. Furthermore, ER-residents, i.e. CALR, P4HB, HSPA5/BiP were found enriched in the COPI fraction. Of the 122 candidates, few proteins e.g. LPL, CGREF1, TGFBI, and LGALS3BP are secreted from the cells.

The core proteome of COPI vesicles as defined above consist with exception of the Rab proteins, luminal NUCB1/2, and the few secreted cargoes exclusively of transmembrane proteins. Since we planned to study CM isoforms, and the only described isoform-specific integrator Scyl1 is a cytosolic protein (Hamlin et al., 2014), we decided to test whether our assay was capable of capturing cytosolic factor that bind to the assembled COPI coat on a vesicle. To this end, the workflow outlined in Fig. 2.5 was modified in three ways. i) Both samples were prepared as actual budding reactions with CM, Arf1, and nucleotides. ii) One reconstitution was performed with GTP while the other one was performed its non-hydrolysable analog GTPγS to stabilize the COPI coat on the vesicles. iii) Isotope-labeled cytosol was added to the budding reaction in order to allow cytosolic factors to bind to COP vesicles during or after their formation.

The cytosol, which was prepared via nitrogen cavitation, was completely depleted in abundant transmembrane proteins of the ER/Golgi Calnexin, ERGIC53, and p24 which are enriched in SIC and present in the whole cell lysate (Fig. 2.7A). As expected, soluble cytosolic proteins ε-COP and Arf1 are completely transferred from the lysate to the cytosol fraction but largely depleted in the SIC. The soluble Hsp70 of the ER, BiP, is also detected in large amounts in the cytosol indicating that organelles did not stay intact during the cytosol preparation (Fig. 7A).

When the cytosol was added to COPI reconstitutions performed with GTP or GTPγS, many proteins displayed a significant enrichment in the sample prepared with the non-hydrolysable analog (Fig. 7B). Unlike expected, the vast majority of these proteins is not part of the cytosol. Among the highest scoring proteins, highlighted in Fig. 2.7B, are the large GTPases atlastin-2/3 (ATL2/3), the ER enzymes acetolactate synthase-like protein (ILVBL), and lanosterol synthase (LSS), as well as transmembrane protein 33 (TMEM33), and adipocyte plasma membrane-associated protein (APMAP) (Fig. 2.7B).

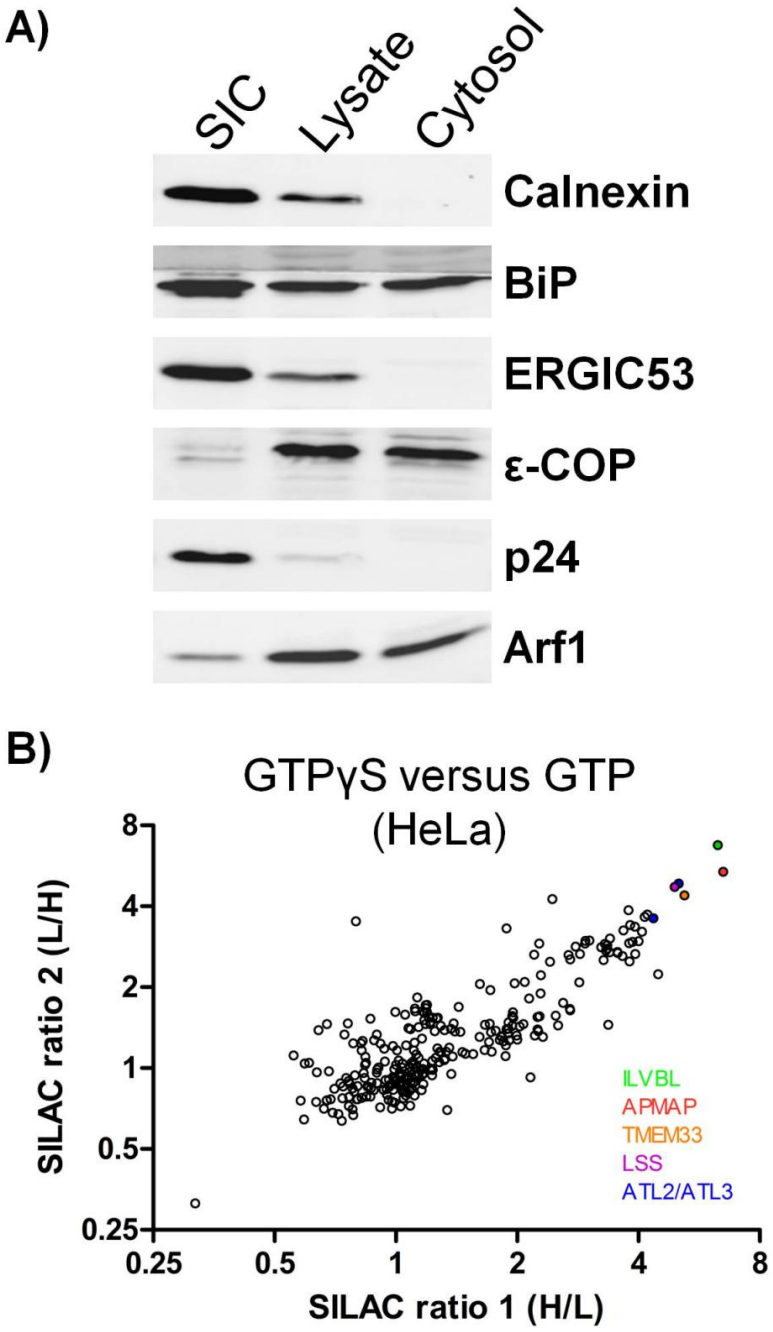

Figure 2.7 Influence of a Non-hydrolysable GTP Analog on COPI Budding in Presence of Cytosol

(A) Western blot analysis of SIC (5 µg), whole cell lysate and a cytosol fraction (both 10 µg). Samples were probed for the presence of the proteins indicated on the right. (B) Scatter plot of SILAC ratios obtained from two independent experiments performed according to workflow in figure 2.5. Both samples were prepared with $CM\gamma_1\zeta_1$, Arf1, and cytosol in the presence of either GTP or GTPγS. Experiments were performed with switched labels. Contaminants were removed from the datasets. Some proteins are highlighted in color. R^2 value of the dataset is 0.78.

Noteworthy, Scyl1 was not detected in the dataset. Only one cytosolic protein known to interact with Arf1 was enriched in the GTPγS vesicle sample, Arfaptin-1. A list showing the 72 proteins enriched more than twofold in either both (mean enrichment) or in the heavy GTPγS sample are displayed in table 2.

Protein.names	Gene.names	ratio 1 (H/L)	ratio 2 (L/H)	Mean SILAC ratio	SEM
Translocon-associated protein subunit alpha	SSR1	6,91		*6,91*	
Acetolactate synthase-like protein	ILVBL	6,29	6,76	6,53	0,23
Translocon-associated protein subunit delta	SSR4	5,95		*5,95*	
Adipocyte plasma membrane-associated protein	APMAP	6,49	5,37	5,93	0,56
Torsin-1A-interacting protein 2	TOR1AIP2	5,62		*5,62*	
Very-long-chain (3R)-3-hydroxyacyl-CoA dehydratase 3	HACD3	5,48		*5,48*	
Atlastin-2	ATL2	5,03	4,86	4,95	0,09
Terpene cyclase/mutase family member;Lanosterol synthase	LSS	4,92	4,72	4,82	0,10
Transmembrane protein 33	SHINC3;TMEM33	5,21	4,39	4,80	0,41
Torsin-1A	TOR1A	4,63		*4,63*	
Cytochrome b5 type B	DKFZp686M0619;CYB5B	4,48		*4,48*	
Atlastin-3	ATL3	4,35	3,61	3,98	0,37
ADP-ribosylation factor-like protein 6-interacting protein 1	ARL6IP1;hCG_1994130	4,21	3,73	3,97	0,24
Sterol-4-alpha-carboxylate 3-dehydrogenase, decarboxylating	NSDHL	4,15	3,65	3,90	0,25
Cleft lip and palate transmembrane protein 1-like protein	CLPTM1L	3,86		*3,86*	
Protein FAM134C	FAM134C	3,78	3,87	3,82	0,05
Vesicle-associated membrane protein-associated protein A	VAPA	4,08	3,22	3,65	0,43
Membrane-associated progesterone receptor component 1	PGRMC1	3,92	3,36	3,64	0,28
Transmembrane and coiled-coil domain-containing protein 1	TMCO1	3,62		*3,62*	
Vesicle-associated membrane protein-associated protein B/C	VAPB	3,81	3,41	3,61	0,20
7-dehydrocholesterol reductase	DHCR7	3,57		*3,57*	
Receptor expression-enhancing protein;Receptor expression-enhancing protein 5	REEP5	4,00	2,97	3,48	0,52
Extended synaptotagmin-2	ESYT2	3,67	3,25	3,46	0,21
PRA1 family protein 3	ARL6IP5	3,87	2,95	3,41	0,46
Membrane-associated progesterone receptor component 2	PGRMC2	4,48	2,23	3,36	1,12
Arfaptin-1	ARFIP1	2,44	4,26	3,35	0,91
Transmembrane protein 43	TMEM43;FLJ00144	3,79	2,91	3,35	0,44
B-cell receptor-associated protein 31	BCAP31	3,93	2,66	3,29	0,63
Fatty acid desaturase 2	FADS2	3,29		*3,29*	
Heme oxygenase 1	HMOX1	3,25		*3,25*	
Catechol O-methyltransferase	COMT	3,58	2,86	3,22	0,36
Extended synaptotagmin-1	FAM62A;ESYT1	3,40	3,03	3,22	0,18
Reticulon;Reticulon-3	RTN3	3,80	2,50	3,15	0,65
Calnexin	CANX	3,65	2,61	3,13	0,52
Reticulon;Reticulon-1	RTN1	3,54	2,70	3,12	0,42
Reticulon	RTN4;NOGOC;Nbla00271	3,55	2,68	3,11	0,44
Fatty acid desaturase 1	FADS1	3,11		*3,11*	

Protein.names	Gene.names	ratio 1 (H/L)	ratio 2 (L/H)	Mean SILAC ratio	SEM
Retinol dehydrogenase 11	RDH11	3,35	2,87	3,11	0,24
NADH-cytochrome b5 reductase;NADH-cytochrome b5 reductase 3;NADH-cytochrome b5 reductase 3 membrane-bound form;NADH-cytochrome b5 reductase 3 soluble form	CYB5R3	3,30	2,90	3,10	0,20
Epoxide hydrolase 1	EPHX1	3,35	2,79	3,07	0,28
V-type proton ATPase subunit S1	ATP6AP1;FLJ00383	3,39	2,70	3,05	0,35
Long-chain-fatty-acid--CoA ligase 3	ACSL3	3,32	2,74	3,03	0,29
Lysophosphatidylcholine acyltransferase 1	LPCAT1;AYTL2	3,23	2,82	3,02	0,21
Dolichyl-diphosphooligosaccharide--protein glycosyltransferase 48 kDa subunit	DDOST	3,02	2,98	3,00	0,02
Signal peptidase complex subunit 2	SPCS2	2,99		*2,99*	
Reticulon	RTN3	2,95	2,97	2,96	0,01
NADPH--cytochrome P450 reductase	POR;DKFZp686G04235	2,95	2,90	2,93	0,02
Thioredoxin-related transmembrane protein 1	TMX1;TXNDC	3,28	2,52	2,90	0,38
Fatty aldehyde dehydrogenase	DKFZp686E23276;ALDH3A2	2,89		*2,89*	
Sarcoplasmic/endoplasmic reticulum calcium ATPase 2	ATP2A2	2,79	2,83	2,81	0,02
Dolichyl-diphosphooligosaccharide--protein glycosyltransferase subunit 1	RPN1	2,86	2,66	2,76	0,10
Aspartyl/asparaginyl beta-hydroxylase	ASPH	2,71		*2,71*	
Lanosterol 14-alpha demethylase	CYP51A1	2,68	2,64	2,66	0,02
AP-1 complex subunit beta-1	AP1B1	2,71	2,54	2,62	0,08
Leucine-rich repeat and calponin homology domain-containing protein 4	LRCH4	1,88	3,31	2,60	0,71
Protein disulfide-isomerase;Protein disulfide-isomerase A3	HEL-S-269;PDIA3	2,27	2,91	2,59	0,32
Protein disulfide-isomerase A6	PDIA6	2,85	2,08	2,47	0,38
ADP-ribosylation factor 4	ARF4	2,41	2,49	2,45	0,04
AP-1 complex subunit mu-1	AP1M1	2,20	2,64	2,42	0,22
Immediate early response 3-interacting protein 1	IER3IP1	3,36	1,45	2,41	0,96
Sarcolemmal membrane-associated protein	SLMAP	2,39		*2,39*	
Glucosidase 2 subunit beta	PRKCSH	2,27		*2,27*	
78 kDa glucose-regulated protein	HEL-S-89n;HSPA5	2,29	2,22	2,25	0,04
Probable glutathione peroxidase 8	GPX8	2,70	1,66	2,18	0,52
Procollagen-lysine,2-oxoglutarate 5-dioxygenase 2	PLOD2	2,60	1,75	2,18	0,43
Emerin	EMD	2,71	1,64	2,17	0,53
AP-1 complex subunit gamma-1	AP1G1	2,16		*2,16*	
Calreticulin	HEL-S-99n;CALR	2,14		*2,14*	
Endoplasmin	TRA1;HEL-S-125m;HSP90B1	2,29	1,90	2,09	0,19
Glutathione peroxidase	GPX8	2,09	2,09	2,09	0,00
Transmembrane emp24 domain-containing protein 5	TMED5	2,50	1,57	2,03	0,46
Aladin	AAAS	1,97	2,07	2,02	0,05

Table 2: Proteins Enriched by GTPγS in the COPI Vesicle Fraction in the Presence of Cytosol

List of proteins enriched in the COPI vesicle fraction yielded with GTPγS compared to GTP, both in the presence of cytosol. Experiments were in general performed according to Fig. 2.5. Vesicles were made from HeLa cells with $CM\gamma_1\zeta_1$ and Arf1 in the presence of labeled/unlabeled cytosol with either GTP or GTPγS. Given are gene and protein names of the identified proteins, the SILAC ratios (H/L or L/H) from each experiment, the mean SILAC ratio, and standard error of the mean (SEM). Displayed are protein with mean SILAC ratios >2 or with a SILAC ratio >2 observed within the experiment in which the GTPγS vesicle sample was heavy labeled (written in italic in the Mean SILAC ratio column).

Since the majority of proteins enriched in GTPγS vesicles were transmembrane proteins, which with high fidelity did not originate from the cytosol (Fig. 2.7A), the possibility was explored that the non-hydrolysable GTP analog had lead to the release of membranes from SIC. To this end, the experiment outlined above was performed this time omitting coatomer in both, the GTP and the GTPγS reconstitution. As can be seen in table 3, a large number of the proteins enriched in the original experiments (with CM) were also enriched in these samples, e.g. atlastins, reticulons, and many other mostly ER resident transmembrane proteins (Tab. 3).

Protein.names	Gene.names	ratio 1 (H/L)	ratio 2 (H/L)	Mean SILAC ratio	SEM
Catalase	CAT	6,77		*6,77*	
Atlastin-2	ATL2	4,00	4,82	4,41	0,41
NADPH--cytochrome P450 reductase	POR;DKFZp686G04235	3,53		3,53	
Extended synaptotagmin-2	ESYT2	3,75	3,25	3,50	0,25
Atlastin-3	ATL3	3,37	3,47	3,42	0,05
Vesicle-associated membrane protein-associated protein B/C	VAPB		3,24	*3,24*	
PRA1 family protein 2	PRAF2		3,24	*3,24*	
Receptor expression-enhancing protein;Receptor expression-enhancing protein 5	REEP5	3,13	3,25	3,19	0,06
Reticulon;Reticulon-3	RTN3	3,12	3,20	3,16	0,04
ADP-ribosylation factor-like protein 6-interacting protein 1	hCG_1994130;ARL6IP1	3,12	3,15	3,13	0,02
Extended synaptotagmin-1	FAM62A;ESYT1	3,00	3,25	3,12	0,13
Calnexin	CANX	3,07	3,16	3,12	0,04
Reticulon;Reticulon-1	RTN1	3,09		*3,09*	
Reticulon-4	RTN4	3,06	3,07	3,06	0,01
B-cell receptor-associated protein 31	BCAP31	2,84	3,16	3,00	0,16

Protein.names	Gene.names	ratio 1 (H/L)	ratio 2 (H/L)	Mean SILAC ratio	SEM
Vesicle-associated membrane protein-associated protein A	VAPA	2,79	3,19	2,99	0,20
Sterol-4-alpha-carboxylate 3-dehydrogenase, decarboxylating	NSDHL		2,93	*2,93*	
PRA1 family protein 3	ARL6IP5	2,83	3,02	2,92	0,10
Membrane-associated progesterone receptor component 1	PGRMC1	2,90	2,81	2,86	0,04
Protein FAM134C	FAM134C	2,49	3,15	2,82	0,33
Epoxide hydrolase 1	EPHX1	2,77	2,70	2,73	0,03
Leucine-rich repeat and calponin homology domain-containing protein 4	LRCH4	2,48	2,88	2,68	0,20
Retinol dehydrogenase 11	RDH11	3,15	2,11	2,63	0,52
Dolichyl-diphosphooligosaccharide--protein glycosyltransferase subunit 1	RPN1	2,49	2,75	2,62	0,13
Membrane-associated progesterone receptor component 2	PGRMC2	2,54	2,64	2,59	0,05
Long-chain-fatty-acid--CoA ligase 3	ACSL3	2,37		*2,37*	
Terpene cyclase/mutase family member;Lanosterol synthase	LSS	2,36		*2,36*	
Protein disulfide-isomerase;Protein disulfide-isomerase A3	HEL-S-269;PDIA3	2,28	2,30	2,29	0,01
Transmembrane protein 33	TMEM33;SHINC3	2,26		*2,26*	
Sarcoplasmic/endoplasmic reticulum calcium ATPase 2;Calcium-transporting ATPase;Sarcoplasmic/endoplasmic reticulum calcium ATPase 1	ATP2A2;DKFZp779O2152;DKFZp779G2251;ATP2A1	2,25		*2,25*	
NADH-cytochrome b5 reductase;NADH-cytochrome b5 reductase 3;NADH-cytochrome b5 reductase 3 membrane-bound form;NADH-cytochrome b5 reductase 3 soluble form	CYB5R3		2,23	*2,23*	
AP-1 complex subunit mu-1	AP1M1	2,13	2,30	2,22	0,09
78 kDa glucose-regulated protein	HEL-S-89n;HSPA5	2,12	2,17	2,15	0,02
Translocon-associated protein subunit delta	SSR4		2,11	*2,11*	
AP-1 complex subunit gamma-1	AP1G1	1,97	2,21	2,09	0,12
Minor histocompatibility antigen H13	HM13		2,07	*2,07*	
Vesicle transport protein GOT1B	GOLT1B	2,07	2,06	2,07	0,01
Serpin H1	SERPINH1	1,84	2,19	2,02	0,17

Table 3: Proteins Enriched by GTPγS in the COPI Vesicle Fraction in the Absence of Recombinant Coatomer

List of proteins enriched in the COPI vesicle fraction when SIC were incubated with GTPγS, Arf1, and cytosol compared to GTP, Arf1, and cytosol. Coatomer was omitted in contrast to the experiments shown in table 2. Experiments were in general performed according to Fig. 2.5. Unlike in the other experiments, labels were not switched. Given are gene and protein names of the identified proteins, the SILAC ratios (H/L) from each experiment, the mean SILAC ratio, and standard error of the mean (SEM). Displayed are proteins with mean SILAC ratios >2 or with a SILAC ratio >2 observed during one of the experiments (written in italic in the Mean SILAC ratio column).

2.3 The Influence of Coatomer Isoforms on the COPI Core Proteome and Vesicle Size

As pointed out in 1.3.3., the function of coatomer isoforms remains largely elusive. One function that coat protein isoforms - especially in the COPII system - have been shown to serve is differential sorting of pivotal proteins into vesicles (Adolf et al., 2016; Mancias and Goldberg, 2007, 2008). Using a baculovirus expression vector system, it has been possible to produce different coatomer isoforms recombinantly (Sahlmuller et al., 2011). The protein complexes, which were purified via an One-STreP-Tag C-terminal of α-COP, are shown on a Coomassie-stained SDS gel in figure 2.8A. When these isoforms are used to reconstitute COPI vesicles *in vitro* with subsequent Western blot analysis of the isotypic COPI vesicles for the presence of COPI core components ERGIC53 and p24, no differential sorting can be observed (Fig. 2.8B and C). The mean incorporation of both proteins in relation to the used SIC is highly similar ranging in case of ERGIC53 from 3.4 % ($CM\zeta_1\mu_2$) to 3.6 %($CM\zeta_2\mu_1$) and 10.9 % ($CM\zeta_1\mu_1$) to 12.2 % ($CM\zeta_2\mu_1$) for p24, respectively (Fig. 2.8C). Incorporation of non-vesicle marker Calnexin was ≪1% (Fig. 2.7B).

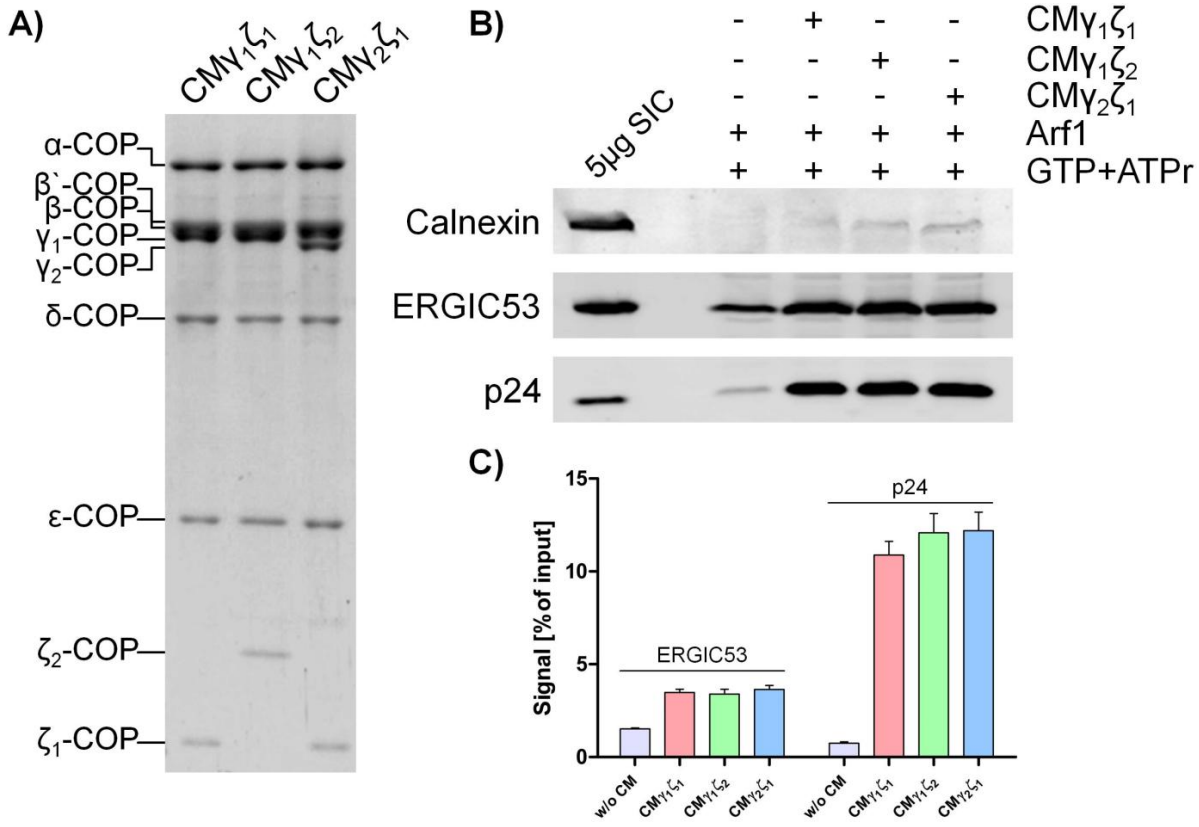

Figure 2.8 Recombinant CM Isoforms: Incorporation of ERGIC53 and p24 into Isotypic COPI Vesicles

(A) Coomassie-stained SDS gel loaded with recombinant coatomer isoforms. (B) Representative Western blot analysis of COPI vesicles reconstituted from SIC HeLa cells using recombinant CM isoforms, Arf1, GTP, and ATP regenerating system (ATPr) with 5 µg of SIC loaded as input. Samples were probed for the presence of the proteins indicated on the left. Vesicles were isolated via differential centrifugation. (C) Quantification of (B); n=8; error bars=SEM.

With our novel COPI proteomics assay, outlined in section 2.1, it was possible to investigate the influence of coatomer isoforms on the COPI vesicle protein content not only for two proteins as shown in figure 2.8, but systematically for several hundred proteins at once. To this end, following the workflow shown in Fig. 2.5, isotypic vesicles were prepared in parallel, purified, and compared by SILAC-based quantitative LC-MS. In order to be able to distinguish between the influence of individual COPI subunit isoforms, isotypic vesicles were reconstituted with $CM\zeta_1\mu_1$ and then compared with vesicles made from either $CM\gamma_1\zeta_2$ or $CM\gamma_2\zeta_1$ coatomer.

Shown in the scatter plots of figure 2.9 is the comparison of isotypic COPI vesicles, differing with respect to the γ-COP subunit. Again, each dot represents a single protein and its respective SILAC ratios obtained from two experiments performed with switched isotope labels. Unlike in figure 2.6, there is no population of proteins which align to a virtual diagonal, but almost all dots crowd around a SILAC ratio of one. While there is virtually no protein that displays a meaningful enrichment in vesicles reconstituted with $CM\gamma_1\zeta_1$ compared to $CM\gamma_2\zeta_1$, very few proteins display slightly increased ratios in $CM\gamma_2\zeta_1$ vesicles (compare Fig. 2.9A and B). These few proteins, which are marked by color in both plots include myosin-9 and myosin-10 (MYH9/10), subunits alpha and beta of the mitochondrial ATP synthase (ATP5B/ATP5A1), mitochondrial Hsp60 (HSPD1), as well as Peroxiredoxin-4 PRDX4 (Fig. 2.9). The highest mean enrichment, 2.4, is scored by ATP5A1. All other proteins display enrichments <2.

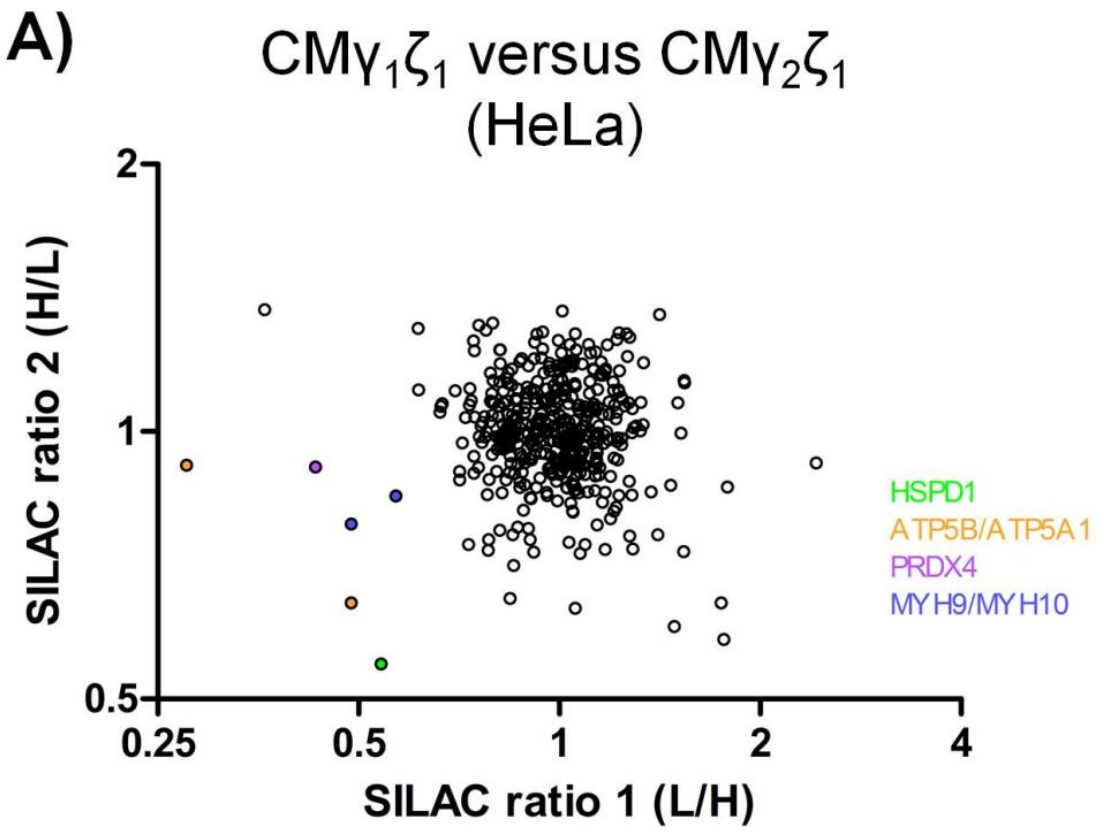

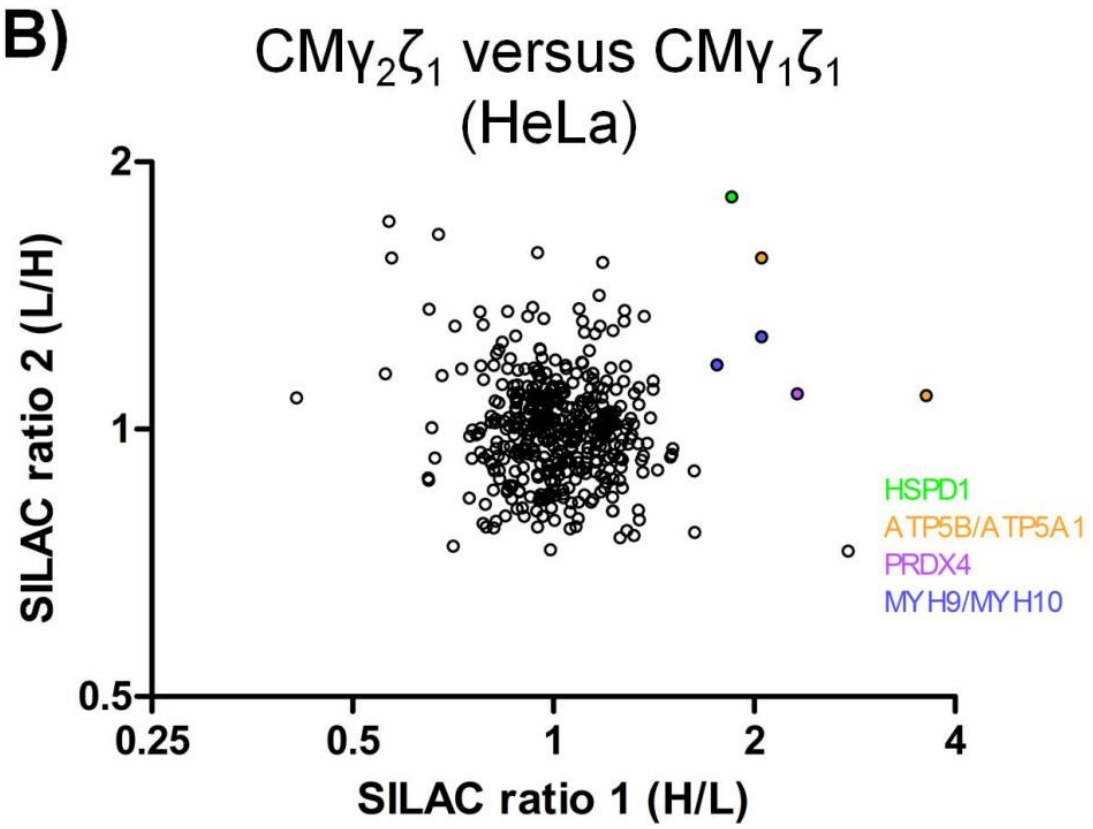

Figure 2.9 Proteomic Comparison of γ-COP-isotypic COPI Vesicles

(A) Scatter plot of SILAC ratios obtained from two independent experiments performed according to workflow in figure 2.5 with two types of isotypic COPI vesicles, $CM\gamma_1\zeta_1$ versus $CM\gamma_2\zeta_1$. Experiments were performed with switched labels. Contaminants were removed from the datasets. Some proteins are highlighted in color. (B) Scatter plot of the inverted SILAC ratios shown in (A) to compare $CM\gamma_2\zeta_1$ versus $CM\gamma_1\zeta_1$. The same proteins are highlighted in color.

In table 4, the 25 proteins with the highest enrichment in vesicles made with $CM\gamma_1\zeta_1$ compared to $CM\gamma_2\zeta_1$ are listed. Conversely, table 5 lists the 25 proteins with the highest SILAC ratios during the comparison of $CM\gamma_2\zeta_1$ versus $CM\gamma_1\zeta_1$ vesicles.

Protein.names	Gene.names	ratio 1: CMγ1ζ1 (L) vs. CMγ2ζ1 (H)	ratio 2: CMγ1ζ1 (H) vs. CMγ2ζ1 (L)	Mean SILAC ratio	SEM
Thioredoxin domain-containing protein 5	hCG_1811539;TXNDC5;STRF8;DKFZp666I134		1,47	*1,47*	
Beta-1,3-galactosyltransferase 6	B3GALT6	1,41	1,35	1,38	0,03
Syntenin-1	SDCBP		1,35	*1,35*	
Ras-related protein Rab-12	RAB12	1,54	1,14	1,34	0,20
Glutaminyl-peptide cyclotransferase-like protein	QPCTL	1,54	1,13	1,34	0,20
N-acetylglucosamine-6-sulfatase	DKFZp686E12166;GNS	1,79	0,87	1,33	0,46
Glucosidase 2 subunit beta	PRKCSH		1,32	*1,32*	
CD276 antigen	CD276		1,31	*1,31*	
Molybdate-anion transporter	MFSD5		1,31	*1,31*	
Zinc transporter 7	SLC30A7	1,51	1,08	1,29	0,21
60S ribosomal protein L27	RPL27	1,27	1,28	1,28	0,00
Carbohydrate sulfotransferase 14	CHST14	1,26	1,29	1,27	0,01
60S ribosomal protein L13	RPL13	1,34	1,20	1,27	0,07
Fukutin-related protein	FKRP	1,23	1,29	1,26	0,03
RING finger and transmembrane domain-containing protein 1	RNFT1	1,52	1,00	1,26	0,26
Aldo-keto reductase family 1 member C1;Aldo-keto reductase family 1 member C2	AKR1C1;AKR1C3;AKR1C2		1,25	*1,25*	
Receptor-type tyrosine-protein phosphatase F;Protein-tyrosine-phosphatase	PTPRF;LAR;DKFZp686B1310		1,25	*1,25*	
ER lumen protein-retaining receptor;ER lumen protein-retaining receptor 3	KDELR3	1,22	1,27	1,24	0,03
Integrin beta;Integrin beta-5	ITGB5	1,27	1,22	1,24	0,02
Guanine nucleotide-binding protein G(I)/G(S)/G(T) subunit beta-2	GNB2		1,22	*1,22*	
Galactosylgalactosylxylosylprotein 3-beta-glucuronosyltransferase 3	B3GAT3	1,18	1,25	1,22	0,04
Chondroitin sulfate synthase 1	CHSY1		1,21	*1,21*	
Nucleoporin NDC1	NDC1	1,32	1,08	1,20	0,12
Alpha-1,6-mannosyl-glycoprotein 2-beta-N-acetylglucosaminyltransferase	MGAT2	1,23	1,17	1,20	0,03
Gamma-glutamyl hydrolase	GGH	1,75	0,64	1,20	0,55

Table 4: Proteomic Comparison of COPI Vesicles: $CM\gamma_1\zeta_1$ versus $CM\gamma_2\zeta_1$

List of the 25 proteins most enriched in the COPI vesicle made with $CM\gamma_1\zeta_1$ in comparison to $CM\gamma_2\zeta_1$. Vesicles were always reconstituted with Arf1 and GTP. Experiments were in general performed according to Fig. 2.5. Given are gene and protein names of the identified proteins, the SILAC ratios (H/L and L/H) from each replicate, the mean SILAC ratio, and standard error of the mean (SEM). Displayed are the 25 proteins with the highest mean SILAC ratios and the proteins with the highest SILAC ratios during the experiment in which the $CM\gamma_1\zeta_1$ vesicle sample was labeled with heavy isotopes (written in italic in the Mean SILAC ratio column).

Protein.names	Gene.names	ratio 1: CMγ2ζ1 (H) vs. CMγ1ζ1 (L)	ratio 2: CMγ2ζ1 (L) vs. CMγ1ζ1 (H)	Mean SILAC ratio	SEM
ATP synthase subunit alpha;ATP synthase subunit alpha, mitochondrial	HEL-S-123m;ATP5A1	3,62	1,09	2,36	1,27
60 kDa heat shock protein, mitochondrial	HSPD1	1,85	1,83	1,84	0,01
ATP synthase subunit beta;ATP synthase subunit beta, mitochondrial	HEL-S-271;ATP5B	2,05	1,56	1,81	0,25
Alpha-1,3-mannosyl-glycoprotein 4-beta-N-acetylglucosaminyltransferase B	MGAT4B	2,77	0,73	1,75	1,02
Peroxiredoxin-4	HEL-S-97n;PRDX4	2,32	1,10	1,71	0,61
Myosin regulatory light chain 12A;Myosin regulatory light chain 12B;Myosin regulatory light polypeptide 9	MYL12A;MYL12B;MYL9	1,69		*1,69*	
Myosin-9	MYH9	2,05	1,27	1,66	0,39
Myosin-10	MYH10	1,76	1,18	1,47	0,29
Sarcoplasmic/endoplasmic reticulum calcium ATPase 2	ATP2A2	1,18	1,54	1,36	0,18
Endoplasmin	TRA1;HEL-S-125m;HSP90B1	1,37	1,34	1,35	0,01
Na(+)/H(+) exchange regulatory cofactor NHE-RF2	SLC9A3R2	1,34		1,34	
DnaJ homolog subfamily C member 13	DNAJC13	1,28	1,36	1,32	0,04
Calreticulin	HEL-S-99n;CALR	1,28	1,32	1,30	0,02
Roundabout homolog 1	ROBO1	1,17	1,41	1,29	0,12
Zinc transporter 1	SLC30A1	1,29		*1,29*	
Membrane-associated progesterone receptor component 2	PGRMC2	1,41	1,13	1,27	0,14
Alpha-1,6-mannosylglycoprotein 6-beta-N-acetylglucosaminyltransferase A	MGAT5	0,95	1,58	1,26	0,32
Glycosyltransferase 8 domain-containing protein 2	GLT8D2	1,63	0,90	1,26	0,36
Calnexin	CANX	1,23	1,29	1,26	0,03
Phosphatidylinositol 4-phosphate 5-kinase type-1 alpha;Putative PIP5K1A and PSMD4-like protein	PIP5K1A;PIPSL	1,41	1,11	1,26	0,15
NADPH--cytochrome P450 reductase	POR;DKFZp686G04235	1,17	1,31	1,24	0,07
Myosin light polypeptide 6	MYL6	1,51	0,95	1,23	0,28
Procollagen-lysine,2-oxoglutarate 5-dioxygenase 2	PLOD2	1,28	1,18	1,23	0,05
Interferon-induced transmembrane protein 3;Interferon-induced transmembrane protein 1;Interferon-induced transmembrane protein 2	IFITM3;IFITM2;IFITM1	1,09	1,37	1,23	0,14
Putative sodium-coupled neutral amino acid transporter 10	SLC38A10	1,34	1,11	1,23	0,12

Table 5: Proteomic Comparison of COPI Vesicles: $CM\gamma_2\zeta_1$ versus $CM\gamma_1\zeta_1$

List of the 25 proteins most enriched in the COPI vesicle made with $CM\gamma_2\zeta_1$ in comparison to $CM\gamma_1\zeta_1$. Vesicles were always reconstituted with Arf1 and GTP. Experiments were in general performed according to Fig. 2.5. Given are gene and protein names of the identified proteins, the SILAC ratios (H/L and L/H) from each replicate, the mean SILAC ratio, and standard error of the mean (SEM). Displayed are the 25 proteins with the highest mean SILAC ratios and the proteins with the highest SILAC ratios during the experiment in which the $CM\gamma_2\zeta_1$ vesicle sample was labeled with heavy isotopes (written in italic in the Mean SILAC ratio column).

As mentioned above, also COPI vesicles formed *in vitro* with different isoforms of ζ-COP were compared systematically by means of SILAC proteomics. The results are shown in figure 2.10. Similar to the comparison of γ-COP-isotypic vesicles, almost all proteins display rather low SILAC ratios. A few of the higher scoring proteins are highlighted in color (Fig. 2.10). In case of ζ_2-COP, there is only one protein which shows a significant mean enrichment, the monocarboxylate transporter 1 (SLC16A1). However, as can be seen in Fig. 2.10B, its SILAC scores are rather divergent, i.e. 6.1 and 1.4. In vesicles made with ζ_1-COP, no protein showed an enrichment >2. The proteins with the highest SILAC ratios, ranging from 1.5-1.7 are the glycosyltransferase POMGNT1, palymitoyltransferase ZDHHC13, the nonaspanin TM9SF1, and trophoblast glycoprotein TPBG (Fig. 2.10).

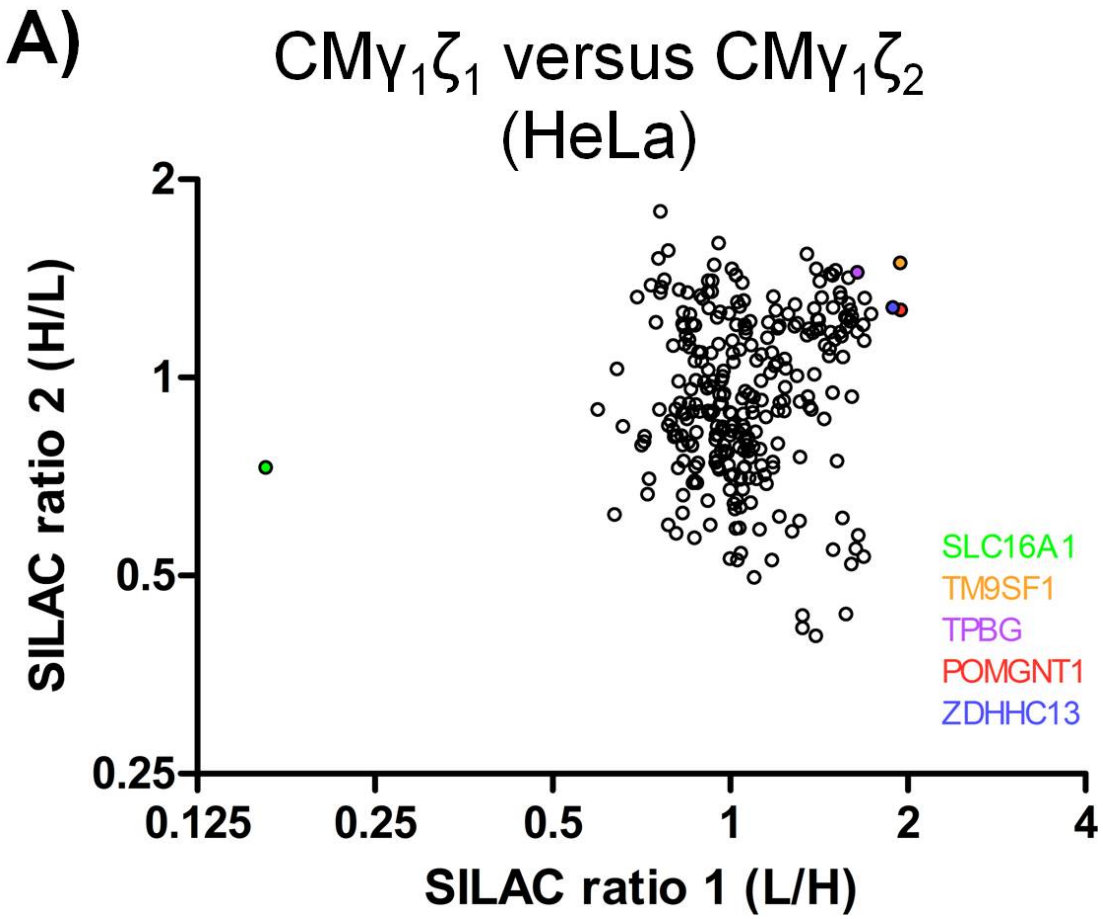

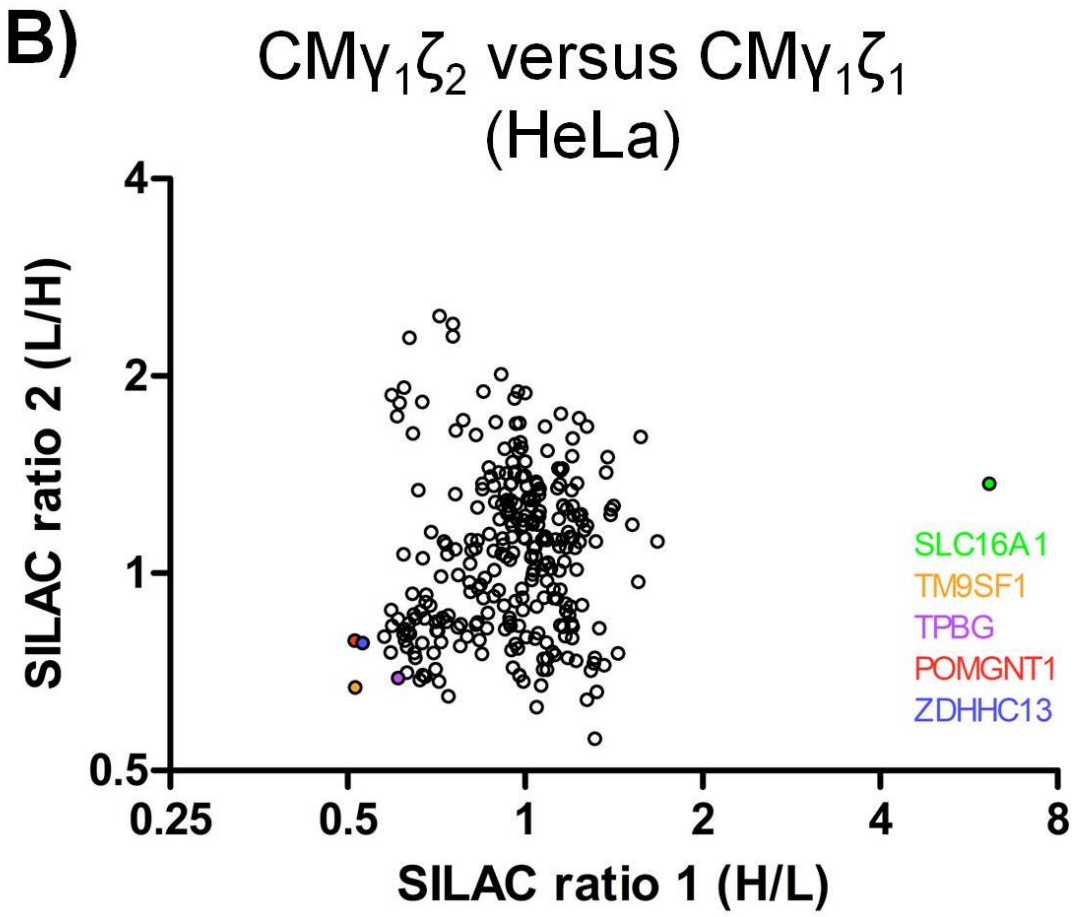

Figure 2.10 Proteomic Comparison of ζ-COP-isotypic COPI Vesicles

(A) Scatter plot of SILAC ratios obtained from two independent experiments performed according to workflow in figure 2.5 with two types of isotypic COPI vesicles, $CM\gamma_1\zeta_1$ versus $CM\gamma_1\zeta_2$. Experiments were performed with switched labels. Contaminants were removed from the datasets. Some proteins are highlighted in color. (B) Scatter plot of the inverted SILAC ratios shown in (A) to compare $CM\gamma_1\zeta_2$ versus $CM\gamma_1\zeta_1$. The same proteins are highlighted in color.

Table 6 and table 7 list the 25 proteins with the highest SILAC ratios in direct comparisons of $CM\gamma_1\zeta_1$ versus $CM\gamma_1\zeta_2$ vesicles (Tab. 6) or $CM\gamma_1\zeta_2$ versus $CM\gamma_1\zeta_1$ vesicles (Tab. 7).

Protein.names	Gene.names	ratio 1: CMγ1ζ1 (L) vs. CMγ1ζ2 (H)	ratio 2: CMγ1ζ1 (H) vs. CMγ1ζ2 (L)	Mean SILAC ratio	SEM
Transmembrane 9 superfamily member 1	TM9SF1	1,94	1,49	1,72	0,22
Immediate early response 3-interacting protein 1	IER3IP1		1,66	*1,66*	
Protein O-linked-mannose beta-1,2-N-acetylglucosaminyltransferase 1	POMGNT1	1,94	1,27	1,61	0,34
Palmitoyltransferase ZDHHC13;Palmitoyltransferase	ZDHHC13	1,88	1,28	1,58	0,30
Trophoblast glycoprotein	TPBG	1,64	1,44	1,54	0,10
Cytochrome b561 domain-containing protein 2	CYB561D2		1,54	*1,54*	
Transmembrane 9 superfamily member 3	TM9SF3;SMBP	1,69	1,32	1,51	0,18
Endoplasmic reticulum mannosyl-oligosaccharide 1,2-alpha-mannosidase;alpha-1,2-Mannosidase	MAN1B1	1,59	1,42	1,50	0,08
Mannosyl-oligosaccharide 1,2-alpha-mannosidase IB	MAN1A2	1,73	1,25	1,49	0,24
Adipocyte plasma membrane-associated protein	APMAP	1,51	1,45	1,48	0,03
Chondroitin sulfate synthase 2	CHPF	1,49	1,43	1,46	0,03
Protein GPR107	GPR107	1,48	1,44	1,46	0,02
Phosphatidylcholine:ceramide cholinephosphotransferase 1	TMEM23;SGMS1		1,45	*1,45*	
Solute carrier family 35 member E1	SLC35E1	1,35	1,54	1,44	0,10
40S ribosomal protein S8	RPS8	1,68	1,20	1,44	0,24
Protein CASP;Homeobox protein cut-like 1	CUX1;Nbla10317;CUX1-RETc;CUX1-RETa	1,54	1,35	1,44	0,10
Glycosyltransferase 8 domain-containing protein 2	GLT8D2	1,59	1,29	1,44	0,15
Polypeptide N-acetylgalactosaminyltransferase;Polypeptide N-acetylgalactosaminyltransferase 1;Polypeptide N-acetylgalactosaminyltransferase 1 soluble form	GALNT1	1,60	1,27	1,43	0,16
Alpha-1,6-mannosyl-glycoprotein 2-beta-N-acetylglucosaminyltransferase	MGAT2	1,54	1,32	1,43	0,11
Protein YIPF3;Protein YIPF3, 36 kDa form III;Protein YIPF	YIPF3	1,40	1,46	1,43	0,03
UDP-glucuronic acid decarboxylase 1	UXS1	1,61	1,24	1,42	0,18
Alpha-1,3-mannosyl-glycoprotein 2-beta-N-acetylglucosaminyltransferase	MGAT1	1,69	1,14	1,41	0,27
Transmembrane protein 165	TMEM165	1,42	1,40	1,41	0,01
Transmembrane 9 superfamily member 4	TM9SF4	1,64	1,17	1,41	0,23
60S ribosomal protein L21	RPL21	1,60	1,22	1,41	0,19

Table 6: Proteomic Comparison of COPI Vesicles: $CM\gamma_1\zeta_1$ versus $CM\gamma_1\zeta_2$

List of the 25 proteins most enriched in the COPI vesicle made with $CM\gamma_1\zeta_1$ in comparison to $CM\gamma_1\zeta_2$. Vesicles were always reconstituted with Arf1 and GTP. Experiments were in general performed according to Fig. 2.5. Given are gene and protein names of the identified proteins, the SILAC ratios (H/L and L/H) from each replicate, the mean SILAC ratio, and standard error of the mean (SEM). Displayed are the 25 proteins with the highest mean SILAC ratios and the proteins with the highest SILAC ratios during the experiment in which the $CM\gamma_2\zeta_1$ vesicle sample was labeled with heavy isotopes (written in italic in the Mean SILAC ratio column).

Protein.names	Gene.names	ratio 1: CMγ1ζ2 (H) vs. CMγ1ζ1 (L)	ratio 2: CMγ1ζ2 (L) vs. CMγ1ζ1 (H)	Mean SILAC ratio	SEM
Monocarboxylate transporter 1	SLC16A1	6,13	1,37	3,75	2,38
Rab-like protein 3	RABL3	1,71		*1,71*	
Roundabout homolog 1	ROBO1	1,57	1,61	1,59	0,02
Talin-1	TLN1	0,72	2,47	1,59	0,88
Moesin	HEL70;MSN	0,75	2,40	1,58	0,82
Synaptophysin-like protein 1	SYPL1	1,54		*1,54*	
Ezrin;Tyrosine-protein kinase receptor	EZR;HEL-S-105;EZR-ROS1	0,75	2,30	1,53	0,77
Reticulon	RTN3	1,52		*1,52*	
Ras GTPase-activating-like protein IQGAP1	IQGAP1;hCG_1991735	1,52		*1,52*	
Golgi-associated plant pathogenesis-related protein 1	GLIPR2;C9orf19	1,49		*1,49*	
Prolow-density lipoprotein receptor-related protein 1;Low-density lipoprotein receptor-related protein 1 85 kDa subunit;Low-density lipoprotein receptor-related protein 1 515 kDa subunit;Low-density lipoprotein receptor-related protein 1 intracellular domain	LRP1	1,48		*1,48*	
40S ribosomal protein SA	RPSA;LOC388524	1,23	1,72	1,48	0,24
Plexin-B2	PLXNB2	1,27	1,68	1,47	0,20
Tubulin beta chain	TUBB;XTP3TPATP1	0,64	2,29	1,46	0,83
Long-chain-fatty-acid--CoA ligase 3	ACSL3	0,91	2,01	1,46	0,55
B-cell receptor-associated protein 31	BCAP31	1,15	1,75	1,45	0,30
Phosphatidylinositol 4-kinase type 2-alpha	PI4K2A	1,38	1,50	1,44	0,06
Fermitin family homolog 2	PLEKHC1;FERMT2	1,00	1,88	1,44	0,44
Brain acid soluble protein 1	BASP1	0,97	1,90	1,43	0,46
Copper-transporting ATPase 1	ATP7A	1,42		*1,42*	
Coatomer subunit epsilon	COPE	1,41		*1,41*	
Polyadenylate-binding protein;Polyadenylate-binding protein 1	PABPC1	1,20	1,61	1,41	0,20
Pyruvate kinase;Pyruvate kinase PKM	HEL-S-30;PKM;PKM2	0,96	1,85	1,40	0,44
Heterogeneous nuclear ribonucleoprotein M	HNRNPM;ORF;HNRPM	1,37	1,43	1,40	0,03
60S ribosomal protein L18	RPL18	1,40		*1,40*	

Table 7: Proteomic Comparison of COPI Vesicles: $CM\gamma_1\zeta_2$ versus $CM\gamma_1\zeta_2$

List of the 25 proteins most enriched in the COPI vesicle made with $CM\gamma_1\zeta_2$ in comparison to $CM\gamma_1\zeta_1$. Vesicles were always reconstituted with Arf1 and GTP. Experiments were in general performed according to Fig. 2.5. Given are gene and protein names of the identified proteins, the SILAC ratios (H/L and L/H) from each replicate, the mean SILAC ratio, and standard error of the mean (SEM). Displayed are the 25 proteins with the highest mean SILAC ratios and the proteins with the highest SILAC ratios during the experiment in which the $CM\gamma_2\zeta_1$ vesicle sample was labeled with heavy isotopes (written in italic in the Mean SILAC ratio column).

Since the COPI coat, unlike the COPII or CCV coat, does not have an outer scaffold layer but is recruited *en bloc*, the size of a vesicle likely is dictated by coatomer. Therefore, we decided to investigate a putative role of CM isoforms in controlling the size of COPI vesicles. To this end, a set of pre-existing negative stain EM images of isotypic COPI vesicles prepared from rat liver Golgi was systematically analyzed. The image quality for all samples was comparable, as can be seen from the examples shown in figure 2.11A-D. In addition to isotypic vesicles (Fig. 2.11B-D), vesicles prepared with rat coatomer (Fig. 2.11A), which represents a physiological mixture of the isoforms, was included in the analysis.

To determine the size of vesicles, we used a semi-automated segmentation approach, which is described in detail in the Methods section. Figure 2.11E shows an example of the vesicle areas that are recognized by the software marked in light green color. The extracted areas, without an overlay of the original EM image are highlighted in Fig. 2.11F. From these areas, the mean diameters of isotypic and rat CM vesicles were calculated (Fig. 2.11G). The mean diameter of all four vesicle types was almost identical, ranging from 73.4 nm to 74.4 nm. Also the standard deviations (SD) were in the same range between 7.7 and 8.9 nm (Fig. 2.11G).

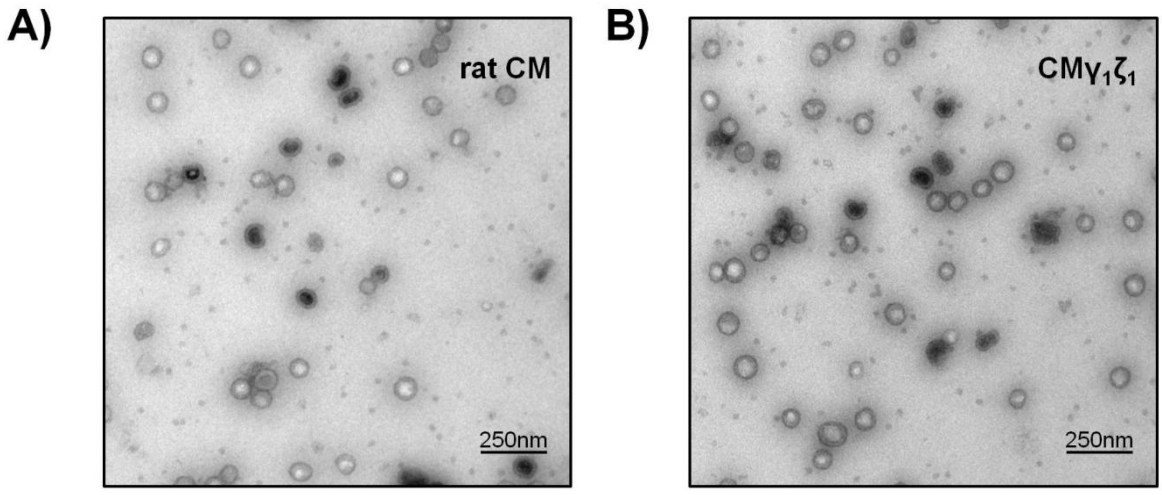

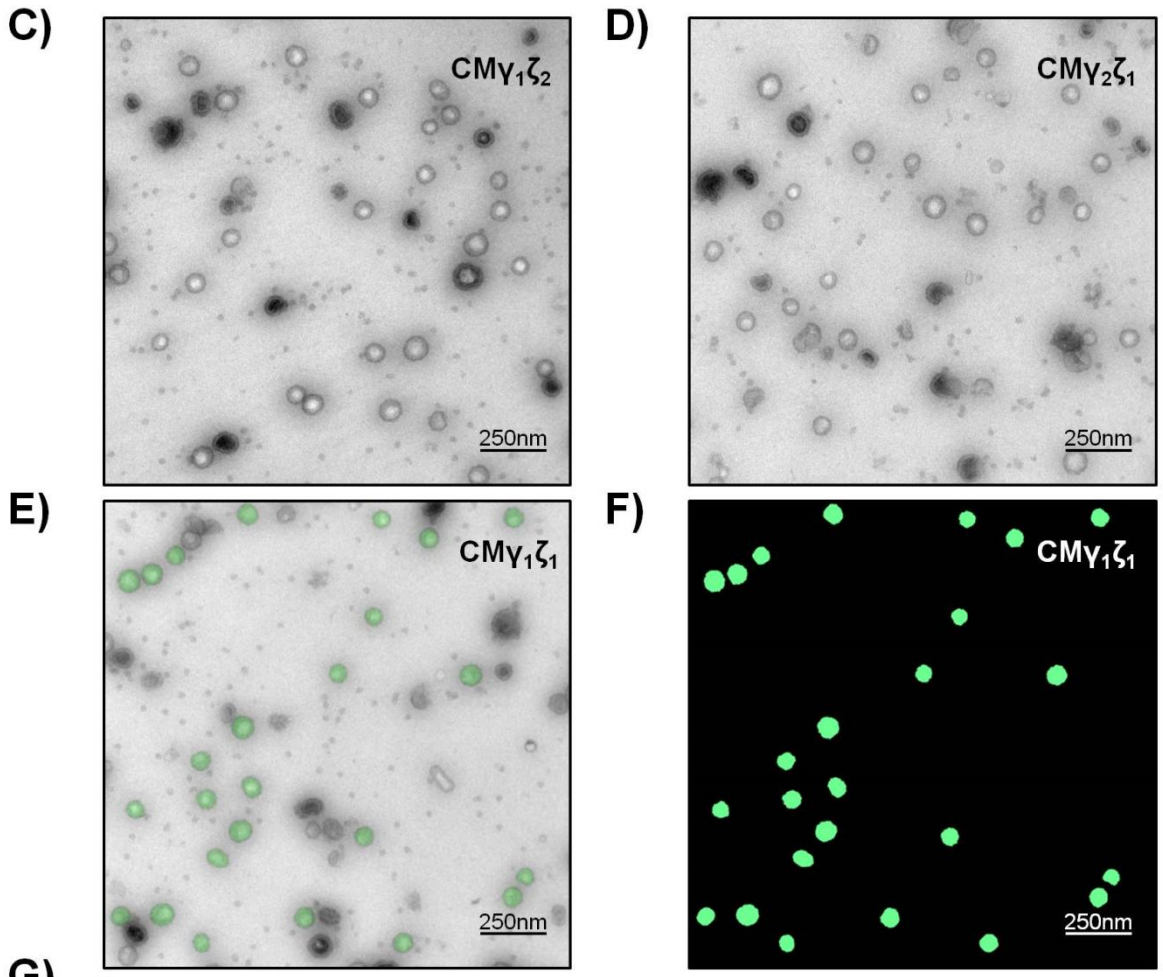

G)

	rat CM	CMγ1ζ1	CMγ1ζ2	CMγ2ζ1
Ø Diameter [nm]	73,8	74,4	74,2	73,4
SD [nm]	7,7	8,9	8,6	8,8
n	78	111	97	79

Figure 2.11 Size Comparison of Isotypic COPI Vesicles

(A-D) Representative negative stain EM images of COPI vesicles reconstituted from rat liver Golgi with either a single CM isoform or an endogenous mixture (rat CM). (E) Example of software-based vesicle area recognition. The areas recognized are colored light green. (F) Picture highlighting the areas recognized in (E) without overlay of the original EM image. (G) Summary of the vesicle size determination. Mean diameters, standard deviations (SD), and sample sizes are given.

2.4 Influence of Arf Isoforms on COPI Vesicle Biogenesis

As pointed out in the Introduction (1.3.3.), coatomer is not the only COPI biogenesis factor which exists as various isotypes. There are in total six isoforms of Arf, five of which are present in humans. In a previous study, performed in our lab, these five isoforms have been studied with regard to their ability to participate in COPI vesicle biogenesis (Popoff et al., 2011b). All human Arfs, except Arf6

were shown to be able to form COPI vesicles from rat liver Golgi. In order to investigate a possible role of the small GTPases in cargo sorting, all isoforms were cloned into a new plasmid so to be able to express them according to our latest, highly efficient expression protocol used for Arf1 (see Materials and Methods). Figure 2.12A shows a Coomassie-stained SDS gel with all five human Arf isoforms. As can be seen, all proteins could be purified with a low level of contaminating proteins. Moreover, for all Arfs only one distinct band can be observed which argues for a high degree of myristoylation of the proteins (Fig. 2.12A). This is further confirmed by the fact that in initial reconstitution experiments with SIC all isoforms except for Arf6 were able to produce COPI vesicles as deduced from the strongly increased GTP-dependent release of marker proteins ERGIC53 and p24 (Fig. 2.12B). Noteworthy, Arf3 seemed to be less capable of producing vesicles compared to all other Arf isoforms (Fig. 2.12B).

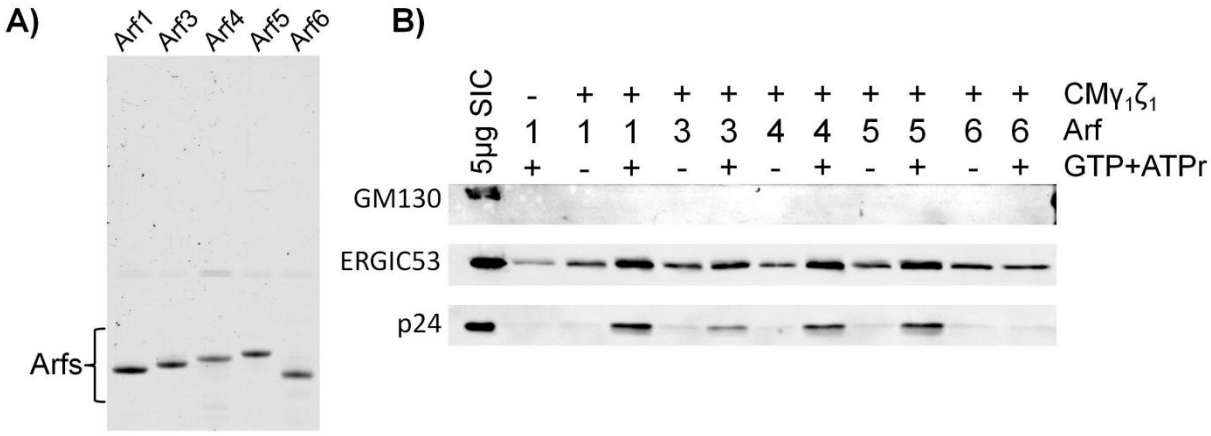

Figure 2.12 Recombinant Arf Isoforms: Ability to Form COPI Vesicles

(A) Coomassie-stained SDS gel loaded with recombinant Arf isoforms. (B) Representative Western blot analysis of a COPI vesicles reconstituted from SIC HeLa using recombinant CM, Arf1 isoforms, GTP, and ATP regenerating system (ATPr) with 5 µg of SIC loaded as input. Samples were probed for the presence of the proteins on the left. Vesicles were isolated via differential centrifugation.

In order to obtain a deeper insight into the protein content of COPI vesicles formed with the different isoforms of Arf, the vesicle proteomics workflow outlined in section 2.1 was employed. Vesicles were produced from heavy and light semi-intact HeLa cells and compared to a light or heavy mock reaction lacking only coatomer. As can be told from the scatter plots of these experiments, presented in figure 2.13A-C, highly correlative datasets could be obtained in all six experiments (Fig. 2.13A-C). This is reflected by high R^2 values of 0.87, 0.89, and 0.81 for experiments with Arf3, Arf4, and Arf5, respectively. Also here, some of the highest scoring proteins are highlighted with color. Several members of the p24/TMED family, nucleobindin 1, and ER cycling proteins ERGIC53 and ERGIC2/3 are among the proteins with the highest SILAC ratios. Moreover, the proteins YIF1A and ERP44, both

of which are also ~sixfold enriched in the COPI proteome obtained with Arf1, exhibit high SILAC scores (Fig. 2.13A-C).

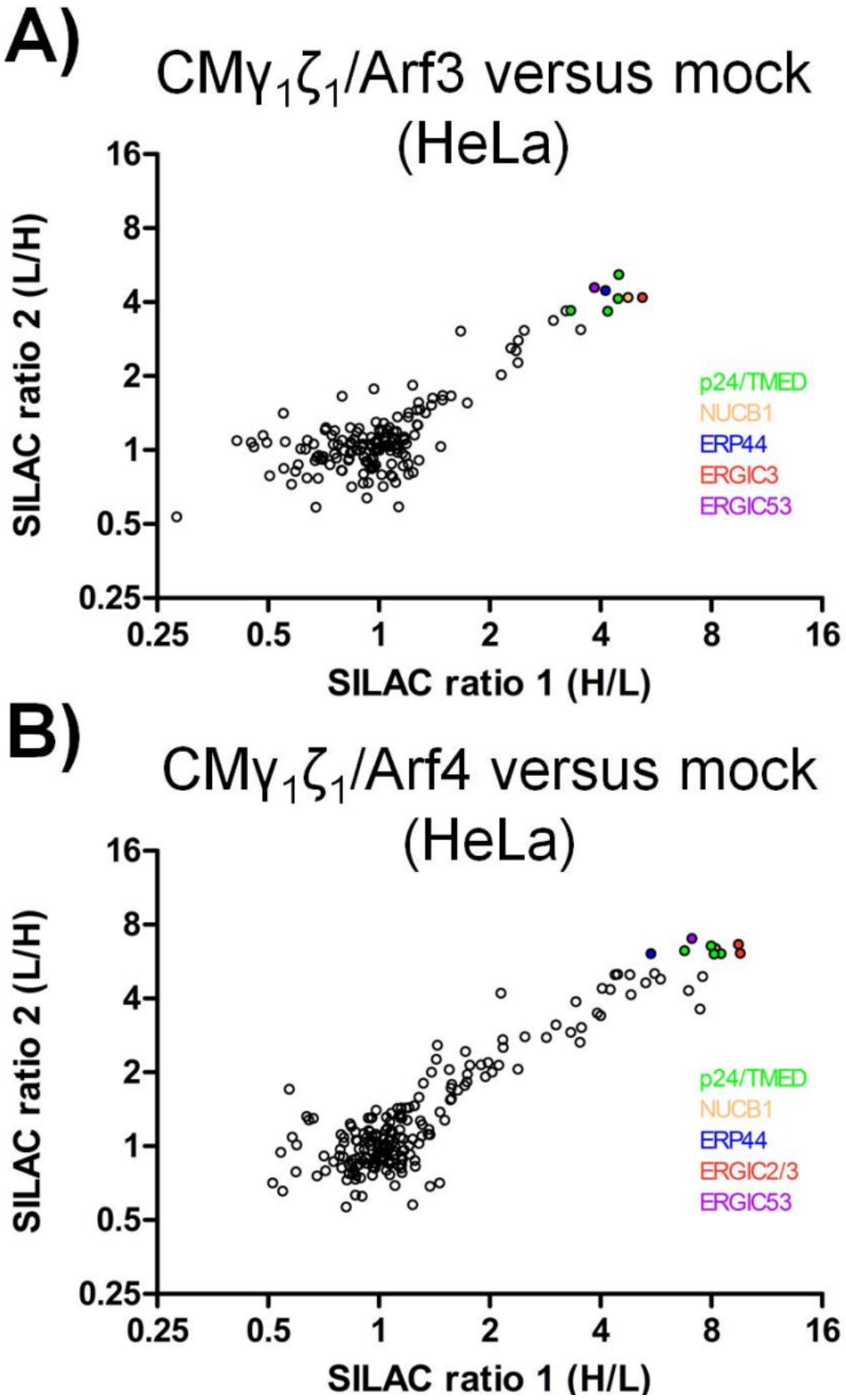

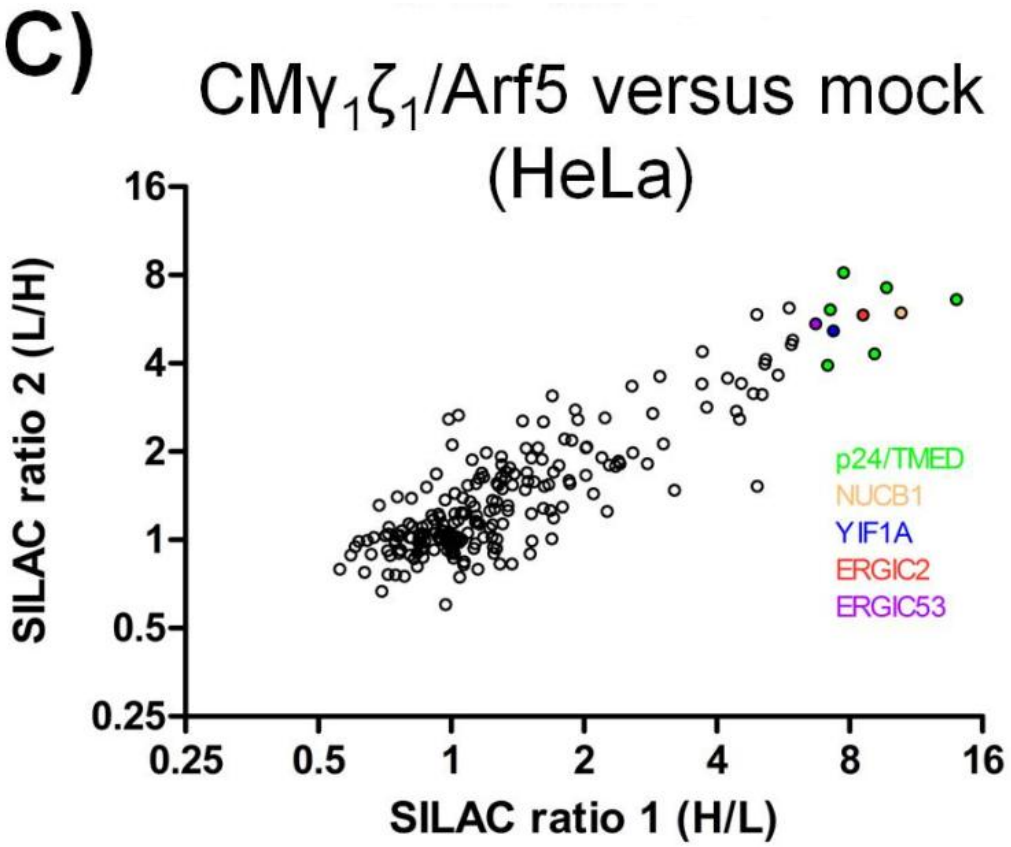

Figure 2.13 The Proteome of COPI Vesicles Made with Different Isoforms of Arf

(A-C) Scatter plot of SILAC ratios obtained from two independent experiments performed according to figure 2.5, with various isoforms of Arf, as indicated above the plots. Experiments were performed with switched labels. Contaminants were removed from the datasets. Some proteins/protein families are highlighted in color. R^2 values of the datasets are 0.87 (A), 0.89 (B), and 0.81 (C).

A comparison of the scatter plot in Fig. 2.6 and the plots shown in figure 2.13 reveals that less peptides and therefore proteins could be identified during the LC-MS runs of COPI samples obtained with Arf4 and Arf5, least with Arf3. Hence, less proteins fulfill the criterion of being twofold enriched in either sample, or the sample in which the vesicle fraction carried the isotope label. These criteria are met by only 25 proteins of the Arf3 datasets, 50 proteins in the datasets obtained with Arf4, and 55 proteins in the datasets produced with Arf5. The vast majority of these proteins are found among the 122 best COPI proteome candidates mentioned earlier. The strong overlap between all COPI proteomic datasets obtained for different Arf isoforms is visualized by the Venn diagram shown in figure 2.14A. Except for eight candidates, all others appear in multiple datasets. Twenty candidates are shared between all four datasets, and they are listed in Fig. 2.14B. Among those candidates are five members of the p24/TMED, ER-Golgi cycling proteins such as ERGIC1 and 2, ERGIC53/LMAN1, or SURF4 and GOLT1B. Also NUCB1 and the SNAREs Sec22b and Stx5 are universally found (Fig. 2.14B).

A)

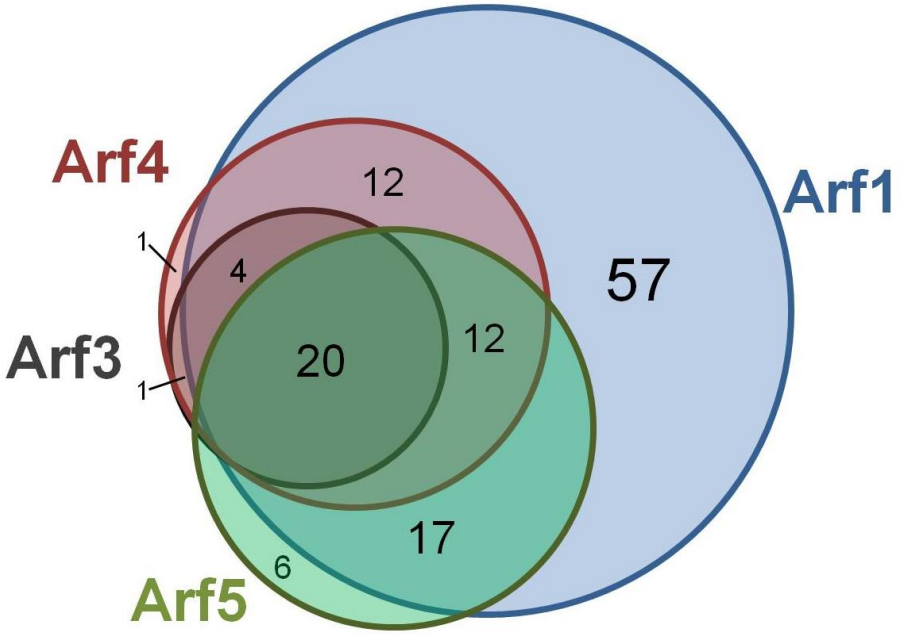

B)

Protein.names	Gene.names
Clusterin;Clusterin beta chain;Clusterin alpha chain;Clusterin	CLU
Endoplasmic reticulum-Golgi intermediate compartment protein 1	ERGIC1
Endoplasmic reticulum-Golgi intermediate compartment protein 2	ERGIC2
Endoplasmic reticulum resident protein 44	ERP44
Vesicle transport protein GOT1B	GOLT1B
Protein ERGIC-53	LMAN1
Vesicular integral-membrane protein VIP36	LMAN2
Nucleobindin-1	NUCB1
Ras-related protein Rab-18	RAB18
Vesicle-trafficking protein SEC22b	SEC22B
Solute carrier family 35 member E1	SLC35E1
Syntaxin-5	STX5
Surfeit locus protein 4	SURF4
Transmembrane emp24 domain-containing protein 10	TMED10
Transmembrane emp24 domain-containing protein 2	TMED2
Transmembrane emp24 domain-containing protein 4	TMED4
Transmembrane emp24 domain-containing protein 7	TMED7
Transmembrane emp24 domain-containing protein 9	TMED9
Protein YIF1B	YIF1B
Zinc finger protein-like 1	ZFPL1

Figure 2.14 Proteomic Comparison of COPI Reconstituted with Different Arf Isoforms

(A) Venn diagram to visualized the overlap of proteins found twofold enriched in COPI proteomic datasets obtained with different isoforms of Arf. Numbers indicate the number of proteins shared between the various datasets. (B) List of the 20 proteins that fulfill the COPI candidate criteria in all four datasets. Given are full protein and gene names.

In the following tables 8-10 (Arf3, Arf4, Arf5) all candidates which are compared in the Venn diagram of Fig. 2.14A are listed more thoroughly.

Protein.names	Gene.names	ratio 1 (H/L)	ratio 2 (L/H)	Mean SILAC ratio	SEM
Transmembrane emp24 domain-containing protein 9	TMED9	4,48	5,19	4,84	0,35
Endoplasmic reticulum-Golgi intermediate compartment protein 3	ERGIC3	5,19	4,17	4,68	0,51
Nucleobindin-1	NUCB1	4,75	4,17	4,46	0,29
Transmembrane emp24 domain-containing protein 10	TMED10	4,47	4,13	4,30	0,17
Endoplasmic reticulum resident protein 44	ERP44	4,12	4,46	4,29	0,17
Protein ERGIC-53	LMAN1	3,85	4,59	4,22	0,37
Transmembrane emp24 domain-containing protein 2	RNP24;TMED2	4,19	3,67	3,93	0,26
Transmembrane emp24 domain-containing protein 4	TMED4	3,32	3,70	3,51	0,19
Transmembrane emp24 domain-containing protein 7	TMED7;TMED7-TICAM2	3,46		*3,46*	
Vesicular integral-membrane protein VIP36	LMAN2	3,22	3,68	3,45	0,23
Surfeit locus protein 4	SURF4	3,54	3,09	3,31	0,23
Vesicle-trafficking protein SEC22b	SEC22B	2,98	3,37	3,17	0,19
Endoplasmic reticulum-Golgi intermediate compartment protein 2	ERGIC2	2,82		*2,82*	
Solute carrier family 35 member E1	SLC35E1	2,48	3,07	2,78	0,29
Zinc transporter 7	SLC30A7	2,72		*2,72*	
Vesicle transport protein GOT1B	GOLT1B	2,39	2,80	2,59	0,20
Immediate early response 3-interacting protein 1	IER3IP1	2,53		*2,53*	
Protein cornichon homolog 4	CNIH4	2,51		*2,51*	
Protein YIF1B	YIF1B	2,36	2,54	2,45	0,09
Syntaxin-5	STX5;STX5A	2,28	2,60	2,44	0,16
Clusterin;Clusterin beta chain;Clusterin alpha chain;Clusterin	CLU	1,67	3,05	2,36	0,69
Endoplasmic reticulum-Golgi intermediate compartment protein 1	ERGIC1	2,38	2,27	2,33	0,06
Ras-related protein Rab-18	RAB18	2,15	2,03	2,09	0,06
Zinc finger protein-like 1	ZFPL1	2,04		*2,04*	
PRA1 family protein 2	PRAF2	2,01		*2,01*	

Table 8: Candidate Proteins for the Core Proteome of COPI Vesicles Reconstituted with Arf3

List of candidates for the COPI core proteome from HeLa cells as determined by two independent experiments performed according to Fig. 2.5. CM$\gamma_1\zeta_1$, Arf3, and GTP were used for all reconstitutions. Given are gene and protein names of the identified proteins, the SILAC ratios (H/L or L/H) from each experiment, the mean SILAC ratio, and standard error of the mean (SEM). Displayed are protein with mean SILAC ratios >2 or with a SILAC ratio >2 in one of the two experiments in which the vesicle sample was labeled with heavy isotopes (written in italic in the Mean SILAC ratio column).

Protein.names	Gene.names	ratio 1 (H/L)	ratio 2 (L/H)	Mean SILAC ratio	SEM
Endoplasmic reticulum-Golgi intermediate compartment protein 3	ERGIC3	9,48	6,64	8,06	1,42
Endoplasmic reticulum-Golgi intermediate compartment protein 2	ERGIC2	9,59	6,11	7,85	1,74
Zinc transporter 7	SLC30A7	7,65		*7,65*	
Nucleobindin-1	NUCB1	8,22	6,39	7,31	0,92
Transmembrane emp24 domain-containing protein 7	TMED7;TMED7-TICAM2	8,50	6,10	7,30	1,20
Transmembrane emp24 domain-containing protein 10	TMED10	8,00	6,55	7,27	0,73
Transmembrane emp24 domain-containing protein 9	TMED9	8,14	6,08	7,11	1,03
Protein ERGIC-53	LMAN1	7,09	7,02	7,06	0,03
Zinc finger protein-like 1	ZFPL1	6,85		*6,85*	
Transmembrane emp24 domain-containing protein 4	TMED4	6,77	6,28	6,52	0,25
Solute carrier family 35 member E1	SLC35E1	7,59	4,91	6,25	1,34
Calumenin	CALU	5,83		*5,83*	
Endoplasmic reticulum resident protein 44	ERP44	5,48	6,09	5,79	0,30
Transmembrane emp24 domain-containing protein 2	RNP24;TMED2	6,94	4,30	5,62	1,32
Transmembrane emp24 domain-containing protein 1	TMED1	7,45	3,62	5,54	1,92
Vesicular integral-membrane protein VIP36	LMAN2	5,61	5,05	5,33	0,28
Protein YIF1A	YIF1A	5,82	4,79	5,31	0,51
Protein cornichon homolog 4	CNIH4	5,05		*5,05*	
Protein RER1	RER1	5,31	4,63	4,97	0,34
Protein YIPF;Protein YIPF5	YIPF5	4,81	5,00	4,91	0,10
Surfeit locus protein 4	SURF4	4,45	5,02	4,74	0,28
VIP36-like protein	LMAN2L	4,71		*4,71*	
Nucleobindin-2;Nesfatin-1	HEL-S-109;NUCB2;Nucb2	4,38	5,00	4,69	0,31
Vesicle-trafficking protein SEC22b	SEC22B	4,84	4,15	4,50	0,35
Clusterin;Clusterin beta chain;Clusterin alpha chain;Clusterin	CLU	4,25	4,35	4,30	0,05
Vesicle transport protein GOT1B	GOLT1B	4,04	4,40	4,22	0,18
Protein kish-A	TMEM167A	3,97		*3,97*	
Transmembrane emp24 domain-containing protein 3	TMED3	3,92		*3,92*	
BET1 homolog	BET1;DKFZp781C0425	3,83		*3,83*	
Immediate early response 3-interacting protein 1	IER3IP1	4,01	3,41	3,71	0,30
Protein YIF1B	YIF1B	3,92	3,49	3,70	0,22
Endoplasmic reticulum-Golgi intermediate compartment protein 1	ERGIC1	3,43	3,88	3,66	0,23
Serpin H1	SERPINH1	3,55	3,05	3,30	0,25
Golgi SNAP receptor complex member 2	GOSR2	2,15	4,20	3,18	1,03
PRA1 family protein 2	PRAF2	3,17		*3,17*	
45 kDa calcium-binding protein	SDF4	3,32	2,92	3,12	0,20
ER lumen protein-retaining receptor;ER lumen protein-retaining receptor 2	KDELR2	3,52	2,65	3,08	0,43
Syntaxin-5	STX5;STX5A	3,03	3,12	3,07	0,05

Protein.names	Gene.names	ratio 1 (H/L)	ratio 2 (L/H)	Mean SILAC ratio	SEM
Ras-related protein Rab-18	RAB18	2,85	2,78	2,81	0,04
Ras-related protein Rab-2A	RAB2;RAB2A	2,49	2,79	2,64	0,15
Transmembrane 9 superfamily member 3	TM9SF3;SMBP	2,17	2,71	2,44	0,27
Neutral alpha-glucosidase AB	HEL-S-164nA;GANAB	2,18	2,53	2,35	0,17
Galactosylgalactosylxylosylprotein 3-beta-glucuronosyltransferase 3	B3GAT3	2,30		*2,30*	
Protein YIPF4	YIPF4	2,39	2,06	2,22	0,16
Peptidyl-prolyl cis-trans isomerase;Peptidyl-prolyl cis-trans isomerase B	HEL-S-39;PPIB	2,12	2,14	2,13	0,01
ER lumen protein-retaining receptor 1;ER lumen protein-retaining receptor	KDELR1	1,98	2,19	2,09	0,11
Protein YIPF3;Protein YIPF3, 36 kDa form III;Protein YIPF	YIPF3	1,72	2,43	2,07	0,36
Ras-related protein Rab-1A	RAB1A	1,90	2,15	2,02	0,13
Polypeptide N-acetylgalactosaminyltransferase;Polypeptide N-acetylgalactosaminyltransferase 1;Polypeptide N-acetylgalactosaminyltransferase 1 soluble form	GALNT1	2,03	2,00	2,01	0,01
Endoplasmin	TRA1;HEL-S-125m;HSP90B1	1,44	2,58	2,01	0,57

Table 9: Candidate Proteins for the Core Proteome of COPI Vesicles Reconstituted with Arf4

List of candidates for the COPI core proteome from HeLa cells as determined by two independent experiments performed according to Fig. 2.5. CM$\gamma_1\zeta_1$, Arf4, and GTP were used for all reconstitutions. Given are gene and protein names of the identified proteins, the SILAC ratios (H/L or L/H) from each experiment, the mean SILAC ratio, and standard error of the mean (SEM). Displayed are protein with mean SILAC ratios >2 or with a SILAC ratio >2 in one of the two experiments in which the vesicle sample was labeled with heavy isotopes (written in italic in the Mean SILAC ratio column).

Protein.names	Gene.names	ratio 1 (H/L)	ratio 2 (L/H)	Mean SILAC ratio	SEM
Transmembrane emp24 domain-containing protein 7	TMED7;TMED7-TICAM2	13,99	6,61	10,30	3,69
Zinc finger protein-like 1	ZFPL1	9,32		*9,32*	
Transmembrane emp24 domain-containing protein 10	TMED10	9,70	7,24	8,47	1,23
Nucleobindin-1	NUCB1	10,47	5,96	8,21	2,26
Transmembrane emp24 domain-containing protein 9	TMED9	7,76	8,16	7,96	0,20
Endoplasmic reticulum-Golgi intermediate compartment protein 2	ERGIC2	8,59	5,85	7,22	1,37
Transmembrane emp24 domain-containing protein 2	RNP24;TMED2	9,12	4,31	6,72	2,40
Transmembrane emp24 domain-containing protein 4	TMED4	7,24	6,10	6,67	0,57
Protein YIF1A	YIF1A	7,36	5,17	6,26	1,10
Protein ERGIC-53	LMAN1	6,71	5,45	6,08	0,63
Transmembrane 9 superfamily member 3	TM9SF3;SMBP	5,83	6,18	6,00	0,17
Transmembrane emp24 domain-containing protein 1	TMED1	7,13	3,93	5,53	1,60
45 kDa calcium-binding protein	SDF4	4,93	5,86	5,39	0,46
Vesicular integral-membrane protein VIP36	LMAN2	5,94	4,80	5,37	0,57

Protein.names	Gene.names	ratio 1 (H/L)	ratio 2 (L/H)	Mean SILAC ratio	SEM
Endoplasmic reticulum resident protein 44	ERP44	5,91	4,64	5,27	0,64
Vesicle-trafficking protein SEC22b	SEC22B	5,17	4,12	4,64	0,52
Solute carrier family 35 member E1	SLC35E1	4,62		*4,62*	
Protein YIPF;Protein YIPF5	YIPF5	5,51	3,65	4,58	0,93
Surfeit locus protein 4	SURF4	5,14	3,97	4,56	0,58
Endoplasmic reticulum-Golgi intermediate compartment protein 1	ERGIC1	5,07	3,14	4,10	0,97
Nucleobindin-2;Nesfatin-1	HEL-S-109;NUCB2;Nucb2	3,71	4,38	4,05	0,33
Polypeptide N-acetylgalactosaminyltransferase;Polypeptide N-acetylgalactosaminyltransferase 1;Polypeptide N-acetylgalactosaminyltransferase 1 soluble form	GALNT1	4,84	3,16	4,00	0,84
Clusterin;Clusterin beta chain;Clusterin alpha chain;Clusterin	CLU	4,55	3,41	3,98	0,57
Vesicle transport protein GOT1B	GOLT1B	4,23	3,56	3,89	0,34
Protein YIF1B	YIF1B	4,43	2,75	3,59	0,84
Golgi integral membrane protein 4	GOLIM4	3,70	3,40	3,55	0,15
Serpin H1	SERPINH1	4,50	2,58	3,54	0,96
Emerin	EMD	3,33		*3,33*	
Peptidyl-prolyl cis-trans isomerase;Peptidyl-prolyl cis-trans isomerase B	HEL-S-39;PPIB	3,80	2,83	3,32	0,48
UbiA prenyltransferase domain-containing protein 1	UBIAD1	3,31		*3,31*	
Alpha-1,3-mannosyl-glycoprotein 2-beta-N-acetylglucosaminyltransferase	MGAT1	2,97	3,61	3,29	0,32
Protein YIPF3;Protein YIPF3, 36 kDa form III;Protein YIPF	YIPF3	2,57	3,35	2,96	0,39
Polypeptide N-acetylgalactosaminyltransferase 10;Polypeptide N-acetylgalactosaminyltransferase	GALNT10	2,84		*2,84*	
Probable glutathione peroxidase 8	GPX8	2,87	2,70	2,78	0,09
Protein RER1	RER1	2,67		*2,67*	
Transmembrane 9 superfamily member 1	TM9SF1	3,03	2,12	2,58	0,45
Alpha-mannosidase 2;Alpha-mannosidase	MAN2A1	2,23	2,61	2,42	0,19
Thioredoxin domain-containing protein 5	hCG_1811539;TXNDC5;STRF8;DKFZp666I134	1,70	3,10	2,40	0,70
Golgi SNAP receptor complex member 1	GOSR1	3,21	1,48	2,34	0,87
Alpha-1,6-mannosyl-glycoprotein 2-beta-N-acetylglucosaminyltransferase	MGAT2	1,91	2,77	2,34	0,43
Ras-related protein Rab-18	RAB18	2,79	1,82	2,30	0,49
Calcium-transporting ATPase;Calcium-transporting ATPase type 2C member 1	ATP2C1	2,58	1,98	2,28	0,30
78 kDa glucose-regulated protein	HEL-S-89n;HSPA5	1,94	2,57	2,25	0,32
Transmembrane 9 superfamily member 4	TM9SF4	2,40	1,85	2,13	0,27
Golgin subfamily B member 1	GOLGB1	2,41	1,82	2,12	0,30
Polypeptide N-acetylgalactosaminyltransferase 2;Polypeptide N-acetylgalactosaminyltransferase 2 soluble form;Polypeptide N-acetylgalactosaminyltransferase	GALNT2	2,36	1,78	2,07	0,29

Protein.names	Gene.names	ratio 1 (H/L)	ratio 2 (L/H)	Mean SILAC ratio	SEM
Protein disulfide-isomerase A6	PDIA6	1,62	2,52	2,07	0,45
Ras-related protein Rab-2A	RAB2;RAB2A	2,20	1,91	2,05	0,14
60S ribosomal protein L13	RPL13	2,03	2,07	2,05	0,02
Ras-related protein Rab-6B	RAB6A;RAB6B	2,02	2,06	2,04	0,02
N-acetylgalactosaminyltransferase 7	GALNT7	2,28	1,80	2,04	0,24
Syntaxin-5	STX5;STX5A	1,88	2,18	2,03	0,15
Inositol monophosphatase 3	IMPAD1	2,02		*2,02*	
Golgi membrane protein 1	GOLPH2;GOLM1	1,81	2,21	2,01	0,20
60S ribosomal protein L18	RPL18	1,45	2,54	2,00	0,54

Table 10: Candidate Proteins for the Core Proteome of COPI Vesicles Reconstituted with Arf5

List of candidates for the COPI core proteome from HeLa cells as determined by two independent experiments performed according to Fig. 2.5. CM$\gamma_1\zeta_1$, Arf5, and GTP were used for all reconstitutions. Given are gene and protein names of the identified proteins, the SILAC ratios (H/L or L/H) from each experiment, the mean SILAC ratio, and standard error of the mean (SEM). Displayed are protein with mean SILAC ratios >2 or with a SILAC ratio >2 in one of the two experiments in which the vesicle sample was labeled with heavy isotopes (written in italic in the Mean SILAC ratio column).

2.5 The COPI Core Proteome of HepG2 Cells and Murine Macrophages

Cells of higher organisms are often highly specialized. In order to fulfill a particular function the morphology, metabolic activity, protein and lipid composition can deviate strongly between different cell types. Hence, after having established a robust COPI proteomics workflow with HeLa cells, we decided to apply our strategy to other, specialized cell types. This was done in order to investigate whether the cell type specialization is reflected by a divergent composition of COPI vesicles. As additional specialized cell types, hepatocellular carcinoma HepG2 cells and immortalized murine macrophages (iMΦ) were chosen, as both of them differ functionally from one another and from HeLa cells. As for HeLa cells, vesicles were produced from unlabeled and labeled HepG2 cells and iMΦ in parallel to a mock reaction without CM. Two experiments, performed with switched labels gave rise to the scatter plots shown in figure 2.15. In all four experiments an average of roughly 3500 peptides and ~600-700 proteins could be identified, which is in the range of what has been previously obtained for experiments with HeLa cells. The correlation of the two experiments with HepG2 cells, which result in an R^2 value of 0.61, was lower than in the same experiment performed with HeLa cells(R^2=0.7) and iMΦ (R^2=0.79), but still decent. Noteworthy, the SILAC ratios obtained from experiments with HepG2 were on average lower compared to both HeLa cells and murine macrophages (compare Fig. 2.15A with Fig. 2.15B and Fig. 2.6).

Some of the highest scoring proteins are highlighted with coloring in the scatter plots of figure 2.15. Again, multiple members of the p24/TMED protein family and nucleobindin 1/2 are amongst the candidates with the highest SILAC ratios. Moreover, the cis-Golgi protein ZFPL1 as well as several solute carrier proteins (SLCs) exhibit high ratios. Apart from the zinc transporters SLC30A5/6 highlighted in the scatter blots of HeLa (Fig. 2.6) and iMΦ (Fig. 2.15B), the putative transporter with undefined substrate SLC35E1 and the putative sodium-coupled neutral amino acid transporter 10 (SLC38A10) show strong enrichment in the COPI vesicle samples. Furthermore, the ER-retrieval receptor RER1 and the nonaspanin family member TM9SF3 in case of HepG2 (Fig. 2.15A) and the glycosyltransferase GALNT1 as well as the Sulfhydryl oxidase 2 (QSOX2) in the iMΦ datasets (Fig. 2.15B) are among the highest scoring proteins.

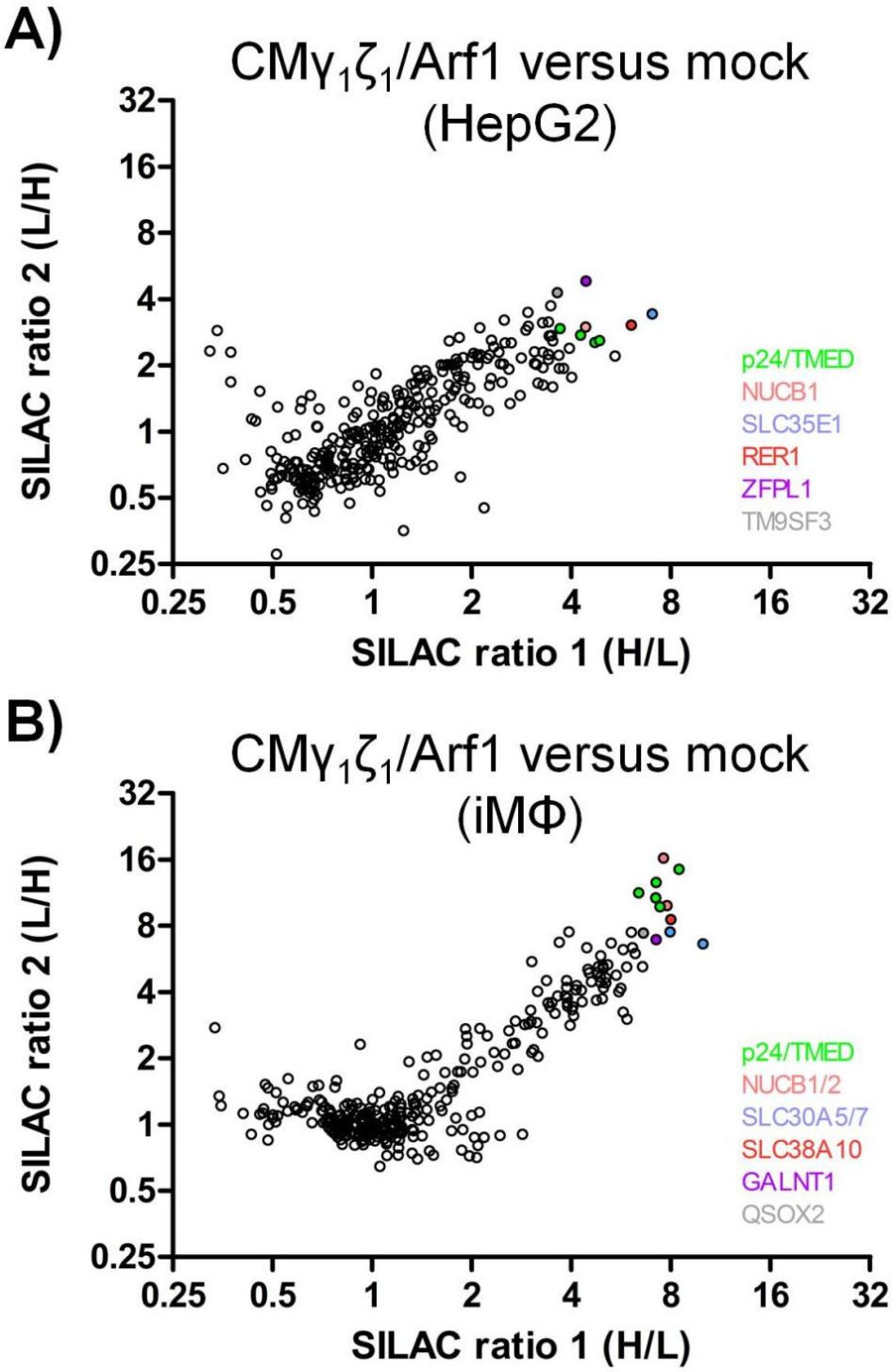

Figure 2.15 The COPI Proteome of HepG2 Cells and Immortalized Murine Macrophages (iMΦ)

(A-B) Scatter plot of SILAC ratios obtained from two independent experiments performed according to figure 2.5 using either SIC HepG2 cells (A) or iMΦ (B) as donor membranes. Experiments were performed with switched labels. Contaminants were removed from the datasets. Some proteins/protein families are highlighted in color. R^2 values of the datasets are 0.61 (A) and 0.79 (B).

From a more general perspective, 69 proteins found in the HepG2 datasets and 144 proteins identified in the iMΦ COPI proteomic experiments fulfill the criteria of twofold enrichment in both

samples or the heavy vesicle sample that had led to our candidate list of the HeLa cell COPI proteome of 122 proteins (see 2.1). A comparison of the COPI proteome candidates from all three tested cell lines is display in the Venn diagram of Fig. 2.16A. A total of 39 proteins is found in all three datasets and listed in Fig. 2.16B. In addition to these ubiquitously identified proteins, 44 proteins are found in two of the three datasets. Due to the great overlap between the datasets, only five of the 69 candidates are uniquely found in the HepG2 COPI proteome. The number of proteins unique to HeLa, HepG2, or iMΦ scales with the total number of candidate proteins identified for the respective cell line. Hence, roughly one third of the HeLa cell COPI proteome candidates (46 proteins) and slightly more than half of the candidates for iMΦ (79 proteins) are found exclusively on the lists of candidates for either cell line.

The list of candidates shared between all three cell lines (Fig. 2.16B) is particularly enriched in ER-Golgi cycling proteins e.g. six members of the p24/TMED family, ERGIC1/2/3, RER1, SURF4, ERGIC53, and KDEL receptor 1. Also ubiquitously found are proteins that serve glycosylation, e.g. B3GAT3, CHST14, MAN1A2, MGAT2, or POMGNT1 (Fig. 2.16B). Furthermore, the ER-Golgi SNAREs Sec22b and Stx5 as well as other proteins implicated in vesicle targeting and fusion (e.g. Rab18, YIPF3, ZFPL1) were found alongside several transporters for calcium (ATP2C1), zinc (SLC30A6/7), or of unknown substrate (SLC35E1). These candidates likely constitute the core machinery of a COPI vesicle.

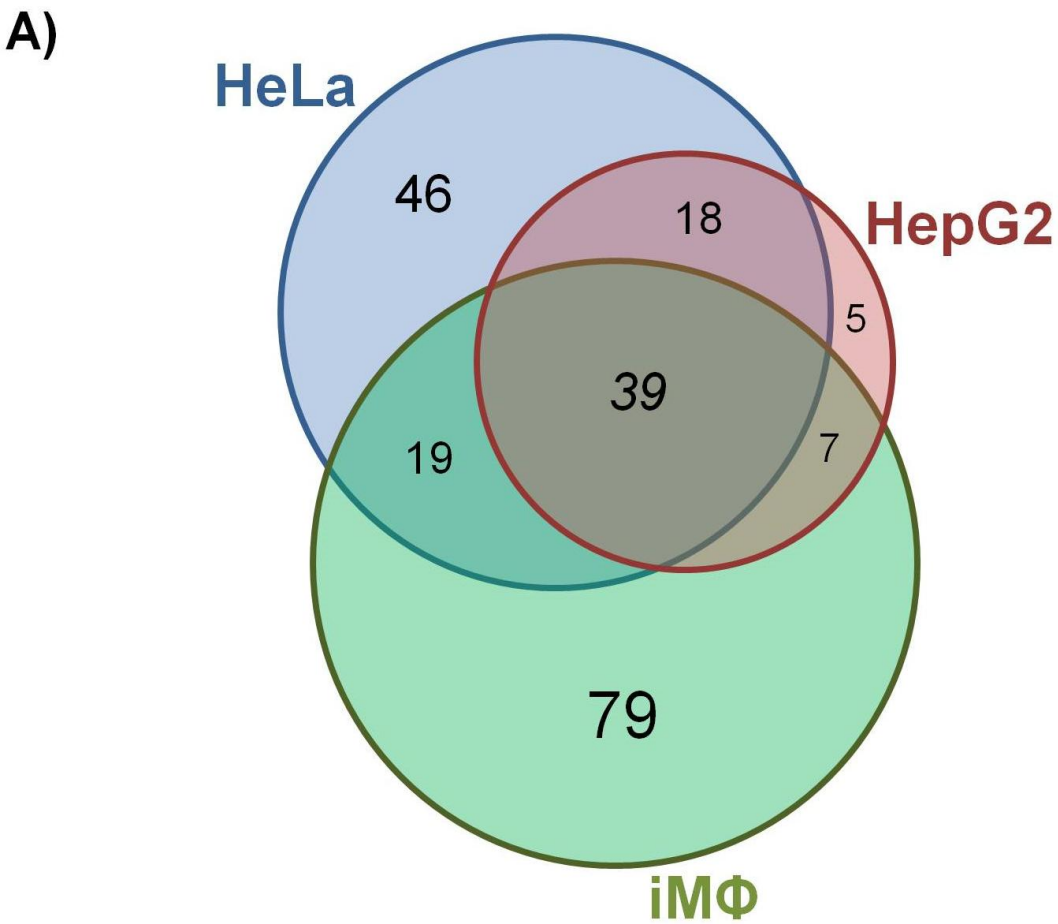

B)

Protein.names	Gene.names
Calcium-transporting ATPase;Calcium-transporting ATPase type 2C member 1	ATP2C1
Galactosylgalactosylxylosylprotein 3-beta-glucuronosyltransferase 3	B3GAT3
Carbohydrate sulfotransferase 14	CHST14
Protein CASP;Homeobox protein cut-like 1	CUX1
Endoplasmic reticulum-Golgi intermediate compartment protein 1	ERGIC1
Endoplasmic reticulum-Golgi intermediate compartment protein 2	ERGIC2
Endoplasmic reticulum-Golgi intermediate compartment protein 3	ERGIC3
Endoplasmic reticulum resident protein 44	ERP44
Polypeptide N-acetylgalactosaminyltransferase 1	GALNT1
Golgin subfamily A member 5	GOLGA5
ER lumen protein-retaining receptor 1;ER lumen protein-retaining receptor	KDELR1
Protein ERGIC-53	LMAN1
Vesicular integral-membrane protein VIP36	LMAN2
Mannosyl-oligosaccharide 1,2-alpha-mannosidase IB	MAN1A2
Endoplasmic reticulum mannosyl-oligosaccharide 1,2-alpha-mannosidase	MAN1B1
Alpha-1,6-mannosyl-glycoprotein 2-beta-N-acetylglucosaminyltransferase	MGAT2
Alpha-1,3-mannosyl-glycoprotein 4-beta-N-acetylglucosaminyltransferase B	MGAT4B
Nucleobindin-1	NUCB1
Nucleobindin-2;Nesfatin-1	NUCB2
Protein O-linked-mannose beta-1,2-N-acetylglucosaminyltransferase 1	POMGNT1
Sulfhydryl oxidase 2	QSOX2
Ras-related protein Rab-18	RAB18
Protein RER1	RER1
Vesicle-trafficking protein SEC22b	SEC22B
Zinc transporter 6	SLC30A6
Zinc transporter 7	SLC30A7
Solute carrier family 35 member E1	SLC35E1
Syntaxin-5	STX5
Surfeit locus protein 4	SURF4
Transmembrane 9 superfamily member 1	TM9SF1
Transmembrane 9 superfamily member 3	TM9SF3
Transmembrane emp24 domain-containing protein 10	TMED10
Transmembrane emp24 domain-containing protein 2	TMED2
Transmembrane emp24 domain-containing protein 4	TMED4
Transmembrane emp24 domain-containing protein 5	TMED5
Transmembrane emp24 domain-containing protein 7	TMED7
Transmembrane emp24 domain-containing protein 9	TMED9
Protein YIPF3;Protein YIPF3, 36 kDa form III;Protein YIPF	YIPF3
Zinc finger protein-like 1	ZFPL1

Figure 2.16 Proteomic Comparison of COPI Reconstituted from Different Cell Types

(A) Venn diagram to visualized the overlap of proteins found twofold enriched in COPI proteomic datasets obtained from different cell lines used as donor membranes. Numbers indicate the number of proteins shared between the various datasets. (B) List of the 39 proteins that fulfill the COPI candidate criteria in all three datasets. Given are full protein and gene names.

Complete lists of the 69 candidates for HepG2 cell COPI proteome (Tab. 11) as well as the 144 candidate identified in iMΦ (Tab. 12) are given below.

Protein.names	Gene.names	ratio 1 (H/L)	ratio 2 (L/H)	Mean SILAC ratio	SEM
Solute carrier family 35 member E1	SLC35E1	7,03	3,42	5,23	1,80
Vesicle-trafficking protein SEC22a	SEC22A	4,87		*4,87*	
Zinc finger protein-like 1	ZFPL1	4,43	4,84	4,63	0,20
Protein RER1	RER1	6,07	3,05	4,56	1,51
Transmembrane 9 superfamily member 3	TM9SF3;SMBP	3,63	4,27	3,95	0,32
Endoplasmic reticulum-Golgi intermediate compartment protein 2	ERGIC2	5,43	2,21	3,82	1,61
Transmembrane emp24 domain-containing protein 9	TMED9	4,87	2,59	3,73	1,14
Nucleobindin-1	NUCB1	4,42	2,99	3,70	0,72
Transmembrane emp24 domain-containing protein 1	TMED1	4,72	2,54	3,63	1,09
cDNA FLJ76981, highly similar to Homo sapiens golgi autoantigen, golgin subfamily a, 5 (GOLGA5), mRNA	GOLGA5	3,47	3,73	3,60	0,13
Transmembrane emp24 domain-containing protein 10	TMED10	4,27	2,74	3,51	0,76
Transmembrane emp24 domain-containing protein 7	TMED7;TMED7-TICAM2	3,70	2,94	3,32	0,38
Alpha-(1,6)-fucosyltransferase	FUT8	3,41	3,15	3,28	0,13
Endoplasmic reticulum mannosyl-oligosaccharide 1,2-alpha-mannosidase;alpha-1,2-Mannosidase	MAN1B1	2,96	3,48	3,22	0,26
GPI ethanolamine phosphate transferase 2	PIGG	3,28	3,12	3,20	0,08
Surfeit locus protein 4	SURF4	3,95	2,39	3,17	0,78
Galactosylgalactosylxylosylprotein 3-beta-glucuronosyltransferase 3	B3GAT3	3,49	2,73	3,11	0,38
Xylosyltransferase 2	XYLT2	3,10		*3,10*	
Transmembrane emp24 domain-containing protein 4	TMED4	3,43	2,72	3,07	0,35
Beta-1,4-galactosyltransferase 7;Xylosylprotein 4-beta-galactosyltransferase	B4GALT7	3,07		*3,07*	
Zinc transporter 6	SLC30A6	3,51	2,59	3,05	0,46
Glutaminyl-peptide cyclotransferase-like protein	QPCTL	2,96	3,01	2,99	0,03
Alpha-fetoprotein	AFP	3,67	2,22	2,95	0,73
Polypeptide N-acetylgalactosaminyltransferase;Polypeptide N-acetylgalactosaminyltransferase 1;Polypeptide N-acetylgalactosaminyltransferase 1 soluble form	GALNT1	2,92	2,90	2,91	0,01
Golgi SNAP receptor complex member 2	GOSR2	4,01	1,77	2,89	1,12
Transmembrane emp24 domain-containing protein 2	RNP24;TMED2	3,79	1,94	2,86	0,92
UbiA prenyltransferase domain-containing protein 1	UBIAD1	2,51	3,21	2,86	0,35
Nucleobindin-2;Nesfatin-1	HEL-S-109;NUCB2;Nucb2	3,41	2,24	2,82	0,58
Transmembrane emp24 domain-containing protein 5	TMED5	3,68	1,94	2,81	0,87
Protein YIPF;Protein YIPF5	YIPF5	3,28	2,30	2,79	0,49
Protein ERGIC-53	LMAN1	3,41	2,13	2,77	0,64
Palmitoyltransferase;Palmitoyltransferase ZDHHC17	ZDHHC17	2,72		*2,72*	
Vesicle-trafficking protein SEC22b	SEC22B	3,09	2,31	2,70	0,39
Protein kish-A	TMEM167A	2,66		*2,66*	

Protein.names	Gene.names	ratio 1 (H/L)	ratio 2 (L/H)	Mean SILAC ratio	SEM
Zinc transporter 7	SLC30A7	2,62		*2,62*	
VIP36-like protein	LMAN2L	3,28	1,95	2,62	0,66
Calcium-transporting ATPase;Calcium-transporting ATPase type 2C member 1	ATP2C1	2,63	2,54	2,58	0,05
Endoplasmic reticulum-Golgi intermediate compartment protein 3	ERGIC3	3,14	2,02	2,58	0,56
Vesicular integral-membrane protein VIP36	LMAN2	3,09	2,04	2,57	0,53
Vesicle transport protein GOT1B	GOLT1B	3,51	1,59	2,55	0,96
Calumenin	CALU	2,55		*2,55*	
Protein O-linked-mannose beta-1,2-N-acetylglucosaminyltransferase 1	POMGNT1	2,12	2,97	2,54	0,42
Mannosyl-oligosaccharide 1,2-alpha-mannosidase IB	MAN1A2	2,52	2,53	2,53	0,01
Ras-related protein Rab-18	RAB18	2,82	2,16	2,49	0,33
Transmembrane emp24 domain-containing protein 3	TMED3	3,29	1,63	2,46	0,83
Polypeptide N-acetylgalactosaminyltransferase 2;Polypeptide N-acetylgalactosaminyltransferase 2 soluble form;Polypeptide N-acetylgalactosaminyltransferase	GALNT2	2,29	2,61	2,45	0,16
Endoplasmic reticulum resident protein 44	ERP44	3,17	1,66	2,42	0,75
Adenosine 3-phospho 5-phosphosulfate transporter 2	SLC35B3	2,33	2,43	2,38	0,05
Protein FAM198B	FAM198B	2,42	2,30	2,36	0,06
Protein YIF1A	YIF1A	2,49	2,03	2,26	0,23
Alpha-1,6-mannosylglycoprotein 6-beta-N-acetylglucosaminyltransferase A	MGAT5	1,84	2,68	2,26	0,42
Endoplasmic reticulum-Golgi intermediate compartment protein 1	ERGIC1	2,59	1,92	2,26	0,33
Sulfhydryl oxidase 2	QSOX2	2,26	2,24	2,25	0,01
Syntaxin-5	STX5;STX5A	2,44	2,04	2,24	0,20
Putative sodium-coupled neutral amino acid transporter 10	SLC38A10	2,23		*2,23*	
Protein YIPF3;Protein YIPF3, 36 kDa form III;Protein YIPF	YIPF3	2,23	2,15	2,19	0,04
Alpha-1,6-mannosyl-glycoprotein 2-beta-N-acetylglucosaminyltransferase	MGAT2	2,12	2,24	2,18	0,06
Beta-1,3-galactosyltransferase 6	B3GALT6	2,16		*2,16*	
Exostosin-like 2;Processed exostosin-like 2	EXTL2	2,07	2,23	2,15	0,08
Protein CASP;Homeobox protein cut-like 1	CUX1;Nbla10317;CUX1-RETc;CUX1-RETa	2,03	2,27	2,15	0,12
Alpha-1,3-mannosyl-glycoprotein 4-beta-N-acetylglucosaminyltransferase B	MGAT4B	1,71	2,58	2,15	0,43
Protein YIPF4	YIPF4	2,10	2,17	2,14	0,04
ER lumen protein-retaining receptor 1;ER lumen protein-retaining receptor	KDELR1	2,80	1,46	2,13	0,67
Thioredoxin domain-containing protein 5	hCG_1811539;TXNDC5;STRF8;DKFZp666I134	2,11		*2,11*	
Fukutin-related protein	FKRP	1,99	2,17	2,08	0,09
Protein YIF1B	YIF1B	2,47	1,67	2,07	0,40
Carbohydrate sulfotransferase 14	CHST14	2,09	2,02	2,05	0,04
Transmembrane 9 superfamily member 1	TM9SF1	1,88	2,17	2,03	0,14

Protein.names	Gene.names	ratio 1 (H/L)	ratio 2 (L/H)	Mean SILAC ratio	SEM
Glycoprotein endo-alpha-1,2-mannosidase-like protein	MANEAL	2,29	1,74	2,01	0,27

Table 11: Candidate Proteins for the Core Proteome of COPI Vesicles of HepG2 Cells

List of candidates for the COPI core proteome from HepG2 cells as determined by two independent experiments performed according to Fig. 2.5. CM$\gamma_1\zeta_1$, Arf1, and GTP were used for all reconstitutions. Given are gene and protein names of the identified proteins, the SILAC ratios (H/L or L/H) from each experiment, the mean SILAC ratio, and standard error of the mean (SEM). Displayed are protein with mean SILAC ratios >2 or with a SILAC ratio >2 in one of the two experiments in which the vesicle sample was labeled with heavy isotopes (written in italic in the Mean SILAC ratio column).

Protein.names	Gene.names	ratio 1 (H/L)	ratio 2 (L/H)	Mean SILAC ratio	SEM
Nucleobindin-1	NUCB1	7,60	16,29	11,94	4,34
Transmembrane emp24 domain-containing protein 7	TMED7	8,45	14,49	11,47	3,02
Transmembrane emp24 domain-containing protein 9	TMED9	7,22	12,62	9,92	2,70
Transmembrane emp24 domain-containing protein 10	TMED10	7,20	10,70	8,95	1,75
Transmembrane emp24 domain-containing protein 2	TMED2	6,40	11,28	8,84	2,44
Nucleobindin-2;Nesfatin-1	NUCB2	7,78	9,89	8,83	1,05
Transmembrane emp24 domain-containing protein 4	TMED4	7,41	9,76	8,58	1,18
Zinc transporter 5	SLC30A5	10,01	6,64	8,33	1,69
Putative sodium-coupled neutral amino acid transporter 10	SLC38A10	8,00	8,56	8,28	0,28
Zinc transporter 7	SLC30A7	7,94	7,50	7,72	0,22
Solute carrier family 35 member E1	SLC35E1	7,45		*7,45*	
Polypeptide N-acetylgalactosaminyltransferase 1;Polypeptide N-acetylgalactosaminyltransferase 1 soluble form	GALNT1	7,21	6,93	7,07	0,14
Sulfhydryl oxidase 2	QSOX2	6,61	7,41	7,01	0,40
Endoplasmic reticulum-Golgi intermediate compartment protein 2	ERGIC2	6,07	7,49	6,78	0,71
Alpha-mannosidase 2	MAN2A1	6,12	6,36	6,24	0,12
Golgi integral membrane protein 4	GOLIM4	6,23	5,99	6,11	0,12
Hexosyltransferase	CHPF2	6,04		*6,04*	
Transmembrane 9 superfamily member 3	TM9SF3	5,74	6,23	5,99	0,25
Alpha-1,3-mannosyl-glycoprotein 2-beta-N-acetylglucosaminyltransferase	MGAT1	5,28	6,68	5,98	0,70
Chondroitin sulfate N-acetylgalactosaminyltransferase 2	CSGALNACT2	5,93		*5,93*	
Endoplasmic reticulum-Golgi intermediate compartment protein 3	ERGIC3	6,57	5,22	5,89	0,68
Xylosyltransferase 2	XYLT2	3,94	7,50	5,72	1,78
Glucoside xylosyltransferase 1	GXYLT1	5,71		*5,71*	
GDP-fucose transporter 1	SLC35C1	5,66		*5,66*	
Endoplasmic reticulum mannosyl-oligosaccharide 1,2-alpha-mannosidase	MAN1B1	5,88	5,20	5,54	0,34
Beta-1,4-glucuronyltransferase 1	B4GAT1	5,53		*5,53*	

Protein.names	Gene.names	ratio 1 (H/L)	ratio 2 (L/H)	Mean SILAC ratio	SEM
Palmitoyltransferase ZDHHC13;Palmitoyltransferase	ZDHHC13	4,46	6,36	5,41	0,95
Vesicular integral-membrane protein VIP36	LMAN2	4,90	5,85	5,38	0,47
Alpha-mannosidase 2x	MAN2A2	5,16	5,32	5,24	0,08
N-acetylglucosamine-1-phosphotransferase subunits alpha/beta;N-acetylglucosamine-1-phosphotransferase subunit alpha;N-acetylglucosamine-1-phosphotransferase subunit beta	GNPTAB	3,67	6,73	5,20	1,53
Transmembrane 9 superfamily member 1	TM9SF1	5,47	4,78	5,13	0,34
Alpha-1,6-mannosylglycoprotein 6-beta-N-acetylglucosaminyltransferase A	MGAT5	4,98	5,23	5,11	0,12
Mannosyl-oligosaccharide 1,2-alpha-mannosidase IB	MAN1A2	5,00	5,12	5,06	0,06
Golgi membrane protein 1	GOLM1	4,83	5,23	5,03	0,20
Ceramide glucosyltransferase	UGCG	5,02		*5,02*	
Protein RER1	RER1	5,64	4,16	4,90	0,74
Transmembrane emp24 domain-containing protein 5	TMED5	5,09	4,63	4,86	0,23
Ectonucleoside triphosphate diphosphohydrolase 7	ENTPD7	4,79	4,91	4,85	0,06
Osteopontin	SPP1	4,85		*4,85*	
Zinc finger protein-like 1	ZFPL1	4,81		*4,81*	
Surfeit locus protein 4	SURF4	5,57	4,01	4,79	0,78
alpha-1,2-Mannosidase;Mannosyl-oligosaccharide 1,2-alpha-mannosidase IA	MAN1A;MAN1A1	4,89	4,68	4,78	0,11
Polypeptide N-acetylgalactosaminyltransferase 2;Polypeptide N-acetylgalactosaminyltransferase 2 soluble form	GALNT2	4,49	5,07	4,78	0,29
Adipocyte plasma membrane-associated protein	APMAP	4,77		*4,77*	
Golgin subfamily A member 5	GOLGA5	5,08	4,40	4,74	0,34
Alpha-1,6-mannosyl-glycoprotein 2-beta-N-acetylglucosaminyltransferase	MGAT2	4,52	4,89	4,71	0,18
Protein ERGIC-53	LMAN1	4,91	4,42	4,67	0,25
Galactosylgalactosylxylosylprotein 3-beta-glucuronosyltransferase 3	B3GAT3	4,67		*4,67*	
Vesicle-trafficking protein SEC22b	SEC22B	5,00	4,18	4,59	0,41
RING finger and transmembrane domain-containing protein 1	RNFT1	4,58		*4,58*	
Carbohydrate sulfotransferase 14	CHST14	4,60	4,46	4,53	0,07
Alpha-1,3-mannosyl-glycoprotein 4-beta-N-acetylglucosaminyltransferase B	MGAT4B	5,74	3,24	4,49	1,25
Phosphatidylinositol glycan anchor biosynthesis, class G	PIGG	5,89	3,01	4,45	1,44
Probable palmitoyltransferase ZDHHC21	ZDHHC21	4,45		*4,45*	
Alpha-1,3-mannosyl-glycoprotein 4-beta-N-acetylglucosaminyltransferase A;Alpha-1,3-mannosyl-glycoprotein 4-beta-N-acetylglucosaminyltransferase A soluble form	MGAT4A	4,41		*4,41*	
Dermatan-sulfate epimerase	DSE	4,96	3,74	4,35	0,61
Complement C1q subcomponent subunit B	C1QB	3,04	5,49	4,27	1,23
Syntaxin-5	STX5A;STX5	4,23		*4,23*	
Protein CASP;Homeobox protein cut-like;Homeobox protein cut-like 1	CUX1	4,15	4,28	4,22	0,06
Molybdate-anion transporter	MFSD5	4,77	3,67	4,22	0,55

Protein.names	Gene.names	ratio 1 (H/L)	ratio 2 (L/H)	Mean SILAC ratio	SEM
Endoplasmic reticulum resident protein 44	ERP44	3,87	4,52	4,20	0,32
Transmembrane 9 superfamily member 4	TM9SF4	4,29	4,08	4,18	0,11
Protein YIPF3;Protein YIPF3, N-terminally processed	YIPF3	4,13	4,09	4,11	0,02
ER lumen protein-retaining receptor;ER lumen protein-retaining receptor 1;ER lumen protein-retaining receptor 2	KDELR1;KDELR2	4,04		*4,04*	
Glycosyltransferase 8 domain-containing protein 1	GLT8D1	3,87	4,19	4,03	0,16
Transmembrane protein 165	TMEM165	4,31	3,61	3,96	0,35
Ectonucleoside triphosphate diphosphohydrolase 4	ENTPD4	3,36	4,52	3,94	0,58
Palmitoyltransferase ZDHHC17	ZDHHC17	3,92		*3,92*	
UDP-glucuronic acid decarboxylase 1	UXS1	3,85		*3,85*	
Adenosine 3-phospho 5-phosphosulfate transporter 1	SLC35B2	3,83	3,84	3,83	0,00
Golgi SNAP receptor complex member 1	GOSR1	3,89	3,76	3,83	0,07
N-acetylgalactosaminyltransferase 7	GALNT7	4,05	3,43	3,74	0,31
Xylosyltransferase 1	XYLT1	3,64	3,83	3,74	0,10
Golgi autoantigen, golgin subfamily b, macrogolgin 1	GOLGB1	3,90	3,57	3,73	0,16
Transmembrane protein 115	TMEM115	3,68		*3,68*	
Protein-tyrosine sulfotransferase 2	TPST2	3,67		*3,67*	
Beta-1,4 N-acetylgalactosaminyltransferase 1	B4GALNT1	3,89	3,46	3,67	0,22
Heparan sulfate 2-O-sulfotransferase 1	HS2ST1	4,02	3,32	3,67	0,35
Glycosyltransferase-like protein LARGE1;Xylosyltransferase LARGE;Beta-1,3-glucuronyltransferase LARGE;Glycosyltransferase-like protein LARGE2;Xylosyltransferase LARGE2;Beta-1,3-glucuronyltransferase LARGE2	LARGE;GYLTL1B	3,63		*3,63*	
Extracellular serine/threonine protein kinase FAM20C	FAM20C	3,16	4,03	3,60	0,43
Endoplasmic reticulum-Golgi intermediate compartment protein 1	ERGIC1	4,06	3,12	3,59	0,47
Polypeptide N-acetylgalactosaminyltransferase;Polypeptide N-acetylgalactosaminyltransferase 12	GALNT12	3,50	3,58	3,54	0,04
Renin receptor	ATP6AP2	3,52		*3,52*	
alpha-1,2-Mannosidase	MAN1C1	3,40	3,57	3,49	0,08
Golgin subfamily A member 2	GOLGA2	3,45	3,43	3,44	0,01
Calcium-transporting ATPase;Calcium-transporting ATPase type 2C member 1	ATP2C1	3,97	2,82	3,39	0,57
Bifunctional heparan sulfate N-deacetylase/N-sulfotransferase 2;Heparan sulfate N-deacetylase 2;Heparan sulfate N-sulfotransferase 2	NDST2	3,57	3,20	3,38	0,18
GPI transamidase component PIG-S	PIGS	3,29		*3,29*	
Soluble calcium-activated nucleotidase 1	CANT1	3,19		*3,19*	
Fukutin-related protein	FKRP	3,19		*3,19*	
Ras-related protein Rab-6B;Ras-related protein Rab-6A	RAB6B;RAB6A	3,01	3,30	3,16	0,15
Phosphatidylinositide phosphatase SAC1	SACM1L	3,08		*3,08*	
V-type proton ATPase subunit S1	ATP6AP1	3,07		*3,07*	

Protein.names	Gene.names	ratio 1 (H/L)	ratio 2 (L/H)	Mean SILAC ratio	SEM
Uncharacterized protein KIAA2013	KIAA2013	3,14	2,90	3,02	0,12
Lysosomal alpha-glucosidase	GAA	3,02	2,94	2,98	0,04
ADP-ribosylation factor-related protein 1	ARFRP1	2,97		*2,97*	
Beta-1,4-galactosyltransferase 5	B4GALT5	3,27	2,60	2,94	0,33
Protein O-linked-mannose beta-1,2-N-acetylglucosaminyltransferase 1	POMGNT1	2,93		*2,93*	
CMP-N-acetylneuraminate-poly-alpha-2,8-sialyltransferase	ST8SIA4	2,98	2,87	2,92	0,05
N-acetyllactosaminide beta-1,3-N-acetylglucosaminyltransferase 2	B3GNT2;B3GNT2	2,88		*2,88*	
Ectonucleoside triphosphate diphosphohydrolase 6	ENTPD6	2,89	2,84	2,87	0,02
Protein FAM134C	FAM134C	2,84		*2,84*	
UDP-GalNAc:beta-1,3-N-acetylgalactosaminyltransferase 1	B3GALNT1	2,84		*2,84*	
Polypeptide N-acetylgalactosaminyltransferase 6	GALNT6	2,71	2,95	2,83	0,12
PRA1 family protein 3	ARL6IP5	2,82		*2,82*	
Neuropilin-2	NRP2	2,80		*2,80*	
Prenylated Rab acceptor protein 1	RABAC1	2,77		*2,77*	
Sterol-4-alpha-carboxylate 3-dehydrogenase, decarboxylating	NSDHL	2,72		*2,72*	
Lactosylceramide alpha-2,3-sialyltransferase	ST3GAL5	2,69		*2,69*	
Glycoprotein-N-acetylgalactosamine 3-beta-galactosyltransferase 1	C1GALT1	2,65		*2,65*	
Transmembrane protein 168	TMEM168	3,08	2,19	2,64	0,44
Trans-Golgi network integral membrane protein 1;Trans-Golgi network integral membrane protein 2	TGOLN1;TGOLN2	2,63		*2,63*	
Protein FAM134B	FAM134B	2,63		*2,63*	
Protein FAM3C	FAM3C	2,59	2,67	2,63	0,04
Lanosterol synthase	LSS	3,17	2,04	2,61	0,56
AHNAK nucleoprotein (desmoyokin)	AHNAK2	2,59		*2,59*	
Deleted in autism protein 1 homolog	DIA1	3,04	2,13	2,59	0,45
Polypeptide N-acetylgalactosaminyltransferase;Polypeptide N-acetylgalactosaminyltransferase 10	GALNT10	2,58		*2,58*	
N-acetyllactosaminide alpha-1,3-galactosyltransferase	GGTA1	2,54		*2,54*	
Zinc transporter 6	SLC30A6	2,54		*2,54*	
Inositol monophosphatase 3	IMPAD1	2,53		*2,53*	
Beta-1,4-galactosyltransferase 1;Lactose synthase A protein;N-acetyllactosamine synthase;Beta-N-acetylglucosaminylglycopeptide beta-1,4-galactosyltransferase;Beta-N-acetylglucosaminyl-glycolipid beta-1,4-galactosyltransferase;Processed beta-1,4-galactosyltransferase 1	B4GALT1	2,71	2,34	2,53	0,18
Protein FAM3A	FAM3A	2,51		2,51	
Transmembrane 9 superfamily member 2	TM9SF2	2,65	2,33	2,49	0,16
Alpha/beta hydrolase domain-containing protein 14A	ABHD14A	2,48		*2,48*	
Endonuclease domain-containing 1 protein	ENDOD1	2,45		*2,45*	

Protein.names	Gene.names	ratio 1 (H/L)	ratio 2 (L/H)	Mean SILAC ratio	SEM
D-glucuronyl C5-epimerase	GLCE	2,12	2,73	2,42	0,31
Ras-related protein Rab-18	RAB18	2,23	2,53	2,38	0,15
Long-chain-fatty-acid--CoA ligase 5	ACSL5	2,33		*2,33*	
Cathepsin B;Cathepsin B light chain;Cathepsin B heavy chain	CTSB	1,92	2,72	2,32	0,40
Golgi apparatus protein 1	GLG1	2,52	2,09	2,31	0,21
Protein GPR107	GPR107	2,75	1,78	2,27	0,49
Protein FAM177A1	FAM177A1	2,34	2,13	2,23	0,10
Alpha-2-macroglobulin receptor-associated protein	LRPAP1	1,93	2,52	2,23	0,30
Membrane-associated progesterone receptor component 2	PGRMC2	2,18		*2,18*	
Neutral cholesterol ester hydrolase 1	NCEH1	2,13		*2,13*	
CMP-N-acetylneuraminate-beta-galactosamide-alpha-2,3-sialyltransferase 1	ST3GAL1	1,94	2,33	2,13	0,19
Granulins;Acrogranin;Granulin-1;Granulin-2;Granulin-3;Granulin-4;Granulin-5;Granulin-6;Granulin-7	GRN	2,40	1,84	2,12	0,28
Lipoprotein lipase	LPL	2,10		*2,10*	
Macrophage metalloelastase	MMP12	2,04		*2,04*	
Prostaglandin G/H synthase 1	PTGS1	2,04		*2,04*	
Monoacylglycerol lipase ABHD12	ABHD12	2,04		*2,04*	
Keratinocyte-associated transmembrane protein 2	9530068E07RIK;KCT2	2,13	1,92	2,03	0,10
Protein GPR108	GPR108	2,02		*2,02*	

Table 12: Candidate Proteins for the Core Proteome of COPI Vesicles of iMΦ

List of candidates for the COPI core proteome from iMΦ cells as determined by two independent experiments performed according to Fig. 2.5. CM$\gamma_1\zeta_1$, Arf1, and GTP were used for all reconstitutions. Given are gene and protein names of the identified proteins, the SILAC ratios (H/L or L/H) from each experiment, the mean SILAC ratio, and standard error of the mean (SEM). Displayed are protein with mean SILAC ratios >2 or with a SILAC ratio >2 in one of the two experiments in which the vesicle sample was labeled with heavy isotopes (written in italic in the Mean SILAC ratio column).

2.6 Sec24D Mutations Causing Syndromic *Osteogenesis Imperfecta*

In addition to the investigation of the COPI vesicle proteome and coatomer and Arf isoforms, as part of this work most recently identified mutations within the COPII coat components Sec24D that cause a syndromic form of *osteogenesis imperfecta* (OI) were studied, using biochemical tools. In the affected families, three mutations were identified, causing either a premature stop-codon (Q208*), a glutamine-proline-conversion (Q978P), or the conversion of serine to phenylalanine in position 1015 (S1015F). Carrying the Q208* and S1015F mutations leads to syndromic OI. A combination of the mutations Q978P and S1015F lead to pregnancy loss (Garbes et al., 2015).

The positions of these point mutations within the crystal structure solved by Mancias and Goldberg (2008) are illustrated in figure 2.17. As indicated, the dimeric Sec23A/Sec24D complex forms an arch on the membrane (Fig. 2.17A). The side view of Sec24D (blue), shown in Fig. 2.17B, reveals a predominantly alpha-helical interaction surface on the edge of the cargo binding COPII subunit. On this side, Sec24D binds to the IxM motif present in Syntaxin5 (Stx5) involving the key residues 834LIL836 (Fig. 2.17C). The point mutations, highlighted in the structure and also in the following are shifted by one amino acid because a Sec24D variant with one additional alanine in position 224 was used for the experiments. Mutation Q979P localizes to an alpha helix very distant from the membrane. Also, the conversion S1016F hits the very end of an alpha helix, closer to the membrane and the Stx5 binding site (Fig. 2.17C).

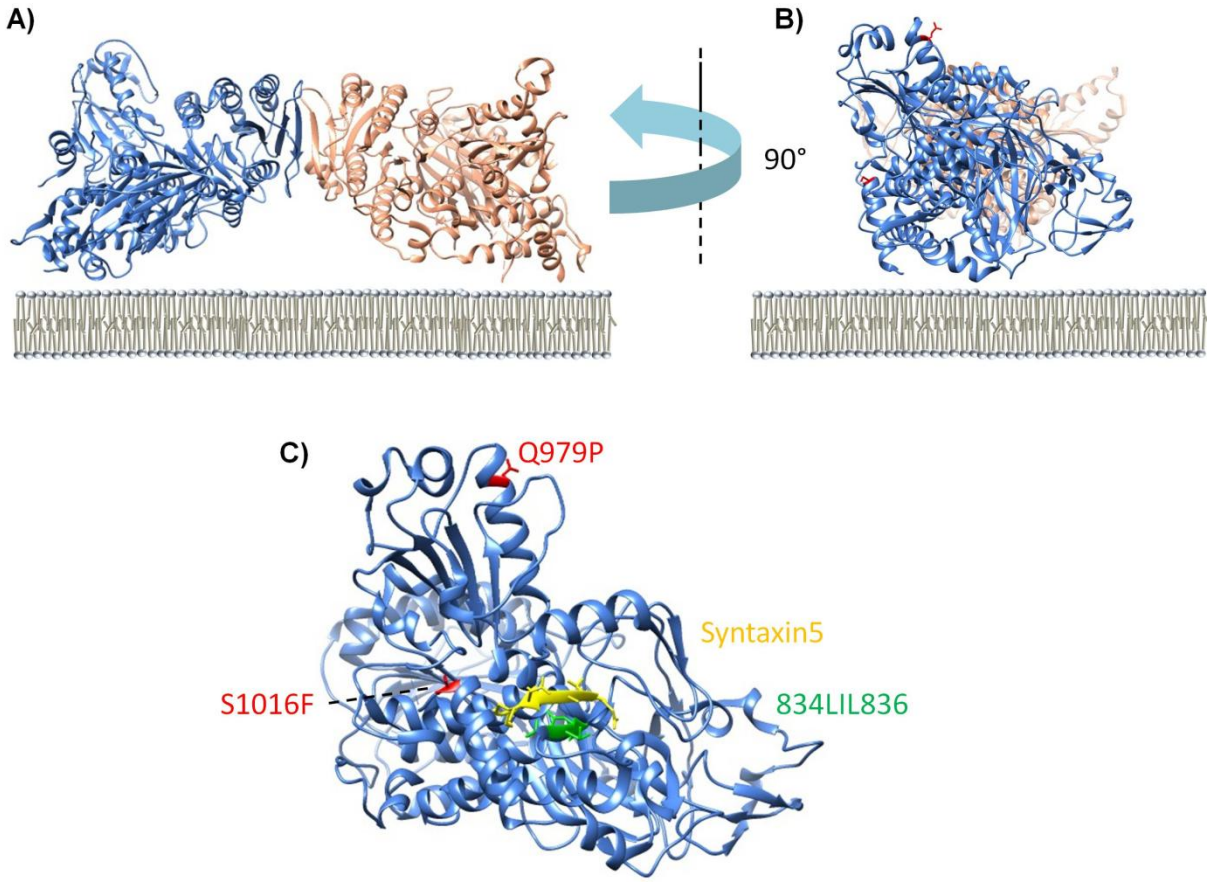

Figure 2.17 Crystal Structure of the Sec23A/Sec24D Complex

(A-C) Crystal structures of the Sec23A/Sec24D complex determined by Mancias and Goldberg (2008): Protein Data Bank accession code 3EFO. Sec23A is colored pink, Sec24D shown in blue. (A) Side view of the dimeric complex with a schematic representation of membrane. (B) Side view of Sec24D after 90° rotation of the structure shown in (A). Sec23A can be seen in the background, a schematic membrane is displayed for orientation. (C) Enlarged side view of Sec24D shown in (B) without Sec23A. The point mutations S1016F, Q979P (both red), as well as the amino acid stretch 834LIL836 (green) that binds to Syntaxin5 (yellow) are highlighted.

In order to study these mutations, we introduced them into the coding sequences of Sec23A/Sec24D expression plasmids. The Q208* mutation that gives rise to a protein shortened by 825 amino acids was excluded from the analysis as the resulting polypeptide surely is non-functional.

Proteins complexes carrying either one of the remaining mutations could effectively be purified (Fig. 2.18). The Sec24D subunit of both variants Sec24D^{Q979P} and Sec24D^{S1016F} is partially degraded. However, the level of degradation is very comparable to the level of degradation observed for wild type Sec24D (Sec24D^{wt}) and the synthetic SNARE-binding mutant (Sec24D^{LIL834AAA}). Also shown are recombinant Sar1B and the outer COPII coat Sec13/Sec31A (Fig. 2.18). These proteins were used in further experiments.

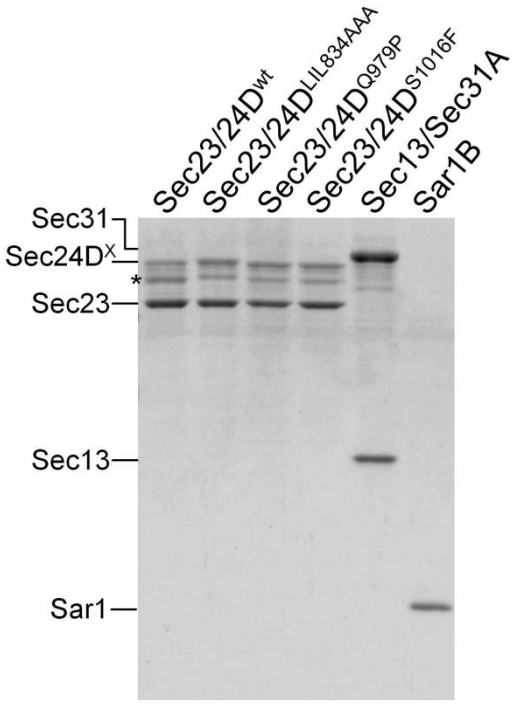

Figure 2.18 Recombinant Wild Type and Mutant COPII Coat Proteins

Coomassie-stained SDS gel loaded with the recombinant COPII coat proteins indicated. Degradation products of the various Sec24D variants are marked by an asterisk (*).

2.7 Mutant Sec24D^{S1016F} is Deficient in ER-Golgi SNARE-Packing

In order to obtain functional insight into the effect of the various mutations, recombinant proteins (Fig. 2.18) were tested in COPII *in vitro* reconstitution experiments. Vesicles were reconstituted from SIC HeLa cells (according to Fig. 2.1) and harvested by high-speed centrifugation at 100.000 ×g as previously described by Adolf et al. (2013). The vesicle samples were subsequently analyzed for the presence of the ER-Golgi cycling protein ERGIC53, as well as the three ER-Golgi SNAREs Syntaxin5, GS27, and Bet1 by Western blot (Fig. 2.19).

Whereas all four variants incorporated highly similar fractions of ERGIC53, packing of SNARE proteins varied significantly between them (Fig. 2.19A and B). COPII samples prepared with Sec24D^{wt} contained between 5.8 and 6.9 % of the SNARE proteins present in the donor SIC. Slightly lower percentages of SNARE-packing were observed for the OI-related variant Sec24D^{Q979P}, ranging from 5.3 to 6.5 % (Fig. 2.19B). The synthetic mutant, Sec24D^{LIL834AAA} is deficient in packing of SNAREs, as has been described earlier (Adolf et al., 2016; Mancias and Goldberg, 2008). This is reflected by the markedly reduced uptake of all three ER-Golgi Q-SNAREs, which drops to 3.5-2.4 % (Fig. 2.19B). A highly similar level of reduction of SNARE-uptake was observed for OI-related variant Sec24D^{S1016F}.

Uptake of all three SNARE proteins was reduced by ~50% with 2.9-3.9 % incorporation of SNAREs present in the SIC (Fig. 2.19B).

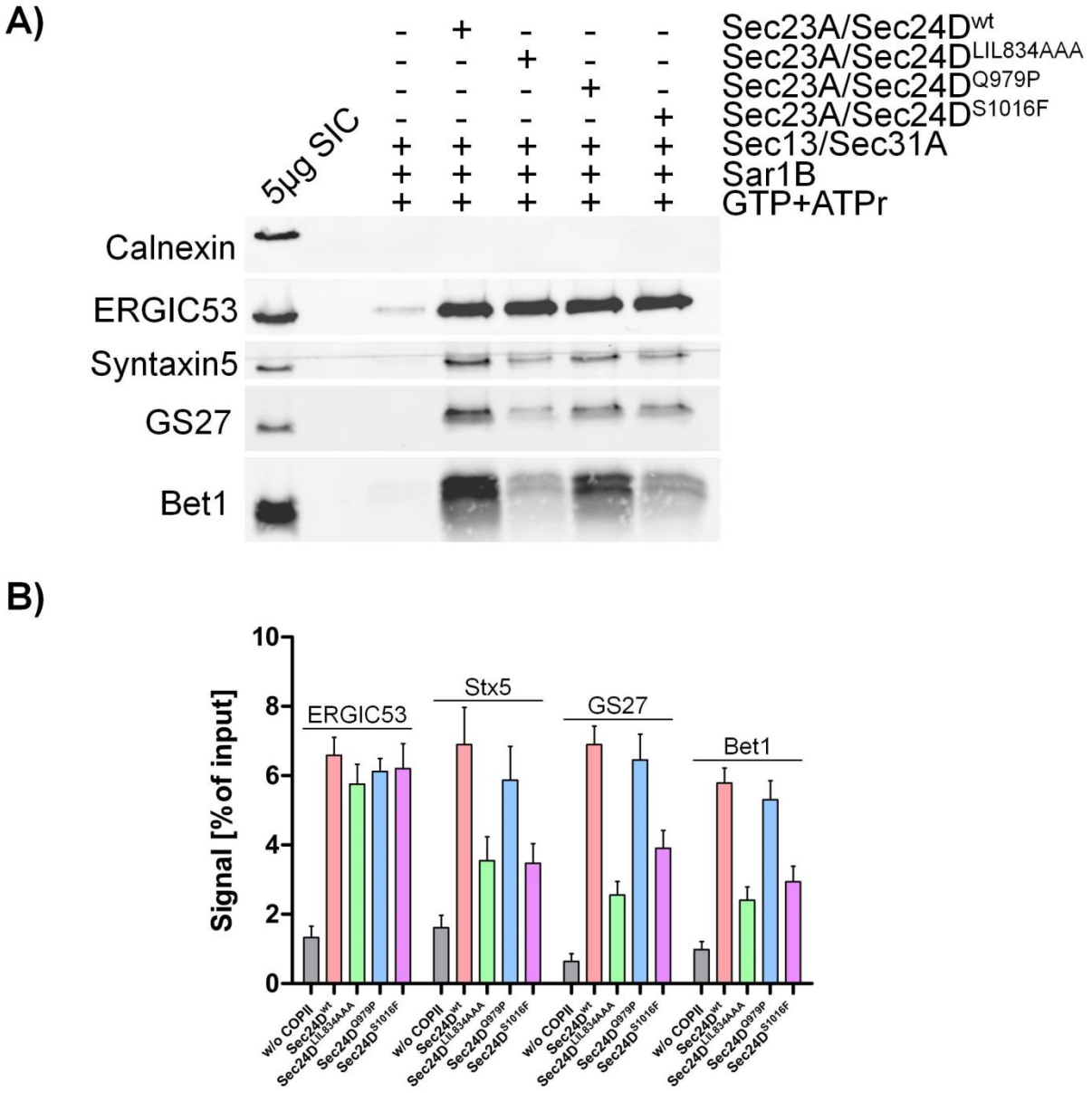

Figure 2.19 Sec24D Variants: Incorporation of ERGIC53 and ER-Golgi SNAREs into COPII Vesicles

(A) Representative Western blot analysis of a COPII vesicles reconstituted from SIC HeLa using recombinant Sar1B, Sec13/Sec31A, Sec23A/Sec24D, GTP, and ATP regenerating system (ATPr) with 5 µg of SIC loaded as input. Samples were probed for the presence of the proteins indicated on the left. Vesicles were isolated via differential centrifugation. (B) Quantification of (A); n=5; error bars=SEM.

To further investigate the SNARE-packing defect observed for the OI-related Sec24D^{S1016F} mutant, pulldown experiments were performed. As has been shown by Mancias and Goldberg (2008), a short peptide motif present in Stx5 binds to Sec24D (see Fig. 2.17C). The binding motif is occluded by a closed conformation that Syntaxins can adopt when the N-terminal H_{abc} domain folds back onto the membrane-proximal region (MacDonald et al., 2010). To overcome this auto-inhibitory state, a

shortened GST-tagged version, Syntaxin5$^{205-328}$-GST, was used for the pulldown experiments lacking both the H_{abc} region and the transmembrane domain. In figure 2.20A, schematic representations of the full length protein (top) and the shortened version used for pulldowns (bottom) are shown. The Stx5 construct was coupled to beads and incubated with the different Sec23A/Sec24D variants. After the incubation, the beads were washed and the bound material analyzed through Western blotting with an antibody against Sec23 and Coomassie staining (CBB). As can be seen in Fig. 2.20B, equal amounts of the Stx5 construct were bound in the different pulldown reactions (compare signals in CBB). Syntaxin5$^{205-328}$-GST pulled down with high efficiency both wild type Sec23A/Sec24D (14.6 %) and the OI-mutant Sec23A/Sec24D^{Q979P} (11.4 %) as deduced from the Sec23 signal (Fig. 2.20B and C). Binding of either Sec23A/Sec24D^{LIL834AAA} (2.8 %) or the second OI-mutant Sec23A/Sec24D^{S1016F} (2.9 %) dropped to the level of the GST control which was 2.7 % of the input (Fig. 2.20B and C).

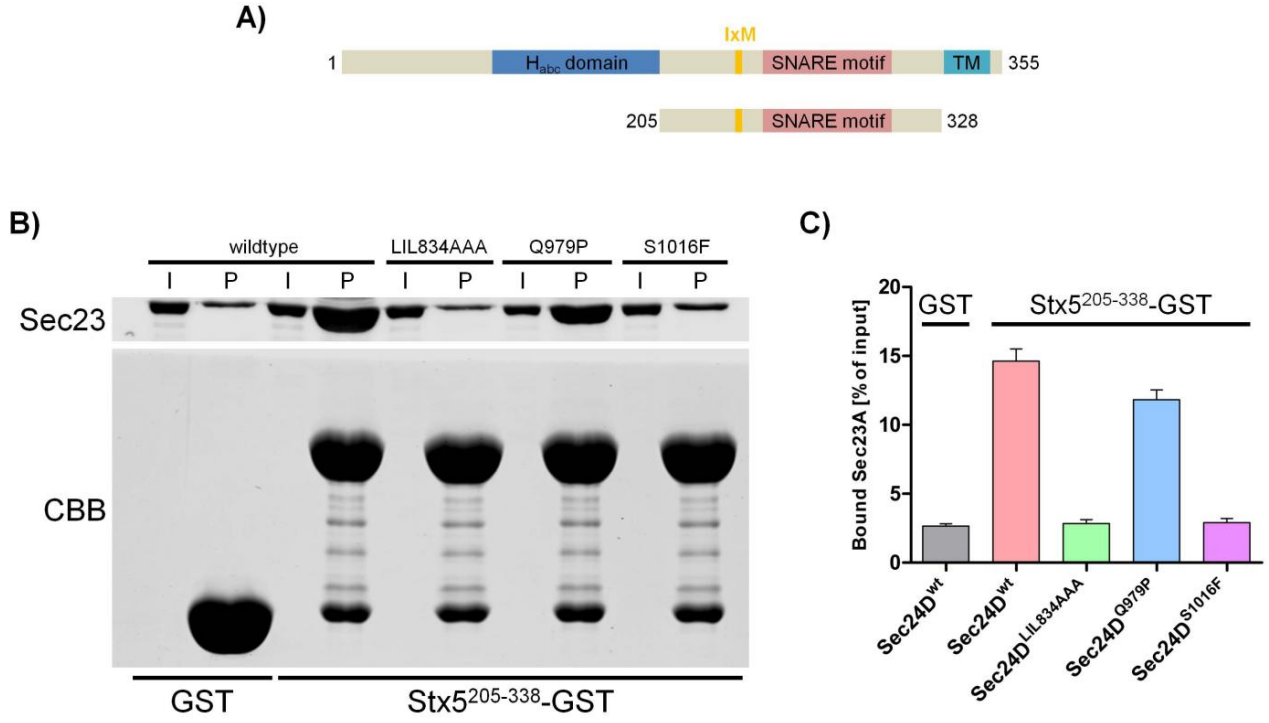

Figure 2.20 Pulldown Experiments: Binding of Sec24D Variants to Syntaxin5

(A) Schematic representation of full length Syntaxin5 (top) with its N-terminal H_{abc} domain, the SNARE motif and the transmembrane (TM) region as well as Syntaxin5$^{205-328}$ used as C-terminal GST-fusion for pulldown experiments. (B) Representative pulldown experiment. Syntaxin5$^{205-328}$-GST and GST control were coupled to beads and incubated with the inner COPII coat variant indicated. Bound material was eluted from the beads with SDS sample buffer, subjected to SDS-PAGE and probed for bound COPII via detection of Sec23 with an antibody. Forty percent of each pulldown reaction (P) was loaded together with 1 % of input (I). Equal loading of the beads was assessed through Coomassie staining (CBB) of the lower part of the gel. (C) Quantification of (B); n=4; error bars=SEM.

2.8 Sec24D Deficient Cells Have Less but Normally Localized ER-Golgi SNAREs

In order to investigate the effect of the mutations in a cellular context, cells from an OI patient ("Lukas") who carries both the Q208* and the S1015F mutation were studied. The cells, which had previously been shown to contain less Sec24D (Garbes et al., 2015), were probed for the presence of transmembrane marker proteins of the early secretory pathway. The amount of Histone H3 (91 %), ER marker protein Calnexin (99 %) and the Golgi SNARE Ykt6 (107 %) were very similar in patient cells compared to CRL-2091 control fibroblasts (Fig. 2.21). The expression of p24 and the ER-Golgi SNARE GS27 were reduced by ~25 % in patient fibroblasts when put into relation to control cells. For the other SNAREs of the ER/Golgi tested, a more strongly reduced protein level was observed. The expression level of GS28 and Sec22b were reduced by more than 40 % in patient cells compared to control fibroblasts. The most significant divergence of protein level was observed for Stx5 and Bet1. For both proteins, a decrease in protein level in patient cell of ~50 % was observed (Fig. 2.21).

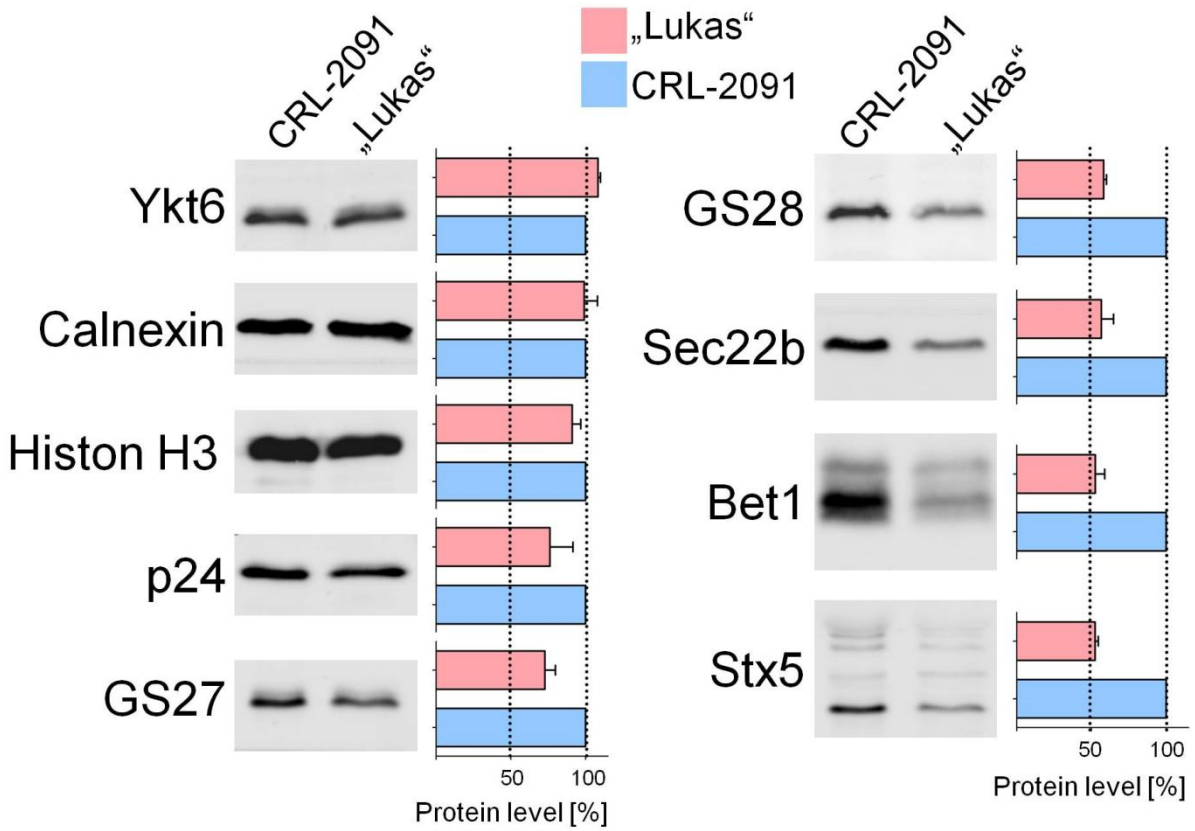

Figure 2.21 Protein Levels of Early Secretory Pathway Membrane Proteins in OI patient Cells and Normal Fibroblasts

Western blot analysis of SIC control fibroblasts (CRL-2091) and OI patient cells ("Lukas"). Of each sample 5 µg were loaded. Proteins detected are indicated on the left side of each blot. Quantifications of the signals in relation to the control cells (100%) are given on the right side of each blot; n=3; error bars=SEM.

In order to investigate if, in addition to a reduced protein level, also the steady state localization of ER-Golgi-SNAREs was changed, confocal immunofluorescence microscopy (IFA) experiments were performed. The Q-SNARE Syntaxin5, the expression of which in patient cells is reduced by almost 50 % (Fig. 2.21), was co-localized with the ER-resident Calnexin (Fig. 2.22) and the ER-Golgi cycling protein p24 (Fig. 2.23). As can be seen in both patient and control cells, there is a strict separation of the signals for Calnexin and Syntaxin5. Calnexin stains the reticular network that fills almost all sections of the cells body, whereas the Syntaxin5 signal is restricted to the Golgi adjacent to the nucleus and additionally dot-like structures (Fig. 2.22).

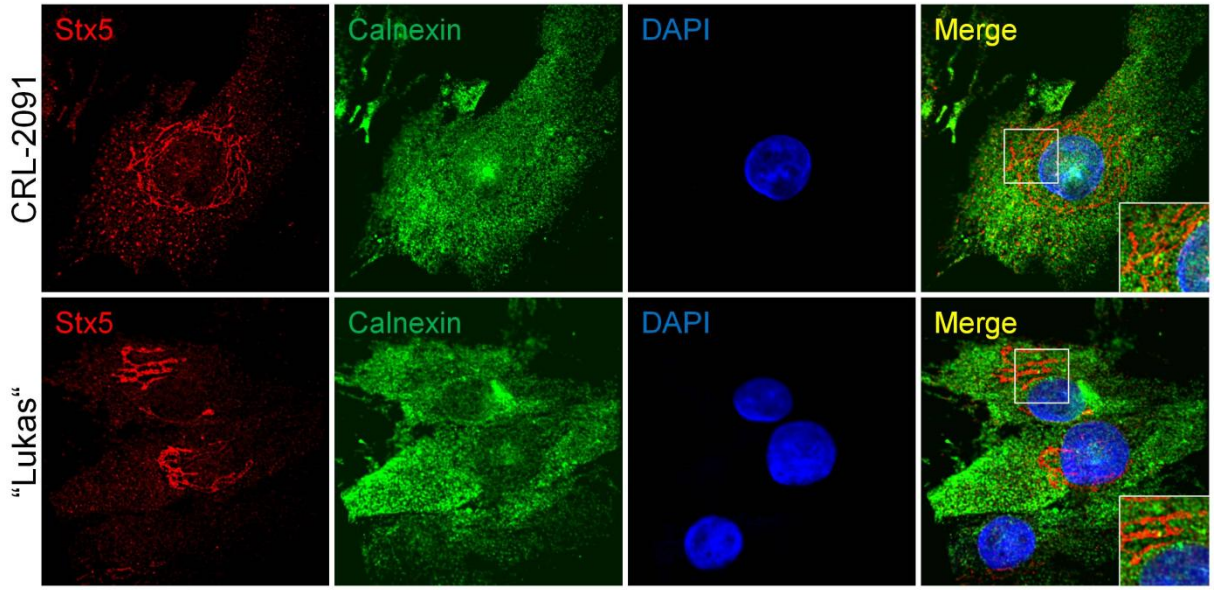

Figure 2.22 IFA: Co-localization of Syntaxin5 and Calnexin in OI patient and control fibroblasts

Methanol-fixated control fibroblasts (CRL-2091) and OI patient fibroblasts ("Lukas") were immune-stained with anti-Calnexin and anti-Syntaxin5 antibodies. Shown are representative images acquired with a spinning disc confocal microscope. Magnification 100×; inlets are marked.

IFA experiments with antibodies against Stx5 and p24 revealed some degree of co-localization, although no perfect merge of signals for the two proteins could be observed (Fig. 2.23). This is generally in line with the fact that p24 cycles in the early secretory pathway and hence localizes at cis-Golgi and the ERGIC under steady-state conditions (Dominguez et al., 1998). Stx5 on the other hand is engaged in at least two different SNARE complexes and is believed to act at the ER-Golgi interface and along the whole cis-to-trans axis of the Golgi (Hong, 2005; Malsam and Söllner, 2011). In general there was no major difference in Stx5/p24 localization between patient cells and control fibroblasts to be observed, except possibly a slightly higher level of co-localization in patient cells.

A more general observation was that control fibroblasts displayed more distinct Stx5-positive punctae compared to Sec24D-deficient “Lukas” patient cells (compare Stx5 signals CRL-2091/”Lukas” in Fig. 2.22 and 2.23).

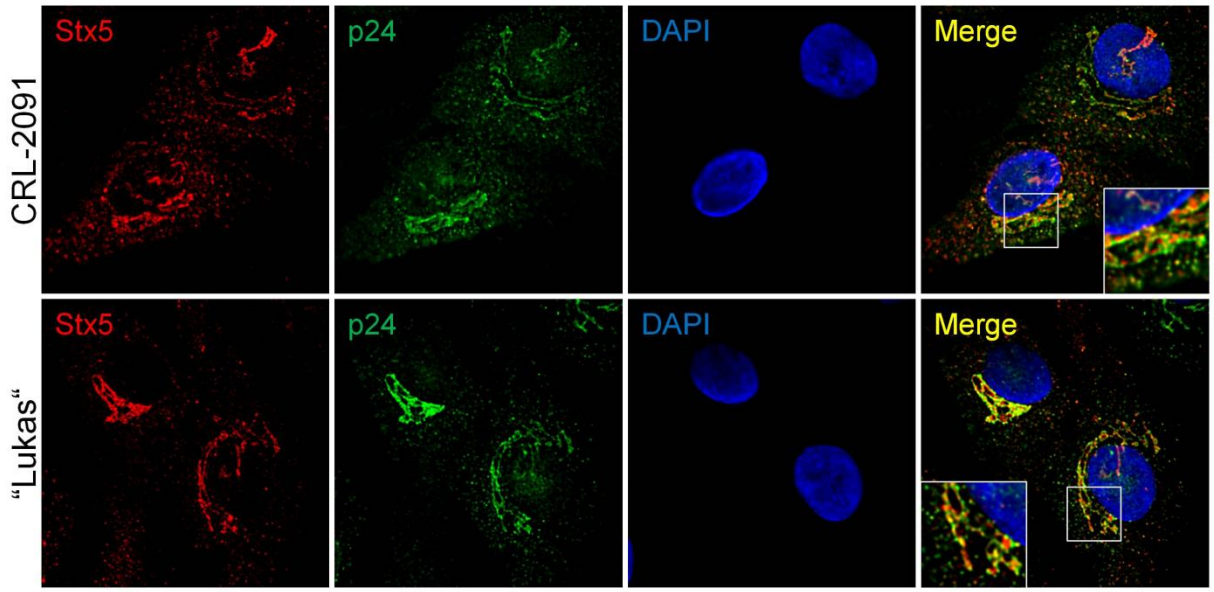

Figure 2.23 IFA: Co-localization of Syntaxin5 and p24 in OI patient and control fibroblasts

Methanol-fixated control fibroblasts (CRL-2091) and OI patient fibroblasts (“Lukas”) were immune-stained with anti-Calnexin and anti-Syntaxin5 antibodies. Shown are representative images acquired with a spinning disc confocal microscope. Magnification 100×; inlets are marked.

3 Discussion

Section 2 shows our results gathered on the proteome of COPI vesicles, the role of coatomer and Arf isoforms, as well as OI-related mutations in Sec24D. In the following these results are discussed with respect to the current knowledge, and I try to suggest how open questions could be addressed further.

3.1 A Novel Proteomic Setup

In section 2.1, our novel proteomic setup to investigate COPI is outlined. Noteworthy, the described setup has been employed to study COPII vesicles in parallel to the presented work on COPI (Adolf et al., unpublished data). With this setup we have unified various aspects of earlier proteomic studies of vesicular carriers and thus generated a simple, reliable, and adjustable workflow for proteomics of vesicles. Many MS studies of transport vesicles used endogenous vesicles, purified from tissue or cell culture (Borner et al., 2006; Hirst et al., 2012; Takamori et al., 2006). The great advantage of this approach is that native vesicles formed not *in vitro* but *in vivo* are captured. For special cases such as synaptic vesicles (SVs), which can be purified with high fidelity, this setup has proven very useful (Takamori et al., 2006). As purification of SVs is performed from brain tissue, however, experiments become more difficult to modulate because of the high demands for genetic manipulation of a whole organism e.g. by knockout/knockin.

Purification of endogenous vesicles from cell culture faces one major experimental challenge: Most vesicle types are ubiquitously found in all cell types and cannot be easily separated from all other classes of vesicles. Hence, there is a distinct issue of vesicle cross-contamination, which needs to be considered. The common vesicle types, COPI, COPII, and CCVs behave very similar during purification procedures such as differential or density gradient centrifugation. This can be deduced from the fact that COPII vesicles, formed *in vitro*, float up to the exact same fractions (2 and 3) of the density gradient shown in figure 2.3 as do COPI vesicles (M.Sc. thesis Manuel Rhiel, Adolf et al., unpublished data). Moreover, in almost all MS datasets presented here, AP-1 and AP-2 complex subunits were identified, indicating that these carriers are not easily separated from COPI and COPII vesicles. Other, earlier purification protocols, e.g. for CCVs (Hirst et al., 2004), or COPI (Gilchrist et al., 2006) were not systematically controlled for the presence of other contaminating vesicle types.

While co-purification of endogenous vesicles is a problem common to all vesicle proteomic setups, unwanted formation of other vesicles is a problem only of *in vitro* reconstitution systems. For example, when cytosol is used to produce COPI vesicles from a Golgi-enriched membrane fraction, formation of other vesicle types is unpreventable as Golgi membranes cannot be purified entirely omitting ER and other membrane contaminants. As a consequence, in a very comprehensive MS study of the ER, Golgi, and COPI vesicles, COPII coat subunits displayed high MS scores in the donor Golgi fraction and the COPI (GTPγS) fraction formed from this Golgi with cytosol (Gilchrist et al., 2006).

While contamination by other classes of newly formed vesicles can be prevented by using purified coat components, as has for example been done for COPII vesicles in yeast (Margulis et al., 2016), removing endogenous contaminations is more difficult. In this concern it has been proven useful to employ a "subtractive" setup. Borner et al. purified a fraction enriched in CCVs from wild type cells and from cells after knockdown of the pivotal CCV component Clathrin heavy chain (Borner et al., 2006). In a comparison of both fractions, the lost/subtracted proteins are the putative CCV proteins. Building on this, the same lab has refined this method by rapidly knocking CCV adaptors "sideways", i.e. tethering them to mitochondria, to investigate their function (Hirst et al., 2012). In the latter study, SILAC labeling was further introduced as the most direct means for quantitative MS in cell culture. With this setup, it is possible to assess the role of single factors during vesicle biogenesis. However, investigating the interplay of several factors at once requires preparation of cell lines with multiple knockins/knockouts and thus advanced genetic manipulation. Moreover, investigating dose-effects for chosen candidates would require fine-tuning of expression levels, e.g. by means of different promoters, complicating the experimental setup further.

In our proteomic setup (Fig. 2.5) we have tried to combine different aspects of vesicular proteomics into a novel, improved workflow. The beneficial aspects of our protocol as well as the drawbacks in comparison to other protocols are listed below.

Benefits of the novel setup:

-Simple cell culture methods; no need for genetic manipulation

-Simple/clear interpretation of MS data (SILAC ratios)

-Highly reproducible (R^2 values between runs usually ~0.7-0.9)

-Unlimited combinations/concentrations of vesicle biogenesis factors can be tested

-Dissection of molecular mechanisms in detail (e.g. through competition/titration of various factors)

Drawbacks of the novel setup: -Requires advanced protein expression/purification skills

-Vesicles are formed *in vitro* (not endogenous)

-potential limitations in capturing cytosolic factors

-Not suitable for new vesicle classes; requires fundamental knowledge of the biogenesis process (*in vitro* reconstitution system)

3.2 What Makes a COPI Vesicle

Sections 2.2 and 2.5 provide insight into protein content of COPI vesicles that were produced in a minimal system from donor membranes of various cell types. Using SILAC-based proteomics, we compared vesicles from reconstitution reactions with a mock vesicles fraction. In the mock fraction, SIC cells were treated with nucleotides and Arf1. The addition of Arf1 to the mock control became necessary as initial experiments, in which the small GTPase was omitted in the mock reaction, showed an enrichment of AP-1, another coat protein known to interact with Arf1 (Stamnes and Rothman, 1993). Having coatomer as the sole difference between both reactions solved this issue.

Using the common criterion of a >twofold enrichment for protein to be considered as candidates for the vesicle proteome resulted in a list of 122 candidate proteins in HeLa cells (Tab. 1). Most of these proteins (102) were identified in 2-3 independent experiments; a minor fraction of 20 proteins was identified in only one MS run. Since these 20 proteins were identified in a vesicles sample from isotope-labeled cells, and thus are no exterior contaminations, they were included as potential candidates into further analyses. The same vesicle versus mock setup was furthermore used to investigate the proteomes of COPI vesicles reconstituted from HepG2 cells (hepatocarcinoma) and iMΦ (murine macrophages). In HepG2 cells, 69 proteins (Tab. 11) and in iMΦ 144 proteins (Tab. 12) could be determined as candidates for the respective COPI proteome within two independent experiments. Of the three candidate lists the mean SILAC ratio was highest for HeLa (mean SILAC ratio 4.5) and lowest for HepG2 cells (mean SILAC ratio 2.82). The 144 candidates identified in iMΦ showed an average SILAC ratio of 4.18. The relatively small number of proteins that fulfill the twofold

enrichment criterion and their low mean SILAC ratio for COPI candidates proteins in HepG2 cells can be explained in several ways. Either, *in vitro* reconstitution of COPI vesicles in these cells is less efficient than in the other two cells lines, or the background that is produced by endogenous, Arf-independent coat proteins and the unspecific release of small membrane fragments during the assays is much higher in HepG2 cells. Conversely, the long list of candidates obtained for murine macrophages possibly reflects a very high suitability of these cells for this assay. Potentially, combining murine cells and murine coatomer enhances the productivity of the assay despite the fact the human and murine coatomer are highly similar (i.e. the largest subunit α-COP is 98.5 % identical).

Of the three candidate lists, 39 proteins are found in all three datasets defining them, with a very high level of fidelity, as core components of COPI vesicles. Another 44 proteins are enriched >twofold in two out of the three datasets, marking them as very good additional candidates for the COPI proteome (Fig. 2.16). Thus, of the 213 individual candidate proteins identified across three cell lines and two species roughly 40 % (83 proteins) are recurring.

The very core of the recurring proteins, the 39 ubiquitously shared proteins, contain a lot of expected, classical COPI proteins but still hint towards an important role for some proteins that has not been appreciated thus far. Classical COPI proteins are for example the various members of the p24/TMED family, which are well characterized single transmembrane proteins that cycle in the early secretory pathway, where they assist COPI biogenesis and transport of GPI anchored proteins (Belden and Barlowe, 2001; Bonnon et al., 2010; Bremser et al., 1999; Dominguez et al., 1998; Gommel et al., 2001). Additional ER-Golgi cycling proteins such as the cargo adaptors ERGIC53 (LMAN1) (Kappeler et al., 1997), the SNAREs Sec22b and Stx5 (Adolf et al., 2016; Hay et al., 1998), or the KDEL receptor (Lewis and Pelham, 1992; Munro and Pelham, 1987) (Fig. 2.16B) are also conserved COPI components. Other proteins, such as the nonaspanins TM9SF1/3, which we define as core components of COPI vesicles (Fig. 2.16B), were only recently characterized and shown to carry distinct KxD/E interaction motifs for COPI transport (Woo et al., 2015). This motif, which is conserved from yeast to human, confers Golgi-retention through interaction with coatomer. Apart from the various cycling proteins, and not unexpected, multiple glycosylation enzyme, i.e. MAN1A2, MAN1B1, MGAT2, MGAT4B, POMGNT1 (Fig. 2.16B) were among the proteins found in COPI vesicles of various cell lines. Whether Golgi-resident enzymes are enriched in COPI vesicles has been controversial since studies that based on the same methodology (immunogold labeling EM) came to opposing conclusion (Martinez-Menarguez et al., 2001; Orci et al., 2000). Several Golgi enzymes within the core COPI proteome strongly argues towards an active uptake of these proteins into COPI vesicles, in line with more recent studies (Eckert et al., 2014; Gilchrist et al., 2006; Rutz et al., 2009).

In general, there is a clear enrichment of putative or known cargo adaptors, vesicle targeting factors, and enzymes among the 39 shared proteins. These core components are strongly enriched in membrane proteins (35 proteins). Most of them have a single TM domain (20 proteins), however, the number of transmembrane spans can go up to ten in case of the calcium-transporting ATPase ATP2C1. The five proteins lacking a TM domain are ERP44, NUCB1/2, and Rab18. ERP44 is an ER-retention factor which possess a C-terminal RDEL signal and forms mixed disulfide bonds in order to retrieve its substrates (Anelli et al., 2003). NUCB1 and NUCB2 are major calcium-binding proteins of the ERGIC and cis-Golgi (Lin et al., 1998). Earlier proteomic studies of the ERGIC (Breuza et al., 2004) and the ER/Golgi and COPI vesicles (Gilchrist et al., 2006) support these findings. Interestingly, Coomassie staining of a fraction enriched in COPI vesicles reveals a distinct band with intensity comparable to those seen for membrane machinery proteins such as p24 and p25 (Rutz et al., 2009). Together with the recurring identification of both proteins with very high SILAC ratios (see Tab. 1, 11-12) this strongly argues for a high concentration of NUCB1/2 inside the lumen of COPI vesicles and a direct link between COPI vesicle transport and calcium homeostasis. Since the overall concentration of nucleobindin in the Golgi lumen is high (Lin et al., 1998) further experiments are required to investigate an active sorting into vesicles.

Another attractive hypothesis is that NUCB1/2 functions as calcium-switchable cargo receptors possibly in addition to its function as buffer for luminal calcium in the Golgi. As the concentration of calcium decreases from the ER towards the TGN (Pizzo et al., 2011), nucleobindins could bind certain proteins at a low calcium concentration (e.g. TGN), and release them at higher concentration (e.g. ER or CGN), or vice versa. Such a mechanism would resemble the pH-dependent binding/release of KDEL clients by their receptor (Wilson et al., 1993).

Of the COPI vesicle core proteome without a TM domain, Rab18 is the only protein localized to the outer leaflet of the vesicle membrane. The fact that Rab18 shows the tightest and most conserved association with COPI is partially surprising. Rab18 has mainly been implicated in lipid droplet (LD) homeostasis (Ozeki et al., 2005), a process in which it seems to interact also with COPI and the tethering complex TRAPPII (Li et al., 2017; Zappa et al., 2017). The identification of this particular Rab family member in our proteomic datasets points towards a significant role for Rab18 in addition to LD homeostasis, potentially in intra-Golgi and ER-Golgi transport. Such a function would be in line with observations made during overexpression and knockdown studies that revealed trafficking defects at these organelles when Rab18 levels were altered (Dejgaard et al., 2008).

One of the recurrent transmembrane proteins worth highlighting is QSOX2 (quiescin Q6/FAD-dependent sulfhydryl oxidase 2). QSOX2 has a single TM domain at its very C-terminus and thus a short cytoplasmic tail with the sequence RVRSRRWKVKHHHPAV (N- to C-terminus). Proteins of

this family serve formation of disulfides and have been previously placed in part to the Golgi complex (Mairet-Coello et al., 2004; Wittke et al., 2003). Here we can show for the first time that QSOX2 is a conserved component of COPI vesicles. Together with its intracellular localization, much argues for a role of COPI in its retention at the Golgi apparatus. As the cytoplasmic tail does not display any of the classical retrieval motifs (e.g. KKxx, KxKxx, KxD/E) further studies are required to determine how QSOX2 is kept at the Golgi complex.

As only Rab proteins (Tab. 1) were be identified as cytosolic factors associated with COPI vesicles, we decided to refine the assay by introducing cytosol to the budding reaction. The cytosol, which was prepared from SILAC-labeled HeLa cells, was depleted in membrane proteins but contained also luminal ER content (Fig. 2.7). In order to capture cytosolic proteins that interact with the COPI coat, vesicles were either prepared with GTP or GTPγS. The use of non-hydrolysable analogs instead of GTP did not result in a decreased level of COPI marker proteins release (Fig. 2.3).

When comparing COPI vesicles made in the presence of cytosol and GTPγS with COPI vesicles made in the presence of cytosol and GTP, 72 proteins showed a twofold enrichment in one to two experiments (Fig. 2.7B and Tab. 1). Unlike expected, the vast majority of these proteins have transmembrane domains and reside in the ER. With the exception of Arfaptin-1, no potential cytosolic COPI interactors could be identified. Arfaptin-1 has been shown to interact with the COPI coat component Arf and to be associated with the Golgi apparatus (Kanoh et al., 1997; Williger et al., 1999). However, as more recent studies place Arfaptin at the TGN (Cruz-Garcia et al., 2013; Man et al., 2011) and the fact that AP-1 coat subunits are enriched in the COPI vesicle fraction produced with GTPγS vesicles (Tab. 2), one cannot conclude with certainty that Arfaptin-1 is a cytosolic interactor of COPI vesicles.

The unexpected finding that many ER resident transmembrane proteins were enriched in the COPI vesicle fraction produced with GTPγS and cytosol prompted us to investigate this observation in more depth. A control experiment without coatomer revealed that many of these ER proteins are released from SIC in the absence of the coat complex (Tab. 3). Notably, many constituents of the tubular ER (reticulons and atlastins) were identified. As atlastins, which are involved in regulation of ER morphology (Zhao et al., 2016) are large GTPases, one possible explanation for this observation is that the tubular ER undergoes shredding due to a constitutive activation of these proteins.

Earlier reports performed with Golgi-enriched membrane fractions and cytosol suggested that non-hydrolysable GTP analogs interfere with the uptake of retrograde and anterograde cargo into COPI vesicles (Lanoix et al., 1999; Nickel et al., 1998). Our proteomic comparison of GTP and GTPγS vesicles and also WB analysis of known COPI marker proteins (Fig. 2.3B) did not hint towards a

defective uptake of these marker proteins when assays are performed with recombinant proteins and SIC.

In a nutshell, what a minimal model COPI vesicle could look like based upon our high fidelity core proteome is shown in figure 3.1. Many of the components are expected and are in agreement with previous findings. Other components, which we could identify consistently in multiple datasets, had not been appreciated as core components of COPI vesicles before.

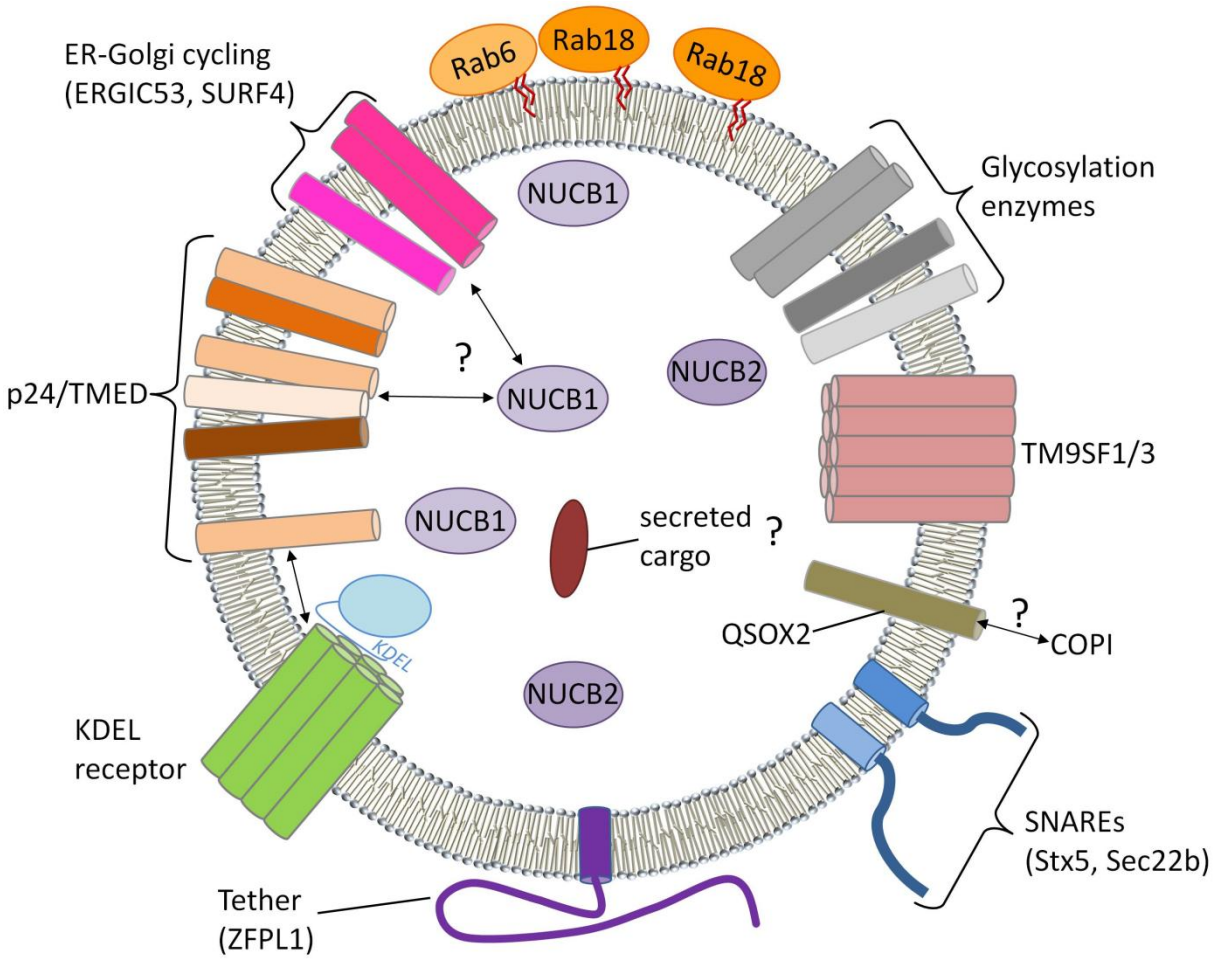

Figure 3.1 Schematic of a Model COPI Vesicle

Schematic drawing of a COPI vesicle based on our proteomic data (Fig. 2.14 and Tab. 1, Tab. 11, and Tab. 12) that highlights commonly known and new features. The vesicle contains mainly TM proteins that cycle between the ER and the Golgi. Our data together with previous observations (see 3.2) suggests that NUCB1/2 are major constituents of the COPI lumen. NUCB1/2 potentially interact with similarly abundant TM proteins for packing into vesicles (e.g. p24 proteins) and serve as cargo-adaptors. Secreted cargo, if present, is found only at low concentration. Glycosylation enzymes are retained by COPI. Targeting/fusion of the vesicle is performed by SNAREs (most prominently Stx5 and Sec22b) as well as tethering factors (ZFPL1) and Rab proteins. Rab18, was the most frequently identified Rab family member associated with COPI. Some core components of COPI vesicles, e.g. QSOX2, are likely retained in the Golgi through interaction with the COPI coat via an unknown mechanism/motif.

However, many open questions concerning the protein content of COPI vesicles remain. Some questions that future research, especially with respect to coatomer and Arf isoforms, could try and answer are mentioned in sections 3.3 and 3.4. Two more general aspects of COPI that could be addressed by future research are discussed below.

i) Role of COPI in the endosomal system

A most recent study in yeast provides strong evidence that COPI plays a role in recycling of the exocytic SNARE Snc1 through recognition of its ubiquitinated form and subsequent trafficking through the endosomal system (Xu et al., 2017). This is in line with earlier studies in mammalian cells which provided evidence for the localization of COPI on endosomes and even suggested vesicle budding at these sites (Aniento et al., 1996; Whitney et al., 1995). A possible role of COP in the endosomal system in mammals could be studied further e.g. by the following experiments:

-Using isolated endosomal membrane fractions for COPI binding/budding studies

-MS analysis of potential endosomal COPI vesicles

-MS of COPI vesicles after temperature block at the TGN (Saraste and Kuismanen, 1984)

-Knocksideways of COPI and monitoring of the effect on the endosomal system (Robinson et al., 2010)

ii) COPI on lipid droplets

Lipid droplets are cellular inclusions that serve the storage of neutral lipids (Guo et al., 2009). LD homeostasis has been previously linked to COPI (Beller et al., 2008; Guo et al., 2008). Transport of proteins to LDs (Soni et al., 2009) and localization and activity of COPI proteins on LDs (Wilfling et al., 2014) has been shown earlier. Most recent studies further linked the tethering complex TRAPP and Rab18 to LD homeostasis (Li et al., 2017; Zappa et al., 2017). This could be further addressed by:

-Using isolated LDs to perform micro LD budding with COPI with subsequent proteomic analysis (Wilfling et al., 2014)

-Interaction studies between LD proteins and the COPI coat components (targeting motifs?)

-Lipidomic analysis of COPI-budded micro LDs and their parental donor LDs

3.3 The Role of Coatomer isoforms

As mentioned in the introduction, coatomer is a heptameric complex. Two of its seven subunits, γ- and ζ-COP, exist as two isoforms. What function these isoforms serve remains largely elusive. A main function that isoforms of coat proteins have been shown to serve is sorting of cargo and machinery. Prominent examples are the isoforms of mammalian Sec24, which pack the ER-Golgi SNAREs (Mancias and Goldberg, 2007, 2008), transporters of the plasma membrane (Farhan et al., 2007; Sucic et al., 2011), and many ER-Golgi cycling proteins (M.Sc. thesis Manuel Rhiel, Adolf et al., unpublished data) into COPII vesicles in an isoform-specific manner. In order to investigate an equivalent function for the isoforms of the COPI coat, we have compared hundreds of COPI vesicle proteins at once in our novel MS setup (Fig. 2.5).

In a direct comparison of $\gamma_1\zeta_1$- and $\gamma_2\zeta_1$-vesicles all proteins crowd around a SILAC ratio of one. No proteins are >twofold enriched in vesicles reconstituted with $\gamma_1\zeta_1$ over $\gamma_2\zeta_1$-vesicles (Tab. 4). A few proteins display a slight enrichment in vesicles formed using $\gamma_2\zeta_1$ (Fig. 2.9 and Tab. 5), however, the most promising candidates based on their SILAC ratios are mitochondrial proteins (HSPD1, ATP5B, and ATP5A1). Abundant proteins such as p24 and ERGIC53, which give highly similar signals in Western blot analyses (Fig. 2.8), display equally similar SILAC ratios in MS experiments. In our datasets ERGIC53 and p24 are slightly more enriched in $\gamma_1\zeta_1$-vesicles as compared to $\gamma_2\zeta_1$-vesicles, showing mean SILAC ratios of 1.11 (ERGIC53) and 1.16 (p24). Since there was a slightly higher incorporation of both proteins by $\gamma_2\zeta_1$ in vesicles assays analyzed by Western blot (Fig. 2.8), these subtle differences, especially since both proteins behave in the same way, are not significant and in the margin of error of this system.

Similarly, a proteomic comparison of COPI vesicles reconstituted with recombinant coatomer containing either ζ_1- or ζ_2-COP did not reveal any major differences. A few proteins (i.e. TM9SF1, TPBG, POMGNT1, and ZDHHC13) are somewhat more enriched in $\gamma_1\zeta_1$- compared to $\gamma_1\zeta_2$-vesicles (Fig. 2.10 and Tab. 6). Of these four potential candidates, TPBG can be discarded because it was not enriched in COPI vesicles made with $\gamma_1\zeta_1$ compared to a control (Tab. 1). The remaining three proteins were found >twofold enriched in COPI vesicles in the same experiments and are thus candidates for the COPI proteome. However, also ERGIC53 (SILAC ratio 1.11) and p24 (SILAC ratio 1.09) were slightly enriched in COPI vesicles prepared with $\gamma_1\zeta_1$- compared to $\gamma_1\zeta_2$ coatomer. Hence, the observed differences for TM9SF1, POMGNT1, and ZDHHC13 are likely to result from a slightly better budding efficacy during these experiments, rather than differential sorting of these proteins by ζ_1-COP. In isotypic vesicles formed by ζ_2-COP, only one protein, the monocarboxylate transporter 1

(SLC16A1) stood out with a rather high mean SILAC ratio of 3.75 (Fig. 2.10 and Tab. 7). However, the two individual SILAC ratios for this protein (6.13 and 1.37) are highly diverging, rendering it a rather weak candidate for being a ζ_2-COP specific client. In summary, it can be concluded that the isoforms of coatomer do not seem to sort the COPI core components differentially.

We furthermore investigated a potential influence of coatomer isoforms on the size of vesicles. In the CCV system it has been shown previously that clathrin adaptor proteins such as AP180 (Zhang et al., 1998) or clathrin assembly lymphoid myeloid leukemia protein (CALM) (Miller et al., 2015) influence the size of endocytic vesicles. Contrary, isoforms of the COPII coat subunit Sec24 in yeast (Sec24p and Lst1p) have been shown to give rise to vesicles with highly similar size and morphology (Miller et al., 2002). To explore this putative function, negatively stained EM images of isotypic COPI vesicles were analyzed systematically using bioinformatics tools for accurate segmentation of objects. The compiled data, presented in figure 2.11, shows that neither isoforms of γ- nor ζ-COP have a substantial influence on the size of COPI vesicles. Indeed, the size of isotypic vesicles was almost identical to that of vesicles reconstituted using an endogenous mix of all CM isoforms represented by rat CM (Fig. 2.11). Noteworthy, the average size of vesicles determined by our approach (~74 nm) matches the size of COPI vesicles determined at the time of their initial discovery (74-76 nm) (Orci et al., 1989). A most recent *in situ* study revealed that COPI vesicles are not uniform with respect to their size and the luminal density under the electron microscope (Bykov et al., 2017). This plasticity is reflected by the standard deviations which range from 7.7 to 8.9 nm (Fig. 2.11).

With our MS and EM data presented throughout this thesis, we can exclude two major functions for the isoforms of CM subunits: i) the uptake of core components into vesicles, and ii) the modulation of COPI vesicle size. This leaves the question regarding a function of these isoforms unanswered. Two previous studies point towards a diverging function of CM isoforms. First, an EM-based study of intracellular coatomer isoform distribution showed that $\gamma_1\zeta_1$ and $\gamma_1\zeta_2$ were preferentially at the cis-Golgi, whereas $\gamma_2\zeta_1$ concentrated at the trans-side (Moelleken et al., 2007). A later study by Hamlin et al. showed that Scyl1, an inactive cytosolic kinase, interacts preferentially with γ_2-COP and class II Arfs (Hamlin et al., 2014). Mutations in Scyl1 have been implicated in the development of neuropathies and liver failure (Schmidt et al., 2007; Schmidt et al., 2015). Scyl1 has furthermore been shown to interact with coatomer (Burman et al., 2008; Ma and Goldberg, 2013), co-localizes with the ERGIC and cis-Golgi as well as COPI coat proteins (Burman et al., 2008), and to influence Golgi apparatus morphology (Burman et al., 2010). Despite these observations, a functional link between COPI and Scyl1 is missing.

The fact that COPI vesicles are not entirely uniform was observed earlier as they can vary largely with respect to their appearance in the electron microscope (Bykov et al., 2017; Donohoe et al., 2007).

Donohoe et al. defined COPIa vesicles in algae and plants, which show a light content and form at the cis-Golgi, and COPIb vesicles that display a strongly stained lumen in EM studies and form at the medial- and trans-Golgi. As we could not observe any visual differences between isotypic vesicles (compare vesicles in Fig. 2.11), a link between the mammalian coatomer isoforms and putative COPIa/b vesicles is highly unlikely. Moreover, a differential interaction of COPI vesicles with various tethers of the Golgi complex have been described (Malsam et al., 2005; Wong and Munro, 2014). While the p115/GM130(GOLGA2) tethering complex selectively associated with COPI vesicles carrying ER-Golgi cycling proteins such as members of the p24 family, the intra-Golgi tethering pair golgin-84(GOLGA5)/CASP(CUX1) was found to tether those vesicles that carry Golgi enzymes (Malsam et al., 2005). Three of these proteins, GM130, golgin-84 and CASP were identified in our datasets of isotypic COPI vesicles. Two of them, golgin-84 and CASP, were furthermore found consistently enriched in COPI vesicles (Fig. 2.16). However, in all comparisons of COPI vesicles made with a single isoform of coatomer, none of the three proteins was significantly enriched. Hence, a functional link between CM isoforms and Golgi tethers is unlikely.

As we could not determine a function for γ- or ζ-COP isoforms, further investigations are required. Three putative functions of coatomer isoforms and how they could be addressed experimentally are listed in the following:

i) Coatomer isoforms could have a specific role in protein sorting in polarized cell type (i.e. neurons)

Isoforms of CM could function similar to isoforms of adaptor protein complexes (see 1.4.3) in sorting of proteins into different trafficking routs. This question could be addressed by:

-Comparative COPI proteomics according to Fig. 2.5 using e.g. a neuronal cell line

-Knockout of isoforms in specific cell lines

-Knocksideways with adjacent purification of endogenous COPI vesicles and MS analysis

-Immunoprecipitation of endogenous COPI vesicles using isoform-specific antibodies

ii) CM isoforms could fulfill a specific function in cargo export or at a certain cellular condition

Using our proteomics approach we were able to identify the core machinery of COPI vesicles. We did not find many cargo proteins, possibly due to their low concentration. During all experiments cells grown under optimal conditions we used. Hence, we did not address a role of CM isoforms under challenging conditions or with a focus on uptake of secreted cargo. A possible role of CM isoforms in these processes could be further challenged by:

-COPI proteomics under stress conditions (e.g. starvation/drug treatment)

-Knockdown/knockout of CM isoforms with concomitant starvation/drug treatment

-Vesicle proteomics using cells with secreted proteins trapped in the ERGIC (15°C) or the TGN (20°C) by temperature block (Saraste and Kuismanen, 1984)

-Using a secreted model protein to assess the effect of CM isoforms on protein secretion via knockdown/knockout

iii) CM isoforms could act in combination with different isoforms of Arf

We have not assessed the possibility that isoforms of CM interact differentially with COPI forming isoforms of Arf.

-COPI proteomics analyzing various combinations of CM/Arf isoforms according to Fig. 2.5

-Bio-ID of CM/Arf isoforms to fish for potential isoform specific interactors

-Competition of different Arfs during vesicle biogenesis (Popoff et al., 2011b)

3.4 The Role Arf Isoforms

In addition to isoforms of the outer COPI coat complex coatomer, we have investigated systematically the function of Arf isoforms. To this end, human Arf isoforms Arf3-6 were cloned into our improved expression system in which the expression of myristoyltransferase (hNMT1) and methionine aminopeptidase (MetAP1) can be induced independently prior to the induction of Arf expression (see Material and Methods). This allowed us to produce Arf isoforms with high purity and a degree of myristoylation close to 100% (Fig. 2.12A). As has been previously shown by Popoff et al. (2011b) in a reconstitution system based on rat liver Golgi membranes and rat liver coatomer, all

isoforms of Arf except Arf6, promote formation of COPI vesicles *in vitro* (Fig. 2.12B). This is in line with the observation that Arf6 localizes to the plasma membrane where it is implicated in playing a role in endocytosis rather than promoting COPI transport (Cavenagh et al., 1996; D'Souza-Schorey et al., 1995). Popoff et al. (2011b) furthermore showed that Arf3 can be outcompeted from COPI vesicles by other Arf isoforms. In agreement with this finding and further studies that place Arf3 at the TGN, where it is specifically activated by the GEF protein brefeldin A-inhibited guanine nucleotide-exchange protein 1 (BIG1) (Manolea et al., 2010), a significantly lower but still appreciable release of ERGIC53 and p24 could be observed when COPI reconstitution from SIC was performed with Arf3 compared to Arf1, Arf4, and Arf5 (Fig. 2.12B). Accordingly, endogenous Arf4 and also Arf5 were found in multiple COPI proteomics datasets (e.g. Arf4 can be found in Tab. 1), while Arf6 was never identified. Whether Arf3 was also present cannot be concluded due to its high sequence similarity to Arf1 that is not resolved by MS.

To challenge a putative role of Arf isoforms in modulating the content of COPI vesicles we used our SILAC-based mass spectrometry setup (Fig. 2.5) to study the content of these carriers prepared with Arf3-5 (Fig. 2.13 and Tab. 8-10). In comparisons of COPI vesicles reconstituted with Arf3-5 with a mock reaction, overall less peptides/proteins were identified compared to samples produced with Arf1. Least proteins were identified with Arf3, again in agreement with previous observations (Fig. 2.12). Only 25 proteins were >twofold enriched in Arf3-COPI vesicles, 50 proteins in COPI vesicles made with Arf4, and 55 proteins in vesicles reconstituted with Arf5 (Tab. 8-10). These 25-56 proteins however, largely overlapped with the COPI proteomics dataset acquired with Arf1 (Fig. 2.14A). Only 8 proteins were not identified with Arf1. These proteins are among the proteome candidates with the lowest SILAC scores. The 6 proteins unique to Arf5 display a mean SILAC ratio of 2.03 including the ribosomal proteins RPL13 and RPL18 which are obvious contaminants. The list of proteins shared between all Arf isoforms (Fig. 2.14B) largely overlaps with the list of proteins identified as COPI protein candidates in different cell lines (Fig. 2.16). Of the 20 proteins shared among all Arf-isotypic COPI vesicles, 17 are found in COPI vesicles made with Arf1 from three different cell types. These proteins include five p24/TMED proteins, the SNAREs Sec22b and Stx5, ER-Golgi cycling proteins such as ERGIC1/2 and LMAN1/2 plus additional targeting factors like ZFPL1 and Rab18 (core components of COPI vesicles as discussed in 3.2).

It can be concluded that the core content of a given COPI vesicle does not depend on usage of a given Arf isoform (Fig. 2.14A), whereas the total yield of reconstituted vesicles, judged by the number of identified peptides and proteins, seems to change. These findings indicate that Arf1 is the most potent small GTPase for COPI vesicle biogenesis. This is in line with the fact that the expression level of Arf1 in rat liver is more than fivefold higher than that of Arf5 and threefold higher than that

of Arf3 (Popoff et al., 2011b). Moreover, knockdown studies performed by the lab of Richard Kahn highlight the importance of Arf1 for COPI transport (Volpicelli-Daley et al., 2005). They found that depletion of a single Arf isoform did not interfere with protein traffic and or Golgi morphology. Only when knocking down two Arf isoforms at a time did they observe phenotypes. Knockdowns of various combinations of Arf3-5 interfered mainly with recycling of the transferrin receptor at the PM, and, when Arf4 was depleted, mislocalization of the KDEL receptor. However, only when Arf1 was knocked down in combination with Arf3-5 did they observe changed Golgi morphology or localization of coatomer (Volpicelli-Daley et al., 2005).

A specialized role for Arf4 and Arf5 is supported by the findings that both proteins respond differently to class I Arfs during BFA treatment. Their membrane association, especially with the ERGIC, seems to much less affected by the drug (Chun et al., 2008; Duijsings et al., 2009). Moreover, Arf4 has been shown to play a role in trafficking of Rhodopsin C at the late Golgi/TGN (Deretic et al., 2005), whereas Arf5 has been implicated in endocytosis of α5β1 intergin (Moravec et al., 2012) and the disease gerodermia osteodysplastica that a cause by mutations of golgin GORAB that interacts specifically with Rab6 and Arf5 (Egerer et al., 2015).

Several aspects of how differential roles of Arf isoforms could be challenged experimentally are already described in the previous section (3.3). Interaction studies between different isoforms of Arf and coatomer as well as uptake of temperature-blocked cargo into COPI vesicles with different Arf isoforms could be tested. A focus of further investigations of Arf isoforms, however, should be placed on their role in post-Golgi trafficking. Multiple studies, cited in this paragraph, forward a role of Arf3-5 in specialized cargo sorting in the TGN/endosomal system. In this respect, the knocksideways approach, which has successfully been used to investigate the role of CCV adaptor proteins (Hirst et al., 2012), would provide a very useful tool, as it could be used in various cell types of interest.

3.5 Syndromic *Osteogenesis Imperfecta* Caused by Compromised ER-Golgi SNARE Sorting?

As part of this study, a most recently discovered link between a syndromic form of OI and mutations within the COPII coat subunit Sec24D was investigated (Garbes et al., 2015). To this end, point mutations found in the patients were introduced to recombinant proteins in order to study their effect on a molecular level. We found that one of the mutations (S1016F) had a strong negative effect on the ability of Sec24D to sort the ER-Golgi Q-SNAREs Stx5, GS27, and Bet1 into COPII vesicles

(Fig. 2.19). The ability of the protein to bind and incorporate ERGIC53 was comparable to the wild type and all other mutants tested, which emphasizes that various independent binding sites are displayed by the COPII coat for active sorting. The second patient-derived mutant COPII variant, Sec23A/Sec24D^{Q979P} showed only minor, ~5-15 %, reduced levels of SNARE-uptake. Since ERGIC53 incorporation was also slightly reduced by ~7 % with this mutant (Fig. 2.19B), it can be concluded that the second mutation has no specific effect on SNARE-sorting. The fact that the Sec23A/Sec24D^{Q979P} did not display a significant impairment of protein uptake is in line with the localization of the regarding glutamate residue in a region distant from the membrane (Fig. 2.17B and C). It is not in immediate proximity to any known binding site for ER export signals. Likewise, the effect observed for the S1016F-mutation is compatible with its localization within the structure, close to the Stx5 binding pocket (Fig. 2.17B and C).

In a previous study we could provide strong evidence that the ER-Golgi Q-SNAREs are sorted into COPII vesicles as a pre-assembled complex via an interaction of Sec24C/D with Syntaxin5 (Adolf et al., 2016). In order to analyze if the ~50 % reduced SNARE-uptake by Sec23A/Sec24D^{S1016F} was a result of a flawed direct interaction between Syntaxin5 and Sec24D, pulldown experiments were performed. As has been previously observed for Sec24C (Adolf et al., 2016), the shortened Syntaxin5 construct Syntaxin5$^{205-328}$-GST displays a very strong interaction also with Sec24D (Fig. 2.20). This interaction was completely abrogated in experiments performed with the binding site mutant Sec23A/Sec24D^{LIL834AAA} (Mancias and Goldberg, 2008) or the OI-patient mutant Sec23A/Sec24D^{S1016F}, coherent with the observations made during the vesicle reconstitution experiments. Here, the second point mutant, Sec23A/Sec24D^{Q979P} showed a minor defect in Sec23A/Sec24D binding (~20 % less than wild type).

Having amounted functional data that showed a major SNARE-sorting defect of one OI-related point mutation, Sec23A/Sec24D^{S1016F}, and no (or potentially a very mild) effect on protein uptake by the second mutation Sec23A/Sec24D^{Q979P}, we decided to study Sec24D-deficiency in a cellular context. To this end, OI-patient derived fibroblasts “Lukas” (genotype Sec24D^{Q208*}/Sec24D^{S1015F}) were analyzed in comparison to a fibroblast control cell line (CRL-2091). Both cells in a first step were studied with respect to the protein level of multiple ER/Golgi proteins (Fig. 2.21). As a general loading control Histone H3 was detected, which showed only a slightly reduced protein level (91 % of control). Also other proteins such as the ER chaperone Calnexin (99 % of control) or the intra-Golgi SNARE Ykt6 (107 % of control) displayed protein levels in patient fibroblasts highly comparable to control cells. Other proteins, such as p24 and GS27 displayed a reduction of ~25 % in “Lukas” fibroblasts. The strongest reduction was observed for the SNAREs Stx5, Bet1, Sec22b, and GS28 (>40-50%). This observation indicates that an impairment of proper trafficking/ER export of proteins can cause their

degradation. Stx5, which binds directly to Sec24D (Fig. 2.20) shows the strongest reduction of protein level in patient cells, together with Bet1, the transport of which is also directly coupled to Stx5 (Adolf et al., 2016). Surprisingly, GS27, which is also part of the ER-Golgi Q-SNARE complex showed only a slightly reduced protein level (Fig. 2.21). Moreover, Sec22b, the R-SNARE that is not sorted by Sec24C/D but by Sec24A/B, displayed a substantially lower protein level, as does the Q-SNARE GS28. Interestingly, p24 displayed a ~25% reduced protein level in patient cells, similar to GS27. Assuming that the reduced protein level of the SNARE-complex partners Stx5, Bet1, GS27, and Sec22b is a result of their miss-sorting, a similar observation for p24 would be perfectly in line with unpublished observation from our lab that shows a Sec24C/D specific sorting of this protein (Adolf et al., unpublished data). Moreover, RNAi experiments from the Hauri lab pointed towards incorporation into COPII vesicles of p24 by Sec24C/D (Bonnon et al., 2010). The down-regulation of the SNARE GS28 makes sense in the light of its involvement in two SNARE complexes with different combination of Stx5, Bet1, Ykt6, and GS15 (Shorter et al., 2002; Xu et al., 2002; Zhang and Hong, 2001). Conversely, the fact that Ykt6 protein levels are not affected by the Sec24D mutations points towards the de-coupling of the fate of this particular SNARE from other interacting SNAREs. Ykt6 has been implicated in ER-Golgi, endosome-TGN, and intra-Golgi transport (Fukasawa et al., 2004; Tai et al., 2004; Xu et al., 2002; Zhang and Hong, 2001). Apart from its engagement in multiple, different trafficking events, Ykt6 is special in that it has no transmembrane domain but is lipidated to enable membrane association (Fukasawa et al., 2004). A large proportion of the protein seems to be in a cytosolic, potentially inactive state (Hasegawa et al., 2004; Zhang and Hong, 2001). All these peculiarities might contribute to its protein levels not responding to perturbation of Sec24D.

Having observed that the protein levels of multiple proteins, especially the ER-Golgi SNAREs, were significantly lower in Sec24D-deficient patient cells compared to control fibroblasts, we decided to probe their intra-cellular localization. One possible effect of the reduced SNARE binding and sorting observed *in vitro* (Figs. 2.19 and 2.20) could be a miss-localization of these proteins. However, in both, control and patient fibroblasts, Syntaxin5 showed a peri-nuclear stain (Figs. 2.21 and 2.22). This is in line with previous IFA observations that localized Stx5 predominantly at the Golgi (Bennett et al., 1993; Subramaniam et al., 1997). No shift towards the ER, here stained with Calnexin (Fig. 2.22) could be observed, as there was no overlap between both signals. Furthermore, both fibroblast lines displayed a highly similar level of co-localization between Stx5 and p24 with possibly a slightly higher degree of co-localization in patient cells (Fig. 2.21). Moreover, the Stx5-positive punctate structures observed in both cell types appeared in general more distinct in OI fibroblasts compared to its control (Figs. 2.22 and 2.23). Taken together, the IFA observations lead to the conclusion that Sec24D deficiency does not cause a major redistribution of Stx5, Calnexin, and p24. The residual incorporation into COPII vesicles, observed for the Sec23/Sec24D^{S1016F} mutant (Fig. 2.19), in addition

to the activity of Sec24C, which possesses the same sorting specificity for p24 (Adolf et al., unpublished data) and the ER-Golgi Q-SNAREs (Adolf et al., 2016; Mancias and Goldberg, 2008), are sufficient to facilitate their proper localization. Potentially, the localization of Stx5 is slightly changed in relation to p24, as has been for some cells. However, most of the times patient and control cells were non-distinguishable during IF assays using antibodies against Stx5/p24. The second general observation, namely weaker, less distinct Stx5 punctae, was made more frequently. Assuming that these structures are either vesicles or sites of vesicle biogenesis (i.e. ERES), a lesser staining with Stx5 is in agreement with the hampered incorporation of this protein into COPII vesicles by the Sec23/Sec24D^{S1016F} mutant (Fig. 2.19) and the reduced Sec24D protein level in these cells due to the premature stop-codon in the second allele (Garbes et al., 2015).

In summary, the experiments show that one of the two point mutations found in Sec24D involved in the development of a syndromic form of OI shows a SNARE sorting and binding defect (Figs. 2.20 and 2.21) that is equivalent to a synthetic mutant designed for this very purpose (Mancias and Goldberg, 2008). The intracellular localization of the Sec24D-interacting SNARE Stx5, however, remained largely unaltered (Figs. 2.22 and 2. 23). This leads to the question of a role for Sec24D in the development of this syndrome, a hallmark of which is the imperfect built of extracellular collagen networks. Mutations within the COPII coat subunit Sec23A were previously linked to Cranio-lenticulo-sutural dysplasia (CLSD), which is also marked by a hampered collagen secretion (Boyadjiev et al., 2006; Fromme et al., 2007). Noteworthy, disruption of the Sec24D gene in the model organisms medaka (Ohisa et al., 2010) and zebrafish (Sarmah et al., 2010) results in highly similar symptoms, namely an imperfect skeletal morphogenesis especially of the craniofacial region due to a hampered secretion of extracellular matrix proteins. Knockdown of Sec24C, which in terms of SNARE-sorting shows the same preferences as Sec24D (Mancias and Goldberg, 2008) did not result in the phenotype of Sec24D disruption (Sarmah et al., 2010). Hence, it can be concluded that the isoforms Sec24D plays a crucial role in ossification and assembly of the extracellular matrix (ECM), potentially in concert with Sec23A (Boyadjiev et al., 2006; Lang et al., 2006).

The export of large cargoes, especially of (pro)collagen (PC) pivotal for ossification and ECM assembly, is highly regulated and involves additional factors such as TANGO1 and cTAGE5 at the ER (Malhotra and Erlmann, 2011, 2015). These factors bind to the inner COPII coat via Sec23. Binding to Sec24C has also been reported, but remains controversial (Ma and Goldberg, 2016; Saito et al., 2009; Saito et al., 2011). In addition, special requirements for vesicle fusion machinery have been pointed out. For secretion of collagen I and collagen VII, the protein Sly1 and the SNAREs Stx18 (collagen VII) and Stx5 (collagen I and VII) have been shown to be crucial (Nogueira et al., 2014). Noteworthy, Stx5

has early been known as one of the SNARE proteins absolutely required for secretion (Gordon et al., 2010).

In conclusion different scenarios why Sec24D deficiency leads to OI are possible. Two of these scenarios as well as arguments for and against them are listed below together with a few experiments that would challenge them:

i) Sec24D is crucial for the formation of large COPII super-carriers.

Pro:

-Sec24D loss in model organisms and syndromic OI patients leads to skeletal morphogenesis defects (Garbes et al., 2015; Ohisa et al., 2010; Sarmah et al., 2010)

-Sec24C knockdown does not resemble Sec24D loss in zebrafish (Sarmah et al., 2010)

-TANGO1/cTAGE5 were shown to interact with both subunits of the inner COPII coat, Sec23 and Sec24 in yeast two-hybrid (Saito et al., 2009)

-Sec24D has been shown to be able and pack procollagen I into COPII vesicles (Gorur et al., 2017)

Contra:

- Positive yeast two-hybrid interaction studies were performed with Sec24C and not Sec24D (Saito et al., 2009)

-TANGO1/cTAGE5 did not interact with Sec24C in pulldown experiments (Ma and Goldberg, 2016)

-packing of procollagen I into COPII vesicles was cytosol-dependent in an *in vitro* system (Gorur et al., 2017)

Experiments to address this hypothesis include:

-Interaction studies between all Sec24 isoforms, especially Sec24D, and TANGO1/cTAGE5 via pulldowns/yeast two-hybrid

-Systematic *in vitro* reconstitution studies to assess packing of procollagens using defined recombinant proteins

-Overexpression of Sec24C in Sec24D deficient cells/fish to test whether the defect can be rescued

ii) ER-Golgi SNARE levels are critical for collagen export and partly controlled by Sec24D

Pro: -Stx5 has been shown to be critical for PC I and VII export (Nogueira et al., 2014)

-ER-Golgi SNAREs expression levels are reduced in OI patient cells (this study)

-Stx5 is important for constitutive secretion (Gordon et al., 2010)

Contra: -Sec24C and Sec24D were shown to be functionally redundant in terms of SNARE sorting (Mancias and Goldberg, 2008)

-No abnormal localization of ER/Golgi proteins in patient cells despite a lower SNARE protein level (this study)

-Stx5 and Bet1 expression levels were up-regulated in cells put under ER stress (Suga et al., 2015)

Experiments to address this hypothesis include:

-To investigate the expression level of ER-Golgi SNAREs (i.e. Stx5, Bet1) in different Sec24 isoform knockdown/knockout cells

-To introduce the Stx5-binding mutation into Sec24C via genome editing and evaluate PC export from the ER

-Overexpression of Stx5/Bet1 in Sec24D-deficient cells

4 Materials and Methods

4.1 Chemicals, Commercial Kits, Supplies, and Instruments

Chemicals, kits for molecular biology and cell culture, disposable plastic ware, proteins (antibodies), DNA, and instrumentation was purchased from one of the companies listed below.

Abcam	Cambridge, UK
Acris (part of OriGene)	Herford, Germany
Affymetrix (part of TFS)	Santa Clara, USA
Anthos Mikrosysteme	Friesoythe, Germany
Assistent	Sondheim, Germany
Axon Labortechnik	Kaiserslautern, Germany
Beckman Coulter	Pasadena, USA
BD Biosciences	Franklin Lakes, USA
Biomers	Ulm, Germany
Bio-Rad	München, Germany
Boehringer	Mannheim, Germany
Carl Zeiss	Oberkochen, Germany
Dr. Maisch HPLC	Ammerbuch-Entringen, Germany
Eppendorf	Hamburg, Germany
Fluka	Taufkirchen, Germany
GERBU Biotechnik	Heidelberg, Germany
GE-Healthcare	Freiburg, Germany
Greiner Bio-One	Frickenhausen, Germany
Heraeus	Hanau, Germany
IBA Lifesciences	Göttingen, Germany
Intavis Bioanalytical Instruments AG	Köln, Germany
Invitrogen (part of TFS)	Carlsbad, USA
Jenway	Staffordshire, UK
LI-CORE	Lincoln, USA
Life Technologies (part of TFS)	Carlsbad, USA
Macherey-Nagel	Düren, Germany
Merck	Darmstadt, Germany

Merck-Millipore/Novagen (part of Merck)	Darmstadt, Germany
Microfluidics Corp.	Westwood, USA
New England Biolabs (NEB)	Frankfurt, Germany
Parr Instruments	Moline, USA
PerkinElmer	Waltham, USA
PeqLab	Erlangen, Germany
Roboklon	Berlin, Germany
Roche	Mannheim, Germany
Roth	Karlsruhe, Germany
Santa Cruz Biotechnology	Heidelberg, Germany
Sarstedt	Nümbrecht, Germany
Sartorius	Göttingen, Germany
Serva	Heidelberg, Germany
Sigma-Aldrich (part of Merck)	Taufkirchen, Germany
Silantes	München, Germany
Sorvall (part of TFS)	Waltham, USA
Source BioScience	Nottingham, UK
Thermo Fisher Scientific (TFS)	Waltham, USA
Qiagen	Hilden, Germany

4.2 Molecular Biology Materials

4.2.1 Enzymes for Cloning

PCRs were performed with Pfu Plus! DNA polymerase (Roboklon). Restriction of plasmids and PCR-generated inserts was carried out using NEB restriction enzymes. Plasmids were usually dephosphorylated using calf intestine alkaline phosphatase (Roche) before ligation with an insert achieved by incubation with T4 DNA ligase (Thermo Fisher Scientific). Colony PCRs were performed with Taq polymerase (Axon).

4.2.2 DNA Ladder

As size standard during agarose gel electrophoresis either 1kb DNA Ladder or 2-Log DNA ladder from NEB were used.

4.2.3 Bacterial Selection Reagents

The following reagents were used for selection of bacterial clones after transformation. They were prepared as stock-solutions (1000×) and diluted in the growth medium down to the final concentration.

Substance	**Storage Temp.**	**Solvent**	**Concentration (final)**
Ampicillin	-20°C	H_2O	100 µg/ml
Bluo-Gal	-20°C	DMF	20 µg/ml
Chloramphenicol	+4°C	Ethanol	25 µg/ml
Gentamicin	+4°C	H_2O	7 µg/ml
Kanamycin	-20°C	H_2O	50 µg/ml
Tetracyclin	-20°C	Ethanol	10 µg/ml

4.2.4 Bacterial Media

Bacteria were usually grown in Luria broth (LB) or on LB agar dishes. After transformation they were grown in super optimal broth with catabolite repression medium (SOC). All media were autoclaved before use.

Medium	**Ingredient**	**Concentration**
LB	Trypton	10 g/l
	Yeast extract	5 g/l
	Sodium chloride	10 g/l
LB agar	Trypton	10 g/l
	Yeast extract	5 g/l
	Sodium chloride	10 g/l
	Agar	15 g/l

SOC	Trypton	10 g/l
	Yeast extract	5 g/l
	Sodium chloride	10 g/l
	Potassium chloride	0.59 g/l
	Magnesium chloride	0.19 g/l

4.2.5 Bacterial Strains

Strain	**Application**	**Source**
E.coli DH5α	Cloning	Invitrogen
E.coli BL21 (DE3)	Protein expression	Invitrogen
E.coli BL21-CodonPlus-RIL (DE3)	Protein expression	Invitrogen
E.coli DH10MultiBac^{Cre}	Cloning/Recombination	Imre Berger (EMBL, Grenoble)

4.2.6 Oligonucleotides

Oligonucleotides were purchased from Biomers. They were used as primers in PCR reactions for molecular cloning of the indicated inserts and for sequencing.

Primer name	**Sequence (5`-3`)**	**Insert**
hArf3 For NcoI	AAAAAACCATGGGCAATATCTTTGG	hArf3
hArf3 Rev HindIII	TTTTTTAAGCTTTTACTTCTTGTTTTTGAGC	hArf3
hArf4 For NcoI	AAAAAACCATGGGCCTCACTATC	hArf4
hArf4 Rev HindIII	TTTTTTAAGCTTTTAACGTTTTGAAAGC	hArf4
hArf5 For NcoI_new	AAAAAACCATGGGCCTCACCG	hArf5
hArf5 Rev HindIII	TTTTTTAAGCTTTTAGCGCTTTGACAGC	hArf5
Sec24D mut2936A-C-fw	GGGTATTATCCCACAAAAGAGGCC	Sec24D-Q979P
Sec24D mut2936A-C-rev	GGCCTCTTTTGTGGGATAATACCC	Sec24D-Q979P
Sec24D mut3047C-T-fw	CGGAGGCTCTTTTTATGTGGATTTCC	Sec24D-S1016F
Sec24D mut3047C-T-rev	GGAAATCCACATAAAAAGAGCCTCCG	Sec24D-S1016F
Sec24D fwd NotI	AAAAAGCGGCCGCATGAGTCAACAAGGTTACGTG	Q979P/S1016F
seq-pFBDM MCSII rev	GCATTCATTTTATGTTTCAGG	Q979P/S1016F
M13-FP	TGTAAAACGACGGCCAGT	for sequencing

M13-RP	CAGGAAACAGCTATGACC	for sequencing
pBakPAC-FP	TAAAATGATAACCATCTCGC	for sequencing
pEGFP-RP	AACAGCTCCTCGCCCTTG	for sequencing
pMON Sequencing 2	AGGAGAGCGCACGAG	for sequencing
recA promoter	TGAGCATACAGTATAATTGC	for sequencing
S-Pr. Sec24D rev	ACCTTGGGTGCTGGATAT	for sequencing
S-Pr. Sec24D rev-2	GGATCTTATGAATATGTTGCC	for sequencing
S-Pr. Sec24D rev-3	GGCCTCGCTGGGGCTGG	for sequencing
T7	TAATACGACTCACTATAGGG	for sequencing

4.2.7 Plasmids

Plasmid name	**Insert(s)**	**Application**	**Creator**
pHV738	hNMT1; hMetAP1	Expression	Simone Röhling
pMON5840-hArf1	hArf1	Expression	Simone Röhling
pET21d-hArf3	hArf3	Cloning	Vincent Popoff
pET21d-hArf4	hArf4	Cloning	Vincent Popoff
pET21d-hArf5	hArf5	Cloning	Vincent Popoff
pET21d-hArf5	hArf6	Cloning	Vincent Popoff
pMON5840-hArf3	hArf3	Expression	This study
pMON5840-hArf4	hArf4	Expression	This study
pMON5840-hArf5	hArf5	Expression	This study
pMON5840-hArf6	hArf6	Expression	This study
pFBDM-HT-hSec23A	hSec23A	Expression	Frank Adolf
pFBDM-HT-hSec23A/24D-LIL834AAA	hSec23A/HT-hSec24D-LIL834AAA	Expression	Frank Adolf
pFBDM-HT-hSec23A/24D-Q979P	hSec23A/HT-hSec24D-Q979P	Expression	This study
pFBDM-HT-hSec23A/24D-S1016F	hSec23A/HT-hSec24D-S1016F	Expression	This study
pFBDM-HT-hSec13/31A	hSec13/HT-hSec31A	Expression	Frank Adolf

4.3 Materials for Protein Biochemistry and Cell Biology

4.3.1 Antibodies

Primary antibodies

Epitope	Clone/Specification	Host	Dilution WB	Dilution IFA	Source
Bet1	sc-136390 (17)	Mouse	1:200	-	Santa Cruz
Calnexin	ab75801	Mouse	1:1000	1:400	Abcam
ERGIC-1	16108-1-AP	Rabbit	1:500	-	Acris
ERGIC-53	sc-365158 (C6)	Mouse	1:200	-	Santa Cruz
γR-COP	(Pavel et al., 1998)	Rabbit	1:5000	-	F. Wieland lab
GM130	610822	Rabbit	1:250	-	BD Biosciences
GS27	sc-135932 (25)	Mouse	1:200	-	Santa Cruz
GS28	sc-15270 (N-16)	Goat	1:100	-	Santa Cruz
Histone H3	ab1791	Rabbit	1:1000	-	Abcam
p24	(Gommel et al., 1999)	Rabbit	1:5000	1:400	F. Wieland lab
Sec22b	sc-101276 (29-F7)	Mouse	1:200	-	Santa Cruz
Sec23	sc-12107 (E-19)	Goat	1:200	-	Santa Cruz
Syntaxin5	sc-365124 (B8)	Mouse	-	1:100	Santa Cruz
Ykt6	sc-30097 (NL-198)	Rabbit	1:100	-	Santa Cruz

Primary antibodies were stored at -20°C diluted in PBST with 1 % (w/v) BSA.

Secondary antibodies

Epitope	Fluorophor	Host	Dilution WB	Dilution IFA	Source
Goat IgG	Alexa-680	Donkey	1:10000	-	Invitrogen
Mouse IgG	Alexa-546	Goat		1:1000	Invitrogen
Mouse IgG	Alexa-680	Goat	1:10000	-	Invitrogen
Rabbit IgG	Alexa-488	Goat		1:1000	Invitrogen
Rabbit IgG	Alexa-680	Goat	1:10000	-	Invitrogen

Secondary antibodies used for Western blot (WB) were diluted in PBST with 1 % (w/v) BSA and stored at 4°C. Antibodies for immunofluorescence assay (IFA) were diluted in PBS with 1 or 5 % (w/v) BSA.

4.3.2 Cell Culture Media

Medium	Supplementation	Concentration (final)
αMEM (Minimum Essential Medium Eagle)	Fetal calf serum (FCS) Penicillin Streptomycin L-glutamine	10 % (v/v) 100 mg/ml 100 mg/ml 2 mM
DMEM (Dulbecco's Modified Eagle's Medium)	Fetal calf serum (FCS) Penicillin Streptomycin L-glutamine (L-proline)	10 % (v/v) 100 mg/ml 100 mg/ml 2 mM (100 mg/l)
Sf9 (GIBCO SF-900 II SFM)	-	-

DMEM and αMEM were usually purchased from Sigma-Aldrich. For SILAC experiments, DMEM with isotope-labeled arginine (Arg-10) and lysine (Lys-8) from Silantes was used. Here, the medium was additionally supplemented with L-proline in order to prevent conversion of arginine to proline (Bendall et al., 2008).

4.3.3 Cell Lines

Cell Line	Species	Application	Source
HeLa	*Homo sapiens*	COPI/COPII reconstitution, WB, SILAC proteomics, cytosol preparation	ACC57 (DMSZ)
HepG2	*Homo sapiens*	COPI reconstitution, WB, SILAC proteomics	-
Immortalized macrophages (iMΦ)	*Mus musculus*	COPI reconstitution, WB, SILAC proteomics	Eicke Latz (Uniklinik, Bonn)
Control fibroblasts	*Homo sapiens*	WB, IFA	Jinoh Kim (UC, Davis); CRL-2091 (ATCC)
Patient fibroblasts "Lukas"	*Homo sapiens*	WB, IFA	Jinoh Kim (UC, Davis); (Garbes et al., 2015)
Sf9	*Spodoptera frugiperda*	Protein expression	Invitrogen

4.3.4 Nucleotides

Nucleotide	Stock conc. [mM]	Source
Adenosine-5`-triphosphate (ATP)	40	Roche
Guanosine-5`-triphosphate (GTP)	25	Affymetrix
Guanosine-5`-O-[γ-thio]-triphosphate (GTPγS)	25	Sigma-Aldrich
Guanosine-5`-O-[β, γ-imido]-triphosphate (GMP-PNP)	25	Sigma-Aldrich

Nucleotides were prepared as stock solutions in 25 mM HEPES pH 7.2 (KOH), 150 mM KOAc, 5 mM MgOAc and stored at -20°C.

4.3.5 ATP Regenerating System (ATPr)

During COPI/COPII budding reactions, an ATP regenerating system was added, as it has been shown to support vesicle biogenesis through an unknown mechanism (Aridor et al., 1995; Aridor et al., 1998).

Component	Stock conc. [mM]	Source
Adenosine-5`-triphosphate (ATP)	40 mM	Roche
Creatine phosphate (CP)	200 mM	Sigma-Aldrich
Creatine kinase (CK)	8 mg/ml	Roche

Components of the ATPr system were prepared as separate stocks in 25 mM HEPES pH 7.2 (KOH), 150 mM KOAc, 5 mM MgOAc. ATP and CP were stored at -20°C. Creatine kinase was stored at -80°C.

4.3.6 Protein Molecular Weight Standard

During SDS-PAGE, Precision Plus Protein™ Prestained Standard from Bio-Rad was used for determination of the apparent molecular masses of proteins. It ranges from 10 to 250 kDa.

4.3.7 Affinity Chromatography

Proteins tagged with polyhistidine were (partially) purified through affinity chromatography with Ni-Sepharose High Performance from GE Healthcare. Coatomer which was tagged with a One-STreP-Tag (OST) that consists of two times Strep-Tag® II was purified with Strep®-Tactin Sepharose® (IBA Lifesciences). For pulldown experiments, GST-tagged proteins were coupled to Glutathione Sepharose 4B (GE Healthcare).

4.3.8 Fast Protein Liquid Chromatography (FPLC) – Gel Filtration

Proteins expressed without an affinity tag or with a polyhistidin tag were purified by gel filtration (size exclusion chromatography). To this end, an Ettan LC FPLC system was used in combination with a Superose6 or a Superdex75 column (both GE Healthcare). For buffer exchange, disposable PD-10 desalting columns were used (GE Healthcare).

4.4 Methods in Molecular Biology

4.4.1 Polymerase Chain Reaction (PCR)

PCRs for the production of inserts were performed with Pfu Plus! DNA polymerase (Roboklon), primers (Biomers) at a concentration of 10-100 µM, 200 µM dNTPs, and 10-50 ng template DNA. They were run in a PCR Spring cycler (Thermo Fisher Scientific). The melting temperature was usually set to 95°C and elongation was performed at 72°C. The elongation times were calculated by assuming that 1 kb of DNA is replicated per minute. The annealing temperatures were determined for each reaction individually.

4.4.2 Overlap Extension PCR

Overlap extension PCRs were performed in order to introduce point mutations into a gene. In a first round, two PCRs were performed to generate fragments of the insert which overlap at the site where

the mutation is to be introduced. These two overlapping fragments are used as templates in a second round of PCR to generate the final insert which covers the whole length of the desired gene and carries the mutation.

4.4.3 Colony PCR

In order to screen for positive clones after a transformation, colony PCRs were performed. To this end, Taq polymerase (Axon) was used instead of a high precision polymerase. Moreover, a bacterial colony served as template for the PCR reaction instead of purified DNA.

4.4.4 Agarose Gel Electrophoresis

Agarose gels were prepared with 1-2 % (w/v) agarose dissolved in TAE buffer (40 mM Tris-HCl pH 8.0, 20 mM acetic acid, 1 mM EDTA), supplemented with 10 µl/l DNA Stain Clear G (Serva). DNA samples were mixed with 5× GelPilot DNA Loading Dye (Qiagen) prior to electrophoresis. Agarose gels were inspected with a Bio-Rad GelDoc system.

4.4.5 Gel Extraction and PCR Purification

Desired PCR fragments and plasmids were routinely purified by gel extraction using a QIAquick Gel Extraction Kit or with a QIAquick PCR Purification Kit (both Qiagen). Kits were used according to the manufacturer's manuals.

4.4.6 Ethanol Precipitation

In order to increase their purity or concentration, DNA samples were subjected to ethanol precipitation. To this end, they were mixed with cold 100 % ethanol (2 volumes) and 3 M sodium acetate (0.1 volume) and incubated at -20°C for 30 min. Precipitated DNA was harvested (14.000 rpm, 15 min, 4°C) and washed once with 1 ml of 70 % (v/v) ethanol (14.000 rpm, 15 min, 4°C). After discarding the ethanol, DNA was dried and resuspended in the desired volume ddH_2O.

4.4.7 Restriction

For subsequent ligation, 5-10 µg of plasmid DNA and 1-5 µg of insert DNA were digested with restriction enzymes purchased from NEB in a recommended buffer for 1-3 h. Fragments were purified by either ethanol precipitation, gel extraction, or using a PCR purification kit (Qiagen). Prior to DNA sequencing, samples were usually subjected to a preparative restriction using 500-1000 µg of plasmid.

4.4.8 Ligation

Prior to ligation, restricted plasmids were treated with calf intestine alkaline phosphatase (CIP) to remove 5` phosphates and prevent re-ligation of partially digested plasmids. After CIP treatment, 50-200 ng of plasmid DNA was mixed with up to 10-fold molar excess of insert in ligation buffer together with T4 ligase (Thermo Fisher Scientific). The reaction was incubated for 1-2 h at room temperature or over night at 16°C before transformation.

4.4.9 Plasmid and Bacmid Preparation

Plasmids were purified using either the NucleoSpin Plasmid Kit (Machery-Nagel) or the QIAprep Spin Miniprep Kit (Qiagen) following the manufacturer's manual. Bacmids were isolated following the instructions of the Bac-to-Bac manual from Invitrogen using the solutions S1-S3 from the NucleoSpin Plasmid Kit (Machery-Nagel).

4.4.10 Transformation of *E.coli*

Chemically competent *E.coli* strains DH5α, BL21 (DE3), and BL21-CodonPlus-RIL (DE3) (all Invitrogen) were transformed via heat shock. The competent cells were carefully mixed with purified plasmid DNA (5-10 ng) or whole ligation reactions, incubated on ice for 30 minutes and subjected to a brief heat shock at 42°C for 45 seconds. The cells were allowed to recover on ice for 2 minutes before

adding 1 ml of SOC medium and incubation at 37°C for 1 h, shaking. Finally, the cells were streaked onto LB agar plates containing the required selection reagents.

DH10MultiBac^{Cre} cells (Imre Berger, EMBL Grenoble) were transformed through electroporation. They were carefully mixed with 10 ng plasmid DNA and incubated on ice for 10-20 minutes. The electroporation was performed in 2mm cuvettes using a GenePulser Xcell™ (Bio-Rad) at 2.5 kV, 200 Ω electrical resistance, and an electrical capacity of 25 µF. Cells were recovered in 1 ml SOC medium shaking at 37°C for 3 h. Recovered cells were streaked into LB agar plates supplemented with the required selection reagents.

4.4.11 Bacterial Expression of ADP-ribosylation Factors

Small GTPases of the Arf family were expressed in *E.coli*. To this end, pMON5480 plasmids encoding one of the five human Arf family members were co-transformed with the pHV738 plasmid, which encodes human glycylpeptide N-tetradecanoyltransferase 1 (hNMT1) and methionine aminopeptidase (hMetAP1), in BL21 (DE3) or BL21-CodonPlus-RIL (DE3) cells (both Invitrogen). Cells containing both plasmids were used to inoculate 100-300 ml of pre-culture which was grown at 27°C or 37°C over night shaking at 180 rpm. Of the pre-culture, 100 ml were used to inoculate a final 2 liter expression culture. The final expression culture was usually incubated at 27°C, for Arf4 and Arf5 occasionally at 37°C, shaking with 180 rpm. The optical density measured at 600nm (OD_{600}) during the expression was monitored using a Jenway 6300 Spectrophotometer (Jenway). Shortly after inoculation of the final expression culture, the BSA/myristate solution was prepared. To this end, 42 mg of sodium myristate (Sigma-Aldrich), dissolved in 3 ml PBS by heating in a microwave was mixed with 20 ml of PBS containing 4.5 % (w/v) fatty acid free BSA (Sigma-Aldrich), pre-heated to 50°C. Once an OD_{600} of approximately 0.6 was reached, the BSA/myristate solution was added. Ten minutes after the addition, IPTG (Gerbu) to a final concentration of 1 mM was added to the culture to induce the expression of hNMT1 and hMetAP1. After 1 h, the expression of the respective Arf protein was induced upon addition of nalidixic acid (dissolved in 300 mM NaOH) to a final concentration of 30 µg/ml. The expression culture was further incubated for 3-4 h before harvest of the cells by centrifugation (4000 ×g, 20 min, 4°C). The harvested cells were usually snap-frozen in liquid nitrogen and stored for later usage at -80°C.

4.4.12 Preparation of Bacterial Glycerol Stocks

Glycerol stocks of transformed bacterial strains were usually used to inoculate over night pre-cultures for protein expression. They were prepared by taking a small aliquot of overnight culture and mixing it with glycerol to a final concentration of 20 % (v/v). The stocks were immediately stored at -80°C.

4.5 Biochemical Methods

4.5.1 SDS Polyacrylamide Gelelectrophoresis (SDS-PAGE)

Standard, discontinuous SDS-PAGE for adjacent Western blotting or to monitor protein purification procedures was performed with a PROTEAN II system (Bio-Rad). For self-casting of gels, 4× stock solutions of the stacking gel buffer (0.5 M Tris-HCl pH 6.8) and the separating gel buffer (1.5 M Tris-HCl pH 8.8) were prepared and stored at 4°C. Gels were casted using Rotiphorese®Gel 30 acrylamide (Roth). The stacking gels were prepared with a final acrylamide concentration of 4 %. For separating gels the concentration was chosen according to the proteins that were to be analyzed ranging from 10 % to 15 % final acrylamide concentration. Samples designated for later MS analysis were separated on pre-cast Novex™ 10% Tris-Glycine Gels using an XCell SureLock™ electrophoresis system (both Invitrogen).

Samples for SDS-PAGE were denatured in 1× SDS sample buffer which was prepared as a 4× stock solution (200 mM Tris-HCl pH 6.8, 40 % (v/v) glycerol, 12 % (v/v) β-mercaptoethanol, 8 % (w/v) SDS, 0.2 % (w/v) bromophenol blue) via heating to 95°C for 5-10 min. Self-casted gels were run in SDS running buffer (25 mM Tris, 192 mM glycine, 0.1 % (w/v) SDS) at a constant electric voltage of 200 V. Pre-casted gels were run in NuPAGE™ MES SDS running buffer (Invitrogen) at 140 V.

4.5.2 Coomassie Staining

Coomassie staining of SDS gels was performed to monitor the purification of proteins, to ensure equal conditions during pulldown experiments, and to stain proteins destined for MS analysis prior to excision from the gel. For purification monitoring and pulldown experiments, SDS gels were stained

with Coomassie Brilliant Blue R250 (Bio-Rad). To this end, the gels were briefly heated in staining solution (0.25 % (w/v) Coomassie Brilliant Blue R250, 40 % (v/v) ethanol, 10 % (v/v) acetic acid) in a microwave and then incubated for approx. 15 minutes. The de-staining was performed by repeatedly incubating the gel in de-staining solution (20 % (v/v) ethanol, 5 % (v/v) acetic acid) with occasional heating in a microwave.

Pre-cast gels loaded with samples for MS analysis were stained with Roti-Blue colloidal Coomassie (Roth) prepared according to the manufacturer`s manual for a minimum of 2 h. Gels were de-stained in de-ionized water.

4.5.3 Western Blot Analysis

Semi-dry Western blotting was performed using a semi-dry Trans-Blot® SD Semi-Dry Transfer Cell from Bio-Rad. Proteins were transferred onto Immobilon®-FL PVDF membranes (Merck-Millipore) at a constant electric voltage of 20 V for 1.5 h after soaking all blot components with transfer buffer (48 mM Tris, 39 mM glycine, 1.3 mM SDS, 20 % (v/v) methanol).

After blotting, membranes were blocked with 5 % (w/v) milk powder dissolved in PBST (35.7 mM Na_2HPO_4, 14.3 mM KH_2PO_4, 136 mM NaCl, 3 mM KCl, 0.05 % (v/v) Tween 20) for 30 minutes at room temperature. Subsequently, the membranes were briefly washed with PBST (3× 5-10 min) and then incubated with first antibodies either for at least 2 h at room temperature or preferably over night in the cold room at 8°C. Membranes were thoroughly washed with PBST (3x 10 min) after incubation with the first antibodies, before detection with fluorophore-coupled secondary antibodies for 30-60 minutes at room temperature. After the final antibody incubation, membranes were again washed with PBST (3× 10 min), and ultimately 2-3x 10 minutes in PBS (35.7 mM Na_2HPO_4, 14.3 mM KH_2PO_4, 136 mM NaCl, 3 mM KCl) before scanning at the LI-COR Odyssey System (LI-COR) run with Image Studio software (Version 2.1.10).

4.5.4 Protein Concentration Determination (Bradford Assay)

Protein concentration was determined using Bio-Rad Protein Assay Dye Reagent (Bradford). After incubation with the dye, absorbance of the samples at 405 nm and 620 nm was measured using an

Anthos Reader 2001 (Anthos). In parallel to the samples which were prepared in triplicates standard samples prepared from BSA-solution of known concentration were measured.

4.5.5 Purification of Untagged ADP-ribosylation Factors

For a regular purification of myristoylated Arf proteins, bacterial pellets originating from four liters of expression culture were first resuspended in 30-50 ml of cold Arf lysis buffer (50 mM Tris-HCl pH 8.0, 1 mM $MgCl_2$, 1 mM DTT, 1 mM GDP, 1 tablet cOmplete™ EDTA-free Protease Inhibitor Cocktail from Roche). Cells were broken during 5-7 runs through a Microfluidizer® (Microfluidics) at an applied pressure of 15.000 psi. Cell debris was removed by ultracentrifugation using a Beckman Coulter Optima™ LE-80L/L-90K ultracentrifuge equipped with a TLA50.2/TFT55.38 rotor (100.000 ×g, 1 h, 4°C). The supernatant was filled up to 200 ml using Arf lysis buffer without GDP. Afterwards, an ammonium sulfate precipitation (ASP) was performed. To this end, the lysate was stirred in an ice-cooled water bath and finely grounded ammonium sulfate was slowly added over a period of 45 minutes until a final concentration of 35-40 % was reached. The supernatant was continued to stir for 45 more minutes before the precipitate was harvested in a Sorvall RC-6 centrifuge equipped with an SLC-1500 rotor (8.000 rpm, 30 min, 4°C). The precipitate was resuspended in Arf lysis buffer with GDP, subjected to ultracentrifugation within a Optima™ TLX ultracentrifuge equipped with TLA45/55 rotor from Beckman Coulter (100.000 ×g, 15 min, 4°C) to remove aggregates and run over a Superdex75 (16/60) column using an Ettan LC FPLC system (both GE Healthcare) with storage buffer (25 mM HEPES pH 7.4 (KOH), 200 mM KCl, 5 mM $MgCl_2$, 1 mM DTT, 1 mM, 10 % (w/v) glycerol) while collecting 0.5 ml fractions. Small samples of the fractions expected to contain the purified proteins were checked via SDS-PAGE with Coomassie staining. Those fractions with little contaminations and decent amounts of purified Arfs were pooled, concentrated using an Amicon® Ultra (10 kDa cut-off) concentrator device (Merck-Millipore), aliquoted, and snap-frozen in liquid nitrogen before long-term storage at -80°C.

4.5.6 Purification of OST-Coatomer

A standard purification of OST-coatomer (One-STreP-Tag C-terminal of α-COP) was performed with two Sf9 cell pellets each originating from 500 ml of expression culture. Cells were resuspended in approx. 30 ml of cold OST buffer (25 mM HEPES pH 7.4 (KOH), 200 mM KCl, 1 mM DTT, 1 mM,

10 % (w/v) glycerol) supplemented with 1 tablet cOmplete™ EDTA-free Protease Inhibitor Cocktail (Roche) and cracked within 5 runs through a Microfluidizer® (Microfluidics) at 15.000 psi. Cell debris was removed via centrifugation with a Beckman Coulter Optima™ LE-80L/L-90K ultracentrifuge equipped with a TLA50.2/TFT55.38 rotor at 100.000 ×g for 1 h at 4°C. The cleared lysate was incubated rotating at 8°C with 2-3 ml of pure Strep®-Tactin Sepharose® beads (IBA) for 2-3 hours. After incubation with the lysate, beads were washed twice with 50 ml of OST buffer by centrifugation in a Megafuge 40R (Heraeus) (2.000 rpm, 5 min, 4°C), transferred to an empty Econo-Pac ®chromatography column and washed once more with 50 ml of the buffer. The protein complex was eluted stepwise (1 ml steps) from the beads with 2.5 mM desthiobiotin (IBA) dissolved in OST buffer. The eluted fractions were analyzed for the presence of protein via the Bradford assay. Those fractions which contained significant amounts of protein were pooled and the proteins concentrated with a 100 kDa cut-off Amicon® Ultra (Merck-Millipore) if necessary. Desthiobiotin was removed from the eluted protein pool via gel filtration using OST buffer without desthiobiotin and a PD-10 desalting column (GE Healthcare). Finally, the protein was aliquoted and stored at -80°C.

4.5.7 Purification of HT-Sec23/Sec24 and HT-Sec13/Sec31 Complexes

Purification of COPII coat components HT-Sec23/Sec24 and HT-Sec13/Sec31 was usually performed with two Sf9 cell pellets originating from 500 ml expression culture, each. The cells were thawed on ice and resuspended in approx. 30 ml cold lysis buffer (25 mM HEPES pH 7.2 (KOH), 500 mM KCl, 5 mM $MgCl_2$, 30 mM imidazole, 0.02 % (v/v) MTG, 1 tablet cOmplete™ EDTA-free Protease Inhibitor Cocktail from Roche). Cells were lysed within 5 runs through a Microfluidizer® (Microfluidics) at 15.000 psi. The lysate was cleared by ultracentrifugation within a TLA50.2/TFT55.38 rotor using a Optima™ LE-80L/L-90K ultracentrifuge from Beckman Coulter (100.000 ×g, 1 h, 4°C) and immediately incubated rotating with 2-3 ml of pure Ni-Sepharose High Performance beads (GE Healthcare) for 2-3 h in the cold room. Following incubation with the lysate, sepharose beads were washed three times with 50 ml of wash buffer (25 mM HEPES pH 7.2 (KOH), 500 mM KCl, 5 mM $MgCl_2$, 50 mM imidazole, 0.02 % (v/v) MTG) in batch via centrifugation (3.000 rpm, 5 min, 4°C). For the elution, beads were transferred to an empty Econo-Pac ®chromatography column. The complexes were eluted in 1 ml steps using elution buffer (25 mM HEPES pH 7.2 (KOH), 500 mM KCl, 5 mM $MgCl_2$, 200 mM Imidazole, 0.02 % (v/v) MTG). After determining the protein concentration with the Bradford assay, those fraction which contained most protein were pooled and the proteins concentrated using a 100 kDa cut-off Amicon® Ultra (Merck-Millipore). From the concentrated Ni-bead eluate, aggregates were removed via ultracentrifugation within an Optima™ TLX

ultracentrifuge equipped with TLA45/55 rotor from Beckman Coulter (100.000 ×g, 15 min, 4°C). Subsequently, the eluate was run over a pre-equilibrated Superose6 column coupled to an Ettan FC FPLC system (both GE Healthcare) with storage buffer (25 mM HEPES pH 7.2 (KOH), 200 mM KCl, 5 mM $MgCl_2$, 10 % (w/v) glycerol, 0.02 % (v/v) MTG) while collecting 0.5 ml fractions. Fractions expected to contain the purified protein complexes were inspected by SDS-PAGE with Coomassie staining. Finally, those fractions which contained stoichiometric amounts of the complexes were pooled, concentrated if necessary, aliquoted, snap-frozen in liquid nitrogen, and stored at -80°C.

4.5.8 COPII Pulldown Assay with Syntaxin5$^{205-328}$-GST

For the pulldown assay, control GST or Stx5$^{205-328}$-GST were centrifuged in a TLA45/55 rotor using an Optima™ TLX ultracentrifuge from Beckman Coulter (100.000 ×g, 1 h, 4°C) to remove protein aggregated. Subsequently, 100 µg of the control GST or 150 µg or the Stx5-GST fragment were incubated with 10 µl of pure Glutathione Sepharose 4B (GE Healthcare) in 0.5 ml of assay buffer (25 mM HEPES pH 7.2 (KOH), 200 mM KCl, 5 mM $MgCl_2$) for 1 h at 8°C, rotating. Following the incubation, the beads were washed twice with 1 ml of assay buffer (3.000 rpm, 2 min, 4°C) using an Eppendorf tabletop centrifuge 5417 R. Afterwards, the beads were in a second round incubated with 30 µg of purified HT-Sec23A/Sec24D variants in a total volume of 0.5 ml for 1 h in the cold room. Subsequently, the beads were again washed twice by centrifugation (3.000 rpm, 2 min, 4°C). Bound material was eluted by boiling the beads in SDS sample buffer. The resulting samples (40 %) were separated by SDS-PAGE and analyzed for the presence of Sec23 by Western blotting. To control for equal loading, the lower part of the SDS gel containing the GST constructs was subjected to Coomassie staining.

4.6 Cell Biology Methods

4.6.1 Tissue Culture of Mammalian Cells

All mammalian cells used in this study were grown adherent in flasks or on dishes. They were cultivated at 37°C in incubators with 5 % CO_2. HeLa cells were grown in αMEM medium (Sigma-Aldrich) but transferred to DMEM for SILAC experiments. All other cells were generally grown

in DMEM (Sigma-Aldrich). Cells were usually grown up to 70-90 % confluency before splitting/dilution using Trypsin-EDTA solution (Sigma-Aldrich).

4.6.2 Freezing of Mammalian Cells

For freezing, cells from one 15 cm dish were trypsinized, harvested by centrifugation (300 ×g, 5 min, 4°C) and gently resuspended in a tiny amount of residual medium. Afterwards, the cells were mixed with 1.5 ml of FCS and incubated on ice for 20 minutes. Finally, the resuspended cells were mixed with 1.5 ml of ice-cold freezing medium (DMEM supplemented with 20 % DMSO) and transferred into Cryo.S™ vials (Greiner Bio-One). The vials were stored at -80°C for 24-48 hours before being transferred to a liquid nitrogen tank.

4.6.3 Mycoplasma Treatment

In order to remove mycoplasma contaminations from the fibroblast cells, they were treated with BM-cyclin (Roche). The treatment was performed following the instructions provided by the manufacturer. Success of the treatment was assessed based on an inspection of the cells using fluorescence microscopy and DAPI staining.

4.6.4 Stable Isotope Labeling by Amino Acids in Cell Culture (SILAC)

For proteomics experiments, HeLa and HepG2 cells, as well as iMΦ were labeled with heavy lysine and arginine. To this end, an SILAC-Lys8-Arg10-Kit (Silantes) was used. To prevent arginine to proline conversion by the cells, the DMEM medium was further supplemented with 200 mg/l of L-proline (Bendall et al., 2008). Cells were cultivated in heavy amino acid containing medium for five passages (approx. 2 weeks) before a small sample was taken. The sample was boiled in SDS-sample buffer, subjected to SDS-PAGE, and analyzed by MS for the incorporation of heavy amino acids. Only when an incorporation >95 % was reached the cells were used for experiments.

4.6.5 Culture of Sf9 Insect Cells

Sf9 insect cells were grown non-adherent in GIBCO SF-900 II SFM medium (Life Technologies) in CELLMASTER Roller Bottles from Greiner Bio-One. The cells were cultured at a temperature of 27°C shaking at 180 rpm. Density of Sf9 cells was monitored every 2-3 days using a Neubauer improved counting chamber (Assistent). In order to provide optimal growth conditions, cells were grown at a density of 0.8×10^6–8×10^6 cell/ml.

4.6.6 Transfection of Sf9 Insect Cells and Baculovirus Production

Transfection of Sf9 cells was performed with isolated Bacmid DNA. To this end, the isolated DNA was dissolved in 20 µl of ddH_2O and subsequently mixed with 200 µl GIBCO SF-900 II SFM medium (Life Technologies). Meanwhile, 15 µl of X-tremeGENE™ HP Transfection Reagent (Roche) were diluted in 100 µl of the Sf9 cell medium. Afterwards, the DNA containing medium and the diluted transfection reagent were mixed. Transfections were always performed in duplicate. Hence, 160 µl of the transfection mixture was added to two wells of a 6-well plate each containing 3 ml of Sf9 cells with a density of 0.25×10^6 cells/ml. The transfected cells were incubated at 27°C for 72h before harvest of the supernatant which contains the first virus generation (P1). To the cells, 3ml of fresh Sf9 cell medium was added and the cells were incubated for 48 more hours. After two days, the cells were resuspended in the medium and harvested in a tabletop centrifuge (13.000 rpm, 1 min). The harvested cells were resuspended in SDS sample buffer, boiled, and a small sample loaded onto an SDS gel followed by Coomassie staining to assess the success of transfection.

From the P1 virus, a second generation of virus (P2) was produced by infecting 50 ml of Sf9 cells with a density of 0.8×10^6 cells/ml with 1 and 2 ml of P1 virus. The virus was expanded for 72h by incubating the infected cells at 27° and shaking with 70 rpm. Following virus expansion, the supernatant containing the P2 virus generation was separated from the Sf9 cells (4.000 rpm, 5 min, 4°C). The different P2 viruses were next tested in small scale expressions before being used on a large scale. To this end, 50 ml of Sf9 cells (2×10^6 cells/ml) were infected with different amounts of P2 virus (between 200-800 µl). Three days after the infection, a small sample of the cells was prepared for analysis via SDS-PAGE and Coomassie staining. The virus concentration which produced the best expression was upscaled and used for final 500 ml expressions.

4.6.7 Preparation of Baculovirus-Infected Cell (BIC) Stocks

For later expressions, stocks of baculovirus-infected Sf9 cells (BIC stocks) were prepared. For this, 200 ml of cells (1×10^6 cells/ml) were infected with the amount of P2 virus used to infect 500 ml expression cultures. The cells were infected with the virus for 24 h. After the infection, the BIC were harvested gently (1.200 rpm, 5 min, 4°C), resuspended in 20 ml of freezing medium (60 % GIBCO SF-900 II SFM medium, 30 % FCS, 10 % DMSO) and aliquoted (usually 1 ml aliquots). The BIC stocks were immediately put to -80°C for 48 h before being transferred to liquid nitrogen for long term storage. Potency of the stocks was tested in small scale test expressions.

4.6.8 Large Scale Expression of Protein Complexes in Sf9 Cells

Large scale expressions of protein complexes, i.e. coatomer, Sec23/Sec24, and Sec13/Sec31 were performed in 500 ml Sf9 cells at a starting density of 2×10^6 cells/ml. The cells were infected with either P2 virus or with BIC stocks using optimal virus titers which have been determined in small scale expressions beforehand. The infected cells were allowed to express the proteins for 72-96 h. After the expression, cells were harvested (2.000 rpm, 5 min, 4°C), snap-frozen in liquid nitrogen and immediately stored at -80°C.

4.6.9 Preparation of Semi-intact Mammalian Cells (SIC)

Semi-intact cells for subsequent vesicle reconstitution assays were prepared basically as described by Mancias and Goldberg (2007). Briefly, mammalian cells grown adherent to 70-90% confluency were detached with Trypsin-EDTA solution (Sigma-Aldrich). The protease was inactivate by adding 300 µl of 1 mg/ml trypsin inhibitor (Sigma-Aldrich) followed by resuspension of the cells in 20 ml of PBS (35.7 mM Na_2HPO_4, 14.3 mM KH_2PO_4, 136 mM NaCl, 3 mM KCl) for one 15 cm dish. The cells were subsequently harvested via centrifugation (300 ×g, 5 min, 4°C) and resuspended again in 10 ml PBS. At this step, cells originating from two 15 cm dishes were combined in one 50 ml falcon tube. Next, 20 µl of 40 mg/ml digitonin (Sigma-Aldrich) was added to each falcon tube, the cells were mixed with the detergent by inversion (3-4 times) and incubated on ice for 5 min. The permeabilization was quenched by adding 30 ml of cold PBS. The now semi-intact cells were harvested (300 ×g, 5 min, 4°C),

resuspended in 50 ml of assay buffer (25 mM HEPES pH 7.2 (KOH), 200 mM KCl, 5 mM $MgCl_2$) and incubated on ice for 10 min for further removal of the cytosol. Afterwards, the SIC were harvested again (300 ×g, 5 min, 4°C) and resuspended in a small volume of assay buffer (0.3-0.5 ml). The protein concentration of the SIC was subsequently determined via the Bradford assay and the cells were used for a reconstitution assay within 1 h after preparation.

4.6.10 Preparation of HeLa Cell Cytosol

For preparation of cytosol, cells from 6 confluent 15 cm dishes were trypsinized and resuspended in 20 ml of PBS (35.7 mM Na_2HPO_4, 14.3 mM KH_2PO_4, 136 mM NaCl, 3 mM KCl) per dish, supplemented with 300 µl of 1 mg/ml trypsin inhibitor (Sigma-Aldrich). The cells were subsequently harvested via centrifugation (300 ×g, 5 min, 4°C), combined, and washed with 50 ml of assay buffer (25 mM HEPES pH 7.2 (KOH), 200 mM KCl, 5 mM $MgCl_2$). After the second harvest, cells were resuspended in a small volume (~1 ml) of assay buffer. Cell lysis was achieved through nitrogen cavitation (800 psi, 30 min, on ice) using a 4639 cell disruption vessel (Parr Instruments). The soluble cytosolic fraction was cleared from debris via centrifugation at 100.000 ×g within an Optima™ TLX ultracentrifuge and a TLA45/55 rotor (Beckman Coulter) at 4°C for 1 h.

4.6.11 *In vitro* reconstitution of COPI and COPII Vesicles from SIC

In vitro reconstitution of COPI and COPII vesicles was essentially performed as described previously by Adolf et al. (2013). Briefly, first recombinant proteins used for reconstitution reactions were centrifuged using a Beckman Coulter Optima™ TLX ultracentrifuge equipped with a TLA45/55 rotor (100.000 ×g, 15 min, 4°C) to remove aggregates. Afterwards, semi-intact cells were prepared as described above. For a regular COPII reconstitution reaction, 200 µg of SIC were incubated with 4 µg of Sar1, 8 µg of HT-Sec23/Sec24, and 10 µg of HT-Sec13/Sec31. COPI reconstitution from 200 µg SIC was performed with 4 µg of Arf and 10 µg of OST-coatomer. For both, COPI and COPII budding reactions, SIC and proteins were incubated with ATP-regenerating system (40 mM creatine phosphate (Sigma-Aldrich), 0.2 mg/mL creatine kinase (Roche), 1 mM ATP (Roche)) and guanine-nucleotide (1 mM GTP (Affymetrix) or 0.2 mM GMP-PNP/GTPγS (Sigma-Aldrich)) for 30 minutes at 30°C in a final volume of 200 or 400 µl of assay buffer (25 mM HEPES pH 7.2 (KOH), 200 mM KCl, 5 mM $MgCl_2$). For some experiments, 150 µg of cytosol per 200 µg of SIC was added to the

incubation. In negative controls either nucleotides or crucial coat proteins were omitted. After 30 min, generated vesicles were separated from SIC via medium-speed centrifugation (14.000 ×g, 10 min, 4°C) in a table top centrifuge. The vesicle containing supernatant was immediately transferred to a fresh tube and the vesicles were either harvested directly by high-speed centrifugation (100.000 ×g, 30 min, 4°C) using a TLA45/55 rotor or subjected to further purification via floatation.

4.6.12 Floatation of Vesicles using an Iodixanol Density Gradient

In order to separate reconstituted vesicles form the excess of recombinant coat proteins, they were subjected to density gradient floatation. To this end, vesicle containing supernatant, obtained after medium-speed centrifugation, was brought to 40% iodixanol concentration and the whole sample was adjusted to 1x assay buffer (25 mM HEPES pH 7.2 (KOH), 200 mM KCl, 5 mM $MgCl_2$). The final volume of the load sample was 700 µl. It was subsequently put into a 4 ml UltraClear™ Thinwall SW-60 Tube (Beckman Coulter), overlaid with 1200 µl of 30% iodixanol and finally 400 µl of 20% iodixanol density gradient matrix both prepared in 1x assay buffer. The gradient was ultracentrifuged over night (14-16 h) at 250.000 ×g and 4°C in a Optima™ LE-80L/L-90K ultracentrifuge equipped with a SW-60 rotor (Beckman Coulter). To initially assess the movement of vesicles, 10 fractions (230 µl) were taken from top to bottom, diluted with 770 µl assay buffer and centrifuged in a TLA45/55 rotor from Beckman Coulter (100.000 ×g, 2 h, 4°C). The harvested material was boiled in SDS sample buffer and subjected to Western blot analysis.

4.6.13 Vesicle Reconstitution for SILAC Proteomics

For a single SILAC mass spectrometry sample, two vesicle reconstitution or a vesicles reconstitution plus a mock reaction were performed in parallel. One of the reactions was performed with light SIC, the other reaction from SILAC-labeled heavy cells. In total, 1200 µg of SIC were used for each condition, split into 6 separate budding reactions. Following the budding reaction, the samples were subjected to floatation within iodixanol density gradients. From each gradient, the top 200 µl were discarded and one major vesicle containing 500 µl fraction taken. This fraction was diluted with 1 ml of assay buffer and subjected to ultracentrifugation using a Beckman Coulter Optima™ TLX ultracentrifuge equipped with a TLA45/55 rotor (100.000 ×g, 2 h, 4°C). The supernatant was again

discarded and the harvested material from each gradient was solubilized within 5 µl of SDS sample buffer and boiling at 95°C for 10 min. All sub-samples were combined into one large sample containing the floated/harvested material from one reaction performed with light and one reaction performed with heavy SIC. The final sample was briefly run into a pre-cast Novex™ 10% Tris-Glycine Gel (Invitrogen), just so that the sample had entered the gel. The gel was subsequently stained with Roti-Blue colloidal Coomassie (Roth), de-stained in de-ionized water and handed over to the MS facility for downstream analyses.

All SILAC experiments were performed at least in duplicate with switched labels to make sure that the labeling procedure had no influence on the cells.

4.7 Imaging, Mass Spectrometry and Data Analysis

4.7.1 Immunofluorescence Assay (IFA) and Confocal Microscopy

For immunofluorescence assays, 0.5-1.0×10^5 cells were seeded onto sterile cover slips (Roth) in a 24-well plate in the evening and cultivated over night for 12-16 h prior to the assay. On the next day, the cells were washed twice with 2-3 ml of PBS (35.7 mM Na_2HPO_4, 14.3 mM KH_2PO_4, 136 mM NaCl, 3 mM KCl) before permeabilization/fixation by incubating the cells with ice-cold, pure methanol for 20 min at -20°C. After incubation with methanol, cells were washed again twice with PBS before incubation with PBS containing 1 % (w/v) BSA (Sigma-Aldrich) for 30-60 minutes at room temperature to prevent later unspecific binding of antibodies. After this blocking step, the cells were incubated with first antibodies, diluted in 1 % BSA-PBS by putting the cover slips onto small drops of the antibody solutions in a humidified Petri dish. Incubation with the primary antibodies was performed over night (12-16 h) at 8°C. On the following day, unbound antibodies were removed by washing the cover slips twice by putting them on drops of PBS and letting them sit for 5-10 minutes. Afterwards, the samples were incubated with secondary antibodies diluted in 1 % (w/v) BSA-PBS for 60 minutes in the dark at room temperature. The cover slips were washed two more times with PBS and once with ddH_2O before mounting onto microscopy glass slides using 5-10 µl of DAPI containing ProLong™ Gold Antifade (Life Technologies). Samples were kept at 8°C in the dark until imaging.

Imaging of the samples was performed at the Nikon Imaging Center at the Heidelberg University using a PerkinElmer ERS-6 spinning disk confocal microscope. Z-stacks were acquired in 150 nm steps with a 100× oil immersion objective using the PerkinElmer Volocity 6.3 software to operate the

microscope. They were further subjected to deconvolution using the Huygens Remote Manager v3.4.1. Downstream processing of the images was done with Fiji/ImageJ 2.0.0-rc-54 software.

4.7.2 Electron Microscopy

Electron microscopy was performed at the Interdisciplinary Center for Neurosciences of the Heidelberg University (IZN). For resin-embedding, *in vitro* reconstituted COPI vesicles were purified via floatation within an iodixanol gradient. Vesicles from three gradients were sequentially harvested by centrifugation (100.000 ×g, 1 h, 4°C) as described above in the presence of 2 % glutaraldehyde (v/v) dissolved in assay buffer (25 mM HEPES pH 7.2 (KOH), 200 mM KCl, 5 mM $MgCl_2$). The vesicles were then resuspended in 10 µl assay buffer and the samples further prepared as described previously by Adolf et al. (2013). Briefly, tannic acid in assay buffer was added to a final concentration of 0.5 % (w/v) and the samples incubated for 1 h. Subsequently, the samples were washed, treated with 2 % (v/v) osmium tetroxide/ 1.5 % (w/v) ferrocyanide and washed again. Finally, samples were stained with uranyl acetate and embedded using glycid ether 100. Ultrathin sections of the embedded samples were further contrasted with uranyl acetate/ lead citrate. Image acquisition was performed at an EM 10 transmission electron microscope from Carl Zeiss operated at 60 kV.

Negative stain EM was performed on vesicles reconstituted as described previously (Beck et al., 2008). Samples were adsorbed onto a carbon grid for 30 min. The sample was subsequently fixed for 10 min by putting it on a drop of 1 % (v/v) glutaraldehyde in assay buffer and then washed in the same way with just buffer three times for 1 min. The samples were then treated with 0.05 % (w/v) tannic acid for 5 minutes and washed again four times with water. Contrasting was achieved by incubating the grids on a drop of water containing 0.4 % (w/v) uranyl acetate/ 1.8 % methyl cellulose on an ice block. Finally, excess of contrasting solution was removed from the grids and they were dried at room temperature.

4.7.1 Size Determination of COPI Vesicles

Bioinformatics to determine the size of vesicles was performed at the Biomedical Computer Vision Group of the Heidelberg University and the DKFZ. Briefly, size determination was achieved by employing the segmentation routine introduced by Dimopoulos et al. which exploits the membrane pattern for the detection of an object boundary (Dimopoulos et al., 2014). We performed a semi-

automated segmentation. First all intact vesicles were localized manually and subsequently used as seeds for the following segmentation. Second, the method described by Dimopoulos et al. (2014) was performed to obtain the membrane profiles of a few examples. Segmented vesicles displaying a low-score were excluded from the further analyses. Finally, the vesicle area enclosed by its membrane was computed from the pixel size information.

4.7.2 Mass Spectrometry of Reconstituted Vesicles

Mass spectrometric analysis was performed at the Core Facility for Mass Spectrometry and Proteomics of the Center for Molecular Biology of the Heidelberg University (ZMBH). In summary, gel pieces were excised, reduced with DTT, alkylated with iodoacetamide and trypsin-digested using a DigestPro MSi platform (Intavis) as described previously (Shevchenko et al., 2006). Following in-gel digest, peptides were analyzed by liquid chromatography with subsequent mass spectrometry (LC-MS). LC was performed with an UltiMate 3000 directly coupled either to an Orbitrap Elite™ or a Q Exactive™ for MS analysis (all instruments from Thermo Fisher Scientific). For analysis with the Orbitrap Elite™, peptides were loaded onto an Acclaim™ PepMap™ 100 C-18 Trap-column (Thermo Fisher Scientific) at a flow rate of 30 µl/min using 0.1 % trifluoroacetic acid. The peptides were eluted from the trap-column and further separated using a 75 µm x 250 mm Acclaim™ PepMap™ 100 C-18 RSLC analytical column (Thermo Fisher Scientific). Elution was performed with a gradient starting with 3 % buffer A (0.1% formic acid, 1 % acetonitrile) and ending with 40 % buffer B (0.1% formic acid, 90 % acetonitrile) over the course of 2 h with a flow rate of 300 nl/min. MS data acquisition was performed through automatic switches between a full scan and up to 30 data-dependent MS/MS scans. For samples analyzed with the Q Exactive™, peptides were directly loaded onto a 75 µm x 300 mm column packed with ReproSil Pur™ C18 AQ (Dr. Maisch HPLC) and eluted with the same 2 h gradient just described. Here, MS data was acquired with automatic switches between a full scan and up to 15 data-dependent MS/MS.

The initial data analysis was performed with MaxQuant v1.5.3.8 (Cox and Mann, 2008). Standard setting for each instrument type were used and a search performed against human or mouse protein databases extracted from UniProt (The UniProt, 2017). Carbamidomethylation of cysteine residues was set as fixed modification. Methionine oxidation, asparagine and glutamine deamination, and N-terminal acetylation were set as variable modifications. The options “match between runs” and “requantify” were both enabled. All results were filtered for a false discovery rate of 1% on a peptide

spectrum match and on protein level. The MaxQuant output files were downstream processed and analyzed using R-Script and Microsoft Excel.

5 Literature

Adolf, F., Herrmann, A., Hellwig, A., Beck, R., Brügger, B., and Wieland, F.T. (2013). Scission of COPI and COPII vesicles is independent of GTP hydrolysis. Traffic *14*, 922-932.
Adolf, F., Rhiel, M., Reckmann, I., and Wieland, F.T. (2016). Sec24C/D-isoform-specific sorting of the preassembled ER-Golgi Q-SNARE complex. Mol. Biol. Cell *27*, 2697-2707.
Aebersold, R., and Mann, M. (2016). Mass-spectrometric exploration of proteome structure and function. Nature *537*, 347-355.
Aguilar, R.C., Boehm, M., Gorshkova, I., Crouch, R.J., Tomita, K., Saito, T., Ohno, H., and Bonifacino, J.S. (2001). Signal-binding specificity of the mu4 subunit of the adaptor protein complex AP-4. J Biol Chem *276*, 13145-13152.
Anderson, R.G., Goldstein, J.L., and Brown, M.S. (1977). A mutation that impairs the ability of lipoprotein receptors to localise in coated pits on the cell surface of human fibroblasts. Nature *270*, 695-699.
Anelli, T., Alessio, M., Bachi, A., Bergamelli, L., Bertoli, G., Camerini, S., Mezghrani, A., Ruffato, E., Simmen, T., and Sitia, R. (2003). Thiol-mediated protein retention in the endoplasmic reticulum: the role of ERp44. EMBO J *22*, 5015-5022.
Aniento, F., Gu, F., Parton, R.G., and Gruenberg, J. (1996). An endosomal beta COP is involved in the pH-dependent formation of transport vesicles destined for late endosomes. J Cell Biol *133*, 29-41.
Antonny, B., Beraud-Dufour, S., Chardin, P., and Chabre, M. (1997). N-terminal hydrophobic residues of the G-protein ADP-ribosylation factor-1 insert into membrane phospholipids upon GDP to GTP exchange. Biochemistry *36*, 4675-4684.
Antonny, B., Madden, D., Hamamoto, S., Orci, L., and Schekman, R. (2001). Dynamics of the COPII coat with GTP and stable analogues. Nat Cell Biol *3*, 531-537.
Appelmans, F., Wattiaux, R., and De Duve, C. (1955). Tissue fractionation studies. 5. The association of acid phosphatase with a special class of cytoplasmic granules in rat liver. Biochem J *59*, 438-445.
Appenzeller-Herzog, C., and Hauri, H.P. (2006). The ER-Golgi intermediate compartment (ERGIC): in search of its identity and function. J Cell Sci *119*, 2173-2183.
Arakel, E.C., Richter, K.P., Clancy, A., and Schwappach, B. (2016). delta-COP contains a helix C-terminal to its longin domain key to COPI dynamics and function. Proc Natl Acad Sci U S A *113*, 6916-6921.
Aridor, M., Bannykh, S.I., Rowe, T., and Balch, W.E. (1995). Sequential coupling between COPII and COPI vesicle coats in endoplasmic reticulum to Golgi transport. J Cell Biol *131*, 875-893.
Aridor, M., Weissman, J., Bannykh, S., Nuoffer, C., and Balch, W.E. (1998). Cargo selection by the COPII budding machinery during export from the ER. J Cell Biol *141*, 61-70.
Avinoam, O., Schorb, M., Beese, C.J., Briggs, J.A., and Kaksonen, M. (2015). ENDOCYTOSIS. Endocytic sites mature by continuous bending and remodeling of the clathrin coat. Science *348*, 1369-1372.
Bagshaw, R.D., Mahuran, D.J., and Callahan, J.W. (2005). A proteomic analysis of lysosomal integral membrane proteins reveals the diverse composition of the organelle. Mol Cell Proteomics *4*, 133-143.
Baltes, J., Larsen, J.V., Radhakrishnan, K., Geumann, C., Kratzke, M., Petersen, C.M., and Schu, P. (2014). sigma1B adaptin regulates adipogenesis by mediating the sorting of sortilin in adipose tissue. J Cell Sci *127*, 3477-3487.
Bannykh, S.I., Rowe, T., and Balch, W.E. (1996). The organization of endoplasmic reticulum export complexes. J Cell Biol *135*, 19-35.
Bantscheff, M., Lemeer, S., Savitski, M.M., and Kuster, B. (2012). Quantitative mass spectrometry in proteomics: critical review update from 2007 to the present. Anal Bioanal Chem *404*, 939-965.
Bard, F., and Malhotra, V. (2006). The formation of TGN-to-plasma-membrane transport carriers. Annu Rev Cell Dev Biol *22*, 439-455.

Barlowe, C., d'Enfert, C., and Schekman, R. (1993). Purification and characterization of SAR1p, a small GTP-binding protein required for transport vesicle formation from the endoplasmic reticulum. J Biol Chem *268*, 873-879.
Barlowe, C., Orci, L., Yeung, T., Hosobuchi, M., Hamamoto, S., Salama, N., Rexach, M.F., Ravazzola, M., Amherdt, M., and Schekman, R. (1994). COPII: a membrane coat formed by Sec proteins that drive vesicle budding from the endoplasmic reticulum. Cell *77*, 895-907.
Barlowe, C., and Schekman, R. (1995). Expression, purification, and assay of Sec12p: a Sar1p-specific GDP dissociation stimulator. Methods Enzymol *257*, 98-106.
Baumann, O., and Walz, B. (2001). Endoplasmic reticulum of animal cells and its organization into structural and functional domains. Int Rev Cytol *205*, 149-214.
Beck, M., Schmidt, A., Malmstroem, J., Claassen, M., Ori, A., Szymborska, A., Herzog, F., Rinner, O., Ellenberg, J., and Aebersold, R. (2011a). The quantitative proteome of a human cell line. Mol Syst Biol *7*, 549.
Beck, R., Prinz, S., Diestelkotter-Bachert, P., Rohling, S., Adolf, F., Hoehner, K., Welsch, S., Ronchi, P., Brugger, B., Briggs, J.A.*, et al.* (2011b). Coatomer and dimeric ADP ribosylation factor 1 promote distinct steps in membrane scission. J Cell Biol *194*, 765-777.
Beck, R., Sun, Z., Adolf, F., Rutz, C., Bassler, J., Wild, K., Sinning, I., Hurt, E., Brugger, B., Bethune, J.*, et al.* (2008). Membrane curvature induced by Arf1-GTP is essential for vesicle formation. Proc Natl Acad Sci U S A *105*, 11731-11736.
Belden, W.J., and Barlowe, C. (2001). Distinct roles for the cytoplasmic tail sequences of Emp24p and Erv25p in transport between the endoplasmic reticulum and Golgi complex. J Biol Chem *276*, 43040-43048.
Beller, M., Sztalryd, C., Southall, N., Bell, M., Jackle, H., Auld, D.S., and Oliver, B. (2008). COPI complex is a regulator of lipid homeostasis. PLoS Biol *6*, e292.
Bendall, S.C., Hughes, C., Stewart, M.H., Doble, B., Bhatia, M., and Lajoie, G.A. (2008). Prevention of amino acid conversion in SILAC experiments with embryonic stem cells. Mol Cell Proteomics *7*, 1587-1597.
Bennett, M.K., Garcia-Arraras, J.E., Elferink, L.A., Peterson, K., Fleming, A.M., Hazuka, C.D., and Scheller, R.H. (1993). The syntaxin family of vesicular transport receptors. Cell *74*, 863-873.
Béthune, J., Kol, M., Hoffmann, J., Reckmann, I., Brügger, B., and Wieland, F. (2006). Coatomer, the coat protein of COPI transport vesicles, discriminates endoplasmic reticulum residents from p24 proteins. Mol Cell Biol *26*, 8011-8021.
Bevis, B.J., Hammond, A.T., Reinke, C.A., and Glick, B.S. (2002). De novo formation of transitional ER sites and Golgi structures in Pichia pastoris. Nat Cell Biol *4*, 750-756.
Bi, X., Corpina, R.A., and Goldberg, J. (2002). Structure of the Sec23/24-Sar1 pre-budding complex of the COPII vesicle coat. Nature *419*, 271-277.
Bi, X., Mancias, J.D., and Goldberg, J. (2007). Insights into COPII coat nucleation from the structure of Sec23.Sar1 complexed with the active fragment of Sec31. Dev Cell *13*, 635-645.
Bianchi, P., Fermo, E., Vercellati, C., Boschetti, C., Barcellini, W., Iurlo, A., Marcello, A.P., Righetti, P.G., and Zanella, A. (2009). Congenital dyserythropoietic anemia type II (CDAII) is caused by mutations in the SEC23B gene. Hum Mutat *30*, 1292-1298.
Bielli, A., Haney, C.J., Gabreski, G., Watkins, S.C., Bannykh, S.I., and Aridor, M. (2005). Regulation of Sar1 NH2 terminus by GTP binding and hydrolysis promotes membrane deformation to control COPII vesicle fission. J Cell Biol *171*, 919-924.
Blagitko, N., Schulz, U., Schinzel, A.A., Ropers, H.H., and Kalscheuer, V.M. (1999). gamma2-COP, a novel imprinted gene on chromosome 7q32, defines a new imprinting cluster in the human genome. Hum Mol Genet *8*, 2387-2396.
Blobel, G., and Dobberstein, B. (1975a). Transfer of proteins across membranes. I. Presence of proteolytically processed and unprocessed nascent immunoglobulin light chains on membrane-bound ribosomes of murine myeloma. J Cell Biol *67*, 835-851.
Blobel, G., and Dobberstein, B. (1975b). Transfer of proteins across membranes. II. Reconstitution of functional rough microsomes from heterologous components. J Cell Biol *67*, 852-862.

Blobel, G., and Sabatini, D.D. (1970). Controlled proteolysis of nascent polypeptides in rat liver cell fractions. I. Location of the polypeptides within ribosomes. J Cell Biol *45*, 130-145.
Blumstein, J., Faundez, V., Nakatsu, F., Saito, T., Ohno, H., and Kelly, R.B. (2001). The neuronal form of adaptor protein-3 is required for synaptic vesicle formation from endosomes. J Neurosci *21*, 8034-8042.
Bobak, D.A., Nightingale, M.S., Murtagh, J.J., Price, S.R., Moss, J., and Vaughan, M. (1989). Molecular cloning, characterization, and expression of human ADP-ribosylation factors: two guanine nucleotide-dependent activators of cholera toxin. Proc Natl Acad Sci U S A *86*, 6101-6105.
Boehm, J., Ulrich, H.D., Ossig, R., and Schmitt, H.D. (1994). Kex2-dependent invertase secretion as a tool to study the targeting of transmembrane proteins which are involved in ER-->Golgi transport in yeast. EMBO J *13*, 3696-3710.
Boehm, M., Aguilar, R.C., and Bonifacino, J.S. (2001). Functional and physical interactions of the adaptor protein complex AP-4 with ADP-ribosylation factors (ARFs). EMBO J *20*, 6265-6276.
Boll, W., Rapoport, I., Brunner, C., Modis, Y., Prehn, S., and Kirchhausen, T. (2002). The mu2 subunit of the clathrin adaptor AP-2 binds to FDNPVY and YppØ sorting signals at distinct sites. Traffic *3*, 590-600.
Boman, A.L., Zhang, C., Zhu, X., and Kahn, R.A. (2000). A family of ADP-ribosylation factor effectors that can alter membrane transport through the trans-Golgi. Mol Biol Cell *11*, 1241-1255.
Bonifacino, J.S., and Glick, B.S. (2004). The mechanisms of vesicle budding and fusion. Cell *116*, 153-166.
Bonifacino, J.S., and Rojas, R. (2006). Retrograde transport from endosomes to the trans-Golgi network. Nat Rev Mol Cell Biol *7*, 568-579.
Bonifacino, J.S., and Traub, L.M. (2003). Signals for sorting of transmembrane proteins to endosomes and lysosomes. Annu Rev Biochem *72*, 395-447.
Bonnon, C., Wendeler, M.W., Paccaud, J.P., and Hauri, H.P. (2010). Selective export of human GPI-anchored proteins from the endoplasmic reticulum. J Cell Sci *123*, 1705-1715.
Borner, G.H.H., Rana, A.A., Harbour, M., Forster, R., Lilley, K.S., Smith, J.C., and Robinson, M.S. (2006). Proteomic analysis of clathrin-coated vesicles. European Journal of Cell Biology *85*, 70-70.
Boyadjiev, S.A., Fromme, J.C., Ben, J., Chong, S.S., Nauta, C., Hur, D.J., Zhang, G., Hamamoto, S., Schekman, R., Ravazzola, M*., et al.* (2006). Cranio-lenticulo-sutural dysplasia is caused by a SEC23A mutation leading to abnormal endoplasmic-reticulum-to-Golgi trafficking. Nat Genet *38*, 1192-1197.
Bremser, M., Nickel, W., Schweikert, M., Ravazzola, M., Amherdt, M., Hughes, C.A., Söllner, T.H., Rothman, J.E., and Wieland, F.T. (1999). Coupling of coat assembly and vesicle budding to packaging of putative cargo receptors. Cell *96*, 495-506.
Breuza, L., Halbeisen, R., Jenö, P., Otte, S., Barlowe, C., Hong, W., and Hauri, H.P. (2004). Proteomics of endoplasmic reticulum-Golgi intermediate compartment (ERGIC) membranes from brefeldin A-treated HepG2 cells identifies ERGIC-32, a new cycling protein that interacts with human Erv46. J Biol Chem *279*, 47242-47253.
Brock, C., Boudier, L., Maurel, D., Blahos, J., and Pin, J.P. (2005). Assembly-dependent surface targeting of the heterodimeric GABAB Receptor is controlled by COPI but not 14-3-3. Mol Biol Cell *16*, 5572-5578.
Brown, H.A., Gutowski, S., Moomaw, C.R., Slaughter, C., and Sternweis, P.C. (1993). ADP-ribosylation factor, a small GTP-dependent regulatory protein, stimulates phospholipase D activity. Cell *75*, 1137-1144.
Burman, J.L., Bourbonniere, L., Philie, J., Stroh, T., Dejgaard, S.Y., Presley, J.F., and McPherson, P.S. (2008). Scyl1, mutated in a recessive form of spinocerebellar neurodegeneration, regulates COPI-mediated retrograde traffic. J Biol Chem *283*, 22774-22786.
Burman, J.L., Hamlin, J.N., and McPherson, P.S. (2010). Scyl1 regulates Golgi morphology. PLoS One *5*, e9537.
Bykov, Y.S., Schaffer, M., Dodonova, S.O., Albert, S., Plitzko, J.M., Baumeister, W., Engel, B.D., and Briggs, J.A. (2017). The structure of the COPI coat determined within the cell. Elife *6*.

Cabrera, M., Muñiz, M., Hidalgo, J., Vega, L., Martín, M.E., and Velasco, A. (2003). The retrieval function of the KDEL receptor requires PKA phosphorylation of its C-terminus. Mol Biol Cell *14*, 4114-4125.

Cacciagli, P., Desvignes, J.P., Girard, N., Delepine, M., Zelenika, D., Lathrop, M., Levy, N., Ledbetter, D.H., Dobyns, W.B., and Villard, L. (2014). AP1S2 is mutated in X-linked Dandy-Walker malformation with intellectual disability, basal ganglia disease and seizures (Pettigrew syndrome). Eur J Hum Genet *22*, 363-368.

Canfield, W.M., Johnson, K.F., Ye, R.D., Gregory, W., and Kornfeld, S. (1991). Localization of the signal for rapid internalization of the bovine cation-independent mannose 6-phosphate/insulin-like growth factor-II receptor to amino acids 24-29 of the cytoplasmic tail. J Biol Chem *266*, 5682-5688.

Caro, L.G., and Palade, G.E. (1964). Protein Synthesis, Storage, and Discharge in the Pancreatic Exocrine Cell. An Autoradiographic Study. J Cell Biol *20*, 473-495.

Casanova, J.E. (2007). Regulation of Arf activation: the Sec7 family of guanine nucleotide exchange factors. Traffic *8*, 1476-1485.

Cavenagh, M.M., Whitney, J.A., Carroll, K., Zhang, C., Boman, A.L., Rosenwald, A.G., Mellman, I., and Kahn, R.A. (1996). Intracellular distribution of Arf proteins in mammalian cells. Arf6 is uniquely localized to the plasma membrane. J Biol Chem *271*, 21767-21774.

Chaudhuri, R., Lindwasser, O.W., Smith, W.J., Hurley, J.H., and Bonifacino, J.S. (2007). Downregulation of CD4 by human immunodeficiency virus type 1 Nef is dependent on clathrin and involves direct interaction of Nef with the AP2 clathrin adaptor. J Virol *81*, 3877-3890.

Chen, H., Fre, S., Slepnev, V.I., Capua, M.R., Takei, K., Butler, M.H., Di Fiore, P.P., and De Camilli, P. (1998). Epsin is an EH-domain-binding protein implicated in clathrin-mediated endocytosis. Nature *394*, 793-797.

Chen, H.J., Yuan, J., and Lobel, P. (1997). Systematic mutational analysis of the cation-independent mannose 6-phosphate/insulin-like growth factor II receptor cytoplasmic domain. An acidic cluster containing a key aspartate is important for function in lysosomal enzyme sorting. J Biol Chem *272*, 7003-7012.

Chen, W.J., Goldstein, J.L., and Brown, M.S. (1990). NPXY, a sequence often found in cytoplasmic tails, is required for coated pit-mediated internalization of the low density lipoprotein receptor. J Biol Chem *265*, 3116-3123.

Chen, X.W., Wang, H., Bajaj, K., Zhang, P., Meng, Z.X., Ma, D., Bai, Y., Liu, H.H., Adams, E., Baines, A.*, et al.* (2013). SEC24A deficiency lowers plasma cholesterol through reduced PCSK9 secretion. Elife *2*, e00444.

Chun, J., Shapovalova, Z., Dejgaard, S.Y., Presley, J.F., and Melancon, P. (2008). Characterization of class I and II ADP-ribosylation factors (Arfs) in live cells: GDP-bound class II Arfs associate with the ER-Golgi intermediate compartment independently of GBF1. Mol Biol Cell *19*, 3488-3500.

Claude, A., Zhao, B.P., Kuziemsky, C.E., Dahan, S., Berger, S.J., Yan, J.P., Armold, A.D., Sullivan, E.M., and Melancon, P. (1999). GBF1: A novel Golgi-associated BFA-resistant guanine nucleotide exchange factor that displays specificity for ADP-ribosylation factor 5. J Cell Biol *146*, 71-84.

Cockcroft, S., Thomas, G.M., Fensome, A., Geny, B., Cunningham, E., Gout, I., Hiles, I., Totty, N.F., Truong, O., and Hsuan, J.J. (1994). Phospholipase D: a downstream effector of ARF in granulocytes. Science *263*, 523-526.

Collins, B.M., McCoy, A.J., Kent, H.M., Evans, P.R., and Owen, D.J. (2002). Molecular architecture and functional model of the endocytic AP2 complex. Cell *109*, 523-535.

Cosson, P., and Letourneur, F. (1994). Coatomer interaction with di-lysine endoplasmic reticulum retention motifs. Science *263*, 1629-1631.

Coutinho, M.F., Prata, M.J., and Alves, S. (2012). Mannose-6-phosphate pathway: a review on its role in lysosomal function and dysfunction. Mol Genet Metab *105*, 542-550.

Cox, J., and Mann, M. (2008). MaxQuant enables high peptide identification rates, individualized p.p.b.-range mass accuracies and proteome-wide protein quantification. Nat Biotechnol *26*, 1367-1372.

Crowley, K.S., Liao, S., Worrell, V.E., Reinhart, G.D., and Johnson, A.E. (1994). Secretory proteins move through the endoplasmic reticulum membrane via an aqueous, gated pore. Cell *78*, 461-471.
Crowley, K.S., Reinhart, G.D., and Johnson, A.E. (1993). The signal sequence moves through a ribosomal tunnel into a noncytoplasmic aqueous environment at the ER membrane early in translocation. Cell *73*, 1101-1115.
Cruz-Garcia, D., Ortega-Bellido, M., Scarpa, M., Villeneuve, J., Jovic, M., Porzner, M., Balla, T., Seufferlein, T., and Malhotra, V. (2013). Recruitment of arfaptins to the trans-Golgi network by PI(4)P and their involvement in cargo export. EMBO J *32*, 1717-1729.
d'Enfert, C., Barlowe, C., Nishikawa, S., Nakano, A., and Schekman, R. (1991). Structural and functional dissection of a membrane glycoprotein required for vesicle budding from the endoplasmic reticulum. Mol Cell Biol *11*, 5727-5734.
D'Souza-Schorey, C., and Chavrier, P. (2006). ARF proteins: roles in membrane traffic and beyond. Nat Rev Mol Cell Biol *7*, 347-358.
D'Souza-Schorey, C., Li, G., Colombo, M.I., and Stahl, P.D. (1995). A regulatory role for ARF6 in receptor-mediated endocytosis. Science *267*, 1175-1178.
D'Souza-Schorey, C., and Stahl, P.D. (1995). Myristoylation is required for the intracellular localization and endocytic function of ARF6. Exp Cell Res *221*, 153-159.
Dalton, A.J., and Felix, M.D. (1954). Cytologic and cytochemical characteristics of the Golgi substance of epithelial cells of the epididymis in situ, in homogenates and after isolation. Am J Anat *94*, 171-207.
Dalton, A.J., and Felix, M.D. (1956). A comparative study of the Golgi complex. J Biophys Biochem Cytol *2*, 79-84.
Davis, C.G., Lehrman, M.A., Russell, D.W., Anderson, R.G., Brown, M.S., and Goldstein, J.L. (1986). The J.D. mutation in familial hypercholesterolemia: amino acid substitution in cytoplasmic domain impedes internalization of LDL receptors. Cell *45*, 15-24.
De Duve, C., and Wattiaux, R. (1966). Functions of lysosomes. Annu Rev Physiol *28*, 435-492.
de Godoy, L.M., Olsen, J.V., Cox, J., Nielsen, M.L., Hubner, N.C., Frohlich, F., Walther, T.C., and Mann, M. (2008). Comprehensive mass-spectrometry-based proteome quantification of haploid versus diploid yeast. Nature *455*, 1251-1254.
Dejgaard, S.Y., Murshid, A., Erman, A., Kizilay, O., Verbich, D., Lodge, R., Dejgaard, K., Ly-Hartig, T.B., Pepperkok, R., Simpson, J.C*., et al.* (2008). Rab18 and Rab43 have key roles in ER-Golgi trafficking. J Cell Sci *121*, 2768-2781.
Dell'Angelica, E.C., Mullins, C., and Bonifacino, J.S. (1999a). AP-4, a novel protein complex related to clathrin adaptors. J Biol Chem *274*, 7278-7285.
Dell'Angelica, E.C., Ohno, H., Ooi, C.E., Rabinovich, E., Roche, K.W., and Bonifacino, J.S. (1997). AP-3: an adaptor-like protein complex with ubiquitous expression. EMBO J *16*, 917-928.
Dell'Angelica, E.C., Puertollano, R., Mullins, C., Aguilar, R.C., Vargas, J.D., Hartnell, L.M., and Bonifacino, J.S. (2000). GGAs: a family of ADP ribosylation factor-binding proteins related to adaptors and associated with the Golgi complex. J Cell Biol *149*, 81-94.
Dell'Angelica, E.C., Shotelersuk, V., Aguilar, R.C., Gahl, W.A., and Bonifacino, J.S. (1999b). Altered trafficking of lysosomal proteins in Hermansky-Pudlak syndrome due to mutations in the beta 3A subunit of the AP-3 adaptor. Mol Cell *3*, 11-21.
Deretic, D., Williams, A.H., Ransom, N., Morel, V., Hargrave, P.A., and Arendt, A. (2005). Rhodopsin C terminus, the site of mutations causing retinal disease, regulates trafficking by binding to ADP-ribosylation factor 4 (ARF4). Proc Natl Acad Sci U S A *102*, 3301-3306.
Dimopoulos, S., Mayer, C.E., Rudolf, F., and Stelling, J. (2014). Accurate cell segmentation in microscopy images using membrane patterns. Bioinformatics *30*, 2644-2651.
Dodonova, S.O., Aderhold, P., Kopp, J., Ganeva, I., Rohling, S., Hagen, W.J.H., Sinning, I., Wieland, F., and Briggs, J.A.G. (2017). 9A structure of the COPI coat reveals that the Arf1 GTPase occupies two contrasting molecular environments. Elife *6*.

Dodonova, S.O., Diestelkoetter-Bachert, P., von Appen, A., Hagen, W.J., Beck, R., Beck, M., Wieland, F., and Briggs, J.A. (2015). VESICULAR TRANSPORT. A structure of the COPI coat and the role of coat proteins in membrane vesicle assembly. Science *349*, 195-198.
Dominguez, M., Dejgaard, K., Füllekrug, J., Dahan, S., Fazel, A., Paccaud, J.P., Thomas, D.Y., Bergeron, J.J., and Nilsson, T. (1998). gp25L/emp24/p24 protein family members of the cis-Golgi network bind both COP I and II coatomer. J Cell Biol *140*, 751-765.
Donaldson, J.G. (2003). Multiple roles for Arf6: sorting, structuring, and signaling at the plasma membrane. J Biol Chem *278*, 41573-41576.
Donaldson, J.G., Cassel, D., Kahn, R.A., and Klausner, R.D. (1992). ADP-ribosylation factor, a small GTP-binding protein, is required for binding of the coatomer protein beta-COP to Golgi membranes. Proc Natl Acad Sci U S A *89*, 6408-6412.
Donohoe, B.S., Kang, B.H., and Staehelin, L.A. (2007). Identification and characterization of COPIa- and COPIb-type vesicle classes associated with plant and algal Golgi. Proc Natl Acad Sci U S A *104*, 163-168.
Doray, B., Lee, I., Knisely, J., Bu, G., and Kornfeld, S. (2007). The gamma/sigma1 and alpha/sigma2 hemicomplexes of clathrin adaptors AP-1 and AP-2 harbor the dileucine recognition site. Mol Biol Cell *18*, 1887-1896.
Drake, M.T., Downs, M.A., and Traub, L.M. (2000). Epsin binds to clathrin by associating directly with the clathrin-terminal domain. Evidence for cooperative binding through two discrete sites. J Biol Chem *275*, 6479-6489.
Duijsings, D., Lanke, K.H., van Dooren, S.H., van Dommelen, M.M., Wetzels, R., de Mattia, F., Wessels, E., and van Kuppeveld, F.J. (2009). Differential membrane association properties and regulation of class I and class II Arfs. Traffic *10*, 316-323.
Dunkley, T.P., Watson, R., Griffin, J.L., Dupree, P., and Lilley, K.S. (2004). Localization of organelle proteins by isotope tagging (LOPIT). Mol Cell Proteomics *3*, 1128-1134.
Dunphy, W.G., and Rothman, J.E. (1985). Compartmental organization of the Golgi stack. Cell *42*, 13-21.
Eckert, E.S., Reckmann, I., Hellwig, A., Röhling, S., El-Battari, A., Wieland, F.T., and Popoff, V. (2014). Golgi phosphoprotein 3 triggers signal-mediated incorporation of glycosyltransferases into coatomer-coated (COPI) vesicles. J Biol Chem *289*, 31319-31329.
Egerer, J., Emmerich, D., Fischer-Zirnsak, B., Chan, W.L., Meierhofer, D., Tuysuz, B., Marschner, K., Sauer, S., Barr, F.A., Mundlos, S*., et al.* (2015). GORAB Missense Mutations Disrupt RAB6 and ARF5 Binding and Golgi Targeting. J Invest Dermatol *135*, 2368-2376.
Essner, E., and Novikoff, A.B. (1961). Localization of acid phosphatase activity in hepatic lysosomes by means of electron microscopy. J Biophys Biochem Cytol *9*, 773-784.
Eugster, A., Frigerio, G., Dale, M., and Duden, R. (2004). The alpha- and beta'-COP WD40 domains mediate cargo-selective interactions with distinct di-lysine motifs. Mol Biol Cell *15*, 1011-1023.
Fagone, P., and Jackowski, S. (2009). Membrane phospholipid synthesis and endoplasmic reticulum function. J Lipid Res *50 Suppl*, S311-316.
Farhan, H., Reiterer, V., Korkhov, V.M., Schmid, J.A., Freissmuth, M., and Sitte, H.H. (2007). Concentrative export from the endoplasmic reticulum of the gamma-aminobutyric acid transporter 1 requires binding to SEC24D. J Biol Chem *282*, 7679-7689.
Faundez, V., Horng, J.T., and Kelly, R.B. (1998). A function for the AP3 coat complex in synaptic vesicle formation from endosomes. Cell *93*, 423-432.
Fenn, J.B., Mann, M., Meng, C.K., Wong, S.F., and Whitehouse, C.M. (1989). Electrospray ionization for mass spectrometry of large biomolecules. Science *246*, 64-71.
Ferguson, S.M., and De Camilli, P. (2012). Dynamin, a membrane-remodelling GTPase. Nat Rev Mol Cell Biol *13*, 75-88.
Fiedler, K., Veit, M., Stamnes, M.A., and Rothman, J.E. (1996). Bimodal interaction of coatomer with the p24 family of putative cargo receptors. Science *273*, 1396-1399.
Fink, J.K. (2013). Hereditary spastic paraplegia: clinico-pathologic features and emerging molecular mechanisms. Acta Neuropathol *126*, 307-328.

Fink, J.K. (2014). Hereditary spastic paraplegia: clinical principles and genetic advances. Semin Neurol *34*, 293-305.
Fleischer, B., Fleischer, S., and Ozawa, H. (1969). Isolation and characterization of Golgi membranes from bovine liver. J Cell Biol *43*, 59-79.
Folsch, H., Ohno, H., Bonifacino, J.S., and Mellman, I. (1999). A novel clathrin adaptor complex mediates basolateral targeting in polarized epithelial cells. Cell *99*, 189-198.
Folsch, H., Pypaert, M., Maday, S., Pelletier, L., and Mellman, I. (2003). The AP-1A and AP-1B clathrin adaptor complexes define biochemically and functionally distinct membrane domains. J Cell Biol *163*, 351-362.
Foster, L.J., de Hoog, C.L., Zhang, Y., Zhang, Y., Xie, X., Mootha, V.K., and Mann, M. (2006). A mammalian organelle map by protein correlation profiling. Cell *125*, 187-199.
Franco, M., Chardin, P., Chabre, M., and Paris, S. (1995). Myristoylation of ADP-ribosylation factor 1 facilitates nucleotide exchange at physiological Mg2+ levels. J Biol Chem *270*, 1337-1341.
Franco, M., Chardin, P., Chabre, M., and Paris, S. (1996). Myristoylation-facilitated binding of the G protein ARF1GDP to membrane phospholipids is required for its activation by a soluble nucleotide exchange factor. J Biol Chem *271*, 1573-1578.
Fromme, J.C., Orci, L., and Schekman, R. (2008). Coordination of COPII vesicle trafficking by Sec23. Trends Cell Biol *18*, 330-336.
Fromme, J.C., Ravazzola, M., Hamamoto, S., Al-Balwi, M., Eyaid, W., Boyadjiev, S.A., Cosson, P., Schekman, R., and Orci, L. (2007). The genetic basis of a craniofacial disease provides insight into COPII coat assembly. Dev Cell *13*, 623-634.
Fryer, L.G., Jones, B., Duncan, E.J., Hutchison, C.E., Ozkan, T., Williams, P.A., Alder, O., Nieuwdorp, M., Townley, A.K., Mensenkamp, A.R.*, et al.* (2014). The endoplasmic reticulum coat protein II transport machinery coordinates cellular lipid secretion and cholesterol biosynthesis. J Biol Chem *289*, 4244-4261.
Fukasawa, M., Varlamov, O., Eng, W.S., Sollner, T.H., and Rothman, J.E. (2004). Localization and activity of the SNARE Ykt6 determined by its regulatory domain and palmitoylation. Proc Natl Acad Sci U S A *101*, 4815-4820.
Futatsumori, M., Kasai, K., Takatsu, H., Shin, H.W., and Nakayama, K. (2000). Identification and characterization of novel isoforms of COP I subunits. J Biochem *128*, 793-801.
Gahl, W.A., and Huizing, M. (1993). Hermansky-Pudlak Syndrome. In GeneReviews(R), M.P. Adam, H.H. Ardinger, R.A. Pagon, S.E. Wallace, L.J.H. Bean, H.C. Mefford, K. Stephens, A. Amemiya, and N. Ledbetter, eds. (Seattle (WA)).
Gaidarov, I., Chen, Q., Falck, J.R., Reddy, K.K., and Keen, J.H. (1996). A functional phosphatidylinositol 3,4,5-trisphosphate/phosphoinositide binding domain in the clathrin adaptor AP-2 alpha subunit. Implications for the endocytic pathway. J Biol Chem *271*, 20922-20929.
Galloway, C.J., Dean, G.E., Marsh, M., Rudnick, G., and Mellman, I. (1983). Acidification of macrophage and fibroblast endocytic vesicles in vitro. Proc Natl Acad Sci U S A *80*, 3334-3338.
Gannon, J., Bergeron, J.J., and Nilsson, T. (2011). Golgi and related vesicle proteomics: simplify to identify. Cold Spring Harb Perspect Biol *3*.
Garbes, L., Kim, K., Rieß, A., Hoyer-Kuhn, H., Beleggia, F., Bevot, A., Kim, M.J., Huh, Y.H., Kweon, H.S., Savarirayan, R.*, et al.* (2015). Mutations in SEC24D, encoding a component of the COPII machinery, cause a syndromic form of osteogenesis imperfecta. Am J Hum Genet *96*, 432-439.
Gaynor, E.C., te Heesen, S., Graham, T.R., Aebi, M., and Emr, S.D. (1994). Signal-mediated retrieval of a membrane protein from the Golgi to the ER in yeast. J Cell Biol *127*, 653-665.
Gilchrist, A., Au, C.E., Hiding, J., Bell, A.W., Fernandez-Rodriguez, J., Lesimple, S., Nagaya, H., Roy, L., Gosline, S.J., Hallett, M.*, et al.* (2006). Quantitative proteomics analysis of the secretory pathway. Cell *127*, 1265-1281.
Gillingham, A.K., and Munro, S. (2007). The small G proteins of the Arf family and their regulators. Annu Rev Cell Dev Biol *23*, 579-611.
Glick, B.S., and Luini, A. (2011). Models for Golgi traffic: a critical assessment. Cold Spring Harb Perspect Biol *3*, a005215.

Glick, B.S., and Nakano, A. (2009). Membrane traffic within the Golgi apparatus. Annu Rev Cell Dev Biol *25*, 113-132.
Glish, G.L., and Vachet, R.W. (2003). The basics of mass spectrometry in the twenty-first century. Nat Rev Drug Discov *2*, 140-150.
Godi, A., Pertile, P., Meyers, R., Marra, P., Di Tullio, G., Iurisci, C., Luini, A., Corda, D., and De Matteis, M.A. (1999). ARF mediates recruitment of PtdIns-4-OH kinase-beta and stimulates synthesis of PtdIns(4,5)P2 on the Golgi complex. Nat Cell Biol *1*, 280-287.
Goffeau, A., Barrell, B.G., Bussey, H., Davis, R.W., Dujon, B., Feldmann, H., Galibert, F., Hoheisel, J.D., Jacq, C., Johnston, M.*, et al.* (1996). Life with 6000 genes. Science *274*, 546, 563-547.
Golgi, C. (1989a). On the structure of nerve cells. 1898. J Microsc *155*, 3-7.
Golgi, C. (1989b). On the structure of the nerve cells of the spinal ganglia. 1898. J Microsc *155*, 9-14.
Gommel, D., Orci, L., Emig, E.M., Hannah, M.J., Ravazzola, M., Nickel, W., Helms, J.B., Wieland, F.T., and Sohn, K. (1999). p24 and p23, the major transmembrane proteins of COPI-coated transport vesicles, form hetero-oligomeric complexes and cycle between the organelles of the early secretory pathway. FEBS Lett *447*, 179-185.
Gommel, D.U., Memon, A.R., Heiss, A., Lottspeich, F., Pfannstiel, J., Lechner, J., Reinhard, C., Helms, J.B., Nickel, W., and Wieland, F.T. (2001). Recruitment to Golgi membranes of ADP-ribosylation factor 1 is mediated by the cytoplasmic domain of p23. EMBO J *20*, 6751-6760.
Gordon, D.E., Bond, L.M., Sahlender, D.A., and Peden, A.A. (2010). A targeted siRNA screen to identify SNAREs required for constitutive secretion in mammalian cells. Traffic *11*, 1191-1204.
Görlich, D., Hartmann, E., Prehn, S., and Rapoport, T.A. (1992). A protein of the endoplasmic reticulum involved early in polypeptide translocation. Nature *357*, 47-52.
Gorur, A., Yuan, L., Kenny, S.J., Baba, S., Xu, K., and Schekman, R. (2017). COPII-coated membranes function as transport carriers of intracellular procollagen I. J Cell Biol *216*, 1745-1759.
Gouw, J.W., Krijgsveld, J., and Heck, A.J. (2010). Quantitative proteomics by metabolic labeling of model organisms. Mol Cell Proteomics *9*, 11-24.
Greenberg, M., DeTulleo, L., Rapoport, I., Skowronski, J., and Kirchhausen, T. (1998). A dileucine motif in HIV-1 Nef is essential for sorting into clathrin-coated pits and for downregulation of CD4. Curr Biol *8*, 1239-1242.
Griffiths, G., and Simons, K. (1986). The trans Golgi network: sorting at the exit site of the Golgi complex. Science *234*, 438-443.
Gruenberg, J., Griffiths, G., and Howell, K.E. (1989). Characterization of the early endosome and putative endocytic carrier vesicles in vivo and with an assay of vesicle fusion in vitro. J Cell Biol *108*, 1301-1316.
Gu, F., Crump, C.M., and Thomas, G. (2001). Trans-Golgi network sorting. Cell Mol Life Sci *58*, 1067-1084.
Guo, X., Mattera, R., Ren, X., Chen, Y., Retamal, C., Gonzalez, A., and Bonifacino, J.S. (2013). The adaptor protein-1 mu1B subunit expands the repertoire of basolateral sorting signal recognition in epithelial cells. Dev Cell *27*, 353-366.
Guo, Y., Cordes, K.R., Farese, R.V., Jr., and Walther, T.C. (2009). Lipid droplets at a glance. J Cell Sci *122*, 749-752.
Guo, Y., Walther, T.C., Rao, M., Stuurman, N., Goshima, G., Terayama, K., Wong, J.S., Vale, R.D., Walter, P., and Farese, R.V. (2008). Functional genomic screen reveals genes involved in lipid-droplet formation and utilization. Nature *453*, 657-661.
Gygi, S.P., Rist, B., Gerber, S.A., Turecek, F., Gelb, M.H., and Aebersold, R. (1999). Quantitative analysis of complex protein mixtures using isotope-coded affinity tags. Nat Biotechnol *17*, 994-999.
Hamlin, J.N., Schroeder, L.K., Fotouhi, M., Dokainish, H., Ioannou, M.S., Girard, M., Summerfeldt, N., Melançon, P., and McPherson, P.S. (2014). Scyl1 scaffolds class II Arfs to specific subcomplexes of coatomer through the γ-COP appendage domain. J Cell Sci *127*, 1454-1463.
Han, X., Aslanian, A., and Yates, J.R., 3rd (2008). Mass spectrometry for proteomics. Curr Opin Chem Biol *12*, 483-490.

Hara-Kuge, S., Kuge, O., Orci, L., Amherdt, M., Ravazzola, M., Wieland, F.T., and Rothman, J.E. (1994). En bloc incorporation of coatomer subunits during the assembly of COP-coated vesicles. J Cell Biol *124*, 883-892.
Hariri, H., Bhattacharya, N., Johnson, K., Noble, A.J., and Stagg, S.M. (2014). Insights into the mechanisms of membrane curvature and vesicle scission by the small GTPase Sar1 in the early secretory pathway. J Mol Biol *426*, 3811-3826.
Harter, C., and Wieland, F.T. (1998). A single binding site for dilysine retrieval motifs and p23 within the gamma subunit of coatomer. Proc Natl Acad Sci U S A *95*, 11649-11654.
Hasegawa, H., Yang, Z., Oltedal, L., Davanger, S., and Hay, J.C. (2004). Intramolecular protein-protein and protein-lipid interactions control the conformation and subcellular targeting of neuronal Ykt6. J Cell Sci *117*, 4495-4508.
Hashimoto, K., Gross, B.G., and Lever, W.F. (1965). Angiokeratoma Corporis Diffusum (Fabry). Histochemical and Electron Microscopic Studies of the Skin. J Invest Dermatol *44*, 119-128.
Hay, J.C., Klumperman, J., Oorschot, V., Steegmaier, M., Kuo, C.S., and Scheller, R.H. (1998). Localization, dynamics, and protein interactions reveal distinct roles for ER and Golgi SNAREs. J Cell Biol *141*, 1489-1502.
Heldwein, E.E., Macia, E., Wang, J., Yin, H.L., Kirchhausen, T., and Harrison, S.C. (2004). Crystal structure of the clathrin adaptor protein 1 core. Proc Natl Acad Sci U S A *101*, 14108-14113.
Hers, H.G. (1963). alpha-Glucosidase deficiency in generalized glycogenstorage disease (Pompe's disease). Biochem J *86*, 11-16.
Hirst, J., Barlow, L.D., Francisco, G.C., Sahlender, D.A., Seaman, M.N., Dacks, J.B., and Robinson, M.S. (2011). The fifth adaptor protein complex. PLoS Biol *9*, e1001170.
Hirst, J., Borner, G.H., Antrobus, R., Peden, A.A., Hodson, N.A., Sahlender, D.A., and Robinson, M.S. (2012). Distinct and overlapping roles for AP-1 and GGAs revealed by the "knocksideways" system. Curr Biol *22*, 1711-1716.
Hirst, J., Borner, G.H., Edgar, J., Hein, M.Y., Mann, M., Buchholz, F., Antrobus, R., and Robinson, M.S. (2013). Interaction between AP-5 and the hereditary spastic paraplegia proteins SPG11 and SPG15. Mol Biol Cell *24*, 2558-2569.
Hirst, J., Bright, N.A., Rous, B., and Robinson, M.S. (1999). Characterization of a fourth adaptor-related protein complex. Mol Biol Cell *10*, 2787-2802.
Hirst, J., Miller, S.E., Taylor, M.J., von Mollard, G.F., and Robinson, M.S. (2004). EpsinR is an adaptor for the SNARE protein Vti1b. Mol Biol Cell *15*, 5593-5602.
Hirst, J., and Robinson, M.S. (1998). Clathrin and adaptors. Biochim Biophys Acta *1404*, 173-193.
Hirst, J., Schlacht, A., Norcott, J.P., Traynor, D., Bloomfield, G., Antrobus, R., Kay, R.R., Dacks, J.B., and Robinson, M.S. (2014). Characterization of TSET, an ancient and widespread membrane trafficking complex. Elife *3*, e02866.
Honda, A., Al-Awar, O.S., Hay, J.C., and Donaldson, J.G. (2005). Targeting of Arf-1 to the early Golgi by membrin, an ER-Golgi SNARE. J Cell Biol *168*, 1039-1051.
Hong, W. (2005). SNAREs and traffic. Biochim Biophys Acta *1744*, 493-517.
Huang, M., Weissman, J.T., Beraud-Dufour, S., Luan, P., Wang, C., Chen, W., Aridor, M., Wilson, I.A., and Balch, W.E. (2001). Crystal structure of Sar1-GDP at 1.7 A resolution and the role of the NH2 terminus in ER export. J Cell Biol *155*, 937-948.
Huizing, M., Boissy, R.E., and Gahl, W.A. (2002). Hermansky-Pudlak syndrome: vesicle formation from yeast to man. Pigment Cell Res *15*, 405-419.
Hunziker, W., Harter, C., Matter, K., and Mellman, I. (1991). Basolateral sorting in MDCK cells requires a distinct cytoplasmic domain determinant. Cell *66*, 907-920.
Huotari, J., and Helenius, A. (2011). Endosome maturation. EMBO J *30*, 3481-3500.
Itzhak, D.N., Tyanova, S., Cox, J., and Borner, G.H. (2016). Global, quantitative and dynamic mapping of protein subcellular localization. Elife *5*.
Izumi, K., Brett, M., Nishi, E., Drunat, S., Tan, E.S., Fujiki, K., Lebon, S., Cham, B., Masuda, K., Arakawa, M.*, et al.* (2016). ARCN1 Mutations Cause a Recognizable Craniofacial Syndrome Due to COPI-Mediated Transport Defects. Am J Hum Genet *99*, 451-459.

Jackson, L.P., Kelly, B.T., McCoy, A.J., Gaffry, T., James, L.C., Collins, B.M., Honing, S., Evans, P.R., and Owen, D.J. (2010). A large-scale conformational change couples membrane recruitment to cargo binding in the AP2 clathrin adaptor complex. Cell *141*, 1220-1229.
Jackson, L.P., Lewis, M., Kent, H.M., Edeling, M.A., Evans, P.R., Duden, R., and Owen, D.J. (2012). Molecular basis for recognition of dilysine trafficking motifs by COPI. Dev Cell *23*, 1255-1262.
Jackson, M.R., Nilsson, T., and Peterson, P.A. (1990). Identification of a consensus motif for retention of transmembrane proteins in the endoplasmic reticulum. EMBO J *9*, 3153-3162.
Jadot, M., Canfield, W.M., Gregory, W., and Kornfeld, S. (1992). Characterization of the signal for rapid internalization of the bovine mannose 6-phosphate/insulin-like growth factor-II receptor. J Biol Chem *267*, 11069-11077.
Jamieson, J.D., and Palade, G.E. (1967). Intracellular transport of secretory proteins in the pancreatic exocrine cell. I. Role of the peripheral elements of the Golgi complex. J Cell Biol *34*, 577-596.
Johnson, K.F., and Kornfeld, S. (1992). A His-Leu-Leu sequence near the carboxyl terminus of the cytoplasmic domain of the cation-dependent mannose 6-phosphate receptor is necessary for the lysosomal enzyme sorting function. J Biol Chem *267*, 17110-17115.
Jones, B., Jones, E.L., Bonney, S.A., Patel, H.N., Mensenkamp, A.R., Eichenbaum-Voline, S., Rudling, M., Myrdal, U., Annesi, G., Naik, S.*, et al.* (2003). Mutations in a Sar1 GTPase of COPII vesicles are associated with lipid absorption disorders. Nat Genet *34*, 29-31.
Kahn, R.A., Cherfils, J., Elias, M., Lovering, R.C., Munro, S., and Schurmann, A. (2006). Nomenclature for the human Arf family of GTP-binding proteins: ARF, ARL, and SAR proteins. J Cell Biol *172*, 645-650.
Kahn, R.A., Kern, F.G., Clark, J., Gelmann, E.P., and Rulka, C. (1991). Human ADP-ribosylation factors. A functionally conserved family of GTP-binding proteins. J Biol Chem *266*, 2606-2614.
Kahn, R.A., Volpicelli-Daley, L., Bowzard, B., Shrivastava-Ranjan, P., Li, Y., Zhou, C., and Cunningham, L. (2005). Arf family GTPases: roles in membrane traffic and microtubule dynamics. Biochem Soc Trans *33*, 1269-1272.
Kanaseki, T., and Kadota, K. (1969). The "vesicle in a basket". A morphological study of the coated vesicle isolated from the nerve endings of the guinea pig brain, with special reference to the mechanism of membrane movements. J Cell Biol *42*, 202-220.
Kanoh, H., Williger, B.T., and Exton, J.H. (1997). Arfaptin 1, a putative cytosolic target protein of ADP-ribosylation factor, is recruited to Golgi membranes. J Biol Chem *272*, 5421-5429.
Kappeler, F., Klopfenstein, D.R., Foguet, M., Paccaud, J.P., and Hauri, H.P. (1997). The recycling of ERGIC-53 in the early secretory pathway. ERGIC-53 carries a cytosolic endoplasmic reticulum-exit determinant interacting with COPII. J Biol Chem *272*, 31801-31808.
Karas, M., and Hillenkamp, F. (1988). Laser desorption ionization of proteins with molecular masses exceeding 10,000 daltons. Anal Chem *60*, 2299-2301.
Karpievitch, Y.V., Polpitiya, A.D., Anderson, G.A., Smith, R.D., and Dabney, A.R. (2010). Liquid Chromatography Mass Spectrometry-Based Proteomics: Biological and Technological Aspects. Ann Appl Stat *4*, 1797-1823.
Karrenbauer, A., Jeckel, D., Just, W., Birk, R., Schmidt, R.R., Rothman, J.E., and Wieland, F.T. (1990). The rate of bulk flow from the Golgi to the plasma membrane. Cell *63*, 259-267.
Kawamoto, K., Yoshida, Y., Tamaki, H., Torii, S., Shinotsuka, C., Yamashina, S., and Nakayama, K. (2002). GBF1, a guanine nucleotide exchange factor for ADP-ribosylation factors, is localized to the cis-Golgi and involved in membrane association of the COPI coat. Traffic *3*, 483-495.
Keen, J.H., Willingham, M.C., and Pastan, I.H. (1979). Clathrin-coated vesicles: isolation, dissociation and factor-dependent reassociation of clathrin baskets. Cell *16*, 303-312.
Kim, J., Kleizen, B., Choy, R., Thinakaran, G., Sisodia, S.S., and Schekman, R.W. (2007). Biogenesis of gamma-secretase early in the secretory pathway. J Cell Biol *179*, 951-963.
Klemm, R.W., Ejsing, C.S., Surma, M.A., Kaiser, H.J., Gerl, M.J., Sampaio, J.L., de Robillard, Q., Ferguson, C., Proszynski, T.J., Shevchenko, A.*, et al.* (2009). Segregation of sphingolipids and sterols during formation of secretory vesicles at the trans-Golgi network. J Cell Biol *185*, 601-612.

Klumperman, J., Schweizer, A., Clausen, H., Tang, B.L., Hong, W., Oorschot, V., and Hauri, H.P. (1998). The recycling pathway of protein ERGIC-53 and dynamics of the ER-Golgi intermediate compartment. J Cell Sci *111 (Pt 22)*, 3411-3425.
Kornfeld, R., and Kornfeld, S. (1985). Assembly of asparagine-linked oligosaccharides. Annu Rev Biochem *54*, 631-664.
Kornfeld, S. (1986). Trafficking of lysosomal enzymes in normal and disease states. J Clin Invest *77*, 1-6.
Kozik, P., Francis, R.W., Seaman, M.N., and Robinson, M.S. (2010). A screen for endocytic motifs. Traffic *11*, 843-855.
Krauss, M., Jia, J.Y., Roux, A., Beck, R., Wieland, F.T., De Camilli, P., and Haucke, V. (2008). Arf1-GTP-induced tubule formation suggests a function of Arf family proteins in curvature acquisition at sites of vesicle budding. J Biol Chem *283*, 27717-27723.
Krauss, M., Kinuta, M., Wenk, M.R., De Camilli, P., Takei, K., and Haucke, V. (2003). ARF6 stimulates clathrin/AP-2 recruitment to synaptic membranes by activating phosphatidylinositol phosphate kinase type Igamma. J Cell Biol *162*, 113-124.
Krieg, U.C., Walter, P., and Johnson, A.E. (1986). Photocrosslinking of the signal sequence of nascent preprolactin to the 54-kilodalton polypeptide of the signal recognition particle. Proc Natl Acad Sci U S A *83*, 8604-8608.
Kuehn, M.J., Herrmann, J.M., and Schekman, R. (1998). COPII-cargo interactions direct protein sorting into ER-derived transport vesicles. Nature *391*, 187-190.
Kuehn, M.J., Schekman, R., and Ljungdahl, P.O. (1996). Amino acid permeases require COPII components and the ER resident membrane protein Shr3p for packaging into transport vesicles in vitro. J Cell Biol *135*, 585-595.
Kuge, O., Dascher, C., Orci, L., Rowe, T., Amherdt, M., Plutner, H., Ravazzola, M., Tanigawa, G., Rothman, J.E., and Balch, W.E. (1994). Sar1 promotes vesicle budding from the endoplasmic reticulum but not Golgi compartments. J Cell Biol *125*, 51-65.
Kural, C., Tacheva-Grigorova, S.K., Boulant, S., Cocucci, E., Baust, T., Duarte, D., and Kirchhausen, T. (2012). Dynamics of intracellular clathrin/AP1- and clathrin/AP3-containing carriers. Cell Rep *2*, 1111-1119.
Kurzchalia, T.V., Wiedmann, M., Girshovich, A.S., Bochkareva, E.S., Bielka, H., and Rapoport, T.A. (1986). The signal sequence of nascent preprolactin interacts with the 54K polypeptide of the signal recognition particle. Nature *320*, 634-636.
Laemmli, U.K. (1970). Cleavage of structural proteins during the assembly of the head of bacteriophage T4. Nature *227*, 680-685.
Lang, M.R., Lapierre, L.A., Frotscher, M., Goldenring, J.R., and Knapik, E.W. (2006). Secretory COPII coat component Sec23a is essential for craniofacial chondrocyte maturation. Nat Genet *38*, 1198-1203.
Langer, J.D., Roth, C.M., Bethune, J., Stoops, E.H., Brugger, B., Herten, D.P., and Wieland, F.T. (2008). A conformational change in the alpha-subunit of coatomer induced by ligand binding to gamma-COP revealed by single-pair FRET. Traffic *9*, 597-607.
Lanoix, J., Ouwendijk, J., Lin, C.C., Stark, A., Love, H.D., Ostermann, J., and Nilsson, T. (1999). GTP hydrolysis by arf-1 mediates sorting and concentration of Golgi resident enzymes into functional COP I vesicles. EMBO J *18*, 4935-4948.
Le Borgne, R., and Hoflack, B. (1998). Mechanisms of protein sorting and coat assembly: insights from the clathrin-coated vesicle pathway. Curr Opin Cell Biol *10*, 499-503.
Lee, F.J., Moss, J., and Vaughan, M. (1992). Human and Giardia ADP-ribosylation factors (ARFs) complement ARF function in Saccharomyces cerevisiae. J Biol Chem *267*, 24441-24445.
Lee, M.C., Orci, L., Hamamoto, S., Futai, E., Ravazzola, M., and Schekman, R. (2005). Sar1p N-terminal helix initiates membrane curvature and completes the fission of a COPII vesicle. Cell *122*, 605-617.
Letourneur, F., Gaynor, E.C., Hennecke, S., Démollière, C., Duden, R., Emr, S.D., Riezman, H., and Cosson, P. (1994). Coatomer is essential for retrieval of dilysine-tagged proteins to the endoplasmic reticulum. Cell *79*, 1199-1207.

Letourneur, F., and Klausner, R.D. (1992). A novel di-leucine motif and a tyrosine-based motif independently mediate lysosomal targeting and endocytosis of CD3 chains. Cell *69*, 1143-1157.
Lewis, M.J., and Pelham, H.R. (1992). Ligand-induced redistribution of a human KDEL receptor from the Golgi complex to the endoplasmic reticulum. Cell *68*, 353-364.
Lewis, M.J., Sweet, D.J., and Pelham, H.R. (1990). The ERD2 gene determines the specificity of the luminal ER protein retention system. Cell *61*, 1359-1363.
Li, C., Luo, X., Zhao, S., Siu, G.K., Liang, Y., Chan, H.C., Satoh, A., and Yu, S.S. (2017). COPI-TRAPPII activates Rab18 and regulates its lipid droplet association. EMBO J *36*, 441-457.
Liang, J.O., and Kornfeld, S. (1997). Comparative activity of ADP-ribosylation factor family members in the early steps of coated vesicle formation on rat liver Golgi membranes. J Biol Chem *272*, 4141-4148.
Lin, P., Le-Niculescu, H., Hofmeister, R., McCaffery, J.M., Jin, M., Hennemann, H., McQuistan, T., De Vries, L., and Farquhar, M.G. (1998). The mammalian calcium-binding protein, nucleobindin (CALNUC), is a Golgi resident protein. J Cell Biol *141*, 1515-1527.
Liu, W., Duden, R., Phair, R.D., and Lippincott-Schwartz, J. (2005). ArfGAP1 dynamics and its role in COPI coat assembly on Golgi membranes of living cells. J Cell Biol *168*, 1053-1063.
Luzio, J.P., Gray, S.R., and Bright, N.A. (2010). Endosome-lysosome fusion. Biochem Soc Trans *38*, 1413-1416.
Luzio, J.P., Pryor, P.R., and Bright, N.A. (2007). Lysosomes: fusion and function. Nat Rev Mol Cell Biol *8*, 622-632.
Ma, D., Zerangue, N., Lin, Y.F., Collins, A., Yu, M., Jan, Y.N., and Jan, L.Y. (2001). Role of ER export signals in controlling surface potassium channel numbers. Science *291*, 316-319.
Ma, W., Goldberg, E., and Goldberg, J. (2017). ER retention is imposed by COPII protein sorting and attenuated by 4-phenylbutyrate. Elife *6*.
Ma, W., and Goldberg, J. (2013). Rules for the recognition of dilysine retrieval motifs by coatomer. EMBO J *32*, 926-937.
Ma, W., and Goldberg, J. (2016). TANGO1/cTAGE5 receptor as a polyvalent template for assembly of large COPII coats. Proc Natl Acad Sci U S A *113*, 10061-10066.
MacDonald, C., Munson, M., and Bryant, N.J. (2010). Autoinhibition of SNARE complex assembly by a conformational switch represents a conserved feature of syntaxins. Biochem Soc Trans *38*, 209-212.
Mairet-Coello, G., Tury, A., Esnard-Feve, A., Fellmann, D., Risold, P.Y., and Griffond, B. (2004). FAD-linked sulfhydryl oxidase QSOX: topographic, cellular, and subcellular immunolocalization in adult rat central nervous system. J Comp Neurol *473*, 334-363.
Majoul, I., Sohn, K., Wieland, F.T., Pepperkok, R., Pizza, M., Hillemann, J., and Söling, H.D. (1998). KDEL receptor (Erd2p)-mediated retrograde transport of the cholera toxin A subunit from the Golgi involves COPI, p23, and the COOH terminus of Erd2p. J Cell Biol *143*, 601-612.
Majoul, I., Straub, M., Hell, S.W., Duden, R., and Soling, H.D. (2001). KDEL-cargo regulates interactions between proteins involved in COPI vesicle traffic: measurements in living cells using FRET. Dev Cell *1*, 139-153.
Malhotra, V., and Erlmann, P. (2011). Protein export at the ER: loading big collagens into COPII carriers. EMBO J *30*, 3475-3480.
Malhotra, V., and Erlmann, P. (2015). The pathway of collagen secretion. Annu Rev Cell Dev Biol *31*, 109-124.
Malhotra, V., Serafini, T., Orci, L., Shepherd, J.C., and Rothman, J.E. (1989). Purification of a novel class of coated vesicles mediating biosynthetic protein transport through the Golgi stack. Cell *58*, 329-336.
Malkus, P., Jiang, F., and Schekman, R. (2002). Concentrative sorting of secretory cargo proteins into COPII-coated vesicles. J Cell Biol *159*, 915-921.
Malsam, J., Satoh, A., Pelletier, L., and Warren, G. (2005). Golgin tethers define subpopulations of COPI vesicles. Science *307*, 1095-1098.
Malsam, J., and Söllner, T.H. (2011). Organization of SNAREs within the Golgi stack. Cold Spring Harb Perspect Biol *3*, a005249.

Man, Z., Kondo, Y., Koga, H., Umino, H., Nakayama, K., and Shin, H.W. (2011). Arfaptins are localized to the trans-Golgi by interaction with Arl1, but not Arfs. J Biol Chem *286*, 11569-11578.
Mancias, J.D., and Goldberg, J. (2007). The transport signal on Sec22 for packaging into COPII-coated vesicles is a conformational epitope. Mol Cell *26*, 403-414.
Mancias, J.D., and Goldberg, J. (2008). Structural basis of cargo membrane protein discrimination by the human COPII coat machinery. EMBO J *27*, 2918-2928.
Mann, M., and Wilm, M. (1994). Error-tolerant identification of peptides in sequence databases by peptide sequence tags. Anal Chem *66*, 4390-4399.
Manolea, F., Chun, J., Chen, D.W., Clarke, I., Summerfeldt, N., Dacks, J.B., and Melancon, P. (2010). Arf3 is activated uniquely at the trans-Golgi network by brefeldin A-inhibited guanine nucleotide exchange factors. Mol Biol Cell *21*, 1836-1849.
Margulis, N.G., Wilson, J.D., Bentivoglio, C.M., Dhungel, N., Gitler, A.D., and Barlowe, C. (2016). Analysis of COPII Vesicles Indicates a Role for the Emp47-Ssp120 Complex in Transport of Cell Surface Glycoproteins. Traffic *17*, 191-210.
Martinez-Menarguez, J.A., Prekeris, R., Oorschot, V.M., Scheller, R., Slot, J.W., Geuze, H.J., and Klumperman, J. (2001). Peri-Golgi vesicles contain retrograde but not anterograde proteins consistent with the cisternal progression model of intra-Golgi transport. J Cell Biol *155*, 1213-1224.
Matsuoka, K., Orci, L., Amherdt, M., Bednarek, S.Y., Hamamoto, S., Schekman, R., and Yeung, T. (1998). COPII-coated vesicle formation reconstituted with purified coat proteins and chemically defined liposomes. Cell *93*, 263-275.
Matter, K., and Mellman, I. (1994). Mechanisms of cell polarity: sorting and transport in epithelial cells. Curr Opin Cell Biol *6*, 545-554.
Mattera, R., Boehm, M., Chaudhuri, R., Prabhu, Y., and Bonifacino, J.S. (2011). Conservation and diversification of dileucine signal recognition by adaptor protein (AP) complex variants. J Biol Chem *286*, 2022-2030.
Maxfield, F.R., and McGraw, T.E. (2004). Endocytic recycling. Nat Rev Mol Cell Bio *5*, 121-132.
Mayor, S., Presley, J.F., and Maxfield, F.R. (1993). Sorting of Membrane-Components from Endosomes and Subsequent Recycling to the Cell-Surface Occurs by a Bulk Flow Process. Journal of Cell Biology *121*, 1257-1269.
Merte, J., Jensen, D., Wright, K., Sarsfield, S., Wang, Y., Schekman, R., and Ginty, D.D. (2010). Sec24b selectively sorts Vangl2 to regulate planar cell polarity during neural tube closure. Nat Cell Biol *12*, 41-46; sup pp 41-48.
Michelsen, K., Schmid, V., Metz, J., Heusser, K., Liebel, U., Schwede, T., Spang, A., and Schwappach, B. (2007). Novel cargo-binding site in the beta and delta subunits of coatomer. J Cell Biol *179*, 209-217.
Michelsen, K., Yuan, H., and Schwappach, B. (2005). Hide and run. Arginine-based endoplasmic-reticulum-sorting motifs in the assembly of heteromultimeric membrane proteins. EMBO Rep *6*, 717-722.
Miller, E., Antonny, B., Hamamoto, S., and Schekman, R. (2002). Cargo selection into COPII vesicles is driven by the Sec24p subunit. EMBO J *21*, 6105-6113.
Miller, E.A., Beilharz, T.H., Malkus, P.N., Lee, M.C., Hamamoto, S., Orci, L., and Schekman, R. (2003). Multiple cargo binding sites on the COPII subunit Sec24p ensure capture of diverse membrane proteins into transport vesicles. Cell *114*, 497-509.
Miller, S.E., Mathiasen, S., Bright, N.A., Pierre, F., Kelly, B.T., Kladt, N., Schauss, A., Merrifield, C.J., Stamou, D., Honing, S*., et al.* (2015). CALM regulates clathrin-coated vesicle size and maturation by directly sensing and driving membrane curvature. Dev Cell *33*, 163-175.
Misra, S., Puertollano, R., Kato, Y., Bonifacino, J.S., and Hurley, J.H. (2002). Structural basis for acidic-cluster-dileucine sorting-signal recognition by VHS domains. Nature *415*, 933-937.
Moelleken, J., Malsam, J., Betts, M.J., Movafeghi, A., Reckmann, I., Meissner, I., Hellwig, A., Russell, R.B., Söllner, T., Brügger, B*., et al.* (2007). Differential localization of coatomer complex isoforms within the Golgi apparatus. Proc Natl Acad Sci U S A *104*, 4425-4430.

Montpetit, A., Cote, S., Brustein, E., Drouin, C.A., Lapointe, L., Boudreau, M., Meloche, C., Drouin, R., Hudson, T.J., Drapeau, P*., et al.* (2008). Disruption of AP1S1, causing a novel neurocutaneous syndrome, perturbs development of the skin and spinal cord. PLoS Genet *4*, e1000296.
Moravec, R., Conger, K.K., D'Souza, R., Allison, A.B., and Casanova, J.E. (2012). BRAG2/GEP100/IQSec1 interacts with clathrin and regulates alpha5beta1 integrin endocytosis through activation of ADP ribosylation factor 5 (Arf5). J Biol Chem *287*, 31138-31147.
Morre, J., Merlin, L.M., and Keenan, T.W. (1969). Localization of glycosyl transferase activities in a Golgi apparatus-rich fraction isolated from rat liver. Biochem Biophys Res Commun *37*, 813-819.
Morris, S.A., Schroder, S., Plessmann, U., Weber, K., and Ungewickell, E. (1993). Clathrin assembly protein AP180: primary structure, domain organization and identification of a clathrin binding site. EMBO J *12*, 667-675.
Mossessova, E., Bickford, L.C., and Goldberg, J. (2003). SNARE selectivity of the COPII coat. Cell *114*, 483-495.
Munro, S., and Pelham, H.R. (1987). A C-terminal signal prevents secretion of luminal ER proteins. Cell *48*, 899-907.
Murphy, J.E., Pleasure, I.T., Puszkin, S., Prasad, K., and Keen, J.H. (1991). Clathrin assembly protein AP-3. The identity of the 155K protein, AP 180, and NP185 and demonstration of a clathrin binding domain. J Biol Chem *266*, 4401-4408.
Nagaraj, N., Wisniewski, J.R., Geiger, T., Cox, J., Kircher, M., Kelso, J., Paabo, S., and Mann, M. (2011). Deep proteome and transcriptome mapping of a human cancer cell line. Mol Syst Biol *7*, 548.
Nakano, A., Brada, D., and Schekman, R. (1988). A membrane glycoprotein, Sec12p, required for protein transport from the endoplasmic reticulum to the Golgi apparatus in yeast. J Cell Biol *107*, 851-863.
Nakatsu, F., and Ohno, H. (2003). Adaptor protein complexes as the key regulators of protein sorting in the post-Golgi network. Cell Struct Funct *28*, 419-429.
Neutra, M., and Leblond, C.P. (1966). Radioautographic comparison of the uptake of galactose-H and glucose-H3 in the golgi region of various cells secreting glycoproteins or mucopolysaccharides. J Cell Biol *30*, 137-150.
Nickel, W., Malsam, J., Gorgas, K., Ravazzola, M., Jenne, N., Helms, J.B., and Wieland, F.T. (1998). Uptake by COPI-coated vesicles of both anterograde and retrograde cargo is inhibited by GTPgammaS in vitro. J Cell Sci *111 (Pt 20)*, 3081-3090.
Nielsen, M.S., Madsen, P., Christensen, E.I., Nykjaer, A., Gliemann, J., Kasper, D., Pohlmann, R., and Petersen, C.M. (2001). The sortilin cytoplasmic tail conveys Golgi-endosome transport and binds the VHS domain of the GGA2 sorting protein. EMBO J *20*, 2180-2190.
Nilsson, T., Jackson, M., and Peterson, P.A. (1989). Short cytoplasmic sequences serve as retention signals for transmembrane proteins in the endoplasmic reticulum. Cell *58*, 707-718.
Nishikawa, S., and Nakano, A. (1993). Identification of a gene required for membrane protein retention in the early secretory pathway. Proc Natl Acad Sci U S A *90*, 8179-8183.
Nishimura, N., and Balch, W.E. (1997). A di-acidic signal required for selective export from the endoplasmic reticulum. Science *277*, 556-558.
Nishimura, N., Bannykh, S., Slabough, S., Matteson, J., Altschuler, Y., Hahn, K., and Balch, W.E. (1999). A di-acidic (DXE) code directs concentration of cargo during export from the endoplasmic reticulum. J Biol Chem *274*, 15937-15946.
Nogueira, C., Erlmann, P., Villeneuve, J., Santos, A.J., Martinez-Alonso, E., Martinez-Menarguez, J.A., and Malhotra, V. (2014). SLY1 and Syntaxin 18 specify a distinct pathway for procollagen VII export from the endoplasmic reticulum. Elife *3*, e02784.
Novick, P., Ferro, S., and Schekman, R. (1981). Order of events in the yeast secretory pathway. Cell *25*, 461-469.
Novick, P., Field, C., and Schekman, R. (1980). Identification of 23 complementation groups required for post-translational events in the yeast secretory pathway. Cell *21*, 205-215.

Novikoff, P.M., Novikoff, A.B., Quintana, N., and Hauw, J.J. (1971). Golgi apparatus, GERL, and lysosomes of neurons in rat dorsal root ganglia, studied by thick section and thin section cytochemistry. J Cell Biol *50*, 859-886.
O'Farrell, P.H. (1975). High resolution two-dimensional electrophoresis of proteins. J Biol Chem *250*, 4007-4021.
O'Kelly, I., Butler, M.H., Zilberberg, N., and Goldstein, S.A. (2002). Forward transport. 14-3-3 binding overcomes retention in endoplasmic reticulum by dibasic signals. Cell *111*, 577-588.
Ohisa, S., Inohaya, K., Takano, Y., and Kudo, A. (2010). sec24d encoding a component of COPII is essential for vertebra formation, revealed by the analysis of the medaka mutant, vbi. Dev Biol *342*, 85-95.
Ohno, H., Aguilar, R.C., Yeh, D., Taura, D., Saito, T., and Bonifacino, J.S. (1998). The medium subunits of adaptor complexes recognize distinct but overlapping sets of tyrosine-based sorting signals. J Biol Chem *273*, 25915-25921.
Ohno, H., Stewart, J., Fournier, M.C., Bosshart, H., Rhee, I., Miyatake, S., Saito, T., Gallusser, A., Kirchhausen, T., and Bonifacino, J.S. (1995). Interaction of tyrosine-based sorting signals with clathrin-associated proteins. Science *269*, 1872-1875.
Ohno, H., Tomemori, T., Nakatsu, F., Okazaki, Y., Aguilar, R.C., Foelsch, H., Mellman, I., Saito, T., Shirasawa, T., and Bonifacino, J.S. (1999). Mu1B, a novel adaptor medium chain expressed in polarized epithelial cells. FEBS Lett *449*, 215-220.
Oka, T., and Nakano, A. (1994). Inhibition of GTP hydrolysis by Sar1p causes accumulation of vesicles that are a functional intermediate of the ER-to-Golgi transport in yeast. J Cell Biol *124*, 425-434.
Ong, S.E., Blagoev, B., Kratchmarova, I., Kristensen, D.B., Steen, H., Pandey, A., and Mann, M. (2002). Stable isotope labeling by amino acids in cell culture, SILAC, as a simple and accurate approach to expression proteomics. Mol Cell Proteomics *1*, 376-386.
Ong, S.E., and Mann, M. (2007). Stable isotope labeling by amino acids in cell culture for quantitative proteomics. Methods Mol Biol *359*, 37-52.
Ooi, C.E., Dell'Angelica, E.C., and Bonifacino, J.S. (1998). ADP-Ribosylation factor 1 (ARF1) regulates recruitment of the AP-3 adaptor complex to membranes. J Cell Biol *142*, 391-402.
Orci, L., Amherdt, M., Ravazzola, M., Perrelet, A., and Rothman, J.E. (2000). Exclusion of golgi residents from transport vesicles budding from Golgi cisternae in intact cells. J Cell Biol *150*, 1263-1270.
Orci, L., Malhotra, V., Amherdt, M., Serafini, T., and Rothman, J.E. (1989). Dissection of a single round of vesicular transport: sequential intermediates for intercisternal movement in the Golgi stack. Cell *56*, 357-368.
Orci, L., Ravazzola, M., Meda, P., Holcomb, C., Moore, H.P., Hicke, L., and Schekman, R. (1991). Mammalian Sec23p homologue is restricted to the endoplasmic reticulum transitional cytoplasm. Proc Natl Acad Sci U S A *88*, 8611-8615.
Otsu, W., Kurooka, T., Otsuka, Y., Sato, K., and Inaba, M. (2013). A new class of endoplasmic reticulum export signal PhiXPhiXPhi for transmembrane proteins and its selective interaction with Sec24C. J Biol Chem *288*, 18521-18532.
Otte, S., and Barlowe, C. (2002). The Erv41p-Erv46p complex: multiple export signals are required in trans for COPII-dependent transport from the ER. EMBO J *21*, 6095-6104.
Owen, D.J., Collins, B.M., and Evans, P.R. (2004). Adaptors for clathrin coats: structure and function. Annu Rev Cell Dev Biol *20*, 153-191.
Ozeki, S., Cheng, J., Tauchi-Sato, K., Hatano, N., Taniguchi, H., and Fujimoto, T. (2005). Rab18 localizes to lipid droplets and induces their close apposition to the endoplasmic reticulum-derived membrane. J Cell Sci *118*, 2601-2611.
Pääbo, S., Bhat, B.M., Wold, W.S., and Peterson, P.A. (1987). A short sequence in the COOH-terminus makes an adenovirus membrane glycoprotein a resident of the endoplasmic reticulum. Cell *50*, 311-317.
Paczkowski, J.E., Richardson, B.C., and Fromme, J.C. (2015). Cargo adaptors: structures illuminate mechanisms regulating vesicle biogenesis. Trends Cell Biol *25*, 408-416.

Palade, G. (1975). Intracellular aspects of the process of protein synthesis. Science *189*, 347-358.
Palade, G.E. (1955). A small particulate component of the cytoplasm. J Biophys Biochem Cytol *1*, 59-68.
Palade, G.E. (1956). The endoplasmic reticulum. J Biophys Biochem Cytol *2*, 85-98.
Palade, G.E., and Siekevitz, P. (1956). Liver microsomes; an integrated morphological and biochemical study. J Biophys Biochem Cytol *2*, 171-200.
Pastor-Cantizano, N., Bernat-Silvestre, C., Marcote, M.J., and Aniento, F. (2017a). Loss of Arabidopsis p24 function affects ERD2 traffic and Golgi structure and activates the unfolded protein response. J Cell Sci.
Pastor-Cantizano, N., Garcia-Murria, M.J., Bernat-Silvestre, C., Marcote, M.J., Mingarro, I., and Aniento, F. (2017b). N-Linked Glycosylation of the p24 Family Protein p24delta5 Modulates Retrograde Golgi-to-ER Transport of K/HDEL Ligands in Arabidopsis. Mol Plant *10*, 1095-1106.
Pavel, J., Harter, C., and Wieland, F.T. (1998). Reversible dissociation of coatomer: functional characterization of a beta/delta-coat protein subcomplex. Proc Natl Acad Sci U S A *95*, 2140-2145.
Pearse, B.M. (1976). Clathrin: a unique protein associated with intracellular transfer of membrane by coated vesicles. Proc Natl Acad Sci U S A *73*, 1255-1259.
Pearse, B.M., and Robinson, M.S. (1984). Purification and properties of 100-kd proteins from coated vesicles and their reconstitution with clathrin. EMBO J *3*, 1951-1957.
Peden, A.A., Oorschot, V., Hesser, B.A., Austin, C.D., Scheller, R.H., and Klumperman, J. (2004). Localization of the AP-3 adaptor complex defines a novel endosomal exit site for lysosomal membrane proteins. J Cell Biol *164*, 1065-1076.
Perkins, D.N., Pappin, D.J., Creasy, D.M., and Cottrell, J.S. (1999). Probability-based protein identification by searching sequence databases using mass spectrometry data. Electrophoresis *20*, 3551-3567.
Pevsner, J., Volknandt, W., Wong, B.R., and Scheller, R.H. (1994). Two rat homologs of clathrin-associated adaptor proteins. Gene *146*, 279-283.
Piper, R.C., and Luzio, J.P. (2007). Ubiquitin-dependent sorting of integral membrane proteins for degradation in lysosomes. Curr Opin Cell Biol *19*, 459-465.
Pizzo, P., Lissandron, V., Capitanio, P., and Pozzan, T. (2011). Ca(2+) signalling in the Golgi apparatus. Cell Calcium *50*, 184-192.
Popoff, V., Adolf, F., Brügger, B., and Wieland, F. (2011a). COPI budding within the Golgi stack. Cold Spring Harb Perspect Biol *3*, a005231.
Popoff, V., Langer, J.D., Reckmann, I., Hellwig, A., Kahn, R.A., Brügger, B., and Wieland, F.T. (2011b). Several ADP-ribosylation factor (Arf) isoforms support COPI vesicle formation. J Biol Chem *286*, 35634-35642.
Porter, K.R., Claude, A., and Fullam, E.F. (1945). A Study of Tissue Culture Cells by Electron Microscopy : Methods and Preliminary Observations. J Exp Med *81*, 233-246.
Porter, K.R., and Kallman, F.L. (1952). Significance of cell particulates as seen by electron microscopy. Ann N Y Acad Sci *54*, 882-891.
Price, S.R., Nightingale, M., Tsai, S.C., Williamson, K.C., Adamik, R., Chen, H.C., Moss, J., and Vaughan, M. (1988). Guanine nucleotide-binding proteins that enhance choleragen ADP-ribosyltransferase activity: nucleotide and deduced amino acid sequence of an ADP-ribosylation factor cDNA. Proc Natl Acad Sci U S A *85*, 5488-5491.
Puertollano, R., Aguilar, R.C., Gorshkova, I., Crouch, R.J., and Bonifacino, J.S. (2001a). Sorting of mannose 6-phosphate receptors mediated by the GGAs. Science *292*, 1712-1716.
Puertollano, R., Randazzo, P.A., Presley, J.F., Hartnell, L.M., and Bonifacino, J.S. (2001b). The GGAs promote ARF-dependent recruitment of clathrin to the TGN. Cell *105*, 93-102.
Randazzo, P.A., and Hirsch, D.S. (2004). Arf GAPs: multifunctional proteins that regulate membrane traffic and actin remodelling. Cell Signal *16*, 401-413.
Redman, C.M., and Sabatini, D.D. (1966). Vectorial discharge of peptides released by puromycin from attached ribosomes. Proc Natl Acad Sci U S A *56*, 608-615.

Rein, U., Andag, U., Duden, R., Schmitt, H.D., and Spang, A. (2002). ARF-GAP-mediated interaction between the ER-Golgi v-SNAREs and the COPI coat. J Cell Biol *157*, 395-404.
Reinhard, C., Harter, C., Bremser, M., Brugger, B., Sohn, K., Helms, J.B., and Wieland, F. (1999). Receptor-induced polymerization of coatomer. Proc Natl Acad Sci U S A *96*, 1224-1228.
Reinhard, C., Schweikert, M., Wieland, F.T., and Nickel, W. (2003). Functional reconstitution of COPI coat assembly and disassembly using chemically defined components. Proc Natl Acad Sci U S A *100*, 8253-8257.
Reitman, M.L., and Kornfeld, S. (1981). Lysosomal enzyme targeting. N-Acetylglucosaminylphosphotransferase selectively phosphorylates native lysosomal enzymes. J Biol Chem *256*, 11977-11980.
Reitman, M.L., Varki, A., and Kornfeld, S. (1981). Fibroblasts from patients with I-cell disease and pseudo-Hurler polydystrophy are deficient in uridine 5'-diphosphate-N-acetylglucosamine: glycoprotein N-acetylglucosaminylphosphotransferase activity. J Clin Invest *67*, 1574-1579.
Ren, X., Farias, G.G., Canagarajah, B.J., Bonifacino, J.S., and Hurley, J.H. (2013). Structural basis for recruitment and activation of the AP-1 clathrin adaptor complex by Arf1. Cell *152*, 755-767.
Robinson, M.S. (2004). Adaptable adaptors for coated vesicles. Trends Cell Biol *14*, 167-174.
Robinson, M.S. (2015). Forty Years of Clathrin-coated Vesicles. Traffic *16*, 1210-1238.
Robinson, M.S., and Bonifacino, J.S. (2001). Adaptor-related proteins. Curr Opin Cell Biol *13*, 444-453.
Robinson, M.S., Sahlender, D.A., and Foster, S.D. (2010). Rapid inactivation of proteins by rapamycin-induced rerouting to mitochondria. Dev Cell *18*, 324-331.
Ross, P.L., Huang, Y.N., Marchese, J.N., Williamson, B., Parker, K., Hattan, S., Khainovski, N., Pillai, S., Dey, S., Daniels, S*., et al.* (2004). Multiplexed protein quantitation in Saccharomyces cerevisiae using amine-reactive isobaric tagging reagents. Mol Cell Proteomics *3*, 1154-1169.
Rossanese, O.W., Soderholm, J., Bevis, B.J., Sears, I.B., O'Connor, J., Williamson, E.K., and Glick, B.S. (1999). Golgi structure correlates with transitional endoplasmic reticulum organization in Pichia pastoris and Saccharomyces cerevisiae. J Cell Biol *145*, 69-81.
Roth, T.F., and Porter, K.R. (1964). Yolk Protein Uptake in the Oocyte of the Mosquito Aedes Aegypti. L. J Cell Biol *20*, 313-332.
Rutz, C., Satoh, A., Ronchi, P., Brugger, B., Warren, G., and Wieland, F.T. (2009). Following the fate in vivo of COPI vesicles generated in vitro. Traffic *10*, 994-1005.
Sabatini, D.D., and Blobel, G. (1970). Controlled proteolysis of nascent polypeptides in rat liver cell fractions. II. Location of the polypeptides in rough microsomes. J Cell Biol *45*, 146-157.
Sabatini, D.D., Tashiro, Y., and Palade, G.E. (1966). On the attachment of ribosomes to microsomal membranes. J Mol Biol *19*, 503-524.
Sahlmuller, M.C., Strating, J.R., Beck, R., Eckert, P., Popoff, V., Haag, M., Hellwig, A., Berger, I., Brugger, B., and Wieland, F.T. (2011). Recombinant heptameric coatomer complexes: novel tools to study isoform-specific functions. Traffic *12*, 682-692.
Saito, K., Chen, M., Bard, F., Chen, S., Zhou, H., Woodley, D., Polischuk, R., Schekman, R., and Malhotra, V. (2009). TANGO1 facilitates cargo loading at endoplasmic reticulum exit sites. Cell *136*, 891-902.
Saito, K., Yamashiro, K., Ichikawa, Y., Erlmann, P., Kontani, K., Malhotra, V., and Katada, T. (2011). cTAGE5 mediates collagen secretion through interaction with TANGO1 at endoplasmic reticulum exit sites. Mol Biol Cell *22*, 2301-2308.
Saraste, J., and Kuismanen, E. (1984). Pre- and post-Golgi vacuoles operate in the transport of Semliki Forest virus membrane glycoproteins to the cell surface. Cell *38*, 535-549.
Sarmah, S., Barrallo-Gimeno, A., Melville, D.B., Topczewski, J., Solnica-Krezel, L., and Knapik, E.W. (2010). Sec24D-dependent transport of extracellular matrix proteins is required for zebrafish skeletal morphogenesis. PLoS One *5*, e10367.
Sato, K., and Nakano, A. (2002). Emp47p and its close homolog Emp46p have a tyrosine-containing endoplasmic reticulum exit signal and function in glycoprotein secretion in Saccharomyces cerevisiae. Mol Biol Cell *13*, 2518-2532.

Sato, K., Sato, M., and Nakano, A. (2001). Rer1p, a retrieval receptor for endoplasmic reticulum membrane proteins, is dynamically localized to the Golgi apparatus by coatomer. J Cell Biol *152*, 935-944.
Schindler, R., Itin, C., Zerial, M., Lottspeich, F., and Hauri, H.P. (1993). ERGIC-53, a membrane protein of the ER-Golgi intermediate compartment, carries an ER retention motif. Eur J Cell Biol *61*, 1-9.
Schmidt, W.M., Kraus, C., Hoger, H., Hochmeister, S., Oberndorfer, F., Branka, M., Bingemann, S., Lassmann, H., Muller, M., Macedo-Souza, L.I*., et al.* (2007). Mutation in the Scyl1 gene encoding amino-terminal kinase-like protein causes a recessive form of spinocerebellar neurodegeneration. EMBO Rep *8*, 691-697.
Schmidt, W.M., Rutledge, S.L., Schule, R., Mayerhofer, B., Zuchner, S., Boltshauser, E., and Bittner, R.E. (2015). Disruptive SCYL1 Mutations Underlie a Syndrome Characterized by Recurrent Episodes of Liver Failure, Peripheral Neuropathy, Cerebellar Atrophy, and Ataxia. Am J Hum Genet *97*, 855-861.
Schmitz, K.R., Liu, J., Li, S., Setty, T.G., Wood, C.S., Burd, C.G., and Ferguson, K.M. (2008). Golgi localization of glycosyltransferases requires a Vps74p oligomer. Dev Cell *14*, 523-534.
Schröder-Köhne, S., Letourneur, F., and Riezman, H. (1998). Alpha-COP can discriminate between distinct, functional di-lysine signals in vitro and regulates access into retrograde transport. J Cell Sci *111 (Pt 23)*, 3459-3470.
Schröder, S., Schimmöller, F., Singer-Krüger, B., and Riezman, H. (1995). The Golgi-localization of yeast Emp47p depends on its di-lysine motif but is not affected by the ret1-1 mutation in alpha-COP. J Cell Biol *131*, 895-912.
Schutze, M.P., Peterson, P.A., and Jackson, M.R. (1994). An N-terminal double-arginine motif maintains type II membrane proteins in the endoplasmic reticulum. EMBO J *13*, 1696-1705.
Schwarz, D.S., and Blower, M.D. (2016). The endoplasmic reticulum: structure, function and response to cellular signaling. Cell Mol Life Sci *73*, 79-94.
Schweitzer, J.K., Sedgwick, A.E., and D'Souza-Schorey, C. (2011). ARF6-mediated endocytic recycling impacts cell movement, cell division and lipid homeostasis. Semin Cell Dev Biol *22*, 39-47.
Schweizer, A., Fransen, J.A., Bächi, T., Ginsel, L., and Hauri, H.P. (1988). Identification, by a monoclonal antibody, of a 53-kD protein associated with a tubulo-vesicular compartment at the cis-side of the Golgi apparatus. J Cell Biol *107*, 1643-1653.
Schweizer, A., Fransen, J.A., Matter, K., Kreis, T.E., Ginsel, L., and Hauri, H.P. (1990). Identification of an intermediate compartment involved in protein transport from endoplasmic reticulum to Golgi apparatus. Eur J Cell Biol *53*, 185-196.
Schweizer, A., Matter, K., Ketcham, C.M., and Hauri, H.P. (1991). The isolated ER-Golgi intermediate compartment exhibits properties that are different from ER and cis-Golgi. J Cell Biol *113*, 45-54.
Semerdjieva, S., Shortt, B., Maxwell, E., Singh, S., Fonarev, P., Hansen, J., Schiavo, G., Grant, B.D., and Smythe, E. (2008). Coordinated regulation of AP2 uncoating from clathrin-coated vesicles by rab5 and hRME-6. J Cell Biol *183*, 499-511.
Serafini, T., Orci, L., Amherdt, M., Brunner, M., Kahn, R.A., and Rothman, J.E. (1991). ADP-ribosylation factor is a subunit of the coat of Golgi-derived COP-coated vesicles: a novel role for a GTP-binding protein. Cell *67*, 239-253.
Sevier, C.S., Weisz, O.A., Davis, M., and Machamer, C.E. (2000). Efficient export of the vesicular stomatitis virus G protein from the endoplasmic reticulum requires a signal in the cytoplasmic tail that includes both tyrosine-based and di-acidic motifs. Mol Biol Cell *11*, 13-22.
Shevchenko, A., Tomas, H., Havlis, J., Olsen, J.V., and Mann, M. (2006). In-gel digestion for mass spectrometric characterization of proteins and proteomes. Nat Protoc *1*, 2856-2860.
Shevchenko, A., Wilm, M., Vorm, O., and Mann, M. (1996). Mass spectrometric sequencing of proteins silver-stained polyacrylamide gels. Anal Chem *68*, 850-858.
Shiba, T., Takatsu, H., Nogi, T., Matsugaki, N., Kawasaki, M., Igarashi, N., Suzuki, M., Kato, R., Earnest, T., Nakayama, K*., et al.* (2002). Structural basis for recognition of acidic-cluster dileucine sequence by GGA1. Nature *415*, 937-941.
Shiba, Y., and Randazzo, P.A. (2014). ArfGAPs: key regulators for receptor sorting. Receptors Clin Investig *1*, e158.

Shibata, Y., Voeltz, G.K., and Rapoport, T.A. (2006). Rough sheets and smooth tubules. Cell *126*, 435-439.
Shorter, J., Beard, M.B., Seemann, J., Dirac-Svejstrup, A.B., and Warren, G. (2002). Sequential tethering of Golgins and catalysis of SNAREpin assembly by the vesicle-tethering protein p115. J Cell Biol *157*, 45-62.
Shteyn, E., Pigati, L., and Folsch, H. (2011). Arf6 regulates AP-1B-dependent sorting in polarized epithelial cells. J Cell Biol *194*, 873-887.
Sickmann, A., Reinders, J., Wagner, Y., Joppich, C., Zahedi, R., Meyer, H.E., Schonfisch, B., Perschil, I., Chacinska, A., Guiard, B.*, et al.* (2003). The proteome of Saccharomyces cerevisiae mitochondria. Proc Natl Acad Sci U S A *100*, 13207-13212.
Siekevitz, P., and Palade, G.E. (1960). A cytochemical study on the pancreas of the guinea pig. 6. Release of enzymes and ribonucleic acid from ribonucleoprotein particles. J Biophys Biochem Cytol *7*, 631-644.
Simpson, F., Bright, N.A., West, M.A., Newman, L.S., Darnell, R.B., and Robinson, M.S. (1996). A novel adaptor-related protein complex. J Cell Biol *133*, 749-760.
Sjostrand, F.S., and Hanzon, V. (1954). Ultrastructure of Golgi apparatus of exocrine cells of mouse pancreas. Exp Cell Res *7*, 415-429.
Slabicki, M., Theis, M., Krastev, D.B., Samsonov, S., Mundwiller, E., Junqueira, M., Paszkowski-Rogacz, M., Teyra, J., Heninger, A.K., Poser, I.*, et al.* (2010). A genome-scale DNA repair RNAi screen identifies SPG48 as a novel gene associated with hereditary spastic paraplegia. PLoS Biol *8*, e1000408.
Sohn, K., Orci, L., Ravazzola, M., Amherdt, M., Bremser, M., Lottspeich, F., Fiedler, K., Helms, J.B., and Wieland, F.T. (1996). A major transmembrane protein of Golgi-derived COPI-coated vesicles involved in coatomer binding. J Cell Biol *135*, 1239-1248.
Soni, K.G., Mardones, G.A., Sougrat, R., Smirnova, E., Jackson, C.L., and Bonifacino, J.S. (2009). Coatomer-dependent protein delivery to lipid droplets. J Cell Sci *122*, 1834-1841.
Spang, A., Matsuoka, K., Hamamoto, S., Schekman, R., and Orci, L. (1998). Coatomer, Arf1p, and nucleotide are required to bud coat protein complex I-coated vesicles from large synthetic liposomes. Proc Natl Acad Sci U S A *95*, 11199-11204.
Spang, A., Shiba, Y., and Randazzo, P.A. (2010). Arf GAPs: gatekeepers of vesicle generation. FEBS Lett *584*, 2646-2651.
Sprangers, J., and Rabouille, C. (2015). SEC16 in COPII coat dynamics at ER exit sites. Biochem Soc Trans *43*, 97-103.
Springer, S., Malkus, P., Borchert, B., Wellbrock, U., Duden, R., and Schekman, R. (2014). Regulated oligomerization induces uptake of a membrane protein into COPII vesicles independent of its cytosolic tail. Traffic *15*, 531-545.
Stagg, S.M., Gürkan, C., Fowler, D.M., LaPointe, P., Foss, T.R., Potter, C.S., Carragher, B., and Balch, W.E. (2006). Structure of the Sec13/31 COPII coat cage. Nature *439*, 234-238.
Stamnes, M.A., and Rothman, J.E. (1993). The binding of AP-1 clathrin adaptor particles to Golgi membranes requires ADP-ribosylation factor, a small GTP-binding protein. Cell *73*, 999-1005.
Stenbeck, G., Harter, C., Brecht, A., Herrmann, D., Lottspeich, F., Orci, L., and Wieland, F.T. (1993). beta'-COP, a novel subunit of coatomer. EMBO J *12*, 2841-2845.
Stephens, D.J. (2003). De novo formation, fusion and fission of mammalian COPII-coated endoplasmic reticulum exit sites. EMBO Rep *4*, 210-217.
Stornaiuolo, M., Lotti, L.V., Borgese, N., Torrisi, M.R., Mottola, G., Martire, G., and Bonatti, S. (2003). KDEL and KKXX retrieval signals appended to the same reporter protein determine different trafficking between endoplasmic reticulum, intermediate compartment, and Golgi complex. Mol Biol Cell *14*, 889-902.
Straus, W. (1964). Occurrence of Phagosomes and Phago-Lysosomes in Different Segments of the Nephron in Relation to the Reabsorption, Transport, Digestion, and Extrusion of Intravenously Injected Horseradish Peroxidase. J Cell Biol *21*, 295-308.

Subramaniam, V.N., Loh, E., and Hong, W. (1997). N-Ethylmaleimide-sensitive factor (NSF) and alpha-soluble NSF attachment proteins (SNAP) mediate dissociation of GS28-syntaxin 5 Golgi SNAP receptors (SNARE) complex. J Biol Chem *272*, 25441-25444.
Sucic, S., El-Kasaby, A., Kudlacek, O., Sarker, S., Sitte, H.H., Marin, P., and Freissmuth, M. (2011). The serotonin transporter is an exclusive client of the coat protein complex II (COPII) component SEC24C. J Biol Chem *286*, 16482-16490.
Sucic, S., Koban, F., El-Kasaby, A., Kudlacek, O., Stockner, T., Sitte, H.H., and Freissmuth, M. (2013). Switching the clientele: a lysine residing in the C terminus of the serotonin transporter specifies its preference for the coat protein complex II component SEC24C. J Biol Chem *288*, 5330-5341.
Suga, K., Saito, A., and Akagawa, K. (2015). ER stress response in NG108-15 cells involves upregulation of syntaxin 5 expression and reduced amyloid beta peptide secretion. Exp Cell Res *332*, 11-23.
Sun, Z., Anderl, F., Fröhlich, K., Zhao, L., Hanke, S., Brügger, B., Wieland, F., and Béthune, J. (2007). Multiple and stepwise interactions between coatomer and ADP-ribosylation factor-1 (Arf1)-GTP. Traffic *8*, 582-593.
Tai, G., Lu, L., Wang, T.L., Tang, B.L., Goud, B., Johannes, L., and Hong, W. (2004). Participation of the syntaxin 5/Ykt6/GS28/GS15 SNARE complex in transport from the early/recycling endosome to the trans-Golgi network. Mol Biol Cell *15*, 4011-4022.
Takamori, S., Holt, M., Stenius, K., Lemke, E.A., Gronborg, M., Riedel, D., Urlaub, H., Schenck, S., Brugger, B., Ringler, P.*, et al.* (2006). Molecular anatomy of a trafficking organelle. Cell *127*, 831-846.
Tanigawa, G., Orci, L., Amherdt, M., Ravazzola, M., Helms, J.B., and Rothman, J.E. (1993). Hydrolysis of bound GTP by ARF protein triggers uncoating of Golgi-derived COP-coated vesicles. J Cell Biol *123*, 1365-1371.
Tarpey, P.S., Stevens, C., Teague, J., Edkins, S., O'Meara, S., Avis, T., Barthorpe, S., Buck, G., Butler, A., Cole, J.*, et al.* (2006). Mutations in the gene encoding the Sigma 2 subunit of the adaptor protein 1 complex, AP1S2, cause X-linked mental retardation. Am J Hum Genet *79*, 1119-1124.
The UniProt, C. (2017). UniProt: the universal protein knowledgebase. Nucleic Acids Res *45*, D158-D169.
Thompson, A., Schafer, J., Kuhn, K., Kienle, S., Schwarz, J., Schmidt, G., Neumann, T., Johnstone, R., Mohammed, A.K., and Hamon, C. (2003). Tandem mass tags: a novel quantification strategy for comparative analysis of complex protein mixtures by MS/MS. Anal Chem *75*, 1895-1904.
Traub, L.M., Ostrom, J.A., and Kornfeld, S. (1993). Biochemical dissection of AP-1 recruitment onto Golgi membranes. J Cell Biol *123*, 561-573.
Tsuchiya, M., Price, S.R., Tsai, S.C., Moss, J., and Vaughan, M. (1991). Molecular identification of ADP-ribosylation factor mRNAs and their expression in mammalian cells. J Biol Chem *266*, 2772-2777.
Tu, L., Tai, W.C., Chen, L., and Banfield, D.K. (2008). Signal-mediated dynamic retention of glycosyltransferases in the Golgi. Science *321*, 404-407.
Unanue, E.R., Ungewickell, E., and Branton, D. (1981). The binding of clathrin triskelions to membranes from coated vesicles. Cell *26*, 439-446.
Ungewickell, E., and Branton, D. (1981). Assembly units of clathrin coats. Nature *289*, 420-422.
Ungewickell, E., Ungewickell, H., Holstein, S.E., Lindner, R., Prasad, K., Barouch, W., Martin, B., Greene, L.E., and Eisenberg, E. (1995). Role of auxilin in uncoating clathrin-coated vesicles. Nature *378*, 632-635.
Varki, A.P., Reitman, M.L., and Kornfeld, S. (1981). Identification of a variant of mucolipidosis III (pseudo-Hurler polydystrophy): a catalytically active N-acetylglucosaminylphosphotransferase that fails to phosphorylate lysosomal enzymes. Proc Natl Acad Sci U S A *78*, 7773-7777.
Vellodi, A. (2005). Lysosomal storage disorders. Br J Haematol *128*, 413-431.
Venditti, R., Wilson, C., and De Matteis, M.A. (2014). Exiting the ER: what we know and what we don't. Trends Cell Biol *24*, 9-18.
Volpicelli-Daley, L.A., Li, Y., Zhang, C.J., and Kahn, R.A. (2005). Isoform-selective effects of the depletion of ADP-ribosylation factors 1-5 on membrane traffic. Mol Biol Cell *16*, 4495-4508.

Votsmeier, C., and Gallwitz, D. (2001). An acidic sequence of a putative yeast Golgi membrane protein binds COPII and facilitates ER export. EMBO J *20*, 6742-6750.
Wakana, Y., van Galen, J., Meissner, F., Scarpa, M., Polishchuk, R.S., Mann, M., and Malhotra, V. (2012). A new class of carriers that transport selective cargo from the trans Golgi network to the cell surface. EMBO J *31*, 3976-3990.
Walter, P., and Blobel, G. (1980). Purification of a membrane-associated protein complex required for protein translocation across the endoplasmic reticulum. Proc Natl Acad Sci U S A *77*, 7112-7116.
Walter, P., and Blobel, G. (1981a). Translocation of proteins across the endoplasmic reticulum III. Signal recognition protein (SRP) causes signal sequence-dependent and site-specific arrest of chain elongation that is released by microsomal membranes. J Cell Biol *91*, 557-561.
Walter, P., and Blobel, G. (1981b). Translocation of proteins across the endoplasmic reticulum. II. Signal recognition protein (SRP) mediates the selective binding to microsomal membranes of in-vitro-assembled polysomes synthesizing secretory protein. J Cell Biol *91*, 551-556.
Wang, C.W., Hamamoto, S., Orci, L., and Schekman, R. (2006). Exomer: A coat complex for transport of select membrane proteins from the trans-Golgi network to the plasma membrane in yeast. J Cell Biol *174*, 973-983.
Waters, M.G., Serafini, T., and Rothman, J.E. (1991). 'Coatomer': a cytosolic protein complex containing subunits of non-clathrin-coated Golgi transport vesicles. Nature *349*, 248-251.
Watkin, L.B., Jessen, B., Wiszniewski, W., Vece, T.J., Jan, M., Sha, Y., Thamsen, M., Santos-Cortez, R.L., Lee, K., Gambin, T.*, et al.* (2015). COPA mutations impair ER-Golgi transport and cause hereditary autoimmune-mediated lung disease and arthritis. Nat Genet *47*, 654-660.
Wegmann, D., Hess, P., Baier, C., Wieland, F.T., and Reinhard, C. (2004). Novel isotypic gamma/zeta subunits reveal three coatomer complexes in mammals. Mol Cell Biol *24*, 1070-1080.
Weissman, J.T., Plutner, H., and Balch, W.E. (2001). The mammalian guanine nucleotide exchange factor mSec12 is essential for activation of the Sar1 GTPase directing endoplasmic reticulum export. Traffic *2*, 465-475.
Whitney, J.A., Gomez, M., Sheff, D., Kreis, T.E., and Mellman, I. (1995). Cytoplasmic coat proteins involved in endosome function. Cell *83*, 703-713.
Whur, P., Herscovics, A., and Leblond, C.P. (1969). Radioautographic visualization of the incorporation of [3H] mannose and [3H] galactose into thyroglobulin by follicular cells of rat thyroids in vitro. J Anat *104*, 582.
Wieland, F.T., Gleason, M.L., Serafini, T.A., and Rothman, J.E. (1987). The rate of bulk flow from the endoplasmic reticulum to the cell surface. Cell *50*, 289-300.
Wiese, S., Reidegeld, K.A., Meyer, H.E., and Warscheid, B. (2007). Protein labeling by iTRAQ: a new tool for quantitative mass spectrometry in proteome research. Proteomics *7*, 340-350.
Wilfling, F., Thiam, A.R., Olarte, M.J., Wang, J., Beck, R., Gould, T.J., Allgeyer, E.S., Pincet, F., Bewersdorf, J., Farese, R.V., Jr.*, et al.* (2014). Arf1/COPI machinery acts directly on lipid droplets and enables their connection to the ER for protein targeting. Elife *3*, e01607.
Williger, B.T., Ostermann, J., and Exton, J.H. (1999). Arfaptin 1, an ARF-binding protein, inhibits phospholipase D and endoplasmic reticulum/Golgi protein transport. FEBS Lett *443*, 197-200.
Wilm, M., Shevchenko, A., Houthaeve, T., Breit, S., Schweigerer, L., Fotsis, T., and Mann, M. (1996). Femtomole sequencing of proteins from polyacrylamide gels by nano-electrospray mass spectrometry. Nature *379*, 466-469.
Wilson, D.W., Lewis, M.J., and Pelham, H.R. (1993). pH-dependent binding of KDEL to its receptor in vitro. J Biol Chem *268*, 7465-7468.
Wittke, I., Wiedemeyer, R., Pillmann, A., Savelyeva, L., Westermann, F., and Schwab, M. (2003). Neuroblastoma-derived sulfhydryl oxidase, a new member of the sulfhydryl oxidase/Quiescin6 family, regulates sensitization to interferon gamma-induced cell death in human neuroblastoma cells. Cancer Res *63*, 7742-7752.
Wong, J.W., and Cagney, G. (2010). An overview of label-free quantitation methods in proteomics by mass spectrometry. Methods Mol Biol *604*, 273-283.

Wong, M., and Munro, S. (2014). Membrane trafficking. The specificity of vesicle traffic to the Golgi is encoded in the golgin coiled-coil proteins. Science *346*, 1256898.
Woo, C.H., Gao, C., Yu, P., Tu, L., Meng, Z., Banfield, D.K., Yao, X., and Jiang, L. (2015). Conserved function of the lysine-based KXD/E motif in Golgi retention for endomembrane proteins among different organisms. Mol Biol Cell *26*, 4280-4293.
Wu, M.M., Llopis, J., Adams, S., McCaffery, J.M., Kulomaa, M.S., Machen, T.E., Moore, H.P., and Tsien, R.Y. (2000). Organelle pH studies using targeted avidin and fluorescein-biotin. Chem Biol *7*, 197-209.
Xie, L., Boyle, D., Sanford, D., Scherer, P.E., Pessin, J.E., and Mora, S. (2006). Intracellular trafficking and secretion of adiponectin is dependent on GGA-coated vesicles. J Biol Chem *281*, 7253-7259.
Xu, P., Hankins, H.M., MacDonald, C., Erlinger, S.J., Frazier, M.N., Diab, N.S., Piper, R.C., Jackson, L.P., MacGurn, J.A., and Graham, T.R. (2017). COPI mediates recycling of an exocytic SNARE by recognition of a ubiquitin sorting signal. Elife *6*.
Xu, Y., Martin, S., James, D.E., and Hong, W. (2002). GS15 forms a SNARE complex with syntaxin 5, GS28, and Ykt6 and is implicated in traffic in the early cisternae of the Golgi apparatus. Mol Biol Cell *13*, 3493-3507.
Yang, J.S., Gad, H., Lee, S.Y., Mironov, A., Zhang, L., Beznoussenko, G.V., Valente, C., Turacchio, G., Bonsra, A.N., Du, G.*, et al.* (2008). A role for phosphatidic acid in COPI vesicle fission yields insights into Golgi maintenance. Nat Cell Biol *10*, 1146-1153.
Yang, J.S., Lee, S.Y., Spano, S., Gad, H., Zhang, L., Nie, Z., Bonazzi, M., Corda, D., Luini, A., and Hsu, V.W. (2005). A role for BARS at the fission step of COPI vesicle formation from Golgi membrane. EMBO J *24*, 4133-4143.
Yates, J.R., 3rd, Gilchrist, A., Howell, K.E., and Bergeron, J.J. (2005). Proteomics of organelles and large cellular structures. Nat Rev Mol Cell Biol *6*, 702-714.
Yehia, L., Niazi, F., Ni, Y., Ngeow, J., Sankunny, M., Liu, Z., Wei, W., Mester, J.L., Keri, R.A., Zhang, B.*, et al.* (2015). Germline Heterozygous Variants in SEC23B Are Associated with Cowden Syndrome and Enriched in Apparently Sporadic Thyroid Cancer. Am J Hum Genet *97*, 661-676.
Yi, E.C., Li, X.J., Cooke, K., Lee, H., Raught, B., Page, A., Aneliunas, V., Hieter, P., Goodlett, D.R., and Aebersold, R. (2005). Increased quantitative proteome coverage with (13)C/(12)C-based, acid-cleavable isotope-coded affinity tag reagent and modified data acquisition scheme. Proteomics *5*, 380-387.
Yin, P., Li, Y., and Zhang, L. (2017). Sec24C-Dependent Transport of Claudin-1 Regulates Hepatitis C Virus Entry. J Virol *91*.
Yoshihisa, T., Barlowe, C., and Schekman, R. (1993). Requirement for a GTPase-activating protein in vesicle budding from the endoplasmic reticulum. Science *259*, 1466-1468.
Zanetti, G., Pahuja, K.B., Studer, S., Shim, S., and Schekman, R. (2011). COPII and the regulation of protein sorting in mammals. Nat Cell Biol *14*, 20-28.
Zappa, F., Venditti, R., and De Matteis, M.A. (2017). TRAPPing Rab18 in lipid droplets. EMBO J *36*, 394-396.
Zaremba, S., and Keen, J.H. (1983). Assembly polypeptides from coated vesicles mediate reassembly of unique clathrin coats. J Cell Biol *97*, 1339-1347.
Zerangue, N., Schwappach, B., Jan, Y.N., and Jan, L.Y. (1999). A new ER trafficking signal regulates the subunit stoichiometry of plasma membrane K(ATP) channels. Neuron *22*, 537-548.
Zhang, B., Koh, Y.H., Beckstead, R.B., Budnik, V., Ganetzky, B., and Bellen, H.J. (1998). Synaptic vesicle size and number are regulated by a clathrin adaptor protein required for endocytosis. Neuron *21*, 1465-1475.
Zhang, R., Sioma, C.S., Wang, S., and Regnier, F.E. (2001). Fractionation of isotopically labeled peptides in quantitative proteomics. Anal Chem *73*, 5142-5149.
Zhang, T., and Hong, W. (2001). Ykt6 forms a SNARE complex with syntaxin 5, GS28, and Bet1 and participates in a late stage in endoplasmic reticulum-Golgi transport. J Biol Chem *276*, 27480-27487.
Zhang, W., Zhou, G., Zhao, Y., White, M.A., and Zhao, Y. (2003). Affinity enrichment of plasma membrane for proteomics analysis. Electrophoresis *24*, 2855-2863.

Zhao, G., Zhu, P.P., Renvoise, B., Maldonado-Baez, L., Park, S.H., and Blackstone, C. (2016). Mammalian knock out cells reveal prominent roles for atlastin GTPases in ER network morphology. Exp Cell Res *349*, 32-44.

Zhao, L., Helms, J.B., Brügger, B., Harter, C., Martoglio, B., Graf, R., Brunner, J., and Wieland, F.T. (1997). Direct and GTP-dependent interaction of ADP ribosylation factor 1 with coatomer subunit beta. Proc Natl Acad Sci U S A *94*, 4418-4423.

Zhao, L., Helms, J.B., Brunner, J., and Wieland, F.T. (1999). GTP-dependent binding of ADP-ribosylation factor to coatomer in close proximity to the binding site for dilysine retrieval motifs and p23. J Biol Chem *274*, 14198-14203.

Zhao, X., Lasell, T.K., and Melançon, P. (2002). Localization of large ADP-ribosylation factor-guanine nucleotide exchange factors to different Golgi compartments: evidence for distinct functions in protein traffic. Mol Biol Cell *13*, 119-133.

6 Appendix

6.1 Abbreviations

AP	Adaptor protein complex
Arf	ADP-ribosylation factor
ATP	Adenosine 5′-triphosphate
Bet1	Blocked in early transport 1 homologue; ER-Golgi Q-SNARE
BFA	Brefeldin A
BSA	Bovine serum albumin
CBB	Coomassie brilliant blue
CCV	clathrin-coated vesicle
CM	Coatomer
COPI	Coat protein complex I
COPII	Coat protein complex II
DMEM	Dulbecco's modified eagle's medium
DMSO	Dimethyl sulfoxide
DNA	Desoxyribonucleic acid
DTT	Dithiothreitol
EDTA	Ethylenediaminetetraacetic acid
ER	Endoplasmic reticulum
ERGIC	ER-Golgi intermediate compartment
GAP	GTPase-activating protein
GBF1	Golgi-specific brefeldin A-resistant factor 1
GDP	Guanosine 5′-diphosphate
GEF	Guanine nucleotide exchange factor
GGA	Golgi-localized, gamma ear-containing, Arf-binding proteins
GM130	Cis-Golgi matrix protein of 130 kDa
GMP-PNP	Guanosine-5′-O-[β,γ-imido]-triphosphate
GP	Glycosylphosphatidylinositol
GS15	Golgi SNARE of 15 kDa; intra-Golgi Q-SNARE
GS27	Golgi SNARE of 27 kDa; ER-Golgi Q-SNARE
GS28	Golgi SNARE of 28 kDa; intra-Golgi Q-SNARE

GST	Glutathione-S-transferase
GTP	Guanosine-5′-triphosphate
GTPγS	Guanosine-5′-O-[γ-thio]-triphosphate
HeLa	Human epithelial cell line derived from cervical cancer
HEPES	4-(2-hydroxyethyl)-1-piperazin-ethansulfonic acid
HepG2	Human cell line derived from hepatic cancer
IFA	Immunofluorescence assay
iMΦ	Immortalized murine macrophages
IP	Immunoprecipitation
IPTG	Isopropyl-1-thio-β-D-galactopyranoside
KDEL	ER-retrieval sequence composed of Lysine (K)-Aspartate (D)-Glutamate (E)-Leucine (L)
kDa	Kilo Dalton
LB	Luria broth
OD	Optical density
p24	Transmembrane emp24 domain-containing protein
PBS	Phosphate buffer saline
PBST	Phosphate buffer saline + Tween 20
PCR	Polymerase chain reaction
psi	Pounds per square inch
PVDF	Polyvinyldifluoride
rpm	Revolutions per minute
Sar1	Secretion-associated and Ras-related protein 1
SDS-PAGE	Sodium dodecyl sulfate-polyacrylamide gel electrophoresis
Sec	Secretion mutant
Sec22b	Vesicle-trafficking protein Sec22b; ER-Golgi R-SNARE
SEM	Standard error of the mean
Sf9 cells	Insect cell line derived from Sf21 (*spodoptera frugiperda)* ovarie cells
SNARE	*N*- ethylmaleimide sensitive-factor attachment receptors
SRP	Signal recognition particle
Stx5	Syntaxin5; ER-Golgi Q-SNARE
TGN	Trans-Golgi network
×g	Times gravity
Ykt6	Synaptobrevin homologueYkt6; intra-Golgi R-SNARE

6.2 Publications

Major parts of this thesis are presented in the following manuscripts:

Rhiel, M., Hessling, B., Gao, Q., Hellwig, A., Adolf, F., and Wieland, F.T. (2017). Quantitative proteomics of isotypic mammalian COPI vesicles. *In preparation*.

Adolf, F., Rhiel, M., Hessling, B., Hellwig, A., and Wieland, F.T. (2017). SILAC-based proteomic profiling of mammalian COPII vesicles. *In preparation*.

Further publications:

Adolf, F., Rhiel, M., Reckmann, I., and Wieland, F.T. (2016). Sec24C/D-isoform-specific sorting of the preassembled ER-Golgi Q-SNARE complex. Mol. Biol. Cell 27, 2697-2707.

Rhiel, M., Bittl, V., Tribensky, A., Charnaud, S.C., Strecker, M., Muller, S., Lanzer, M., Sanchez, C., Schaeffer-Reiss, C., Westermann, B., Crabb, B.S., Gilson, P.R., Külzer, S., and Przyborski, J.M. (2016). Trafficking of the exported P. falciparum chaperone PfHsp70x. Sci Rep 6, 36174.

Acknowledgement

First and foremost I am grateful to Prof. Dr. Felix T. Wieland for giving me the opportunity to work in his lab, his interest in my project, our fruitful discussions and for always being open-minded about new ideas.

I would also like to thank Prof. Dr. Thomas Söllner for being my second referee and a vital member of my technical advisory committee during the last three years.

I am grateful to Prof. Dr. Sabine Strahl and Prof. Dr. Matthias Mayer for kindly agreeing to be on my defense committee.

I would like to thanks Dr. Rainer Beck for serving as third member of my technical advisory committee and his valuable input.

I am grateful to all members of the Wieland lab, past and present, for their advice, helpful discussions, and support. Special thanks to Jan Brod for being not only a good colleague but a good friend.

I would further like to thank Dr. Bernd Hessling, Andrea Hellwig, and Qi Gao for being wonderful collaborators.

I am deeply grateful to family. I have to thank my parents Rita and Erhard and my brother Fabian for their unconditional support, encouragement, and love.

I would furthermore like to thank Rita and Hans for their support and hosting me on countless weekends.

Finally I have to thank my significant other Sabrina. I could not have done it without you. You still are the best ☺